CONTAINS PULLOUTS

CU 15814

Thesis

L2595

DYNAMIC BEHAVIOUR OF LINKAGE MECHANISMS

by

R. S. HAINES

A thesis submitted for the degree of Doctor or Philosophy in the Faculty of Engineering at the University of Newcastle upon Tyne.

September 1982

To Gillian

'The discovery of instances which confirm a theory means very little
if we have not tried, and failed, to discover refutations.
In order to make the method of selection by elimination work,
and to ensure that only the fittest theories survive,
their struggle for life must be made severe for them.'

Sir Karl Popper

SUMMARY

General: The thesis concerns the prediction and control of vibrations in planar, kinematically determinate linkage mechanisms operating in a continuous manner, typically driven by a crankshaft. An array of simplified models of linkage components is used to assess the likely significance of the many factors concerned, assuming the components to be of realistic proportions. It is concluded that the effects of joint clearance and (in some cases) driving system flexibility, rather than link flexibility per se, are likely to be the crucial factors. Attention is therefore focused on the former factors in the chapters that follow.

Clearance Effects: The literature on the two-dimensional dynamic effects of clearance ("ludodynamic" effects) in revolute joints is critically reviewed, with the conclusion that existing theoretical models need to be simplified to be of use for preliminary design synthesis, and that more discriminating experimental work is needed before any of the theories can be applied with confidence. A new theory is developed with a view to meeting the former need, the results being presented in the form of a design chart. An account is then given of the design, development and use of a novel experimental apparatus for studying a number of relevant aspects of the ludodynamic behaviour of a revolute joint. The new theory is supported in some respects for larger clearances (250 μm on 50mm diameter) but for smaller clearances (65 & 20 μm) the air 'squeeze film' is found to play an increasingly dominant role.

Drive Flexibility Effects: The effects of driving system flexibility are approximately governed by an inhomogeneous Hill's equation. A numerical method is used to find the harmonic composition of the steady state solutions of this equation. A rule for predicting resonant and unstable speeds is hypothesized: it is shown to give excellent results, but the response at off-resonant speeds also has a large high-frequency element in some cases.

Synthesis: A convenient method for modifying undesirable dynamic performance in a linkage mechanism is the attachment of auxiliary masses or springs. A method is developed for the efficient optimisation of counterweights by a weighted root mean square criterion, subject to bounds on the physical parameters. A known method for synthesis of auxiliary springs by the use of precision points in the objective function is extended, and methods for optimising the spacing of the precision points are introduced.

ACKNOWLEDGEMENTS

This thesis is based on research carried out in the period 1977-1982 with the financial support of Science and Engineering Research Council grants GR/A/28374 and GR/B/37943, and using the facilities of the Stephenson Engineering Laboratory, the Computing Laboratory (NUMAC) and the University Library at the University of Newcastle upon Tyne.

The author would like to thank all concerned for this support, in particular Prof. Leonard Maunder who, as holder of the grant, Director of the Stephenson Laboratory and supervisor of this thesis, made it all possible - and enjoyable. It is also the author's pleasure to acknowledge the advice and encouragement of Professor Maunder and former colleagues at the Department of Mechanical Engineering, not least those whose collaborative contributions are referred to below, and to thank the following for the assistance referred to:-

Mrs. Sheila Stone, for typing the thesis (and much other essential documentation of the work) with pleasant efficiency and dependable precision; Mr. Deiter Hofmann and Dr. Ryzard Godlewski (German and Russian translation respectively); Mr. Tony McGilvray (photography) and the many staff of the Stephenson Laboratory workshops who at various stages contributed, by component manufacture and practical advice, to the construction of the experimental apparatus.

STATEMENT OF ORIGINALITY

Except where indicated to the contrary, this thesis describes the sole and original work of the author. The following specific contributions by colleagues are described in the text:-

Dr. R. Godlewski (Visiting Fellow) collaborated on the design of some parts of the experimental apparatus, as recorded in Chapter 5. The components of the apparatus were made by the staff of the departmental workshop.

The method used in Chapter 7 (described in 10. S - T) is a development of a method explored by Professor H. Tamura while at Newcastle on a Senior Visiting Fellowship.

Mr. C. M. Boivin wrote the major part of a computer program based on the author's work described in Sections 8B and C. Some results from this program are discussed in Section 8C, and shown in Section 10 U.

Dr. I.I. Esat collaborated on a study of spring balancing, some aspects of which are presented in Section 8D, and wrote the computer program which was adapted by the author to illustrate the techniques developed in Section 8E.

The thesis has not been submitted to any other university, or submitted previously to the University of Newcastle upon Tyne.

CONTENTS

		Page
CH. 1	INTRODUCTION	1
1A:	Classes of mechanism	1
1B:	Types of problem	3
1C:	External influences on research trends	6
1D:	Modern developments in planar mechanism theory	8
1E:	Outline of ensuing argument	12
CH. 2	SIGNIFICANCE OF FACTORS AFFECTING LINKAGE VIBRATIONS	14
2A:	Purpose, method & scope of this chapter	14
2B:	Typical links	15
2C:	Fundamental frequency ratio	17
2D:	Harmonic spectrum of forcing terms	20
2E:	Damping ratio	22
2F:	Approximate analysis of coupler link vibrations	23
2G:	Effect of axial loads on coupler link vibrations	28
2H:	Coupling effect of end loads & link foreshortening	31
2I:	Effect of crank speed variation on link vibrations	34
2J:	Neglected effects in coupler link vibrations	36
2K:	Vibrations in cases (ii) to (iv)	41
2L:	Comparison with previous investigations	44
2M:	Conclusions of chapter	48
CH. 3	A CRITICAL SURVEY OF 'LUDODYNAMIC' INVESTIGATIONS	50
3A:	Scope and arrangement of chapter	50
3B:	Motion in contact: general	52
3C:	Motion in contact: simulations	55
3D:	Motion in contact: experimental results	58
3E:	Motion across the clearance	60
3F:	Impact and rebound stage	62
3G:	Restoration of contact	66
3H:	Provisional assessment & priorities for investigation	67
3I:	Supplementary review	69
CH. 4	AN APPROXIMATE THEORY OF THE LUDODYNAMIC BEHAVIOUR OF A REVOLUTE JOINT IN A GENERAL LINKAGE	72
4A:	Aims & assumptions	72
4B:	Development of the general theory	74
4C:	Preliminary testing of theory	80
4D:	Use of the general theory in design	82
4E:	Extension to 'free flight' and 'impact' phases	84
4F:	Features & limitations of the theory	87
4G:	Conclusions of chapter	89

(Page)

CH. 5 RIG DESIGN & DEVELOPMENT 90

5A: Introduction 90
5B: Requirements 91
5C: Basic configuration 92
5D: Exciters 93
5E: Transducers 94
5F: Alignment & adjustment features 96
5G: Development of exciter system 98
5H: Development of displacement transducer system 99
5I: Performance tests: exciters 101
5J: Performance tests: instrumentation 103
5K: Mechanical system dimensions and properties 105

CH. 6 AN EXPERIMENTAL STUDY OF LUDODYNAMICS 107

6A: Introduction 107
6B: Compliance tests 108
6C: Drop tests 112
6D: Flypast test (detailed): standard build 114
6E: Series of flypast tests: standard build 119
6F: Effect of varying inertia parameters 123
6G: Effect of reducing clearances 127
6H: Conclusions of chapter 130

CH. 7 THE STEADY-STATE RESPONSE OF FORCED HILL'S EQUATIONS 132

7A: Introduction 132
7B: Method 133
7C: Application to flexible drive - general study 135
7D: Application to flexible drive - case study 142
7E: Application to end-loaded coupler 145

CH. 8 DEVICE SYNTHESIS 146

8A: Aims and scope 146
8B: The effects of counterweights 147
8C: Counterweight synthesis 152
8D: The effects of springs 158
8E: Spring synthesis 162

CH. 9 A REVIEW OF THE INVESTIGATION 169

9A: Overview 169
9B: The ludodynamic investigation 171
9C: The investigation of Hill's equation 177
9D: The prediction of linkage mechanism vibrations 180
9E: The control of linkage mechanism vibrations 185
9F: SUMMARY OF CONCLUSIONS 188

APPENDICES

A1

10A: The influence of design speed and stress level on the frequency ratio A1
10B: Upper bounds for amplitudes of harmonic components of excitation A3
10C: Development of approximate equations for coupler-link vibrations A5
10D: The effect on resonant vibrations of an impulse-like component in the periodic excitation A9
10E: The effect of a step change in the end load on coupler vibrations A10
10F: The effect of rotation on a slightly curved beam A11
10G: The effect of axial compliance of adjacent links on bending vibrations A12
10H: Approximations following from the small-clearance assumption A13
10I: Derivation of following-mode equation A15
10J: Derivation of standard flypast equation A16
10K: Procedure used for constructing Figure 79.a A17
10L: Derivation of free-flight trajectory and impact equations A19
10M: Procedure for constructing Figure 104.a/.b A21
10N: Variation of inertial parameters A22
10P: Adjustment & alignment of experimental rig A23
10Q: Calibration of transducers A27
10R: Recording of experimental signals A29
10S: Steady state solutions of a Hill's equation with forcing term A30
10T: Stability of solutions of Hill's equation A32
10U: Edited output of program 'MUSCLE' A33

BIBLIOGRAPHY A35

NOTE ON CROSS REFERENCES

Bibliographic sources: Names in BLOCK CAPITALS with or without lower case suffixes, e.g. (BLOGGS a), BLOGGS & BLIGGS or BLIGGS ET AL(b) refer to the list of bibliographical sources given in alphabetical order at the end of the thesis.

Sections: (6E) means Section E of Chapter 6.

(E) means Section E of the current chapter.

Other items: (figures, tables, equations, definitions etc.).

These are identified by a single series of location codes of the form

98·f (for example), where

'98' refers to page 98, including the facing page, and

'·f' refers to an item identified by a marginal mark ·f.

Where the page number is omitted, the current page should be understood.

NOTES ON NOMENCLATURE

Owing to the diverse nature of the sub-problems treated in this thesis, a uniform nomenclature would be unwieldy and has not been attempted except on a chapter-by-chapter basis. The principal nomenclature for each chapter is recorded briefly on the title page for that chapter for ease of reference. Other symbols are defined at the point of use.

The following signs are used throughout:-

$\dot{}$ (dots over symbol): differentiation with respect to time.

$\underline{\ }$ (bar under symbol): matrix (upper case symbols), or column vector (lower case symbols).

^{T} (superscript to symbol): transpose of matrix/column vector.

CHAPTER 1

INTRODUCTION

(None of the material in this chapter has been published previously).

1. INTRODUCTION

1A: CLASSES OF MECHANISM

A "linkage mechanism" is an assembly of components that are linked together by joints so as to constrain their relative motion; but that definition conceals a great variety of form and versatility of function. This two-fold diversity results in their being rather little of value that one can say about the complete class of linkage mechanisms, and it is usual for investigations to be focused upon some or other sub-class. A brief examination of some of the main dividing lines is a first requirement for making clear the scope and context of the present investigation.

Pure/hybrid: As well as 'pure' linkage mechanisms whose essential elements consist only of links and joints, there are 'hybrid' mechanisms that incorporate other devices such as gears or cams. The latter in general are more expensive to manufacture and are more dependent on quality of manufacture, but they do provide a greater flexibility of design and may therefore provide a solution where no 'pure' linkage mechanism can be found to fit the bill. A pure linkage may of course be driven by a system of cams and/or gears.

Planar/spatial: Planar linkages, in which all the intended motions are parallel to a single plane, are usually preferred where the function to be carried out is essentially one or two-dimensional. Spatial linkages are obviously necessary to fulfil functions whose definition involves three dimensions, but some spatial linkages can also be used in place of planar linkages. As with hybrid linkages, this option provides more scope for the designer at the probable expense of greater costs of manufacture; the total space required for operation is also likely to be larger. Nevertheless, there are probably some instances where a simple spatial mechanism is able to replace a relatively complex planar linkage to advantage.

Kinematic determinacy: In the great majority of applications, the motion of the linkage mechanism (as idealised at the drawing board) is determined by the motion of a number of actuators (most usually one) corresponding to the number of kinematic degrees of freedom of the linkage. Such a linkage mechanism can be described as 'fully constrained' or 'kinematically determinate'.

Intermittent/continuous: The functional division between mechanisms that operate intermittently (such as switchgear) and those that operate continuously in cycles is obviously one that has a considerable influence on the characteristic design problems that arise. Continuously operating mechanisms are usually driven by means of a crankshaft or by a cam or cams.

Except where stated to the contrary, the linkages referred to in this thesis are assumed to be pure, planar, kinematically determinate, and continuously operated by a single crankshaft or camshaft running at nominally constant speed. It may be noted that the majority of practically important continuously operating mechanisms probably fall within the scope of this definition. The restriction to a single drive is purely to simplify the formulation, and most of the results could be extended to multiple-drive mechanisms with little amendment.

1B: TYPES OF PROBLEM

The class of linkage mechanisms defined in Section A provides a mechanical design problem with a very large number of variables and possibly significant criteria of performance, related in ways that are often highly non-linear. As a result, the 'brute force' approach to design - wherein every conceivable design variable, constraint and objective is incorporated in a model and an "optimum" found by an automatic search procedure with random start - is simply not feasible. Nor is it likely to become so, since, even if computer power continues to increase exponentially, the problem of adequately specifying all the constraints and penalty functions for any particular application will remain prohibitive. It is therefore necessary, as STARR has observed, to break the design problem down into a number of stages, in each of which a certain subset of the design variables is chosen in the light of certain aspects of the desired performance, taking account of certain phenomena.

Thus the theoretical problems that arise can be classified in four ways, namely, by the relation of the problem to the design process, by the design variables to be taken as fixed, by the aspects of performance in question, and by the phenomena to be taken into account in the model used.

Design Process: The distinction between the "analysis" and "synthesis" types of problem is very familiar. Synthesis usually requires either the inversion or the repeated application of one or more analysis techniques; the latter may also be required after the synthesis step in order to provide data for a subsequent stage in the design, and/or to check the validity of the assumptions made during the synthesis. Thus a particular system to be analysed may give rise to a spectrum of techniques of varying degrees of sophistication. To guide the initial stages of synthesis a heuristic method may be appropriate, that is to say one whose validity or accuracy is uncertain but which nevertheless provides valuable insights, and/or indicates trial solutions with a fair chance of success. At the other end of the spectrum, the 'post-synthesis' analysis may take the form of a simulation incorporating as many aspects of behaviour as are understood.

Table 4·a:

Design Features

Symbol	Portmanteau term	Meaning in this thesis
T	TYPE (or topology)	How many links, which joined to which, how.
G	GEOMETRY	Dimensions relating joint locations in each link.
S	STRUCTURE	Sizes, shapes, materials of complete joints+links.
D	DEVICES	Design variables of auxiliary devices as below:
├ D_i	" (inertial)	Auxiliary links; simple or geared counterweights.
└ D_c	" (non- ")	Springs, dashpots.

Table 4·b:

Aspects of Performance

Portmanteau term	Meaning in this thesis	Dominant Design Features
MOBILITY	Degrees of freedom, orders of families of curve generated, etc.	T
MOTION	Angular and linear displacements and associated derivatives and ratios	TG
IMBALANCE	Combined moment of momentum and components of linear momentum; net torque and components of force transmitted to frame	T G S D_i
ENERGY TERMS	Mean and instantaneous power consumption, variations in stored energy, energy dissipation in specified modes, overall energy efficiency	T G S D_i D_e
INTERNAL LOADS	Internal forces, moments at any point including joint loads	
FLEXIBILITIES	Properties of separate links and instantaneous combined values	
NAT. FREQS.		
STRESSES & STRAINS	Peak and effective values in links and at joints	
STABILITY	Applies both to vibrations and to speed variations	

Table 4·c

Phenomena included or excluded

Symbol	Description
n	Nominal behaviour
e	External (functional) loads
i	Inertial loads, device loads
g	Gravitational loads
q	Quasi-static elastic deflections
s	Driving speed fluctuations
d	Driving torque fluctuations
f	Friction
t	Tolerances
c	Clearances in joints
v	Vibratory deflections
o	Out-of-plane effects

Design variables fixed: The complete description of a linkage will comprise a description of all the features listed in Table 4.a. Each introduces a number of design variables, which may be regarded as fixed or otherwise at any point in the design. It can be seen that the listed features form a natural sequence, symbolically 'TGSD', in that the definition of one feature implies the prior definition (even if only provisionally) of the features preceding it in the sequence.

Aspects of performance: The potentially interesting aspects of performance of a linkage mechanism are grouped in Table 4.b, which also shows the design features that influence each aspect (in the simplest applicable model). It can be seen that as the features of a design are defined in sequence, the aspects of performance become fixed in a related sequence.

Phenomena included: Table 4.c gives the range of phenomena that might be taken into account in theoretical models of linkage mechanisms. The inclusion of some of these phenomena has a considerable effect on the nature of the analysis or synthesis problem, so that it is possible to distinguish a number of significantly different problem 'levels' or topics of enquiry, as proposed for example by SKREINER or by ERDMAN & SANDOR. As both of their classifications have some limitations, an alternative (in the same spirit) is presented as Table 5.a, to be used in conjunction with the preceding tables to generate more specific 'topics', as below.

The sequential character of the design features and the related aspects of performance is reflected in the traditional serial design strategy, wherein T,G,S,D, are each optimised in turn, taking account mainly of the aspects of performance that are nominally completely predictable at each stage. If the more complex phenomena are taken into account, however, all of the features of the design are brought into play in an interactive manner, as indicated in the third column of Table 5.a. Thus it can be argued that in the final stages of optimisation of a high-performance linkage, a more integrated strategy may be better; that is to say, the Geometry, Structure and Devices may all be amended in turn in the course of a single iteration. Nevertheless, success in this approach will still depend on the serial synthesis of the general outlines of the mechanism, and on a clear understanding of how the different features separately affect the performance.

Table 5.a .

Fields of Enquiry

Topics	Phenomena: definitely included	Phenomena: possibly included	Relevant design features	Time dependence
KINEMATICS	n		T G	Soluble at arbitrary intervals
LUDOKINEMATICS	nc, nt, nct		T G	Soluble at arbitrary intervals
STATICS	ne	gfo	T G	Soluble at arbitrary intervals
KINETOSTATICS	nei	gfo	T G S D	Soluble at arbitrary intervals
KINETOELASTOSTATICS	neiq	gfo	T G S D	Soluble at arbitrary intervals
ENERGY DYNAMICS	neis	qgo	T G S D	Soluble at arbitrary intervals
TIME DOMAIN DYNAMICS	neisd	gf	T G S D	Integration over time necessary
KINETOELASTODYNAMICS	neiv	gsdf	T G S D	Integration over time necessary
LUDODYNAMICS	neic	gsdfv	T G S D	Integration over time necessary
3-D DYNAMICS	neisdo	gfcv	T G S D	Integration over time necessary

A serial approach will therefore be assumed throughout this thesis.

It is now possible to identify in outline the topics of enquiry to be given particular attention in this thesis. Central to Chapter 2 will be a comparison between a kinetoelastostatic analysis and a kinetoelastodynamic analysis of motion in simplified links. Chapters 3-6 will concern ludodynamic analysis and synthesis. Chapter 7 is devoted to the kinetoelastodynamics of drive systems and of end-loaded links. Chapter 8 will deal with methods of device synthesis on the basis of kinetostatic synthesis.

It may be helpful to spell out the definitions of the two unfamiliar terms above (formally defined in Table 5.a). 'Kinetoelastostatic' indicates that inertial forces are calculated as though the links were rigid, but that the elastic deflections resulting from such forces are taken into account. 'Ludodynamic' is a term newly minted to identify the important class of dynamic problem in which clearance at the joints is taken into account. (Since clearance is sometimes described as 'play' in English, and 'jeu' and 'spiel' are the normal terms in French and German usage, the classical prefix 'ludo-' seems an obvious choice).

1C: EXTERNAL INFLUENCES ON RESEARCH TRENDS

The pattern woven by linkage mechanism research in the last decade or so reveals a number of threads whose origins lie outside the subject itself, and whose influence can also be seen in the course taken by the present investigation.

Development of computing power: If the dramatic advances made in the power and economy of electronic computing have not entirely eliminated interest in the older methods, they have certainly shifted into the realm of the answerable a great many questions that previously lay well outside, and the result has inevitably been a considerable interest in exploiting these new possibilities in some highly number-intensive projects, those of DUBOWSKY & GARDNER (a,b) and FUNABASHI & OGAWA being good examples. More recently, as the "microchip" has put programmable computing power within reach of every designer, a revived concern has been shown for the efficient solution of relatively small problems, by workers such as MILNER & SMITH, and WALDRON & KUMAR.

Another consequence of the march of the microchip is, of course, that mechanisms whose function is essentially to process information, in products such as cash-registers and typewriters, are rapidly becoming obsolete. Fortunately for researchers in the field, linkages in other roles seem likely to prove harder to replace, and as BROOKE has argued, even calculating mechanisms will still be needed for certain harsh environments.

New manufacturing techniques: The increasing use of numerically controlled machine tools has tended to reduce the cost penalty of devices such as hybrid and spatial linkages. This is possibly one factor underlying the extensive amount of effort devoted to spatial links in the last decade.

Environmental concerns: It is now history that a gradual increase in concern for natural resource integrity and environmental quality, a by-product of developing affluence, crystallised at the start of the seventies as a qualitative change in the self-image of Industrial Man. For the engineering profession the effect has been felt most sharply in the much greater public

attention paid to health and safety at work, and (with the assistance of OPEC) to energy conservation. For the machinery researcher the particular 'pollution' issue brought into prominence has been that of noise and vibration.

Economic pressures: The secular economic trend towards increasing productivity has continued to create a need for higher machinery speeds, with the implied threat of greater noise and energy dissipation.

The influence upon this thesis of the first of these trends has been somewhat back-handed. There is always a danger of the sophistication of numerical simulations outstripping both the intuitive understanding necessary in order that the computer is asked the right questions, and the empirical knowledge of the factors that control "second order" effects. Thus the growth of number-intensive research can paradoxically be seen as underlining the need for more simplified heuristic models, as well as for fundamental experimental studies. In the event, the investigation reported here has developed mainly along these two lines, although the simplified and abstracted model of ludo-dynamic phenomena to be presented in Chapter 4 will be seen to depend upon computing power for the revelation of some of its properties, and Chapter 8 will look forward to the incorporation of the results in advanced techniques of computer aided design.

The last two "external influences" sketched in this section were seen to lead to immediately contradictory objectives. Their reconciliation will depend on a greater ability to interpret and control the effects of transmitted dynamic loads, of elastic compliance, of backlash and of friction and other modes of energy dissipation. It is this class of problem (taken as a whole but with friction given only cursory consideration) that provides the main connecting theme of this thesis. Examples of the many reports of previous research in these fields are given below. It should be recognized that whatever advances are made can be used as readily to increase speeds at existing vibration levels as to reduce vibration levels at existing speeds (or to progress along some middle road, for that matter). The techniques themselves are quite indifferent to such choices.

1D: MODERN DEVELOPMENTS IN PLANAR MECHANISM THEORY

This preliminary overview of investigations in the previous decade related to the class of mechanism identified in Section A will spotlight published papers that review parts of the field, and work that has had a particular influence on the investigation reported here. Under the last heading work by other researchers at Newcastle upon Tyne - the 'Newcastle school' - is obviously particularly relevant.

Kinematic synthesis: This is the 'classic' problem in the field of mechanism design, so it is not surprising that this is the subject of the largest portion of the relevant literature. THOMPSON reviewed the literature up to 1973, distinguishing the two major schools: precision point synthesis based on Burmester theory, and numerical optimisation with or without constraints. Contrary to Thompson's prediction that the latter would prevail, both schools have continued to flourish, and the method of SPITZNAGEL & TESAR could be regarded as a synthesis: an iteratively optimised choice of precision points. At Newcastle, OLDHAM (a) described the advantages of concentrating on the class of 'dyadic' linkages, consisting of an actuator pair with any number of dyads (Assur groups of lowest order) attached in sequence: this class permits systematic solution of the kinematic equations in closed form and includes a high proportion of the planar linkages actually used in industry. OLDHAM (b) proceeded to develop a program 'PSALM' for the kinematic synthesis of dyadic linkages by means of a 'Simplex' search routine.

Dynamic analysis: Since SKREINER outlined the problems and possibilities posed by the incorporation of dynamic analysis in linkage mechanism design, the major advance has been the development of a number of computer programs that solve the kinematic and dynamic equations of a more or less arbitrary mechanism, having automatically formulated them from a symbolic description of the topological and geometric structure of the linkage. PAUL surveyed these projects, emphasising the mathematical relationships between the different formulations used.

Dynamic synthesis: STARR provided an overview of this varied and growing field. Some of its more significant subdivisions are considered under the headings that follow.

Device synthesis: LOWEN & BERKOF (a) reviewed the wide variety of methods that had been proposed prior to 1968 for 'balancing' linkage mechanisms, mostly using inertial devices. BERKOF ET AL.(a) reviewed further papers up to 1976. The majority of recent English language papers on inertial device synthesis have utilized BERKOF & LOWEN(a)'s method of 'Linearly Independent Vectors' (which has the advantage of being applicable to dynamic as well as to kinetostatic cases, although not to kinetoelastodynamic or ludodynamic cases). The exception to this rule is that investigations in this field involving numerical searches have not taken the linear dependencies (associated with kinematic loop closure) into account. Among the latter investigations, that reported by DRESIG & SCHÖNFELD is notable for the efficiency and versatility of the program package described. WALKER at Newcastle paid more attention to the constraints on the counterweight dimensions, the intelligible specification of weighting factors and the inclusion of joint loads in the criteria of performance; he also tested the effects of counterweights experimentally.

Computer Aided Design: A number of writers have examined the developments referred to above from the point of view of the CAD principles involved: KAUFMAN has treated the dynamic analysis programs in this way, for example. Optimisation techniques have often been treated in their own right, with mechanism synthesis merely providing a case study, but more recently it has been suggested (most explicitly by DATSERIS & FREUDENSTEIN) that this 'black box' approach is not very healthy, and that optimisation techniques closely tailored to the particular circumstances of mechanism design are likely to prove of greater practical value. In a similar spirit AFIMAWALA & MAYNE have developed a technique of interactive optimisation that helps to develop the user's intuitive understanding of the problem.

Kinetoelastodynamics: ERDMAN & SANDOR's review in 1972 served to relate this topic to a wider context. LOWEN & JANDRASITS' review in the same year provided far more detail on the methods, assumptions and quantitative results of the various authors. A later paper by JANDRASITS & LOWEN(a) extended their survey to 1976. A number of significant subdivisions emerge from these reviews. Some authors considered only transverse link deflections and loads, others allowed for various axial effects. Some simulated the motion from chosen initial conditions, others sought the components of the steady-state solution, others again concentrated on the stability of the homogeneous terms: a few considered the synthesis problem, defined as minimising the sections subject to constraints on the stresses and deflections. Some expressed the deflections in terms of assumed normal modes of the separate links while others considered the complete linkage as an elastic structure at each instant and others used lumped masses. At Newcastle, SMITH studied the stability of a highly flexible coupler, using assumed modes; OLDHAM later refined Smith's method and achieved better agreement with experimental measurements.

In many of these investigations the links analysed or tested were given very flimsy sections. The reason given was that this was believed to provide a more stringent test of the theory, and/or that the deflections were easier to measure experimentally. However, SANDERS & TESAR have argued that for links with realistic sections a kinetoelastostatic solution with axial effects omitted is adequate. Some deficiencies in their treatment (and in some other papers in this field) will be rectified in Chapter 2 of this thesis, with the effect that SANDERS & TESAR's central conclusion is reinforced in some cases, but not in cases where certain imperfections in the joints or drive systems are found.

Friction: This topic seems to have been given relatively little attention in recent years in the context of linkage mechanisms. KRANIASKAS at Newcastle made a thorough empirical study of the frictional behaviour of a PTFE-based bearing for a switchgear mechanism. More recently, IMAM ET AL. have suggested an approximate closed-form modification of previous 'friction-circle' based methods for incorporating classical Coulomb friction in dynamic analysis computations, and THRELFALL described the adaption of the program DRAM to incorporate a fairly realistic model of dry friction, including surface elastic effects. A very recent paper by ROONEY & DERAVI proposed a tangent function to approximate the displacement/load relationship at a dynamic frictional interface.

Ludokinematics & Ludodynamics: An important paper by DUBOWSKY & GARDNER (b) included a useful survey of work in these fields up to 1975. Early dynamic work treated the motion as one-dimensional, so that the problem became similar to problems involving backlash in other systems, such as gears, cams, impact dampers and pneumatic machinery. At Newcastle WILSON studied the two degree of freedom motion of the slider in a sliding joint with clearance, in the form of a piston and cylinder. The case of two-dimensional motion within the clearance at a revolute joint has given rise to quite a substantial literature, which will be fully reviewed in Chapter 3 of this thesis. The contribution of the Newcastle school (in the persons of FAWCETT & BURDESS and GRANT) has been concerned with methods of design to avoid loss of contact, and thus impact, entirely; an approach taken also by EARLES & WU.

1E: OUTLINE OF ENSUING ARGUMENT

It is contended that the factors considered in the preceding sections together provide good grounds for investigating the major determinants of the dynamic performance of a certain class of mechanisms, whose kinematic design is taken to be (at least provisionally) already completed. The class (to recapitulate) comprises pure linkage mechanisms of the planar, kinematically determinate, single input, continuously operating type. Real mechanical systems of this class - found in a wide variety of practical applications and giving rise to a complex of interrelated phenomena - require a variety of analytic and synthetic tools for their optimal dynamic design. The subject of this thesis is the identification and provision of those tools, without restriction to any specific application, phenomenon or theoretical framework.

Taking each chapter in turn, Chapter 2 concerns a wide range of factors that could affect vibrations in realistic linkages. These will be examined with the aid of a number of highly simplified models in order to establish the typical orders of magnitude of certain terms. It will be argued that, with certain exceptions, even high speed linkages are unlikely to have natural frequencies of the same order as the driving speed, and in consequence - in contrast to the current prevailing academic paradigm - that significant linkage vibrations are most likely to be the result of impacts or similarly impulsive loads, not the regular kinematic accelerations. Since joint clearance is a ubiquitous potential source of impacts, ludodynamic problems will be identified as an appropriate focus for the major part of the investigation. Flexibility in drive systems and the associated Hill's equations will be taken as a secondary topic of interest.

It is found to be appropriate to concentrate on two-dimensional ludodynamics of revolute joints. The published literature will be fully reviewed in Chapter 3, with selective reference to papers dealing with the one-dimensional problem where appropriate. The main needs will be identified as lucid heuristic models to guide the initial stages of design synthesis, and better empirical data to back up more sophisticated models for final 'tuning' of the designs.

In an attempt to meet the first need, a novel approximate theory of ludodynamics will be presented in Chapter 4, which reduces the problem to a function of three dimensionless parameters. The region in parametric space

within which impacts are predicted to occur will be shown by means of a contour map of the surface that contains this region. A method for predicting impact magnitudes on a similar basis will be proposed.

Chapter 5 will describe the design and development of an experimental rig for the purpose of testing the theory described in Chapter 4, and for providing empirical data of more general application in accordance with the needs identified in Chapter 3. The use of this rig and the results obtained will be reported in Chapter 6.

In Chapter 7 the class of Hill's equations relevant to vibrations in linkage drive systems will be studied, and spectral analyses of some steady-state forced solutions presented as a pointer to the conditions in which such vibrations may exacerbate the effects of link flexibility.

The ultimate aim of this work is to lead to better linkage designs. Thus in Chapter 8 methods of synthesis of auxiliary devices for controlling dynamic performance will be considered. The limitations of existing methods for the synthesis of counterweights and springs will be indicated and several new methods will be developed.

Chapter 9 will review the entire investigation and consider some implications.

Most chapters have one or more associated appendices. These are gathered together at the end of the thesis, under the convenient heading of Chapter 10.

CHAPTER 2

SIGNIFICANCE OF FACTORS AFFECTING LINKAGE VIBRATIONS

(The material in this chapter is a considerably extended version of a study published as reference HAINES(a)).

Principal nomenclature for this chapter is given overleaf: this nomenclature also applies to the appendices to this chapter, namely Sections 10A, and 10C to G.

2. SIGNIFICANCE OF FACTORS AFFECTING LINKAGE VIBRATIONS

2A: PURPOSE, METHOD & SCOPE OF THIS CHAPTER

The object of the study presented in this chapter is to distinguish the factors most likely to be significant in the vibration of practical linkages of the class specified in Section 1A, in order to suggest guidelines for the early stages of linkage design and priorities for further research. Since a broad and only partially characterised class of linkages is under consideration, rigorous demonstration will not be possible, but intuitive judgement will be backed up by the analysis of simplified models to provide plausible guidelines.

The starting point is that the linkage is assumed to have been designed initially to be of adequate strength and stiffness according to the rigid-body method, with idealised joints. On this basis, assumptions will be introduced and justified concerning the nature of the component undergoing the most significant vibratory deflection (Section B), the fundamental frequency ratio (Section C), the shape of the harmonic spectrum of the exciting terms (Section D), and the degree of damping (Section E). With further assumptions made on a provisional basis, the response of the resulting model of a coupler-type link will be determined and related to the response predicted by a kinetoelastostatic approximation (Section F).

The effect of relaxing some of the restrictive assumptions made in the foregoing sections will be considered in Sections G to J, while vibrations in different kinds of component (links with overhung masses, tie rods and drive shafts) will be briefly considered in Section K. Section L provides a selective review of previous investigations in the light of this investigation. Conclusions regarding recommended design practice and priorities for extending the investigation are presented in Section M.

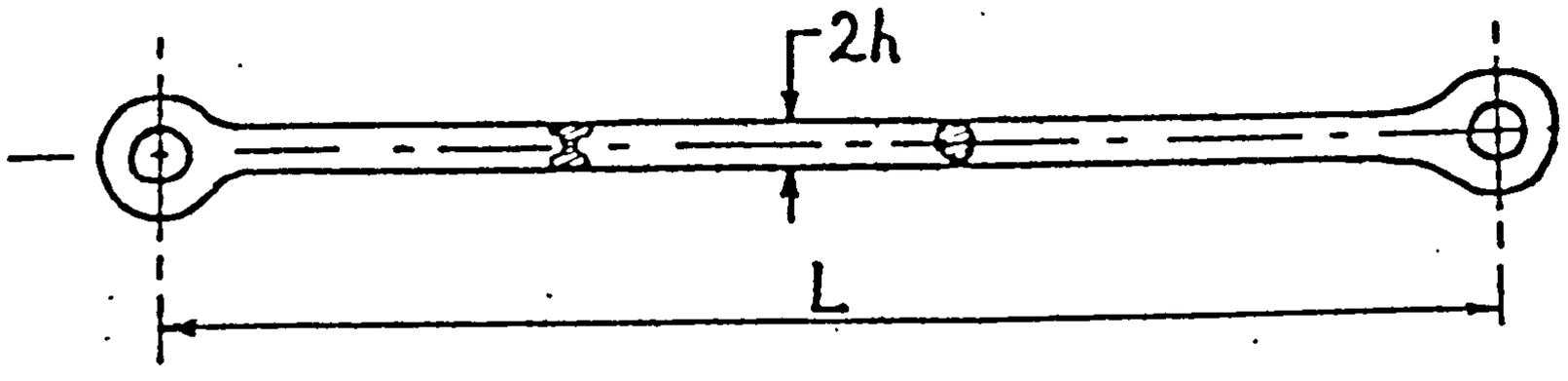

15·a: Case (i), 'coupler' link

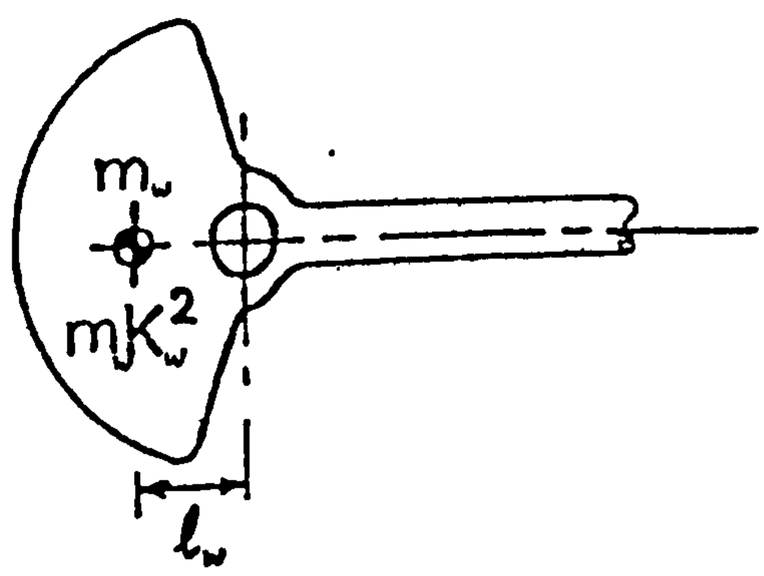

15·b: Case (ii), counterweighted link

2B: TYPICAL LINKS

Four idealised cases will be considered representing the different circumstances in which vibrations might reasonably be expected. Case (i) will be considered in detail, the other cases being considered briefly for contrast.

Case (i): 'Coupler link'. This is a revolute-jointed binary link not subject to any transverse loading other than its own weight and inertia. In these circumstances such links can be relatively slender in section, so are more likely to suffer from dynamic effects.

For a sound design, the cross-section could range from circular to I-section with the major axis in the plane of the inertial loads (see.a). For a particular type of application the cross-sectional area (a), modulus (Z) and second moment of area in the bending plane (I) can be taken to be proportional to h, h^2 and h^3 respectively, where h is the depth of section, assumed for simplicity to be uniform along the length (L) of the link.

The magnitude of h is assumed to be sufficient to ensure that the maximum stresses in bending and in tension/compression under rigid body loading are no more than respective permitted design values, and also to ensure that the Euler buckling load exceeds the greatest rigid-body end-load by a suitable factor of safety - say four. (The peak rigid body tensile and compressive end-loads are assumed to be similar).

The link is assumed to have a length/depth ratio of no more than 100, corresponding to a slenderness ratio (L/K where $I=aK^2$) of up to 350. OLDHAM (b, p12-12) suggested that the former limit in current practice (in 1977) was about 22, so this allows a good margin for changes in practice.

If nominal direct bending strains of up to $\varepsilon \approx 1/1000$ occur, the maximum bending deflection is y where $y.2r_{min} \leqslant (L/2)^2$ and the minimum radius of curvature r_{min} is given by h/ε; thus $y/L \leqslant (L/2h) \times (\varepsilon/4) \leqslant 0{\cdot}025$. That is to say, nominal bending deflections of up to a few percent of the length may be designed for.

Case (ii): 'Counterweighted link'. In this case the link is assumed to be weightless but attached to a heavy rigid inertia (see Figure 15.b). This represents in extreme form the vibratory effect of heavy non-structural moving

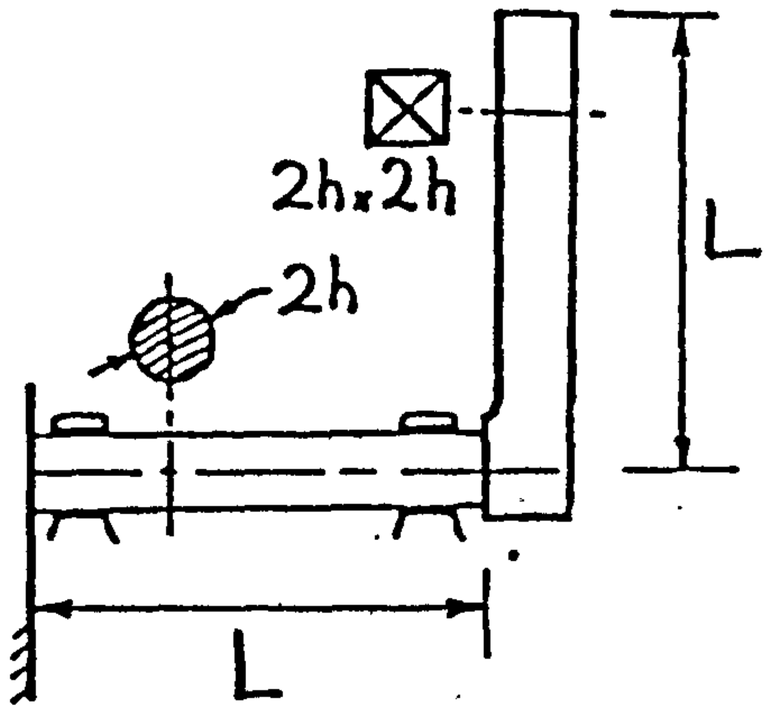

16·a: 'SIMILAR' SHAFT & CRANK

parts, such as counterweights or driven components.

Case (iii): 'Flexible drive'. In this case the linkage itself is rigid but driven by a light flexible shaft of radius r_s. Flexibility in other elements of the driving system such as driving belts, the motor field and even the crank could be considered as included in the nominal 'flexible shaft'. Here it should be appreciated that there is a sense in which shafts can be regarded as inherently more flexible than links, as a class. In the simple case of a shaft and 'similar' crank shown opposite (.a), for example, it is easy to establish that more than 85% of the total flexibility at the output end is contributed by shaft torsion.

Case (iv): 'Tie rod'. A light elastic rod carrying a heavy mass m_o at one end is subject to axial oscillations, with a peak acceleration $\bar{A}_a$, at the other. This represents the case in which longitudinal deflections provide a significant mode of vibration. (Although the longitudinal natural frequency of a pinned-pinned link is usually well above its bending frequency, if both ends of the link are attached to assemblies with a high effective inertia at the terminals, a longitudinal vibratory mode of considerably lower frequency than the pinned-pinned longitudinal mode will be introduced. A number of previous workers have overlooked this.)

2C: FUNDAMENTAL FREQUENCY RATIO

A key design variable regarding the vibrations of cyclic mechanisms is the "fundamental frequency ratio", Ω, which is defined here as the ratio of the lowest frequency of free vibration of the structure to the cyclic driving frequency. (The reciprocal of this definition is sometimes used). The first thing to establish is the likely magnitude of that ratio. SANDERS & TESAR suggested that for realistic links the frequency ratio is unlikely to be less than about 20. Although many of the studies reported in the literature involved considerably lower ratios, the links in question are sometimes explicitly acknowledged to be unrealistic, e.g. JANDRASITS & LOWEN(b) referred in a footnote to "..realistic mechanisms with...vastly stiffer beams...", and THOMPSON & GHANDI observed: "...the cross sectional shape.. is adopted for simulation purposes to accentuate the deflections...it is not proposed as a viable engineering design."

(The stiffness in the plane of motion in the cases referred to was in fact considerably less than that in the transverse plane, contrary to the "rational" practice for practical links suggested in the previous section.)

It is often argued, for example by ERDMAN & SANDOR and by LAWRENCE & ALEXANDER, that lower ratios will prevail as mechanisms are designed for higher speeds. The crucial question here is whether the practical limit on such a trend would really be excessive flexibility (low Ω), or whether lack of strength would prove more restrictive. The latter possibility has been suggested by Witfeld, in a German paper reviewed by LOWEN & JANDRASITS.

The strength limitation can be defined, as appropriate, in terms of limiting values (σ_l etc.) on the nominal direct stress and strain (σ, ε), or torsional stress and strain (τ, γ). For a given (kinematically specified) mechanism and given design crank speed ω there will be a minimum cross-section (as defined by h or r_s) below which the stresses due to rigid-body loading exceed the relevant limit. The cross-section will also determine the natural frequency and hence the frequency ratio at design speed, Ω.

These relationships are developed in Appendix 10A. In case (i) it is found that, for a material of density μ/g and Young's Modulus E,

$$\Omega = \left(\frac{\pi^2}{8}\right)\left(\frac{h}{k}\right)\left(\frac{1}{\varepsilon_l}\right)\left(\sqrt{\frac{\mu}{Eg}}\right)\left(\frac{\bar{A}}{\omega^2}\right)\omega \ ,$$

where $\bar{A}$ is the peak transverse acceleration.

In this expression the first term in a constant, so by assumption is the second, and so are the third and fourth for a given material. The fifth is a constant for a given linkage geometry and is typically of the order of the crank length: it could be termed the "equivalent centrifugal radius", C. The presence of the sixth term then shows that for a case (i) link in a linkage of given geometry and material, the frequency ratio Ω increases with increased design speed.

In case (ii), taking the overhung mass (m_ω) to be constant, with a constant radius of gyration (K_ω) and overhung by a constant amount (ℓ_ω) it is found that

$$\Omega = 3^{1/2} L^{-1/2} m_\omega^{1/6} \ell_\omega^{2/3} (K_\omega^2 + \ell_\omega^2)^{-1/2} (I/h^4)^{-1/6} E^{-1/6} \varepsilon_\ell^{-2/3} C^{2/3} \omega^{1/3} \qquad .a$$

where in this case C is defined in terms of the peak transverse acceleration and angular acceleration of the mass ($C_1\omega^2$, $B\omega^2$ respectively) as $C = C_1 + BK_\omega^2/\ell_\omega$.

It can again be seen that all the terms in the expression for Ω except the last term are constant by assumption for a given material and linkage geometry. Thus in this case, too, increased design speeds lead to increased values of Ω.

If in case (iii) only the shaft radius is assumed to be increased with increased design speed, it emerges similarly that

$$\Omega \propto \omega^{1/3} \qquad .b$$

If the linkage design also varies with ω, Ω increases more rapidly with ω.

In the last case a significant point is that the length of a drive shaft can be increased indefinitely without running into any limit associated with quasi-static stresses. There is therefore a clear possibility that the lowest natural frequency for a practical linkage will be associated with shaft torsion rather than with link flexure. This was the case, for example, in the linkage studied by WALKER.

In case (iv) the dimensions of the tie-rod may be governed by the avoidance of overload in tension/compression or by the avoidance of buckling. In the first case the frequency ratio Ω is found to be no less than $\sqrt{(C/L\varepsilon_\ell)}$ where $C = \bar{\lambda}_a \omega^2$. If the rod is of slender proportions a larger cross-

sectional area, a, may be necessary to avoid buckling, so the frequency ratio must be higher. The above expression therefore provides a lower limit. Assume for example that $\varepsilon_\ell = 0{\cdot}001$ and c is approximately equal to the crank radius; then it is seen that $\Omega \geqslant 10$ provided that the link in question is no more than ten times the crank radius. The latter criterion is probably met for the large marjority of mechanisms, if not all.

The arguments above all assume that design stress limits are constant. In practice, of course, as design speeds are raised it is likely that stress limits will be pushed upwards; nevertheless, in the light of the fact that in cases (i) to (iii) frequency ratios increase with design speed for a constant design stress, it does not seem reasonable to sustain the view that frequency ratios will undergo a major reduction as a result of a requirement for increased design speeds. It will consequently be assumed in this chapter that $\Omega \geqslant 10$.

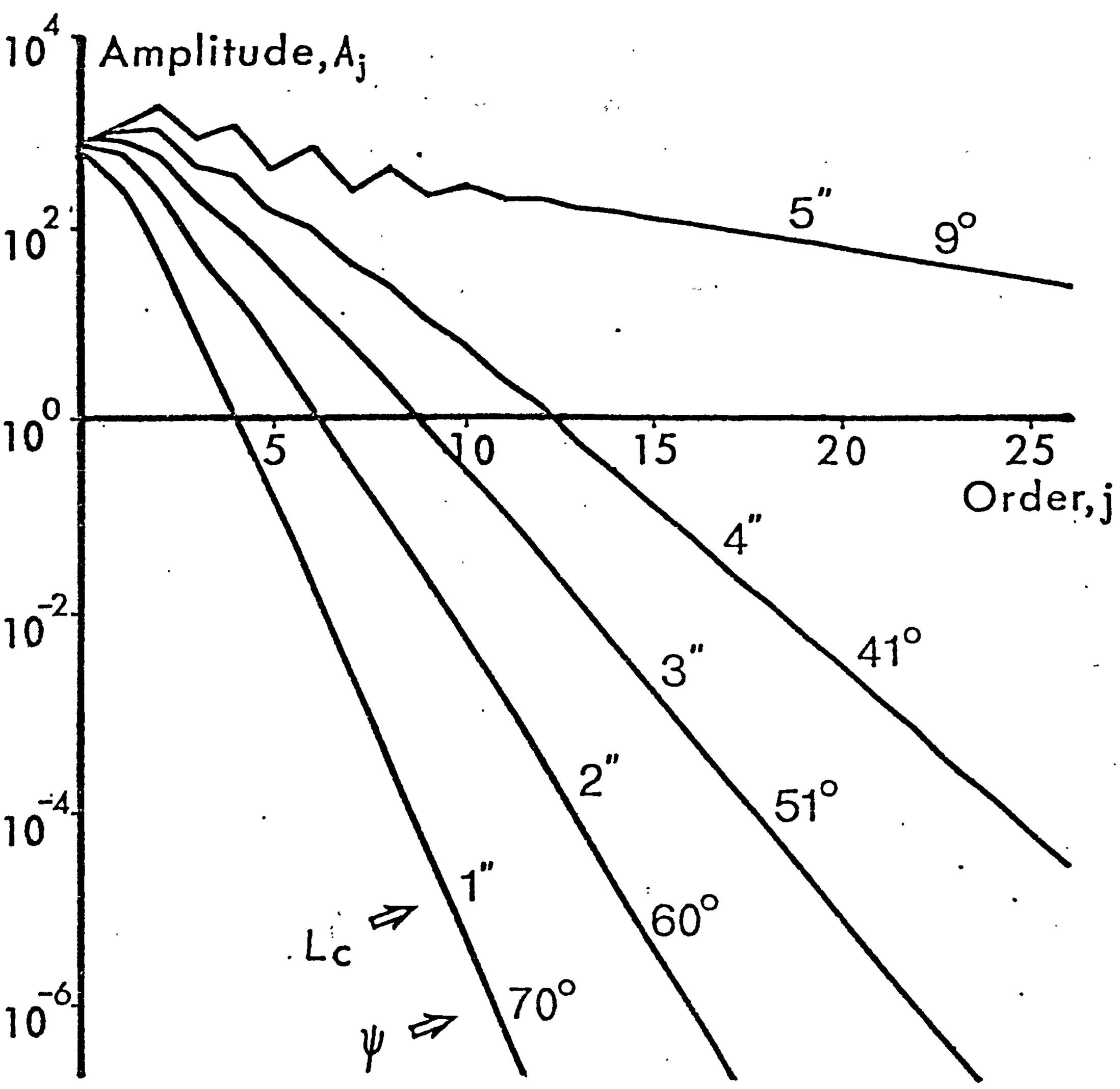

20.a: Excitation spectra for a family of four-bar chains

2D: HARMONIC SPECTRUM OF FORCING TERMS

The assumption of a frequency ratio of not less than 10 to 1 focuses attention on the order of magnitude of the tenth and higher harmonics of the forcing terms, which could potentially provoke resonant vibration. This will emerge from a study of the typical shape of the frequency spectrum of the excitation, that is the variation of A_j with j where A_j is the amplitude of the j'th harmonic in the exciting function.

The writer has shown in a paper reproduced as an Appendix to this thesis (section 10B) that in general A_j is subject to the following upper limits:

$$A_j \leq (2/\pi)(R'_p/j^p) \qquad \text{.b}$$

$$A_j \leq (2/\pi)(R_p/j^{p+1}) \qquad \text{.c}$$

where R'_p is the peak-to-peak range and R_p the "cumulative range" (sum of all maxima less sum of all minima within a cycle) of $d^pA(\phi)/d\phi^p$, ϕ being the phase angle of the drive (crank angle) measured in radians.

Consider for example the case $p=0$. Since $R'_0 \leq 2\bar{A}$ it is seen that $(A_j/\bar{A}) \leq (4/\pi)$; and indeed $(jA_j/\bar{A}) \leq (4/\pi)$ if there is only one maximum within each cycle of $A(\phi)$ so that $R_0 \equiv R'_0$. These relations throw light on a variety of special cases.

The special feature of crankshaft-driven linkage mechanisms is that all the derivatives of the ideal kinematic motion are continuous analytic functions, so that in practice the calculated ranges of the successive derivatives, R'_p do not grow out of bounds, at least provided that extreme transmission angles are avoided. Accordingly, for higher values of j, equation .c shows that A_j is effectively bounded by curves proportional to high negative powers of j.

This is illustrated in the figure opposite, which shows the logarithmic harmonic spectrum of $A(\phi)$ for a family of four-bar chains differing only in the crank-length L_c. $A(\phi)$ is here identified with the transverse acceleration of the undeflected mid-point of the coupler, for reasons to be explained in section F. The case with $L_c = 3''$ in the figure corresponds precisely to the mechanism described by SANDERS & TESAR. The minimum transmission angle ψ is also shown in the figure: a commonly recommended practical design rule is that the transmission angle should not fall below 50^o, and in accordance with the basic assumption of sound design, this rule will be

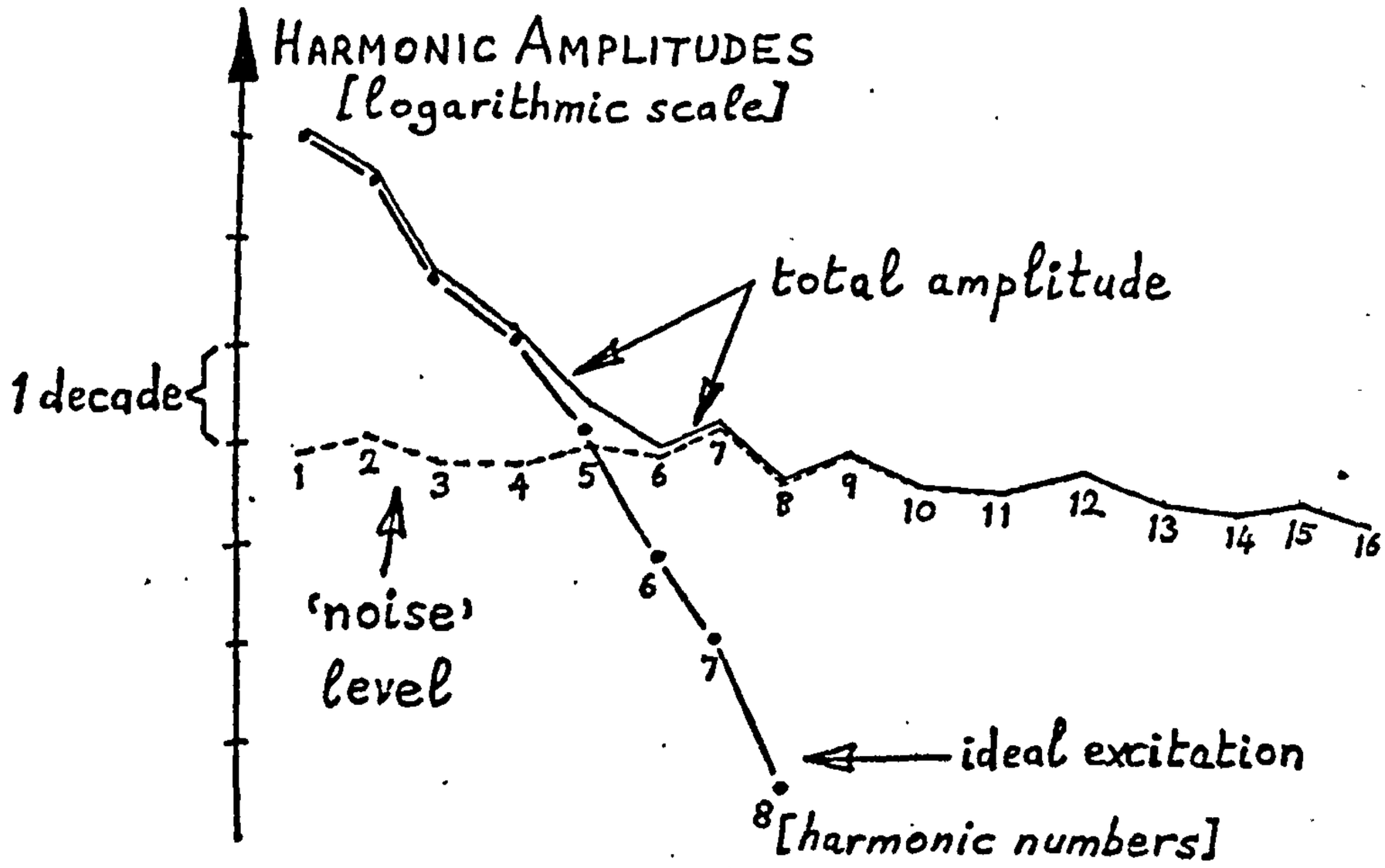

21.a: Effect of irregularities on excitation spectrum

assumed here. Thus cases with $R_c \geqslant 4^{\circ}$ will be disregarded; for the other cases it can be seen that A_j decays rapidly and persistently, as suggested by the qualitative argument in the previous paragraph. Indeed, beyond the first three or four harmonics a good approximation to a straight line is obtained, so we can write $A_j \approx A^* \varrho^j$ where $\varrho < 1$, $j > 3$ (say). A similar trend has been observed for other four-bar chains studied by the author, and it is suggested that this is probably characteristic of crankshaft-driven linkage mechanisms, with ideal joints.

In other mechanisms R_p is only defined for low values of p, up to $(q-1)$ say: for example for a tangent-flank cam the follower acceleration is only piecewise-continuous, so R_1 is undefined and $q = 1$. In such cases the upper bound on A_j is proportional to j^{-q}. For more sophisticated cam profiles q may equal 2 or 3.

If significant Coulomb friction is present, there will be a discontinuity in the frictional torque at the joints when the relative motion changes sign. This will similarly give rise to an excitation spectrum with $q = 1$. If backlash or other source of impact is present, and if this is represented as a Dirac impulse, q will equal 0. (More realistically, if the impulse occurs in a finite time T_I, A_j will be approximately constant for all j up to but excluding frequencies of the order of T_I^{-1}).

The latter "noise" effects will be additional to the ideal-joint excitation, so that the total excitation will have a spectral shape something like that sketched opposite (full line). That is to say - a crucial point - that at the higher frequencies the kinematic excitation is irrelevant.

2E; DAMPING RATIO

The effect of the high frequency components of the excitation may be limited by damping. The total damping effect, being dependent on a variety of energy dissipation processes that are difficult to model reliably, is notoriously difficult to predict. Since losses at kinematic joints are involved as well as material damping and air damping, a critical damping ratio of $c = 0{\cdot}01$ may be considered a reasonably conservative design value for many applications, and will be assumed in what follows unless otherwise stated. This compares for example with a value of 0.015 reported by GOLEBIEWSKI & SADLER, based on the measured logarithmic decrement of a transient. Similarly, LAWRENCE & ALEXANDER reported empirical values of 0.015 and 0.030 for two links.

•a

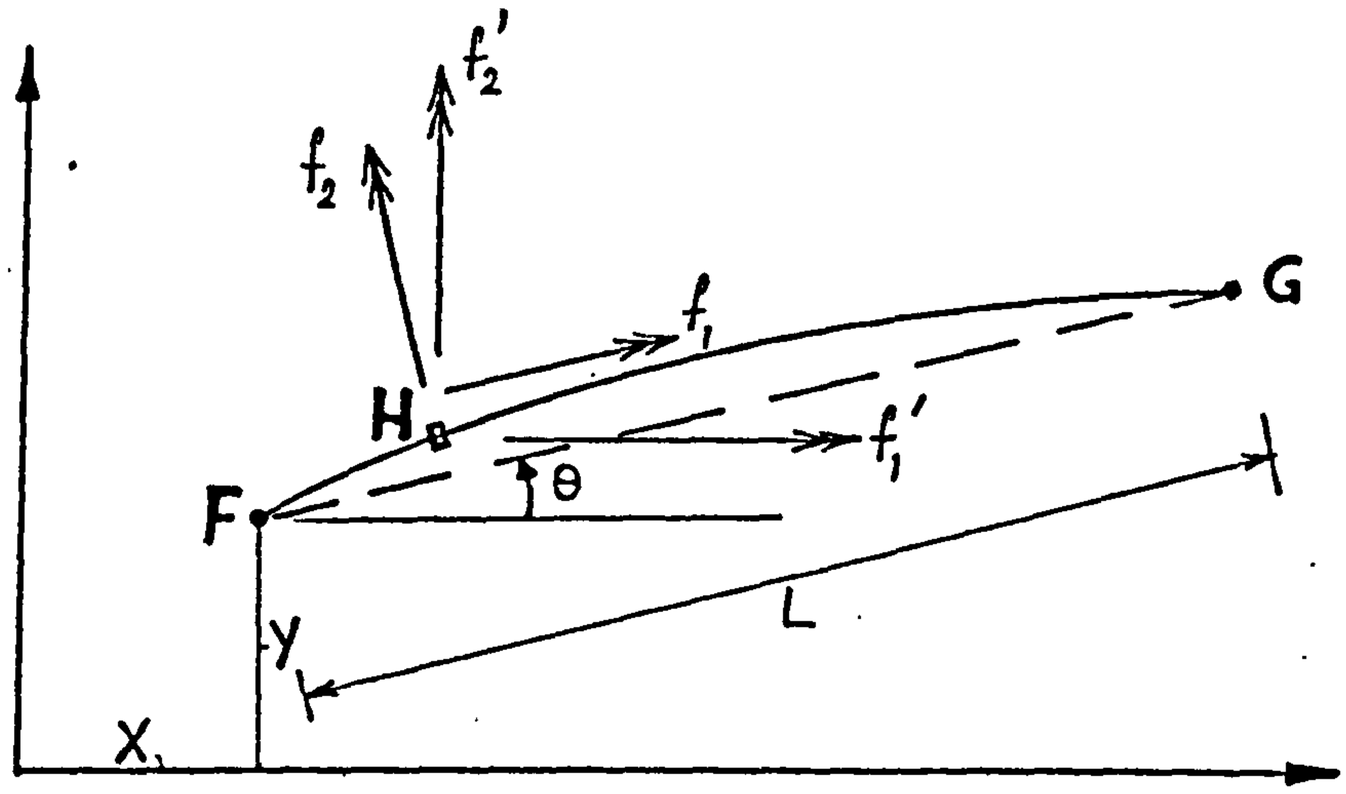

Suffix '$_o$' indicates original state

•b

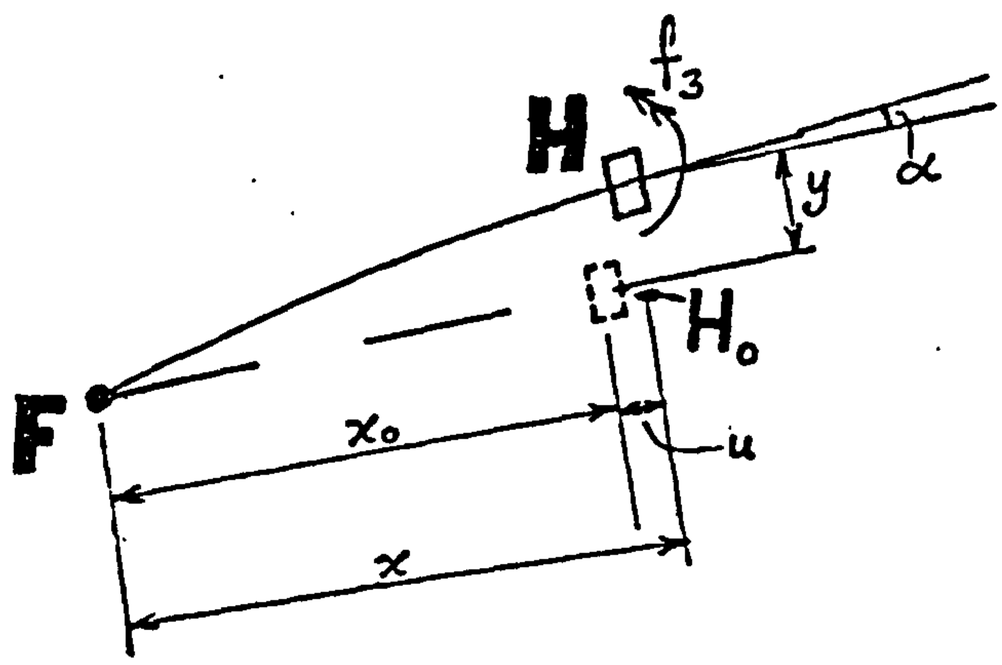

•c

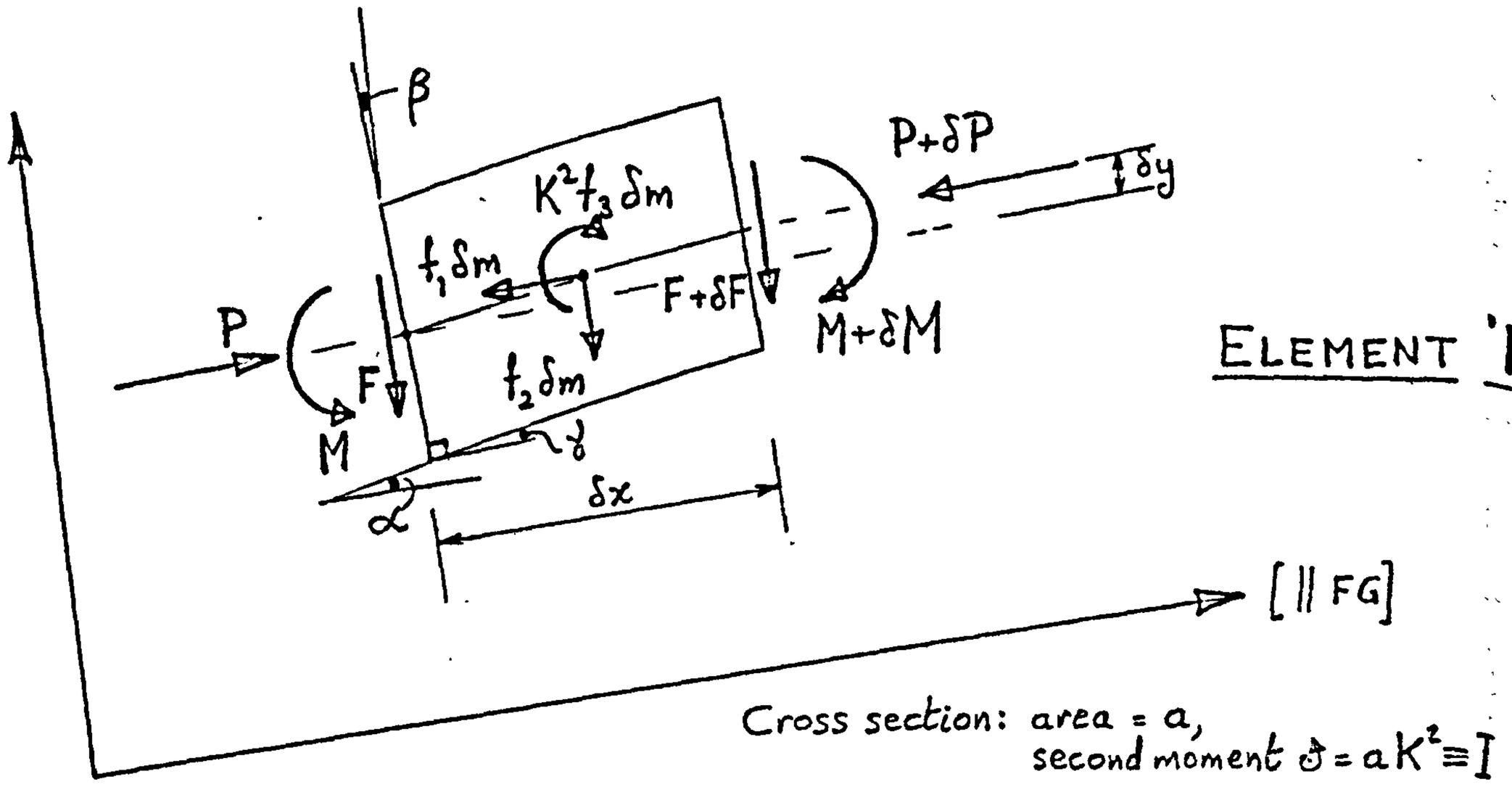

ELEMENT 'H'

Cross section: area = a,
second moment $\vartheta = aK^2 \equiv I$

23 •a—•c: Deflections and loads for a coupler link.

Symbol: variants	Meaning
A:	Acceleration of link:
A_m; A_e	transverse, at midpoint; transverse, end wrt midpt.
A_j A_k A_{kj}	transverse components (see * below & 24·c)
A_I; A_a	component due to impact; axial
a	Area of cross-section of link.
C	'Equivalent centrifugal radius' (acceleration/ω^2)
c: c_k	Damping ratio (damping factor/critical damping): see *.
D:	Dynamic magnifier applied to vibratory amplitude:
D_{kj}; D_r	for specified component (see *); at resonant peak;
D_I	additional magnifier associated with impact (26·c).
E	Young's modulus of elasticity.
e	Radial clearance at joint.
F	Shear force in beam.
f: $f_1 f_2 f_3 f_1' f_2'$	Acceleration of element of link (see figure, 23·a/b).
G	Shear modulus of elasticity.
g	Gravitational acceleration.
H:	Factor applied to bending stiffness, due to P (p. 28):
H_k H_{kj}; H_T	for specified component (see *); overall.
h	Semi-height of link section.
I	Second moment of area of link section.
i	Square root of -1.
J: J_1; J_2; J_ϕ	Effective moment of inertia: of crank; rocker; linkage.
j	Order of term in (Fourier) time series expansion.
K: K; K_w	Radius of gyration: of link section; of counterweight.
k	Order of mode of vibration.
L: L_c	Length of link: of crank.
ℓ: ℓ_h; ℓ_w	Length of part of link: half overall length; offset of counterweight.
M	Bending moment at specified section of link.
m: m; m_w; m_e	Mass: of link; of (counter)weight; effective value.
P: P_c	(Compressive) axial load in link: Euler critical value.
p	Number of differentiations performed on excitation.
Q	Velocity ratio (output/input) for 4-bar mechanism.
q	1 + highest p for which differentiated function is bounded.
R_p: R_p'	'Cumulative range' (see p.A3) of p'th derivative of forcing function; its peak-to-peak range.
r_s	Radius of shaft.
S	Stiffness of shaft.
s	Slenderness ratio, L/K for link.

T: T; T_I	Time duration: of non-contact phase; of impulse.
t	Time as variable.
U	Foreshortening of link (= -u at end of link).
u	Longitudinal deflection at point on link.
v: v_1; v_2	Modal amplitude: of cosine term; of sine term.
X: X_F	Global Cartesian coordinate: of joint F.
x	Distance along link.
Y: Y_F; Y_w	Global Cartesian coordinate: of joint F; of counterweight.
y: y_k	Transverse deflection: k'th modal component (see *);
y_{ks}; y_s	quasi-static component; quasi-static, at midpoint.
z:	Dynamic error in deflection (value - quasi-static value):
z_k z_{kj}; z_r	component values (see *); resonant component.
z: z_m	Error due to centrifugal effect: at midpoint.
α	Rotation of centreline of element from rigid position.
β	Rotation of cross-section of element from rigid position.
γ: γ_ℓ	Shear strain in element (see 23·c): limiting design value.
Δ	Ratio, longitudinal/transverse vibration amplitude.
ε: ε_ℓ	Direct strain: limiting design value.
ζ	Timoshenko's shape factor for shear rigidity.
η	Relative jerk between members of joint.
θ	Inclination of link centreline to global reference axis.
Π	Magnitude of brief impulse applied to system.
μ	Mass density of link.
σ: σ_ℓ	Direct stress: limiting design value.
τ: τ_ℓ	Shear stress: limiting design value.
Φ	Torsional deflection of drive shaft.
ϕ	Input shaft angle.
ψ	Transmission angle (angle between adjacent links).
ξ	Coefficient of damping in drive shaft.
Ω	Ratio of natural frequency to driving frequency.
ω: ω; ω_1	Frequency: of crank rotation; fundamental natural (bending);
ω_{1L}; ω_{1T}; ω_1*	ditto (longitudinal); ditto (torsional); ditto (corrected).

* Note, these subscripts have the consistent meaning indicated:-

j	Associated with the j'th harmonic of the excitation.
k	Associated with the k'th mode of vibration.
(Omission of j	or k implies that all harmonics or modes are included).
o	Undeformed value.
—	(Overbar) indicates peak magnitude over the cycle.

2F: APPROXIMATE ANALYSIS OF COUPLER LINK VIBRATIONS (Case 1)

In order to gain an understanding of the implications of the typical features identified in sections C-E, the kind of component defined as case (1) (light coupler) will now be studied in detail, with additional simplifications introduced for the time being.

Thus it will be assumed that the rigid driving crank rotates at constant speed, that the frame is sufficiently rigid and massive not to deflect, and that the joints are free of both friction and backlash. Furthermore the link is assumed to be straight when undeflected, and symmetrical (and symmetrically loaded and constrained) about the plane of motion.

Additional simplifications will be introduced in the course of the analysis, wherever possible after explicitly formulating the term that is dropped. The effects of these various simplifications will be considered in sections G to J.

The formal development of the equation of motion is given in Appendix 10C. In this section the methods used will be described and the resulting equations presented and evaluated.

Kinematics: Figure .a/b shows a link operating under the conditions described. The deflected position of the element is given in complex form by $X+iY+(x+iy)\exp(i\theta)$. The components of velocity and acceleration are obtained from the derivatives of this expression. It is noted that $\dot{x} \equiv \dot{u}$, the Coriolis term ($2\dot{u}\dot{\theta}$) is neglected, and α is approximated by dy/dx. Letting A_m be the transverse acceleration of the undeflected midpoint, and A_e the transverse acceleration of the ends about the middle, the transverse acceleration f_2 at x reduces to

$$f_2 = A_m + A_e(1-2x/L) - \ddot{y} - y\dot{\theta}^2 \qquad .d$$

Equilibrium equations: From the equations of equilibrium of the loads on an elemental transverse slice (assumed not to warp), including the d'Alembert loads, it is found (see Figure .c) that

$$\frac{\partial^2 M}{\partial x^2} = \frac{f_2 m}{L} + P\frac{d^2y}{dx^2} - K^2\frac{m}{L}\frac{\partial f_3}{\partial x} - \frac{mf_1}{L}\frac{\partial y}{\partial x}. \qquad .e$$

The last two terms will be neglected for the time being.

Elastic equation: The axial and shear deformations given in Appendix 10C are neglected for the purpose of this section, the bending deflections being dominant in typical coupler links. Then $\beta = \alpha$. $\sin\alpha$, $\cos\alpha$ are approximated by α, 1. By twice differentiating the bending equation it is found that

$$\frac{\partial^2 M}{\partial x^2} = -EI\frac{\partial^4 y}{\partial x^4} . \qquad \text{.a}$$

Equation of motion: The three equations reproduced above lead to the general equation of motion.* Expanding both the deflection y and the distributed transverse inertial load as Fourier (sine) series, and equating coefficients, it is found that each term in the series is associated with a different normal mode. (INGLIS suggests this method for a similar problem).

Now the deflection of mode k is divided into two components, the quasi-static component y_{ks} and the dynamic error z_k where $y_{ks} + z_k \equiv y_k$. The former is given by

$$(1 - P/k^2 P_c)\, y_{ks} = 4A_k / \pi k^5 \omega^2 \Omega^2 \qquad \text{.b}$$

where ω is the driving speed, $\Omega\omega$ the first transverse natural frequency with no end load, P_c the first Euler critical end load and A_k is defined by

$$A_k \equiv \begin{cases} A_m & | k \text{ odd} \\ A_e & | k \text{ even} \end{cases} \qquad \text{.c}$$

It can be seen that if $A_m \approx A_e$ the quasi-static deflection in the second mode is of the order of 32 times smaller than that in the first.

For a first assessment of the dynamic error the end-load is omitted, and a small damping term is included so that conditions at resonance can be properly represented. Then it is found that

$$\ddot{z}_k + 2\omega\Omega k^2 \tau_k \dot{z}_k + \omega^2\Omega^2 k^4 z_k = -4\ddot{A}_k/(\pi k^5 \omega^2 \Omega^2). \qquad \text{.d}$$

* P is approximated at all x by the instantaneous mean of $P_{(x=0)}$ and $P_{(x=L)}$

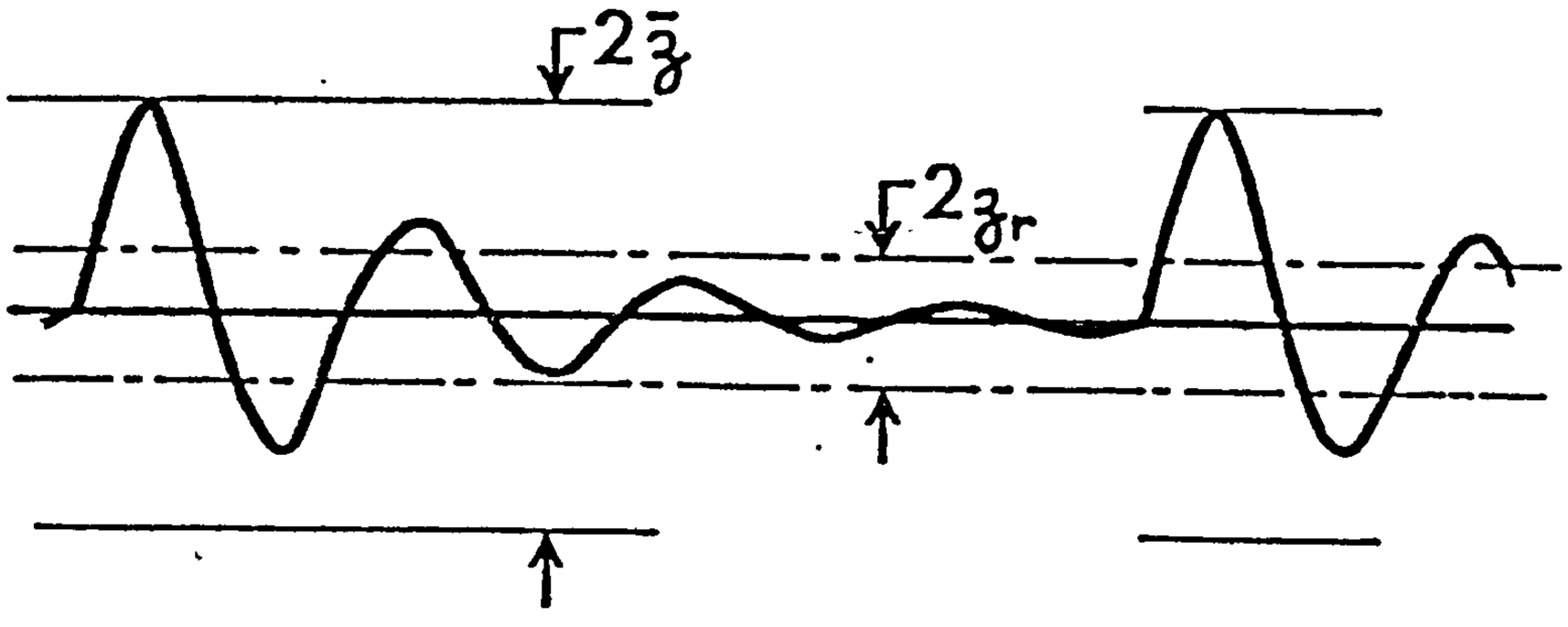

26.a: Limiting form of high-frequency response

may be necessary to consider the contribution of frequencies adjacent to the resonant frequency. In practice, the worst case occurs when the high frequency disturbance due to a given excitation waveform is largely confined to a small part of the total period, so that the case of an instantaneous impulse, periodically repeated, is approached. This may be termed a 'quasi-impulse'. In this case all the high-frequency components of the excitation are closely in phase at one instant in the cycle. The consequence, as shown in Figure ·a, is that the high frequency dynamic error at this point in the cycle ($\bar{z}$) may be considerably greater than the magnitude of the resonant component alone (z_r), which only gives the mean high-frequency error over the cycle. An analysis of this extreme case, given in Appendix 10D, shows that if the ratio ($\bar{z}/z_r$) is defined as the 'impulsive magnifier' D_I, then ·b

$$D_I \doteq (2\pi c/\Omega)/(1-\exp(-2\pi c/\Omega)). \qquad \cdot c$$

This extreme case can be taken as providing an upper limit for the more general case. Thus a conservative estimate of $(\bar{z}/\bar{y}_s)$ is $D_I D_r A_{kj}/k^5\bar{A}$. It may be seen that the expression for D_I approaches unity for the case $2\pi c \ll 1/\Omega$, and that $D_I D_r$ approaches $(\pi\Omega)$ for the case $2\pi c \gg 1/\Omega$. For $c=0{\cdot}01$, $\Omega=10$ gives $D_I=1{\cdot}35$ and $\Omega=20$ gives $D_I=1{\cdot}75$, so that the effective magnifier at resonance, $D_I D_r$, is still only about 90 in the latter case.

Evaluation: In the light of the arguments advanced in section 2D about the variation of A_j with j (in the case of ideal joints & crank drive), the insignificant nature of most of the error terms arising from the kineto-elastostatic approximation when $\Omega \geq 10$ is now clearly apparent. For we have from equations 20·c, 25·a/b: $z_{11}/\bar{y}_s \leq 1/25\pi \approx 1\%$. The second and third harmonics may lead to errors of a few percent in the first mode, but thereafter the reduction in A_j can be expected to outweigh the increase in j^2. The normalised resonant error in the first mode, on the other hand, is seen to be of the order of 5-10% for $\Omega=10$ in the case $L_c=3''$ on Figure 20·a, although it falls below the 1% mark if Ω is increased to 13. Thus it seems that the error due to the kinetostatic approximation begins to become significant when the assumed limits of frequency ratio and transmission angle are both approached, but not otherwise.

For $\Omega \geq 10$, $k = \underline{2}$ the resonant harmonic is the 40th or above, so it is clear that errors arising from resonance in this and higher modes will be completely negligible.

Stresses: Since the dynamic error in the deflection has been shown to be so dominated by the first mode, the expression for the amplitude of the normalised dynamic error in the deflection can also serve to give the normalised dynamic error in the bending stresses (which are related to the beam curvature d^2y/dx^2) and the normalised dynamic error in the transverse loads at the joints (which depends on the slope dy/dx at the ends). For simplicity, then, the following sections will focus on corrections to the deflection term, it being understood that this also serves as proxy for the load and stress terms.

Higher modes: note:- It should be stressed that the overwhelming case indicated above for neglecting modes above the first depends on the separation into 'quasi-static' and 'dynamic error' components. That is, although the second and third modes may be detectable in the total response (as other workers have noted), they are almost entirely accounted for in the quasi-static term, and can safely be neglected if this is separated out as described above.

2G: EFFECT OF AXIAL LOADS ON COUPLER LINK VIBRATIONS (Case i)

It has been suggested that in a well-designed mechanism for normal applications the end-loads do not exceed (say) one fourth of the Euler buckling load. The effect of an end load of such a magnitude - excluded entirely after equation 24·b in section F - will now be examined.

The variation of axial load along the link will be neglected at first. Thus equations A7·f, A7·g, A7·h, A7·i will apply.

Quasi-static effect: Equation A7·g shows that the effect of a (compressive) end load is to reduce the stiffness associated with the k'th mode by a factor H_k equal to $[1-(P/k^2P_c)]$. In the case assumed, H_1 may vary between 0.75 and 1.25, H_2 between 0.94 and 1.06, etc.

If the maximum value of $|P|$ does come near these limits, the effect on the first mode is correspondingly significant, and therefore would best be taken into account in estimating the quasi-static deflection. Because of the dominance of the first mode, it would usually be adequate to divide the total peak quasi-static deflection by H_1 (using the appropriate instantaneous value of P). ROARK & YOUNG give tables (9b) that permit a more accurate calculation.

Corrected equation of motion: The undamped equation of motion for the dominant first mode, from A7·g, can be written in the form

$$\ddot{y}_1 + \omega^2\Omega^2 H_1 y_1 = \omega^2\Omega^2 y_{1s} \qquad \cdot a$$

where y_{1s} is the quasi-static deflection without end-load correction. However, z_1 is now defined as the error incurred in using the corrected quasi-static approximation, that is $z_1 = y_1 - y_{1s}/H_1$. Then the equation of motion for z_1 becomes ·b

$$\ddot{z}_1 + \omega^2\Omega^2 H_1 z_1 = \ddot{y}_{1s}/H_1 + 2\dot{H}_1\dot{y}_{1s}/H_1^2 - 2\dot{H}_1^2 y_{1s}/H_1^3 + \ddot{H}_1 y_{1s}/H_1^2 \qquad \cdot c$$

This equation will be studied by dividing the complete cycle up into periods of slowly and rapidly varying end-load.

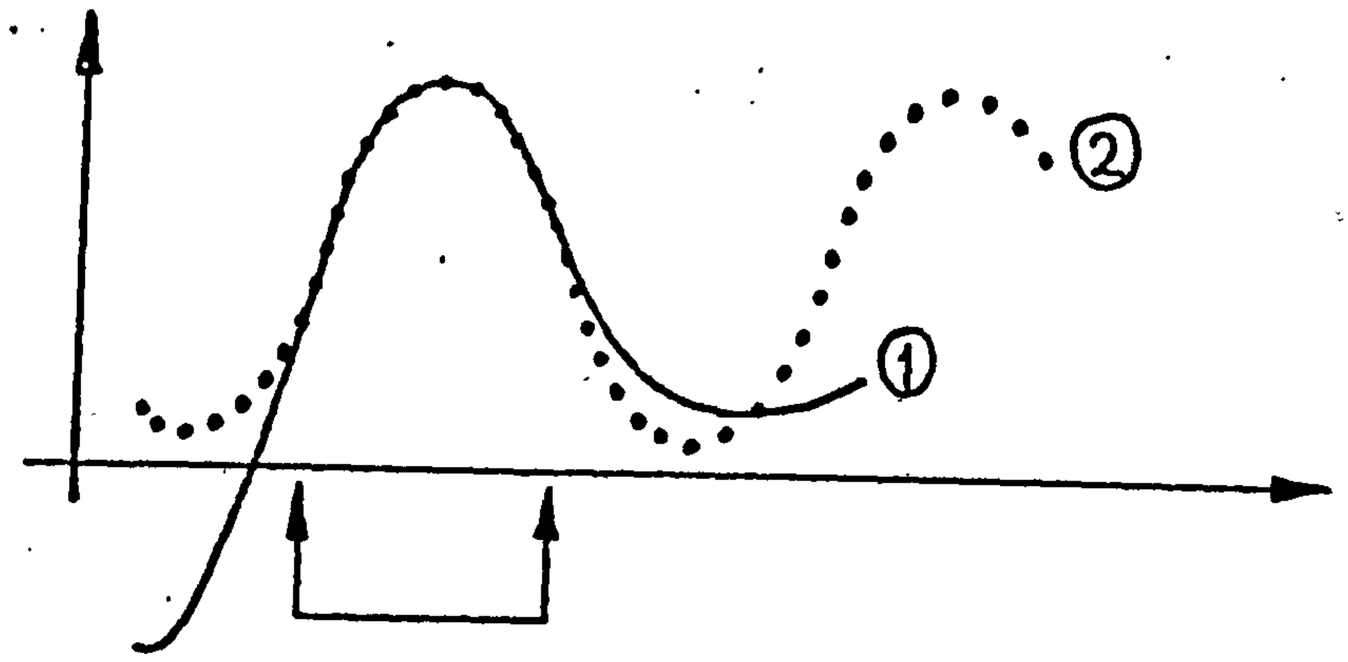

[① approximates to ② over the interval shown.]

29.a: Approximation of 'slowly varying' end load

Slowly varying end-load: Suppose that during part of the cycle y_{1s} and P approximate over small intervals to sine waves (see figure) whose amplitudes are of the order of magnitude of $\bar{y}_s$ and $P_c/4$ (or less) respectively and whose angular frequencies are of the order of ω (or less). Then it can be seen that the forcing terms (right hand side) of the equation for z_1 (28·c) are all of a similar order of magnitude, and small compared with the order of magnitude of the forcing terms in the otherwise similar equation for y_1 (28·a). Thus there is no significant build-up of error during these parts of the cycle.

If there is a quasi-impulse (cf p. 26·b) in the transverse loading while the end-load is varying slowly, the effect is the same as that considered in Section F (p25→26), except that Ω becomes $\Omega\sqrt{H_1}$ and the effective excitation is increased by a factor $1/H_1$.

Rapidly varying end-load: To understand the effect of a rapid change in the end-load, let us consider the extreme case of a step change. The result is a step change in H_1 and thus (considering $z_1 = y_1 - y_{1s}/H_1$) a step change in z_1, to be followed by transient vibration in proportion to the step-size. If Ω approximates to an integer, resonant magnification of this vibration also occurs. The analysis of this case, given in Appendix 10E, is similar to that of a quasi-impulse in the transverse inertial load, and shows that the normalised peak dynamic error due to such a step (for $\Omega = 10$, $\tau = 0{\cdot}01$, $H_1 = 0{\cdot}75$ minimum) is about $9j\,H_{1j}$ where H_{1j} is the j'th harmonic of H_1.

Considering that the end-load on the link under consideration arises from the acceleration of other links, the observations in section 2D about the frequency content of the transverse acceleration can also be applied to the frequency content of H_1. (The effect of variation in H_1 due to vibrations of other links will be considered in the next section). Since the range of H_1 is by assumption no more than 0.5, the amplitude of the first harmonic is not more than $(2/\pi) \times 0{\cdot}5$, i.e. about 0.3. Thus for well-designed mechanisms (as discussed in section D), the tenth harmonic, $H_{1,10}$ is likely to be of the order of (say) 0.0003, giving a normalized error of less than 3%.

Effect of variations in axial load along the length: In practice, the axial load will usually vary along the length of the link. Neglecting the small changes in longitudinal acceleration due to the transverse deflection, it is

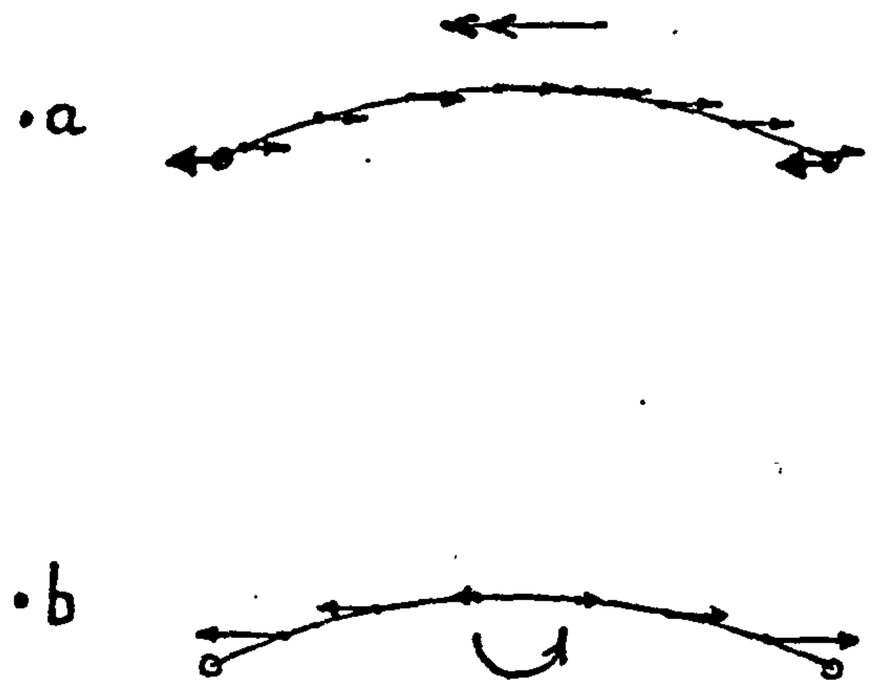

30.a/.b: Distribution of axial components of rigid-body d'Alembert load.

clear that:

(i) longitudinal acceleration of the mid-point of the link will introduce an axial load varying linearly along the length, and

(ii) rotation of the link about its mid-point will introduce a tensile axial load varying parabolically along the length.

Figures ·a and ·b show the distribution of the additional d'Alembert load, supposing the deflected shape to be that predicted without allowing for this additional loading. In figure ·a the resulting bending moment is evidently skew-symmetric about the centre, and so has no effect of the mid-point deflection.

The bending effect of the load distribution shown in figure ·b can be readily estimated to a first approximation, by approximating the deflection shape by a parabola. It is shown in an Appendix (10F) that the effect is to reduce the midpoint deflection by a proportion $(0{\cdot}56/\Omega^2)(\dot{\theta}/\omega)^2$ where $\dot{\theta}$ is the angular velocity of the link under consideration. Since we are assuming $\Omega \gg 10$ and $\dot{\theta}$ is normally of the same order as ω or less, it is seen that this effect modifies the deflection by the order of $\frac{1}{2}\%$ or less, so its neglect is justified.

2H: COUPLING EFFECT OF END LOADS AND LINK FORESHORTENING

In the cases analysed so far, the vibrations in each link were found to be independent. In cases where link foreshortening and axial joint loads are both significant, this result does not apply: in general, the foreshortening does work against the axial load, so that vibratory energy is transferred between the links and the equations of motion are coupled.

Foreshortening effect: Referring to equation A6·f, the foreshortening of the link due to curvature is given by

$$U = \tfrac{1}{2}\int_0^L (\partial y/\partial x)^2\, dx. \qquad \cdot a$$

For a static uniformly distributed transverse load, with associated midpoint deflection $\bar{y}_s$,

$$(\partial y/\partial x) = (16\bar{y}_s/5L^4)(4x^3 - 6x^2L + L^3) \qquad \cdot b$$

leading to a foreshortening of $(2176\,\bar{y}_s^2)/(875\,L)$, that is about $0{\cdot}249\,\bar{y}_s^2/L$. For the first mode of deflection alone,

$$(\partial y/\partial x) = (\pi y_1/L)\sin(\pi x/L) \qquad \cdot c$$

leading to a foreshortening of $(\pi^2 y_1^2/4L)$, , that is about $0{\cdot}247 y_1^2/L$, which is not significantly different from the former result for the same mid-point deflection $(y_1 = \bar{y}_s)$. Thus in most cases the total foreshortening is given to a good approximation by $(\pi^2/4L)$ times the square of the total mid-point deflection. This deflection can be written as $(y_s + z)$ where in this case y_s is the quasi-static mid-point deflection allowing for the rigid-body end-load, and z is the total mid-point dynamic error. As the dynamic error in every case investigated so far has been quite small compared with $\bar{y}_s$, it is reasonable to approximate the foreshortening U by $(\pi^2/4L)(y_s^2 + 2z\,y_s)$ so that an equation of motion linear in z will be obtained. $\cdot d$

Differentiating the expression for U twice with respect to time leads to

$$\ddot{U} = (\pi^2/2L)(\ddot{y}_s(y_s+z) + \dot{y}_s^2 + 2\dot{z}\dot{y}_s + y_s\ddot{z}). \qquad \cdot e$$

In line with the foregoing, (y_s+z) will be approximated by y_s, and $\dot{z}\dot{y}_s$ will be assumed small compared with $\ddot{z}y_s$, leading to

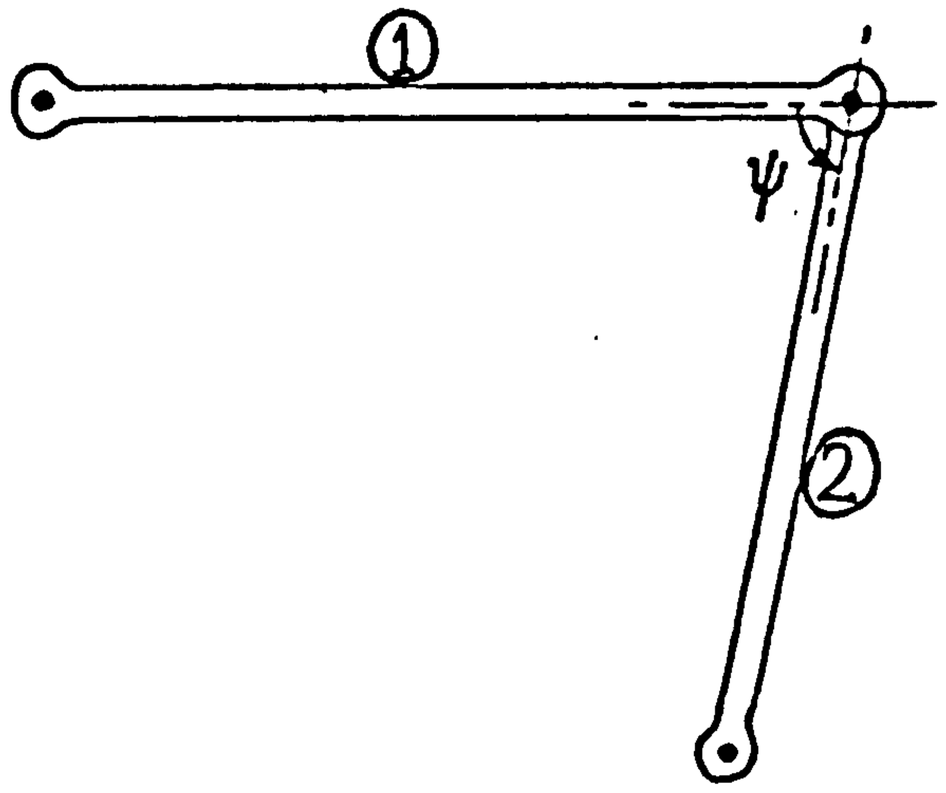

32.a: Dyad with possible vibration coupling via foreshortening effect

$$\ddot{u} = (\pi^2/2L)(\ddot{y}_s y_s + \dot{y}_s^2 + y_s \ddot{z}).$$

According to the assumptions in section 2B, $y_s/L \leq 0{\cdot}025$ (for each link), so $\ddot{u}$ is an order of magnitude smaller than $\ddot{z}$ or $\ddot{y}_s$ (whichever is larger).

Implications: A formal analytic treatment of the implications of this foreshortening is beyond the scope of this chapter, but physical reasoning can provide definite pointers. Consider the dyad shown opposite, whose links are indicated by suffices ① and ② and are assumed to have broadly similar dimensions. The transmission angle ψ is assumed, as previously, to remain fairly close to the right angle. The variation in length of link ② has the effect of imposing an additional transverse acceleration on link ① related to and of the same order as $\ddot{u}_②$. This term appears in the equation of motion along with $\ddot{z}$ and $\ddot{y}_s$ which are an order of magnitude larger. Thus in general it is reasonable to expect that the foreshortening of link ② would not change the order of magnitude of $z_①$ (and conversely).

This reasoning falls down, however, if a dominant harmonic component in the term $\ddot{u}_②$ is close to the natural frequency of link ①, so that energy flows in the same direction between the two links for several vibratory cycles. If such coupling takes place to the maximum extent, all the vibratory energy associated with link ② would be transferred to link ① at some point in the cycle, and vice versa. Thus in round terms the consequence would be a doubling of the peak dynamic error in each link.

If the dominant component of the variation of $y_{②s}$ is the 1st harmonic, and the dominant component of $z_②$ is the 10th harmonic of the crank speed ($\Omega_② \doteqdot 10$), $y_{②s}\ddot{z}_②$ will be mainly 9th and 11th harmonics (by trigonometrical product formulae). Thus if $\Omega_①$ is about 9 or 11 the above conditions for significant coupling will be met. More generally, it appears that designs for which the values of Ω in adjacent links differ by about 1 or about 2 may experience exacerbated vibrations due to the coupling effect considered above, and it would be advisable for designers to avoid such a condition if possible.

Relation to vibratory end load: As in static problems the incremental transverse displacements due to incremental axial loads (on an already deflected beam) are related by the reciprocal theorem to incremental axial displacements due to incremental transverse loads, so the effect of vibratory foreshortening is likewise inseparable from the effect of vibratory end loads.

The case of two similar adjacent links vibrating in an approximately perpendicular configuration (see figure 32.a) provides a simple example. The flow of energy from link ① to link ② due to axial vibratory end-motions of link ① can be seen in two ways. From the point of view of link ② it is work done against transverse vibratory joint loads, and affects the motion of link ② as considered under the previous heading. From the point of view of link ① it is work done by axial vibratory joint loads. Thus we conclude that the effect of the latter is significant as and when the effect of the former is also significant.

2I: EFFECT OF CRANK SPEED VARIATION ON LINK VIBRATIONS

Variations in the angular speed of the driving link might be divided into "wow" - cyclic speed variations due to the finite inertia and torque capacity of the driving system; "flutter" - high frequency variations due to flexibility of the driving system; and "blip", momentary accelerations due to pulses in the driving torque, as may arise for example from a thyristor-controlled motor. This section will be confined to the consideration of the effects of "wow", the effects of "blip" and "flutter" being considered in sections J and K (case iii) respectively.

To gain an insight into the effect of wow, then, let us consider the cases of a crank-rocker mechanism and a drag-link mechanism in both of which the mass of the coupler can be represented as two point masses at the joints, and so can be 'lumped' together with the crank and rocker or follower. It will also be assumed that the cyclic speed variation is controlled largely by the effect of a flywheel rather than by the motor speed control system, and that potential energy variations are not significant. Then the kinetic energy of the system is constant, so that $\frac{1}{2}J_1\omega^2+\frac{1}{2}J_2Q^2\omega^2$ is constant where J_1 is the lumped inertia at the crank, J_2 that at the rocker, ω the crank speed and Q the velocity ratio. Thus ω is greatest when $|Q|$ is least, and conversely. The acceleration of the output link is $(dQ/d\phi)\omega^2+Q\dot{\omega}$, rather than $(dQ/d\phi)\omega^2$ in the nominal (ω constant) case. The implications will be considered separately for the two types of mechanism indicated.

Crank-rocker mechanism: The greatest acceleration of the rocker occurs near the instant when Q changes sign, and is therefore nearly equal to $\dot{Q}\omega$. Since ω is at its maximum at this point, the effect is that the peak rocker acceleration (and thus the level of vibration to be expected in the rocker) is somewhat greater than in the nominal case with the same mean value of ω. In well-designed mechanisms, however, the speed variation is usually no more than a few percent, so that the percentage underestimate of $((dQ/d\phi)\omega^2)_{max.}$ being about twice the percentage speed variation (from the mean), is unlikely to be very significant.

The transverse acceleration of the coupler is greatest in the part of the cycle when the coupler is nearly perpendicular to the crank, which is when $|Q|$ is near its maximum and ω is therefore depressed. The centripetal

acceleration of the crank/coupler joint is thereby reduced, and thus so also is the transverse acceleration of the coupler - so that in this case the neglect of the speed variation is conservative. Similar observations apply to the coupler in a crank-slider mechanism.

Crank-follower (drag link) mechanism: The follower acceleration is greatest when $dQ/d\phi$ is near its maximum, which is roughly mid-way between the points of minimum and maximum Q, so that ω is close to its nominal value. However, $\dot{\omega}$ has an opposite sign to $dQ/d\phi$, so that the total follower acceleration will usually be reduced by the effect of speed variation.

The kinetic energy associated with rotation of the coupler is usually considerably smaller than that associated with its translation, so that the restriction on the mass distribution of the coupler in the above treatment does not seriously put in question the qualitative conclusions drawn.

It may be concluded that the neglect of crank speed variation is conservative for some types of mechanism but not for others, but in any case does not affect the order of magnitude of the peak inertial loading provided that the speed variation is itself of a smaller order than the mean speed.

2J: NEGLECTED EFFECTS IN COUPLER LINK VIBRATIONS

The order of magnitude or character of the terms and effects neglected in the previous sections will now be examined relatively briefly, to ascertain whether there are circumstances of practical relevance in which these omissions may be significant.

Effect of frame vibrations: The inertially generated load transmitted to the frame provides a classic problem of linkage mechanism dynamics. The load is usually estimated on rigid-link assumptions. Provided that the mechanism itself meets the various criteria of sound design noted in this chapter, this method appears to be appropriate, and the major difficulties lie in the field of synthesis, considered in Chapter 8. For present purposes, however, it is also necessary to consider the possibility of interaction between linkage and frame vibrations.

Considering that the benefit obtainable from lightening moving links is considerably greater than that obtainable from lightening the frame, the natural frequencies of vibration of a rigidly-mounted frame seem in practice likely to be of a higher order than those associated with link vibrations. On these grounds substantial coupling effects would not be expected. This is as much as to say that if the link vibrations are predicted to be seriously affected by frame vibrations, the frame design itself will probably not prove viable.

If the frame is mounted on soundly-designed anti-vibration mountings, the natural frequency of this system will be well below the operating crank-speed, so the additional (high frequency) effect on the moving links should not be significant. One requirement of 'soumd design' implicit in this argument is that the response of the suspension should not include an out-of-plane component, which would lead to gyroscopic effects.

Effect of backlash and other irregularities: The effect of clearances in the joints is that impulses may be generated when relative motion across the clearance takes place. Suppose that the relative acceleration between the two members of the point is ηt from the moment when the contact force drops to zero to the moment when contact is remade, time τ later, after relative motion across the diametral clearance $2e$. Then the relative displacement

x is $\eta t^3/6$ and so $T=(12e/\eta)^{1/3}$. The impact velocity is thus $3\eta(12e/\eta)^{2/3}$ that is about $10(2e)^{2/3}\eta^{-1/3}$. As noted in section D, such an irregularity gives rise to a flat inertial load or acceleration spectrum: every harmonic component of the latter up to a high order is of magnitude $A_I \doteq (10\omega/\pi)(2e)^{2/3}\eta^{-1/3}$, say $3\omega(2e)^{2/3}\eta^{-1/3}$. For a mechanism with a crank length of L, and motion bearing some resemblance to harmonic motion, the nominal peak acceleration will be of order $\omega^2 L$; similarly a preliminary estimate of the order of magnitude of η might be $\omega^3 L$. The ratio of A_I to the nominal peak acceleration is therefore of the order of $3(2e/L)^{2/3}$.

Thus even for a close-fitting bearing with $2e \approx 10^{-4}L$, A_I may approach 1% of the peak nominal acceleration. Since the effect of A_I may be subject to a resonant dynamic magnifier of the order of 50, it appears that this effect could in some cases be significant compared with the nominal deflection, and could indeed be the dominant source of dynamic error.

Other sources of discontinuous excitation such as "blips" in the crank speed due to impulses in the driving torque are even more difficult to quantify, but considering that the observations about the shape of the harmonic spectrum for backlash apply here as well, it is clear that any such effect ought to be considered seriously as a likely culprit if serious vibrations occur in a practical mechanism.

$y_k\dot{\theta}^2$ term: The combination of bending deflection y and angular motion of the link $\dot{\theta}$ gives rise to a term $y\dot{\theta}^2$ in equation A6·e, leading to a term $y_k\dot{\theta}^2$ in A7·g. $\dot{\theta}$ is usually of the order of the driving speed or less, whereas the preceding term in equation A7·g is of the order of $100y_k\omega^2$ or more for $\Omega \geqslant 10$. Thus the effect of the $y\dot{\theta}^2$ term is to introduce an extra variation in the coefficient of y_k of no more than 1%. Considering that variations of up to 10% due to an axial load variation have already been considered and found to have only minor effects, the omission of the $y_k\dot{\theta}^2$ term is clearly justified.

Interaction with axial vibrations: The ratio of the natural frequency of longitudinal vibration of a simple beam pinned at the ends to that of transverse vibration is $(L/\pi K)$ where K is the radius of gyration of the cross section. We have assumed an upper limit of $L/K = 350$; it seems

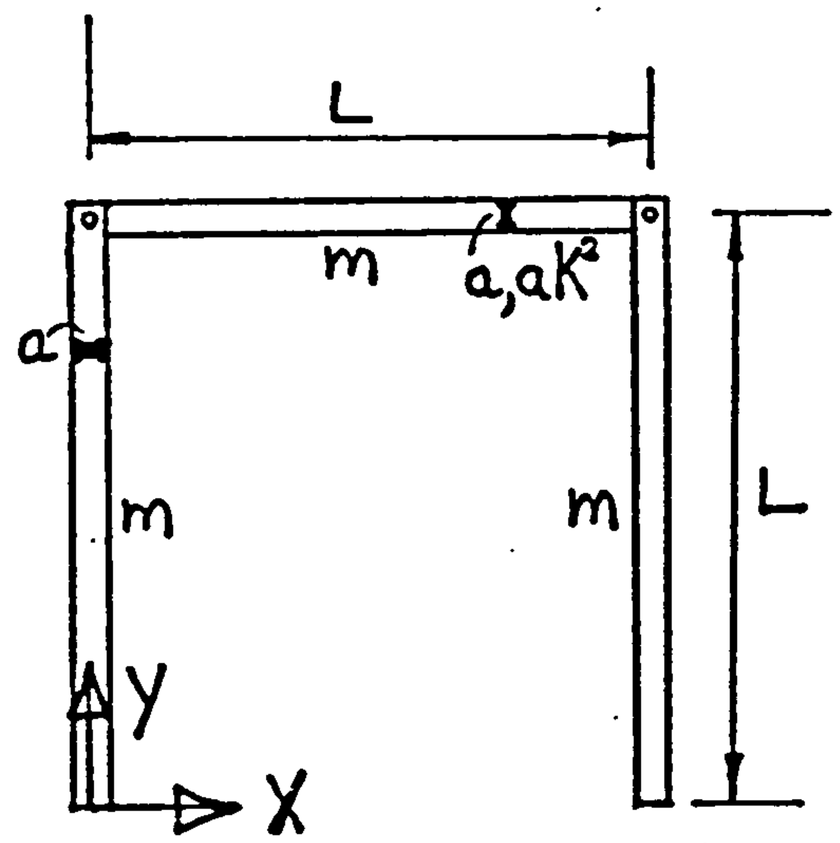

38.a: Example of axial/bending interaction

L/K	Δ	Γ
39.887	0.020	0.988
28.545	0.040	0.975
23.569	0.060	0.964
20.626	0.080	0.953
18.629	0.100	0.942
17.163	0.120	0.931
16.027	0.140	0.921
15.114	0.160	0.911
14.359	0.180	0.902
13.721	0.200	0.893

TABLE 38.b: Approximate mode shape factor & frequency correction factor for system in 38.a

unlikely that links will be significantly vibration-prone unless L/K is at least 1/10 of this value, so that the longitudinal: transverse frequency ratio is of the order of 10:1. As a consequence such a link can be assumed to respond to longitudinal loading at frequencies of the order of ω_1 (the fundamental frequency in bending) as if it were a light longitudinal spring: that is, the axial strains associated with vibrations can be taken to be constant along the link. Such axial strains in a given link could affect the transverse vibrations in an attached link and/or in the given link itself. These two effects will be considered in turn.

Two-link case: To gain an idea of the significance of the first kind of interaction noted above, let us consider vibrations of the system shown in Figure 38·a, such that the two parallel links vibrate longitudinally and the third link vibrates transversely. By the reasoning above, we can assume that in conditions of free vibration the deflection in the Y- direction is everywhere $(\Delta v Y/L + v \sin(\pi X/L)) \sin(\Gamma \omega_1 t)$. In this expression Γ represents the ratio of the natural frequency to that calculated with the longitudinal elasticity neglected, and Δ represents the ratio of the amplitudes of longitudinal and transverse vibrations. With Γ and Δ found by the Rayleigh-Ritz method, the effect is as shown in Table 38·b. The working is given in Appendix 10G.

The table shows that for $L/K \geqslant 35$, the dynamic component of deflection is only increased by about 3% due to the increased flexibility, and the natural frequency is only reduced by about 2%. Indeed, values of L/K considerably lower than this do not show a great effect. (If the designer was relying on tuning to minimise vibrations the frequency effect would certainly be significant, but in this chapter the conservative assumption of resonant conditions has proved sustainable throughout).

The system shown in Figure 38·a is admittedly simplified in several respects, but at least some are negligible. If one of the ends of the X-direction beam was fixed (representing attachment to a rigid crank) the longitudinal flexibility correction would hardly be any worse. Non-perpendicularity of the links would affect the result, but not its order of magnitude (one would suppose) provided that reasonable transmission angles were maintained. An important qualification, however, is that the results would obviously not be relevant if the L/K ratios of the adjoining links were markedly different:

in particular, transverse vibration in a link with L/K near the lower limit assumed, associated with longitudinal vibration in a link with L/K nearer the upper limit would present a picture very different from Table 38·b. Since in this case it is the longitudinal vibration that provides the most serious problem, however, it is better to treat it as an extension of Case (iv).

One link case: The interactions between longitudinal and transverse vibrations in the same link are omitted in two respects in Appendix 10C.

Firstly, x and L are approximated by x_o and L_o. As the differences are orders of magnitude smaller than L itself this clearly does not cause a significant error.

Secondly, the 'Coriolis' term $2\dot{u}\dot{\theta}$ is dropped from equation A5·e. This term has the effect of an additional transverse excitation. The components of u most likely to cause trouble are those near the first transverse natural frequency $\Omega\omega$. The displacement amplitude of this component cannot be greater than $L\varepsilon_\ell$, so that $\dot{u}$ is of the order of $\frac{1}{2}\omega\Omega L\varepsilon_\ell$ at the mid-link position. Taking $\dot{\theta}$, as before, as of the order of ω, the omitted term is of the order of $\varepsilon_\ell\Omega\omega^2 L$ or less. Since the larger terms included are normally of the order of $\omega^2 L$, the omitted term is likely to be two orders of magnitude smaller, so that omission is also justified.

'Timoshenko beam' terms: The effect of the rotary inertia of the beam element (the term $(-K^2m/L)\partial f_3/\partial x$ in equation A6·d) and of shear deformation (first equation at A6·f) are both accounted for in the Timoshenko model of beam vibration. According to McCALLION the effect is to reduce the first natural frequency from ω_1 to a value ω_1^*, given by

$$(\omega_1-\omega_1^*)/\omega_1 = \pi^2(1+E/\zeta G)/s^2 \qquad \cdot a$$

where S is the slenderness ratio, L/K and ζ is a shear coefficient dependent on the cross section. According to McCALLION the best available estimate for the shear coefficient for a rectangular section is $\zeta = 0{\cdot}851$. Assuming as previously that $S \geqslant 35$ for a potentially troublesome link, it follows that for a rectangular steel section

$$(\omega_1 - \omega_1^*)/\omega_1 < 0.017 \qquad \text{.a}$$

This suggests that for the cases of interest the Timoshenko beam terms are not significant, unless a cross-section with a much poorer shear coefficient than the rectangular section is used in conjunction with a rather low slenderness ratio.

Link curvature: If a link is substantially curved or dog-legged in or out of the plane of motion, it is clear that the analysis given in this chapter is quite inapplicable. A major degree of coupling between end-loads and transverse deflections is likely to occur, and longitudinal stiffnesses may be much reduced, with adverse effects on the natural frequency. A theoretical study by BADLANI & MIDHA of a link curved in the plane unfortunately fails to illuminate the problem since the parameters quoted by the authors fall in the unstable region of the Matthieu equation stability chart; the main effect of the small initial curvature is to introduce an assymetric exciting term, without which the instability is masked by the nominally exact symmetry of the slider-crank arrangement. SUNADA & DUBOWSKY described a promising finite element method for treating links of any three-dimensional form, but this is limited by the neglect of axial loads on the questionable grounds that most studies of straight links have found these terms to be negligible. In short, the effects of link curvature remain a significant field for future investigations.

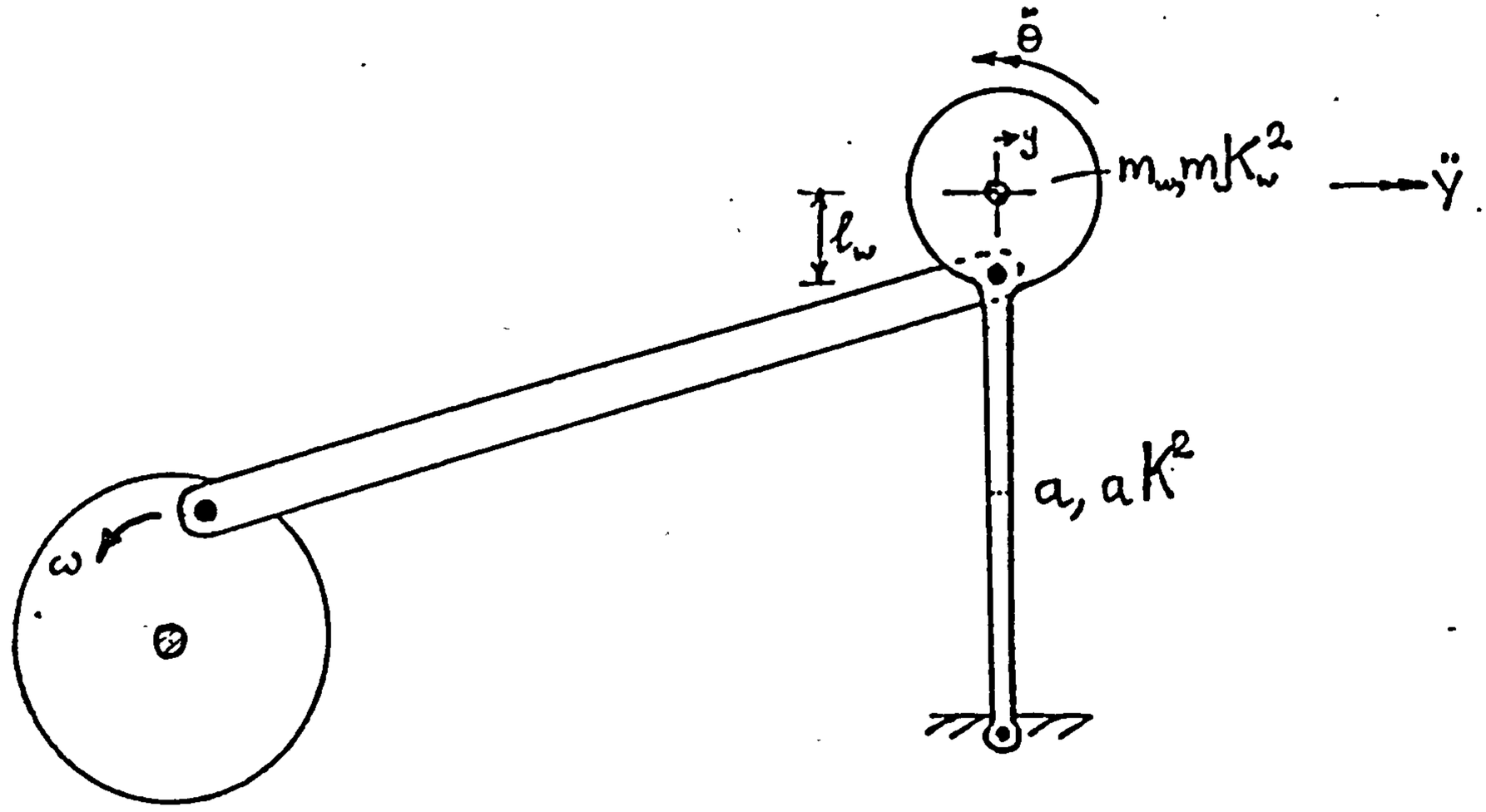

41.a: 'Typical' case of light link with overhung mass

2K: VIBRATIONS IN CASES (ii) TO (iv)

Case (ii): light link with overhung mass: In this case the dominant mode of vibration is deflection y of the mass m_w against the bending stiffness $m_w\Omega^2\omega^2$ of the link. The d'Alembert moment acting on the overhang will be $m_w K_w^2\ddot{\theta} + m_w\ddot{y}\ell_w$, where $\ddot{y}$ and $\ddot{\theta}$ are the rigid-body transverse acceleration and angular acceleration of the overhung mass (see Figure ·a for example).

Then with end-load and damping omitted the transverse equation of motion must be

$$m\ddot{y} + m\omega^2\Omega^2 y = -mA(\phi) \qquad \Big| \; A \equiv \ddot{y} + K_w^2\ddot{\theta}/X \qquad \cdot b$$

As for equation A7·a in Appendix 10C, this equation can be elucidated by expressing y as the sum of a 'quasi-static' and a 'dynamic error' term. Without spelling out every step, it is clear that by this means conclusions similar to those in Section F may be drawn regarding the relative magnitudes of the quasi-static deflection, the low frequency component of dynamic error, and the resonant component of dynamic error, provided that similar assumptions are made about the frequency ratio, damping factor and excitation spectrum.

In evaluating the effect of end-loads in case (ii), obviously the axial component of the inertial load on the overhung weight must be taken into account along with the joint reaction. A further difference is that the first mode shape is not a half-sine wave as in case (i), but comprises a series of Fourier components, each of which is amplified by the relevant factor $1/H_k$ defined as for case (i) (Section 2G, p28). The net effect is therefore a change in the total effective stiffness by a factor H_T that is a function of (P/P_c) but is only roughly approximated by $(1-P/P_c)$. Tables in ROARK & YOUNG (Table 9b, case 3e, "$a=0$") again provide for a more accurate calculation. The similarity of the values given in these tables for uniformly distributed load (corresponding to case (i)) and concentrated moment at the end (corresponding to case (ii)) suggests that the qualitative conclusions of Section G can reasonably be extended to case (ii).

In some positions, an overhung mass may affect the axial natural frequency of the link, such as in the case of an overhung mass at the coupler end of the rocker in a crank-rocker mechanism (see ·a). If the coupler is light the ratio of axial to bending natural frequency is $\sqrt{[(\ell_w^2+K_w^2)/3K^2]}$, which is

likely to be considerably more than unity in view of the assumptions being made; thus the bending mode remains the more critical.

Case (iii): flexible shaft: As in Case (ii), there is only one degree of freedom in this case. The equation of motion can be derived from a power balance:

$$-S\theta\dot{\phi} = d/dt\,[\tfrac{1}{2} J_{\phi+\theta} (\dot{\phi}+\dot{\theta})^2] + \zeta \dot{\theta}^2 \qquad \text{.a}$$

where θ is the torsional deflection of the drive shaft, S its stiffness, $J_{\phi+\theta}$ is the generalised (effective) inertia of the linkage referred to the input and the last term represents the effect of damping. Since it is assumed that $\theta \ll 2\pi$, this can be reduced to

$$\ddot{\theta} + [(\dot{J}_\phi + \zeta)/J_\phi]\dot{\theta} + [(S + \tfrac{1}{2}\ddot{J}_\phi)/J_\phi]\theta = -\tfrac{1}{2}[\dot{J}_\phi/J_\phi]\dot{\phi} \qquad \text{.b}$$

which is basically a Hill's equation, modified by inhomogeneous and first order terms.

If the crank and coupler of a four-bar chain are massless compared with the rocker, the effective inertia at the crank falls to zero at the instant when the crank and coupler are in line. This extreme case points to the fact that the variation in the coefficient of θ can easily be a large fraction of its mean value. Moreover, the dominant components of both the torque fluctuation and the inertia variation are likely to be at twice the driving speed.

These facts suggest that where the input system stiffness is inadequate, the torsional oscillations set up may be not only significant in magnitude but also rich in harmonic content. Since torsional oscillations in the crank-shaft are transmitted by the kinematic relationship to all driven links, the last point is particularly significant. The effect is that if a linkage contains both a flexible shaft and flexible links, the harmonic spectrum of the accelerations at the joints may be much worse than calculated from rigid body assumptions, so that the links may well experience flexural vibrations that would not be expected by consideration of the values of Ω for the links alone.

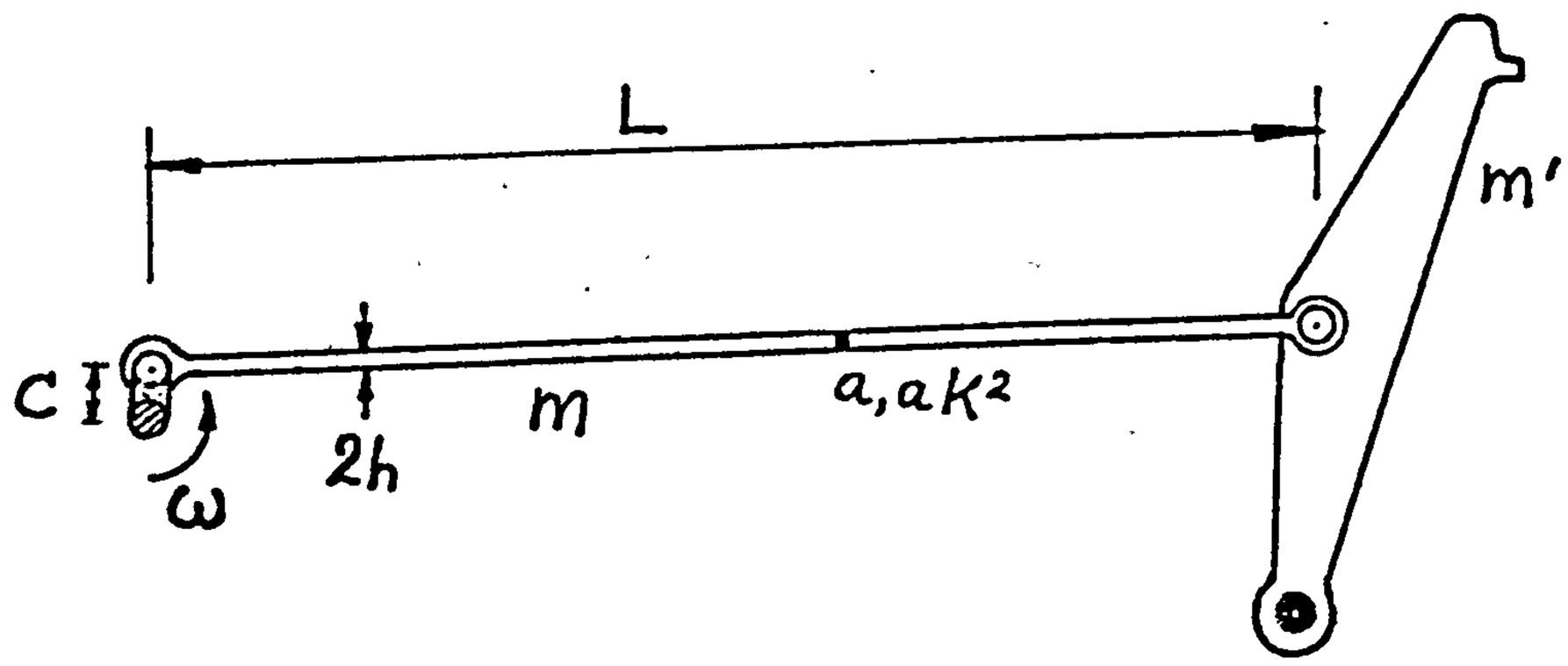

43.a: Typical case where axial vibrations matter

Case (iv): tie rod: The dominant mode of vibration is axial motion U of the mass m_w against the tensile stiffness $m_w\omega^2\Omega^2$ $(=Ea/L)$. The d'Alembert load on the mass will be $-m_w\ddot{X}$ where $\ddot{X}$ is the acceleration of the other end of the rod. Thus the undamped equation of motion is

$$m_w\ddot{U} + m_w\omega^2\Omega^2 U = -m_w A_a(\phi) \qquad \Big| A_a \equiv \ddot{X} \qquad \cdot b$$

This is similar to the equation obtained for Case (ii), and similar consequences follow.

There is one important complication, however. The figure $(\cdot a)$ shows a typical practical situation for which Case (iv) provides an idealisation: a slender coupler connects a massive rocking component to a rigid crank. Let the effective mass of the rocker at the coupler joint be m'. If this is large enough the axial natural frequency may fall as low as the bending natural frequency; that is

$$(Ea/m'L) \approx \pi^4 (Ea/mL)(K^2/L^2) \qquad \cdot c$$

The ratio of the peak rigid-body tensile stress ($\omega^2 C m'/a$ approx.) to the peak rigid-body bending stress ($\omega^2 C mLh/16aK^2$ approx.) is then about $L/6h$. Since the coupler is assumed to be slender, this indicates that the critical stress therein is likely to be that due to the axial load. The dynamic error in this stress may be significantly modified, however, by coupling with bending vibrations in the same link, since changes in link length due to bending and due to axial strains are both associated with vibratory motion of the heavy rocker.

2L: COMPARISON WITH PREVIOUS INVESTIGATIONS

The physical understanding of the relevant phenomena, gained in the previous sections, can be usefully compared with the results of more detailed investigations of more specific problems.

Unfortunately the parameters of many of the studies make them of rather little relevance to the questions of interest here. The deliberate choice of artifically weak cross-sections for some investigations has been noted in Section 2C. Other investigations have been concerned with the behaviour of links at improbably high stress levels. For example, LOWEN & JANDRASITS cite results by VISCOMI & AYRE contrasting linear and non-linear solutions for a steel link. The quoted deflections of 3.8 inches (linear) and 1.56 inches (non-linear) for a twelve inch coupler with 2h = 0.5 inches imply stress levels of some hundreds of tons per square inch. WILLMERT ET AL. contrasted kinetoelastostatic and kinetoelastodynamic solutions for an aluminium link at stresses of up to 50,000 pounds per square inch at the design speed. As this speed lies between two resonant speeds (third and fourth order), still higher stresses could be expected while running up to speed.

Some noteworthy points emerge, however. Even under the extreme conditions referred to, VISCOMI & AYRE found the higher modes to have negligible effects. JANDRASITS & LOWEN(b) found the effects of coupling between two highly flexible links to be quite negligible in their numerical simulations: they correctly stressed that this result depended on the assumption of a rigid crank. (Due to the presence of an overhung mass on one link the uncoupled natural frequencies would not have been close in this case). NATH & GHOSH included a very full array of small order terms in a finite-element analysis and found that the higher order acceleration terms played a very small part in the transient solution even for the extreme cases studied. On the other hand the effect of vibratory end loads was found to be fairly significant in these cases. (These authors also placed particular stress on their treatment of driving cranks, as being driven by systems of no inertia: not surprisingly, the cranks exploit this freedom by vibrating merrily, but the realism of this assumption seems dubitable).

Three studies with experimental support are of particular interest. SANDERS & TESAR performed a theoretical exercise similar to that in Section 2F above, and obtained an equation similar to equation 25.a except in two respects.

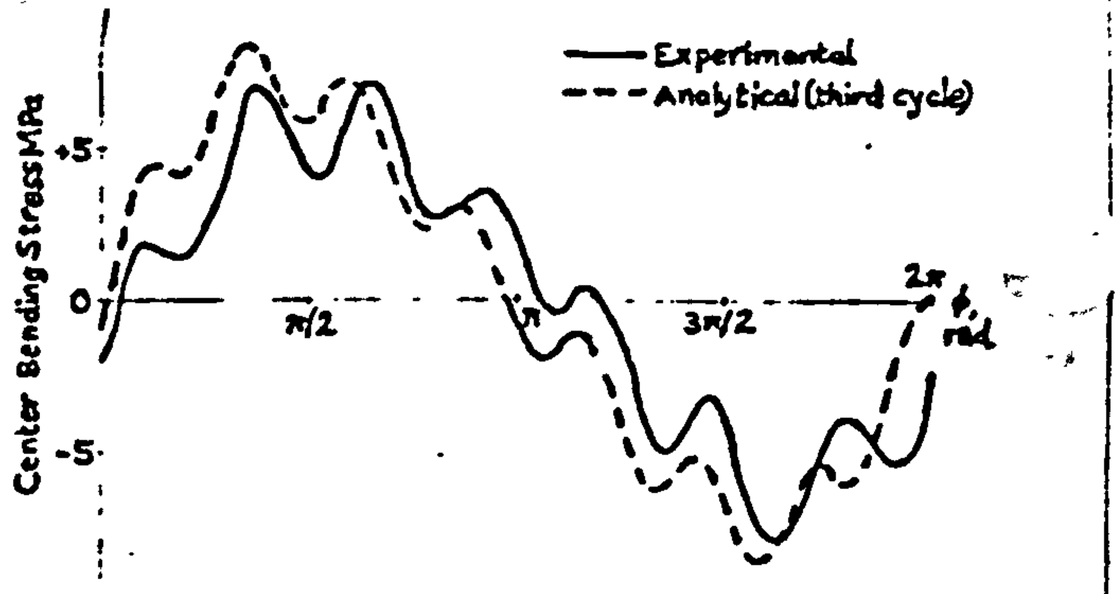

[ex: Fig. 9] Bending stresses at the midpoint of the connecting rod of a slider-crank linkage ($L_c = 0.25L$, $L_s = 0$, $\omega = 400$ rpm)

45 • a: 'Steady state' vibrations, ex. GOLEBIEWSKI & SADLER

Firstly, the exponent of k was 5 rather than 9. This stemmed from the fact that these workers used an "equivalent load" at the mid-point of the beam to represent the distributed inertial load. This is in fact equivalent as regards the mid-point deflection but not as regards the modal composition of the deflection, and therefore gives erroneous results when used in a dynamic problem. Their conclusion, that modes higher than the first can be neglected, is in fact reinforced by the corrected analysis given here.

The second point of variance in SANDERS & TESAR's treatment is that they included a "transient" term (without damping). They did not identify the non-steady initial conditions associated with this transient, but the conditions in question appear to be that $z = \dot{z} = 0$ at zero crank angle. There appears to be no physical justification for such an assumption, and in fact this transient term appears to have been confused with the natural frequency (resonant) component of the <u>steady-state</u> response, since the measured value of the latter was subsequently compared with the theoretical transient. Surprisingly there is quite good agreement. An important point is that the measured value is in fact very much larger than the steady state term of the theoretical solution. It is difficult to explain this except as indicating the presence of some additional source of excitation, e.g. backlash.

A similar situation arose in an earlier study by GOLEBIEWSKI & SADLER. They obtained theoretical curves using numerical integration from "zero initial conditions for deflections and their derivatives .... at crank angle $\phi = 0$," and stated that zero damping was assumed. Since the stated initial conditions are not steady-state conditions the simulation must include a "transient" or arbitrary magnitude which, owing to the omission of damping, never disappears as it would in the real world. The apparent similarity between simulated and experimental curves is therefore spurious. (This is particularly clear in the Figure (.a) reproduced here, in which the experimental curve shows the same values of stress and rate of change of stress at $\phi = 2\pi$ as at $\phi = 0$ but the simulated curve certainly does not; confirming the <u>non</u>-steady nature of the latter in contrast to the former). Thus the experimentally recorded vibrations are again not accounted for by the theory, and again an additional source of excitation is the simplest explanation.

JANDRASITS & LOWEN(a,b) published a very thorough study of vibrations in a highly flexible link with overhung mass. They clearly spelt out the need to exclude transients from the solution (in the Appendix of their paper (b)).

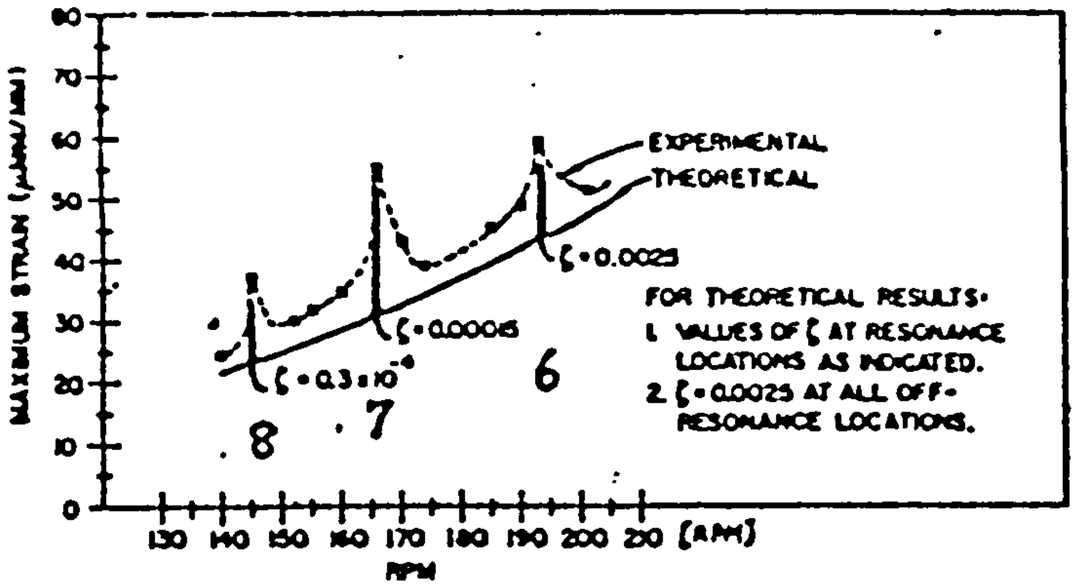

[ex:Fig. 14] Comparison between experimental and theoretical results: corrected maximum strain at bottom gage location

46.a: Contrasting resonance curves, ex JANDRASITS & LOWEN(b).

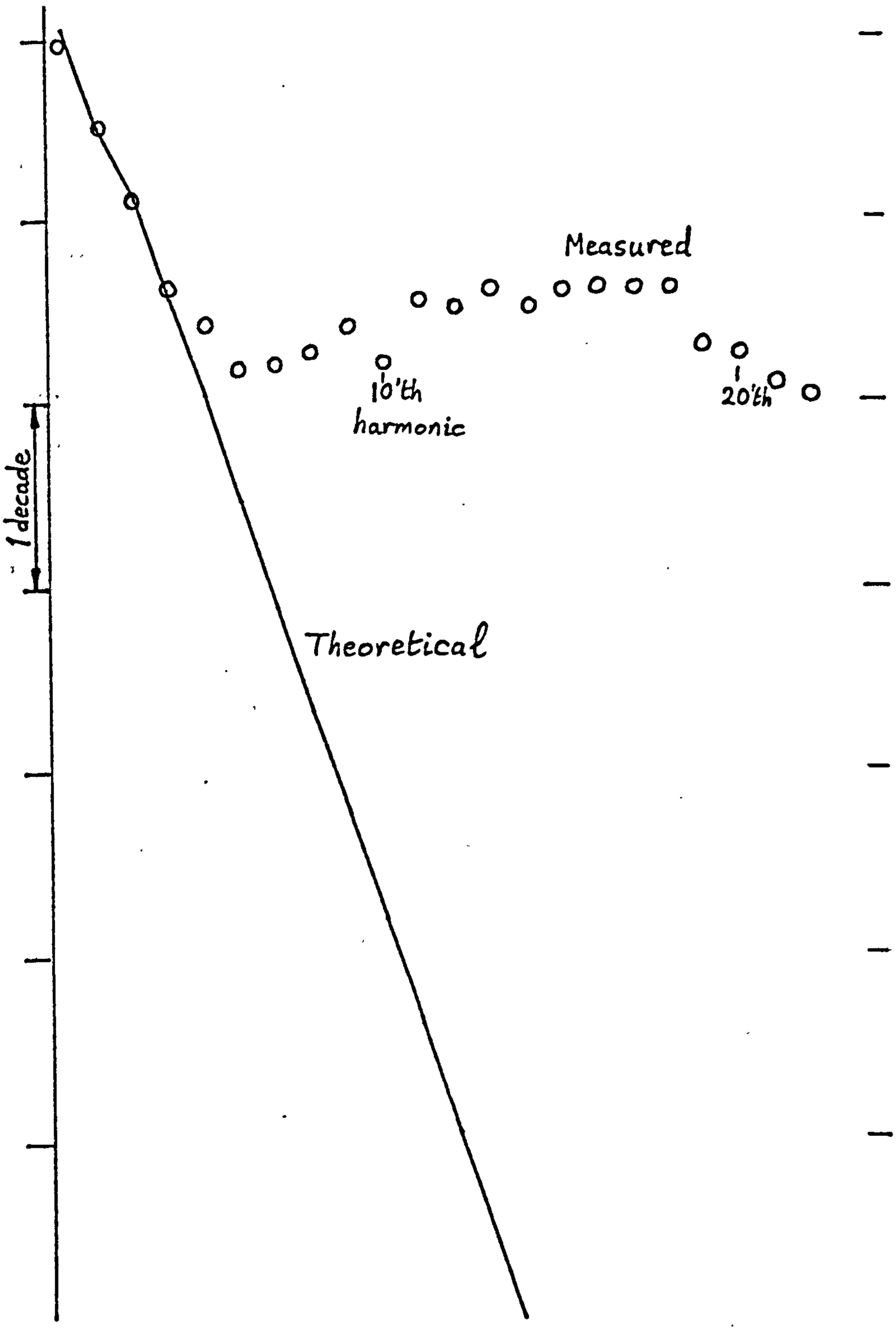

46.b: Frequency content of sewing machine needle holder acceleration

Their well-documented experimental results were particularly interesting: time-domain curves showed apparently good agreement, but the frequency domain comparison showed two revealing anomalies (see the reproduced figure •a.).

Firstly, the amplitudes of the resonant peaks could only be matched by using very different damping factors at each speed, and secondly the band-widths of the peaks were in practice at least an order of magnitude greater than predicted. Since the peaks all correspond to vibration at the same natural frequency (excited by different harmonics of the excitation) such differences in apparent damping can hardly be explained by the simplified model of damping used (as suggested by the authors). The second discrepancy suggests that the true damping factor is much higher than any of the extremely small values assumed and more like the order of 0.01 found in other experiments (see Section 2D). Thus instead of explaining the experimental resonances by applying enormous and greatly varied dynamic magnifiers to vanishingly small equilibrium amplitudes - the mechanism is kinematically very well-proportioned, so the frequency spectrum declines very sharply - we can deduce that the actual equilibrium amplitudes are both much larger and much more equal in size than those of the simulation. This is just as would be expected if there was any kind of discontinuous excitation arising from the joints or drive system (c.f. Figures 21•a,46•b).

A comparable phenomenon has been observed in measurements on an industrial sewing machine taken by two students under the supervision of the writer's colleague Dr. J.N. Fawcett. Briefly, a light piezo-electric accelerometer was attached to the needle holder and the signal therefrom was passed through a frequency analyser. An example of the results obtained is shown by the open circles in Figure •b (based on a private communication from Trenholme & Weighell). The full line shows the frequency composition of the calculated rigid body acceleration, which at low frequencies agrees well with the measurement. In addition, however, there is seen to be a significant level of vibration present at twenty and more times the crank speed. As the 20'th harmonic and above of the kinematic acceleration is clearly quite negligible, imperfections must again be inferred as the source of excitation.

A similar example is found in OLDHAM(b)'s frequency analysis of the signal from a strain-gauged coupler in a four-bar mechanism. He observed that the second and third natural frequencies at 75 Hz and 169 Hz (at about 14 dB less than the magnitude of the first: ibid, Fig. 14.3a) were visible at a

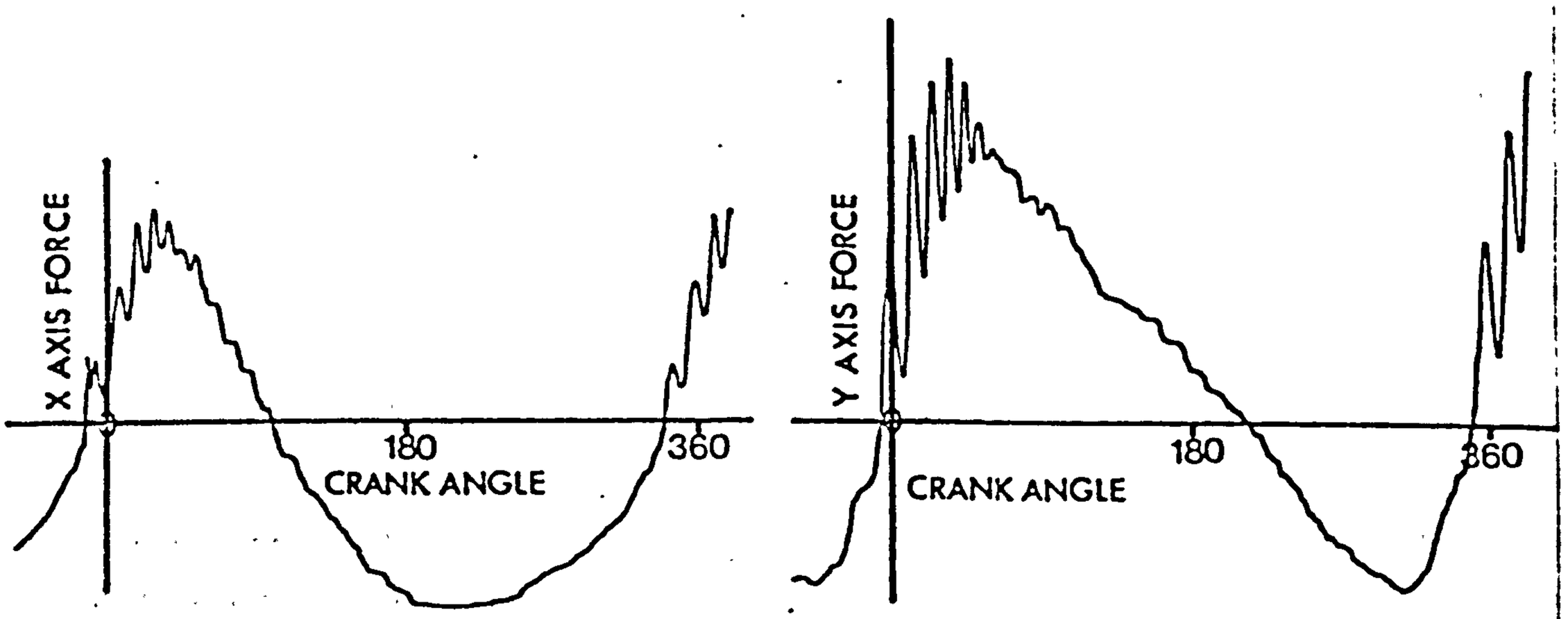

[ex: FIGURE 5.9] ROCKER/FRAME FORCE FOR 170 R.P.M.

47. a: Measured joint force for a 'rigid' linkage, ex WALKER

driving frequency of 2.5 Hz, implying that harmonics up to the 60'th and above are present in the motion; yet a Fourier analysis of the theoretical model showed the 32'nd harmonics of the kinematic terms to be of the order of 10^{-14} times those of the first (ibid., p14-7). (In the case quoted $|P/P_c|$ is estimated by the present writer not to exceed about 0.2, so the frequency variation should not affect the order of the result).

Walker observed yet another similar phenomenon in an investigation into the effect of balance weights on a supposedly rigid six-bar linkage. Loads transmitted at the frame joints were recorded by means of Piezo-electric bi-axial shear load transducers. Figure •a shows the cyclic variation of one component of the load, without balance weights. The frequency of the very evident vibration agrees with that predicted for the torsional mode of vibration of the drive shaft, but the relevant (nineteenth) harmonic of the predicted torque fluctuation is far too small to account for such a response. As the drive system included a flexible coupling driving a heavy flywheel, excitation from this source can be confidently ruled out, leaving joint backlash as the most obvious diagnosis.

Conclusions of review: It has been found that significant second-order and non-linear effects associated with link flexibility have not been clearly demonstrated except under conditions of, apparently, little practical relevance. Nevertheless there is a variety of experimental evidence that significant vibrations sometimes occur which cannot be accounted for by the inertial excitation arising from nominal kinematic accelerations. The frequency domain characteristics of this "anomalous" vibration, where known, appear to be consistent with discontinuous sources of excitation.

2M: CONCLUSIONS OF CHAPTER

The foregoing study suggests a number of objectives for the design of high-speed linkage mechanisms without excessive vibrations.

Input system: Particular attention should be paid to minimising the flexibility of the drive shaft and crank (if any). The natural frequency of the vibratory mode involving shaft torsion and/or bending of the input link should preferably exceed (say) twenty times the driving speed at all points in the cycle. The same would apply to intermediate shafts or bell-cranks. Motor controls should not produce pulses in the driving torque.

Frequency ratios: For each coupler-type link the natural frequency of bending should be estimated as though the link were 'simply supported' at its ends. If the link actuates considerably heavier links, the least natural frequency of the link in tension/compression should be estimated, treating the link in question as a light spring and the driven links as an attached equivalent mass. Each frequency so calculated should exceed ten times the driving speed, for crank-driven mechanisms with normal transmission angles and no discontinuities in loading. For cam-driven mechanisms, mechanisms with unusually severe transmission angles, or mechanisms where the function involves discontinuous external loads, considerably higher natural frequencies should be designed for. The bending natural frequencies of adjacent links should in any case differ by at least three times the fundamental driving frequency.

Joints: Impacts due to backlash should be eliminated and Coulomb friction minimised.

Curved links: Curvature or dog-legging of links should be avoided, whether in or out of the plane of motion.

If all the above objectives are satisfactorily achieved, the following procedure is appropriate for estimating loads and deflections.

First approximation: The loads at any instant should be found by the rigid-body method, and the deflections at any instant found by treating the inertial loads thus found as external loads applied statically, axial loads in binary links being neglected.

Second approximation: The end-loads found by the rigid body method should be taken into account in calculating the quasi-static bending deflection and the corresponding stresses for binary links: variations in axial load along the length should be neglected, the instantaneous mean of the two end loads being used, for example in conjunction with the tables for simultaneous axial and transverse loading in ROARK & YOUNG. The dynamic error should be estimated by considering only one mode of bending vibration per flexible link, without coupling. The dynamic error associated with the lower harmonics of the transverse acceleration at the mid-point should be estimated by equation 25·a, and the dynamic error associated with the harmonic nearest resonance should be estimated by applying an impulsive magnifier (equation 26·c) as well as an appropriate resonant magnifier to the corresponding harmonic of the quasi-static deflection.

Provided that the "second approximation" terms are found to be of an order smaller than the first approximation terms, further terms may be neglected.

Priorities for more detailed work: The broad investigation reported in this chapter has highlighted a number of topics requiring more detailed analysis. In view of the variety of cases where vibrations have been measured at an order of magnitude not predicted by sound theory, there seems to be little point in either refining or simplifying existing techniques without accounting for such "anomalous" vibration. Accordingly the major aim of the ensuing investigation will be to develop an improved understanding of one likely culprit: the effects of clearance at revolute joints.

Among the other points at which the simplified analysis described above breaks down, excessive flexibility of the input system has been identified as a probably significant factor in practical applications. Thus a secondary aim will be to elucidate the properties of Hill's equations of the type concerned.

CHAPTER 3

(Most of the material in this chapter has been published in the form of reference HAINES b; Section A is considerably modified, however, and Section I is entirely new).

Principal nomenclature

e	Radial clearance at joint.
M	Representative mass of linkage.
R	Magnitude of joint reaction force, calculated without clearance.
R_{min}	Locally minimum value of R with respect to time.
$\dot{\vartheta}$	Angular orientation (with respect to axis in ground) of joint reaction force vector without clearance.
$\dot{\vartheta}_o$	Value of $\dot{\vartheta}$ at instant when $R = R_{min}$.

3. A CRITICAL SURVEY OF 'LUDODYNAMIC' INVESTIGATIONS

3A: SCOPE AND ARRANGEMENT OF CHAPTER

Definition of problem: revolute joints in linkage mechanisms may take a number of technical forms: notably, rolling element bearings; plain journal bearings with oil supplied continuously so as to maintain a hydrodynamic regime; plain journal bearings with some form of boundary lubrication, as provided for example by oil-impregnated bearing sleeves - or just occasional applications of the oilcan; and journal bearings with solid (e.g. PTFE) lubrication. It is the third and fourth types that most obviously raise the question of vibration due to motion within the clearance, and it is this class that is the subject of the following survey. (The question of the motion of the pin within a hydrodynamically lubricated journal bearing has given rise to a large literature in its own right, of course).

The dynamic effects of clearance may be an important factor in many different classes of machine system, such as gear trains, cam-pushrod systems, pneumatic tools, and reciprocating heat engines - the problem of 'piston slap' - as well as in linkage mechanisms. Provided that the motion across the clearance is essentially one-dimensional, all of these cases have a substantial degree of similarity. In the case of revolute joints in linkage mechanisms, however, the problem usually involves two significant components of force and displacement, and this markedly changes its character. If in the one-dimensional case the contact force at the clearance location never changes sign, so that contact is never lost, then the system may be analysed - and the contact force predicted - as though there were no clearance. In the two-dimensional case, however, even if the two members (pin and journal) are in continuous contact, the possibility of relative movement around the 'clearance circle' modifies the system response, so that even the contact force cannot be predicted with confidence. This distinction marks a major division in the literature.

Considering that all the evidence of ludodynamically induced vibrations referred to in the last chapter was associated with revolute joints, it is appropriate to focus the following survey on studies of the two-dimensional behaviour of the latter. Studies of one-dimensional systems will be considered, however, to the extent that the techniques or results are applicable to the two-dimensional case.

Papers covered: The theoretical papers by Rao and by Bahgat et alia were considered by the writer to be so seriously flawed as to have no value. (Among other things, RAO omitted the transverse component of the inertial load on the coupler of a crank-slider mechanism; BAHGAT ET AL & OSMAN ET AL solved the equations of motion of the systems they studied as though the displacements, velocities and accelerations were wholly unrelated variables: thus they were left with more variables than independent equations, and the answers they obtained were arbitrary, not to say wholly implausible). These papers will accordingly not be considered further.

A number of authors have considered the purely kinematic consequences of joint clearance. (DUBOWSKY & GARDNER(b) have briefly reviewed these papers up to 1975). This is another quite separate issue that will not be considered here.

Subject to the aforementioned restrictions and omissions, the following survey is intended to be comprehensive as far as the English-language literature is concerned; a few non-English papers are also covered.

Arrangement: For a complete description of the phenomena under study, it is necessary to consider the following phases:

(i) Relative motion around the "clearance circle" up to the point where contact is lost.
(ii) Relative motion acrosss the clearance circle up to impact.
(iii) Interaction during the period of impact, and subsequent rebound.
(iv) Restoration of lasting contact.

In practice, it is likely that useful predictions can be obtained short of complete simulation. Nevertheless the above sequence will be used for convenience as a framework for the survey. The main focus will be on stage (i), which will be subdivided into general, mostly qualitative considerations; numerical simulations; and experimental results; in Sections B, C, D respectively. Investigations relating to stages (ii), (iii) and (iv) are then reviewed in Sections E, F, G respectively.

Sections B to G cover, more particularly, the papers that were reviewed in 1978, and therefore provide the background to the conclusions then drawn (presented in Section H) and the subsequent work described in Chapters 4 to 6. For completeness, the papers published or located subsequently are reviewed in a supplementary Section I.

3B: MOTION IN CONTACT : GENERAL

As GRANT & FAWCETT(b) have stressed, the motion-in-contact stage is in one sense the most important, since if loss of contact can be avoided the remaining stages never arise. FURUHASHI ET AL(a) have argued that even following contact loss, the motion quickly reconverges to the trajectory predicted on the assumption that contact is continuous. EARLES & WU(b) have contributed the valuable suggestion that if loss of contact is predicted, the margin by which the relevant threshold is breached will probably give a useful measure of the ensuing impact.

'Flypast' theories: The conditions leading to contact loss have been discussed in general terms by FAWCETT & BURDESS(a), EARLES & WU(b,c) and GRANT & FAWCETT(b). Fawcett and Burdess suggested that contact loss is likely to occur when the bearing force (calculated for zero clearance) undergoes a significant reduction in magnitude and rapid reversal in direction, an incident that may conveniently be termed a "fly-past". The important implication is that loss-of-contact occurrences might be predicted from examination of such incidents alone, the rest of the bearing force locus being ignored, as having relatively little effect.

More explicitly, Earles and Wu suggested that the effect of any given locus might be expressed as a function solely of (R_{min}) and ($\dot{\psi}_0$), where (R_{min}) is the minimum magnitude of the zero-clearance bearing force, ψ is its orientation, and $\dot{\psi}_0$ is the value of $\dot{\psi}$ when $R = R_{min}$. The argument here is essentially that $\dot{\psi}_0$ provides a measure of the disturbance at the joint and R_{min} provides a measure of its ability to withstand this disturbance without contact loss: Earles and Wu stressed that the criterion $R_{min}=0$ is very rarely met for a revolute joint. A brief examination of the implications of this assumption will be helpful for the subsequent discussion.

Firstly, it may be noted that whereas there appears to be no physical reason why a large value of $\dot{\psi}$ at some instant should affect the integrity of contact at that instant, the cumulative effect of the sudden increase and decrease in $\dot{\psi}$ during a flypast would indeed provide a serious disturbance, and the peak value ($\dot{\psi}_0$ in effect) provides a simple measure of the severity of the complete incident. Quantitatively, the level of "disturbance" might be represented by the excess of kinetic energy in the system, above that indicated by a zero-clearance analysis: then the supposition is that a flypast

defined by a given value of $\dot{\gamma}_0$ will give rise to a correlated increase in this "disturbance energy" - at least for a given linkage.

This interpretation leaves it unclear whether the effect of such incidents is distinct (as assumed implicitly by Earles and Wu) or cumulative - that is, whether the disturbance produced by one fly-past might be expected to die away before the next occurrence. This depends on the degree of damping in the system as well as the interval between successive flypasts, but estimating the damping effect even of a known coefficient of Coulomb friction is not straightforward in this situation.

One further qualitative deduction that can be made is that the most likely period for contact loss is shortly <u>after</u> $R = R_{min}$, since at $R = R_{min}$ the disturbance energy will in general still be accumulating rapidly.

<u>Earles' criterion</u>: Based on experimental work (considered in section D), EARLES & WU(b) proposed the criterion: contact maintained if $(\dot{\gamma}_0/R_{min}) < 1$ (rad/N/s). Although the attempt to identify a simple design criterion of this nature is clearly a valuable approach, the general applicability of this criterion must be in doubt at present, since (as the authors stress) it <u>cannot be cast in dimensionless form</u>. .a

By contrast, let us consider a dimensional analysis of the computer simulations by the same authors (EARLES & WU a). In the case of simulated motions of geometrically similar linkages in a horizontal plane (the clearance being excluded from the condition of geometrical similarity) there are four independent variables - clearance, driving speed, density and representative link-length, say - as against three arbitrary dimensional units. Thus the system may be defined by any one dimensionless group. A convenient group is $(\dot{\gamma}_0^2 e M/R_{min})$, where e is the radial clearance and M the mass of a representative link. Then similar values of this group would lead to similar simulated motions, so that the criterion for simulated contact loss must be a function of this group rather than of $(\dot{\gamma}_0/R_{min})$. This conflict in criterion perhaps indicates that a rather different mechanism of contact loss is involved in practice from that in the computer model. (Further light will be shed on this question in the next chapter). .b

GRANT & FAWCETT(b) have interpreted the Earles and Wu criterion as indicating that the actual point in the cycle at which contact is lost would correspond to $\dot{\vartheta}/R = 1(\text{rad/N/s})$. The arguments given above suggest this to be mistaken, however, since this condition would normally be met for the first time <u>before</u> R reaches R_{min}.

TEXT BOUND INTO

THE SPINE

Authors	References											
DUBOWSKY	a											
DUBOWSKY & GARDNER		b	a,b									
EARLES & WU				a								
WU & EARLES					●							
FURUHASHI ET AL						a,b						
MORITA ET AL						●						
GRANT & FAWCETT							c					
HAMMERSCHMIDT								●				
MIEDEMA & MANSOUR									●			
ROGERS & ANDREWS										●		
SERGEEV & YUDIN											●	
SHIMOJIMA ET AL												●
Assumptions/cases considered												
a)Links:(1)rigid;(2)deflect as Euler beams	1	2	2	1	1	1	1	1	1	1	1	1
b)Bearing surfaces:(1)rigid; (2) deflect elastically	2	2	2	1	1	1	1	2	1	2	1	1
c)Damping:(1)absent;(2)tangential Coulomb friction at joints; (3)viscous damping at bearing surface, radial and tangential;(4)ditto, radial only;(5)damping of output motion;(6)viscous damping of all motions.	3 + 5	3	3	1	1	6	1	4	5	3	1	* + 5
d)Drive has defined:(1)velocity; (2)torque;(3)inertia;(4)flexibility.	2	4	1	3	1	*	1	1	1	1	1	*
e)Linkage:(1)4-bar;(2)crank-slider;(3)other.	2	3	1	1	3	1	1	3	2	2†	2	2
f)Clearance at:(1)1 joint; (2)>1joint.	1	2	2	1	1	*	1	1	1	2	1	*
g)Clearance,e:(1)e<<gross motion;(2) e unrestricted.	2	1	1	2	2	2	2	2	2	2	2	2
h)Simulation begins:(1)when system quiescent;(2)at arbitrary phase.	2	2	2	1	1	2	1	2	2	2	2	2
i)Run time,T:(1)T<1 cycle; (2)to limit cycle;(3): (1)≡(2)	2	3	3	1	1	2	1	1	2	2	1	3

*: Assumption (2) included in formulation, but (1) explicitly or apparently adopted for case study presented.

†: Uses a "self-formulating" program which could equally be applied to many other linkages.

Table 55.a: Simulations of Motion-in-Contact Stage

3C: MOTION IN CONTACT : SIMULATIONS

Theoretical simulations of two-dimensional motion during contact at revolute joints have been reported in the references indicated in Table •a. This also summarizes the cases considered and the stated or apparent assumptions made in each case. It is seen that the simulations differ in a number of significant respects. The most suitable assumptions may vary to some extent from case to case, but some general observations may be offered.

Damping: The variation in assumptions concerning damping may be particularly important, since this affects the extent to which successive flypasts interact and the rate of convergence to a limit cycle. For this reason the inclusion of some appropriate form of damping seems to be desirable. In one model (c(3) in Table •a) there is a damping force at the bearing that is parallel, proportional, and opposed to the relative velocity vector. Although not unreasonable during the impact phase, this assumption leads to possibly questionable consequences during the continuous contact phase, namely a drag force proportional to the sliding velocity but independent of the radial load, and capable of dissipating more energy than in the impact phase. Experimental elucidation would be valuable here.

Multiple clearances: Heading 'f' in Table •a raises the question whether clearances at more than one joint introduce significant phenomena that cannot be predicted from a study of the clearances one at a time. The results of DUBOWSKY & GARDNER(b) suggest one such phenomenon in that impact in one joint is predicted to provoke immediate contact loss in another.

Size of clearance: Assumption 'g(1)' in Table •a arises from the unique treatment by DUBOWSKY & GARDNER(a,b) of the effect of clearance as a small order perturbation of the ideal kinematic motion. Since clearances are typically at least three orders of magnitude smaller than link lengths, the justification for this assumption seems to be beyond doubt. Thus, in view of the relative analytical simplicity and greater accuracy and computational efficiency that it makes possible, the perturbation approach should in the author's opinion be the preferred approach for future investigations. A further reduction in calculation time may be gained by the careful selection of starting conditions, as indicated by h(1) in Table •a .

Misalignment: It seems likely that the remaining differences between the models have relatively little effect on the behaviour during this phase. One restriction common to the models is the assumption that all the inertial forces and reactions lie in the same plane. Considering that a "planar" model with realistic clearances is strictly a spatial mechanism, even fairly small departures from the assumed condition may conceivably have a large effect on the likelihood or severity of contact-loss; if so, this would represent a major limitation on the existing analyses.

Oscillations: The simulation reported by HAMMERSCHMIDT does not include extended periods of contact. The others do, and all agree in predicting that loss of contact occurs shortly after a flypast. EARLES & WU(a), FURUHASHI ET AL(a,b), GRANT, MIEDEMA & MANSOUR, and ROGERS & ANDREWS all show or report circumferential oscillations superimposed on the zero-clearance motion: this may be regarded as a visible manifestation of the "disturbance energy" considered in the previous section! A paper by WU & EARLES states that "from the initial position the curves [with and without clearance] are identical up to the point when contact is lost", but WU makes it clear that this only refers to the gross motion, the oscillations being ignored. By contrast, FURUHASHI ET AL(a,b) stress that these circumferential oscillations may lead to considerable vibratory variations in both the driving torque and the joint forces, although this effect only appears for relatively large clearances (0.08mm). (In their simulations, in fact, contact loss does not occur except with still larger clearances). Oscillations are not visible in SHIMOJIMA ET AL's model but this may be due to almost critical damping caused by high friction at the output slider.

DUBOWSKY & GARDNER(b) do not show or comment on the circumferential motion in the time domain, but a polar plot makes it clear that during this phase of the motion radial oscillations are negligible. ROGERS' & ANDREW's simulation, by contrast, shows radial oscillations of about 15% of the size of the circumferential oscillations, which would throw some doubt on the models that assume rigid bearing surfaces, since the threshold for loss of contact might be considerably modified by such oscillations.

Pseudo-impact model: An alternative approach to that considered so far has been described by TOWNSEND & MANSOUR(a,b) (see also MANSOUR & TOWNSEND); that

is, to eliminate this phase altogether from the simulation procedure, so that it is represented in practice by a rapid succession of small impacts. As these authors point out, however, this procedure leads to problems when friction and imperfect resilience are included; and it does not readily lend itself to design for avoidance of true contact loss. (The actual procedure used in these references is questioned below).

3D: MOTION IN CONTACT ; EXPERIMENTAL RESULTS

Relevant experimental results have been reported by EARLES & WU(b,c), EARLES & KILIÇAY(a), FAWCETT & BURDESS(a), FURUHASHI ET AL(b), MORITA ET AL., GRANT & FAWCETT(a,b) and SHIMOJIMA ET AL. Earles and others measured the acceleration due to impact, so the only information revealed about the motion-in-contact phase is the circumstances in which it ceases to be continuous. The criterion "contact maintained if $\dot{\imath}_o/R_{min} < 1$(rad/N/s)" was obtained by extrapolation from an empirical formula that was fitted to the impact acceleration levels recorded in cases where contact was not maintained.

No attempt to test this criterion against the actual thresholds of contact loss observed in the full set of experiments was reported. GRANT's results were reported (GRANT & FAWCETTa) as confirming the Earles and Wu criterion. However, the agreement is only qualitative and does nothing to discriminate between this criterion and a variety of possible alternative criteria, the experiment not having been designed principally for this purpose. For example, impacts are recorded (albeit small) for $\dot{\imath}_o/R_{min}$ as low as 0.32, whereas no impacts are recorded (at small clearance) in one case where $\dot{\imath}_o/R_{min}$ is as high as 220. (Values calculated by the present author, following Grant's method).

Grant also measured the relative motion at the joint, (GRANT, GRANT & FAWCETTb). The results are not presented in the time domain, so some difficulties of interpretation arise, but they appear to suggest that oscillations are rapidly damped. Radial oscillations appear to be quite significant, but as the displacement transducers are only mounted on one side of the joint it is not possible to eliminate the effect of out-of-plane angular oscillations which could produce similar measurements.

FAWCETT & BURDESS(a) measured the contact force, but presented this only in Cartesian components. The oscillations following impact were found to die out after about 1/6th of a cycle.

Shimojima et alia, like Grant, measured the relative displacement on only one side of a bearing, using a stroboscopic optical method (which assumes the existence of a stable limit cycle). The clearance in this case was exceptionally high (1 mm radial) and the friction force was comparable to the inertia force, so the results may be atypical. There is some evidence of circumferential oscillation. The points where no-contact was recorded do not agree very well with the points predicted.

Earles and Kiliçay recorded accelerations on a special linkage with clearance at two revolute joints, but found no evidence of contact loss at one being affected by the other.

Morita et al measured the fluctuations in driving torque and found good agreement in frequency and magnitude with the predicted fluctuations associated with circumferential oscillations without contact loss. This important result demonstrates the reality and significance of the circumferential oscillations, and provides some support for the assumption of rigid bearing surfaces during this phase, and for the dissipative damping model assumed in FURUHASHI ET AL(a). Evidence of contact loss was seen in some cases, but the threshold for contact loss did not agree with that predicted.

3E: MOTION ACROSS THE CLEARANCE

Some of the simulations discussed under the previous heading also cover motion after loss of contact (DUBOWSKY, DUBOWSKY & GARDNERa,b, HAMMERSCHMIDT, MIEDEMA & MANSOUR, ROGERS & ANDREWS, SERGEEV & YUDIN, SHIMOJIMA ET AL). In addition, GRANT postulated that the end of the trajectory (impact point) would be in line with $\dot{s}$ at $R = R_{min}$, but offered no justification for this.

Apart from the effect on computation efficiency, it seems likely that the different assumptions indicated in Table 55.a have little effect during this phase of the motion. An additional assumption introduced by DUBOWSKY & YOUNG for a simulation of a one-dimensional case is that friction (Coulomb and viscous) occurs on the thrust faces of the joint. This phenomenon, which reduces the magnitude of the succeeding impact, may be significant for linkages acting in a non-vertical plane.

TOWNSEND & MANSOUR describe a technique for approximating the time between "closely spaced impacts". In fact, the method they describe involves a truncated Taylor series which seems to amount to their disregarding the curvature of the clearance circle in comparison with the curvature of the relative flight-path: for example, it yields an infinite time interval if the relative flight-path is a straight line (equivalent to $\ddot{\theta}_s = 0$ in their notation). As the justification for this is not clear, the writer cannot accept the results obtained by this method (MANSOUR & TOWNSEND) on the strength of the arguments reported.

Severity of impact: The purpose of simulating this phase is to predict the velocity and angle of approach at the end of the phase, and thus the severity of the ensuing impact. In most cases the results are presented in terms of some measure of the latter such as peak force or acceleration, but in reviewing these results it should be borne in mind that they are also affected by the precise mechanism of impact, considered in the next section.

The most consistent finding is that the level of impact, by a variety of measures, increases at an increasing rate with the magnitude of clearance. This has been both predicted (by DUBOWSKY, DUBOWSKY & GARDNERa,b and MANSOUR & TOWNSEND) and found experimentally (EARLES & WU b,c, FAWCETT & BURDESSa). This increase is much less marked at higher frequencies in a simulation that incorporates bearing compliance (DUBOWSKY) presumably because elastic deflect-

ions then have a relatively greater effect. The predicted level of impact has also been found to vary with such parameters as the velocity of the drive shaft (DUBOWSKY). The experimentally determined levels of impact have likewise been related to other factors, such as the margin by which the empirical loss of contact criterion is breached (EARLES & WUb,c) and the relative angular acceleration at the joint (EARLES & KILIÇAYa). More generally, Dubowsky has drawn a comparison between the variation in predicted impact levels and that obtained from a simplified, one dimensional analogue known as an impact pair (DUBOWSKY), and an improved version known as an impact beam (DUBOWSKY & GARDNERa). MIEDEMA & MANSOUR have highlighted the predicted clustering of the points of major impact on the bearing and journal surface. All these results suggest possible design guidelines, subject to the limitations of the various models as noted previously.

3F: IMPACT AND REBOUND STAGE

Ideally, a theory of the impact and rebound stage should be able to predict the components of the rebound velocity, the frequency content of the impulse generated, and the peak stress at the contact region. A great many theoretical and experimental investigations into impact in general have been carried out over a long period, a classic compilation of the less recent work being given by GOLDSMITH. However, little of this knowledge is strictly applicable to the case of impact that concerns us here, namely impact between highly conformable surfaces, at low approach speeds (because of the small clearance) and arbitrary approach angles, of beam-like bodies at arbitrary orientations.

Spring-damper models: Because of the conformable profiles and low approach speeds, it has been argued (see DUBOWSKY & YOUNG, HUNT & CROSSLEY) that the energy loss at impact is likely to be associated with material damping (rather than micro-plastic deformation), which suggests a "Kelvin-Voigt" model (spring and damper in parallel) for the contacting surfaces. The spring function for this model may be taken to be that given by a form of Hertzian contact theory (cf HUNT & CROSSLEY, ROARK & YOUNG Ch.5) which, although strictly a static theory, can give good approximations of impact behaviour according to GOLDSMITH; or a piecewise-linear approximation to this. For small clearances, however, this may be inappropriate since the length of the contact zone may not be negligible in comparison with the radius of curvature (see ESHWAR). DUBOWSKY & YOUNG cite a numerical solution for the latter case which gives a significantly higher stiffness. There is some dispute over whether the piecewise-linear approximation is acceptable: DUBOWSKY & YOUNG's results suggest that it is, while those of VELUSWAMI ET AL suggest that it is not.

Several workers, notably DUBOWSKY & FREUDENSTEIN have assumed a linear viscous damping law for the Kelvin-Voigt model with a coefficient obtained by analogy with non-impactive vibration. However, from a close examination of the differences between the latter case and the vibro-impact case, HUNT & CROSSLEY followed by HERBERT & McWHANNEL have argued that the damping coefficient in the case of vibroimpact should be proportional to a power 'n' of the spring force, adopting in practice the assumption that $n=1$ on the grounds of analytic convenience. The advantages of this modification are claimed by

HUNT & CROSSLEY to be a better representation of the variation of impactive energy loss with approach velocity and by HERBERT & McWHANNEL to be a more realistic frequency content in the impulse generated. In both of these investigations quantitative results have been derived using GOLDSMITH's empirical data, HERBERT & McWHANNEL's "direct" method being the more general. Experimental tests of the Hunt and Crossley modification have been reported by HAYASHI ET AL. and VELUSWAMI ET AL. as favourable in the case of spheres and plates, but reported by CROSSLEY ET AL. as unfavourable in the case of cylinders and plates. OLĘDZKI ET AL. have argued that the classic results can be better reproduced by using a quadratic damping law independent of the spring force; with supporting results from a Geneva mechanism (OLĘDZKI & SZYDLOWSKI).

Effect of link compliance: The character of impact between beam-like bodies has long been known to differ significantly from that of impact between compact bodies, but studies of the former have been focused on either purely longitudinal (compressive) or purely transverse (bending/shear) impact. Of the 2-D investigations reviewed here, only DUBOWSKY & GARDNER(a,b) take any account of the beam-like character of typical mechanism links, by including a modal analysis of bending in their simulations. The effects of axial loading, and of elastic deformation of the bearing housing under "tensile" impact, are excluded. Nevertheless, their simulations show a substantial reduction in the impact levels when the bending flexibility is included, leading to the suggestion that a calculated reduction in the link sections may be used to improve performance. Results by DUBOWSKY & YOUNG provide some experimental support for this approach, and for the Kelvin-Voigt model in general, in the case of a revolute joint subject to one-dimensional vibro-impact. Further experimental support has recently been reported by DUBOWSKY & MOENING, for a non-revolute joint. One apparent implication of the effect of link resilience is that the rebound velocity for a given approach velocity may vary with the position of the point of impact with respect to the two members.

Pulse shape: The phenomena considered in the previous paragraph must also significantly affect the pulse shape; indeed, in view of the complex shape of the bodies surrounding a pin and journal, a finite element analysis as described by BECKETT ET ALIA may be the only way to establish the pulse

shape with sufficient accuracy to permit "tuning" of gaps in the frequency content, as suggested by HERBERT & McWHANNEL. Even then, the frequency spectrum may well change significantly with the clearance, and thus with the age of the bearing; and furthermore even very small misalignments at the point of impact have been found by CROSSLEY ET AL. to have a considerable effect on the period of contact.

Momentum exchange models: An approach altogether simpler than the Kelvin-Voigt model is that based on momentum exchange and an assumed "coefficient of restitution". This treats the impact phase as taking place in an instant, i.e. a period of negligible duration compared with that of the other phases. This leads to a problem considered in the next section and rules out a direct prediction of the maximum stress generated or the frequency content of the impulse, although the former could be determined by a separate analysis, such as that of JOHNSON. In simulations using this method by MANSOUR & TOWNSEND, MIEDEMA & MANSOUR, TOWNSEND & MANSOUR and SHIMOJIMA ET AL. a constant coefficient of restitution has been assumed, so the results are presumably more approximate than those obtainable using the Kelvin-Voigt model.

Tangential effects: The effect of oblique angles of approach has not received great attention in the present context. Some investigators using spring-damper models have postulated that the damping force diametrically opposes the relative velocity of approach (see Table 5.a). As noted in section C,this has questionable consequences during the continuous contact phase, but these would be effectively reduced by using the HUNT & CROSSLEY modification (damping coefficient proportional to normal load), since the normal load is typically much smaller during the continuous contact phases than during the impact phases. Tangential elastic forces and Coulomb friction at impact are not incorporated in any of the spring-damper models, but friction is included by MIEDEMA & MANSOUR and TOWNSEND & MANSOUR in their momentum exchange models. In a different context Cunningham and Goldsmith have shown the peak stress generated by impact at angle θ to the normal to be approximately proportional to the cosine of θ (see GOLDSMITH), while the work of MAW ET AL. has demonstrated some counter-intuitive results. However, neither these three degree of freedom studies (of impact between a sphere and a beam or plate) nor a one degree of freedom analogue suggested by DIX are

directly applicable to the present case, which is essentially a two degree of freedom case.

Model sensitivity: VELUSWAMI ET ALIA have pointed out that since one-dimensional vibro-impact involves a sequence of rebounds, a small discrepancy in the model may lead to cumulative errors so that the system converges to a different limit cycle. By contrast, since the bouncing motion in the two-dimensional case is characteristically interrupted by periods of sliding in which the different predicted trajectories converge, the need for an accurate model of impact is somewhat reduced and in this case some of the sophistications discussed above may prove to be superfluous.

3G: RESTORATION OF CONTACT

If a (non-zero) constant coefficient of restitution model is used to simulate impact, a non-zero rebound velocity is always obtained, so restoration of continuous contact is never directly predicted, although experiments show that it certainly occurs. A variety of methods of dealing with this have been reported.

TOWNSEND & MANSOUR(a) ignore the motion-in-contact mode entirely, being content to reproduce it approximately with a close succession of small pseudo-impacts. MIEDEMA & MANSOUR assume that continuous contact is restored unless the analysis of that mode predicts the immediate re-loss of contact, in which case presumably the "coefficient of restitution" equation is introduced to determine the rebound velocity. SERGEEV & YUDIN do not consider this problem, their method being apparently equivalent to the assumption of zero coefficient of restitution. WILSON & FAWCETT ignore the rebound velocity if it falls below a threshold value. TATARA shows in a different context that the spring-damper model implies a coefficient of restitution that varies (down to zero) with the effective external force present at the point of impact.

The first method is computationally not ideal (see also comments in Section E). The justification for the second and third methods is questionable, while the fourth is necessarily arbitrary. Tatara's method would seem to offer the basis for resolving this problem more satisfactorily.

3H: PROVISIONAL ASSESSMENT & PRIORITIES FOR INVESTIGATION

The problem of sensibly two-dimensional vibro-impact at revolute joints has been shown to provide an important field of enquiry with some interesting and distinctive characteristics. In addition to some broad guidelines (both theoretical and empirical) for estimating the overall level of performance that may be expected, a wide array of theoretical techniques is available for simulating, in specific cases, each stage of the cyclic behaviour.

General models: The broad guidelines for the largely one-dimensional case, such as those provided by Dubowsky's "Impact Pair" and "Impact Beam", are of value in the initial stages of design synthesis. Earles' investigations provide a first approach to the development of a similar tool for the two-dimensional case. Further investigation is necessary to clear up the dimensional anomaly of his empirical criterion in its present form and to relate it to theoretical studies.

Simulations and experiments: For simulations the main question is what set of simplifying assumptions to adopt. The following assumptions may be considered for simulations of the motion-in-contact and motion-across-clearance stages:-

- The clearance is very small by comparison with the gross displacements of the links.
- Loss of contact is a function solely of "flypast" incidents in the ideal joint load locus (rather than the entire locus).
- Such incidents are distinct rather than cumulative in their effects.
- Loss of contact at a given joint is not materially affected by clearance elsewhere.
- Loss of contact is not materially affected by elastic compliance of the joint elements; by imperfect alignment or imperfectly coplanar inertial forces; or by the specific character of the energy dissipation function, provided that it is sufficient to suppress any cumulative effect from successive cycles.

For simulation of the impact stage, the simplest assumption is that impact is instantaneous and that the coefficient of restitution is not affected by imperfect alignment, by the gross geometry of the linkage pair forming the joint or by the speed or angle of relative approach. More sophisticated methods involve assumptions of a law of damping during finite periods of compression and recovery.

The simulations reported cover widely varied levels of sophistication, although every simulation incorporates at least one of the above simplifications and no simulation incorporates them all. Experimental investigation of the behaviour has been less complete, serving on the whole to confirm the broad applicability of particular theoretical models in a range of typical instances rather than to delineate their limits of applicability, or to discriminate between competing models. It appears likely that the minimum set of assumptions necessary to yield the desired information will vary from application to application, but the evidence reviewed does suggest that simulations using the simplest set of assumptions would adequately predict at least some features of the behaviour in at least some cases.

Priorities: Two priorities may be identified for the subsequent investigation. Firstly, a theoretical analysis using the full set of simplifying assumptions should be attempted in the hope of extracting general design guidelines and providing a consistent theoretical framework for the empirical approach of Earles and his colleagues. Secondly, an empirical investigation should be mounted with the express purpose of discriminating between the competing models for each aspect of the problem.

3I: SUPPLEMENTARY REVIEW

This section covers papers published, located or translated since 1978. Although placed here for ease of reference, it may be appropriately read after Chapters 4 to 6.

Contact loss: Theoretical studies of the conditions leading to contact loss were carried out by DUBOWSKY ET AL and by HAINES(c). (The content of the latter study is incorporated in Chapter 4 of this thesis, so will not be considered here). Dubowsky et al's model comprised a heavy bearing pin with no attached linkage, moving freely in a journal: the latter was constrained to move in an elliptical path in the horizontal plane at circular frequency ω. In the special case of a circular path, "Earles' criterion" taken literally predicts that contact loss becomes inevitable in this model if ω is sufficiently reduced, which the authors regarded as physically incredible. They proposed an alternative criterion, but as this still leads to the conclusion that contact loss becomes inevitable as $\omega \to 0$ for any non-circular path, thus hardly seems any more realistic. One of the sets of simulations predicted that contact loss would be affected by ω for a given path and clearance, and is therefore not a function solely of the dimensionless group $\dot{\gamma}_o^2 e M / R_{min}$ suggested in Section 3B, above; that group being independent of ω in this application. The sensitivity to ω may be related to the surface elasticity included in the model, which was regarded by the authors as a key factor.

EARLES & KILICAY(b) published further experimental evidence in support of Earles' contact loss criterion, now expressed in the form: contact maintained if $(\dot{\gamma}/R)_{max} < 1$ (rad/N-sec) throughout the cycle. Qualitatively, the determining role of flypasts is established beyond reasonable doubt by this work (as well as by that of FUNABASHI ET AL a,b considered below). The quantitative prediction was stated in summary to be borne out in each of the many cases where the criterion was met, whereas contact was stated to be lost in every case where $\dot{\gamma}/R$ exceeded 3 (rad/N-sec) at least once in the cycle (though not at every flypast for which $\dot{\gamma}/R$ exceeded 3, which is surely more to the point). The specific cases cited (and others cited by KILICAY) make it clear that this refers to the bearings with wider clearances (e.g. 90 μm on a 25 mm pin), the tighter bearings (e.g. 15 μm) usually remaining apparently impact-free. The experimental test of contact loss was a "significant" disturbance in the signals from accelerometers mounted close

to the bearings in question. Considering the numerous predictions and growing experimental evidence (cf. MORITA ET AL and below) that sudden sharp accelerations at flypasts are a normal feature of ludodynamic behaviour even where contact is maintained, it must be questioned whether this form of test can actually distinguish a true impact. Whether the impulsive acceleration appears "significant" is then in some part a function of the transducer gain.

Simulations and experimental results: FUNABASHI ET AL(a,b) carried out a comprehensive theoretical and experimental investigation into all aspects of ludodynamic behaviour in a crank-slider mechanism with a single clearance and a crank-rocker mechanism with multiple clearances. Measurements of both displacement and load showed good agreement with the simulations (although no attempt was made to identify stringent test conditions such as contact-loss thresholds); the main discrepancy was attributed to drive-shaft elasticity. Multiple clearances were found to increase the severity of the driving torque fluctuations. Interesting features of the published measurements include a major impulse just before loss of contact (Fig. 12d of Ref.a); distinct impulses at flypasts with no detected loss of contact (Figs. 5a(i) and 6a of Ref.b); major impulses after very small separations, occurring just after a flypast (Figs. 5a(iii) and 6c of Ref. b).

Similar phenomena can be seen in measurements by HAIN, on a scotch yoke mechanism incorporating a sliding block with clearance in the revolute joint. Two periods of contact loss led to modest impulses in the measured torque, but far greater impulses were recorded with no measured contact loss: these occurred just after rapid changes in the contact angle.

Simulations by HAMMERSCHMIDT & STRUMPFEL that incorporated bearing surface flexibility showed marked radial oscillations in the continuous contact phase, but these were largely absent in the corresponding experimental results. (The latter result must cast some doubt on the simulations of DUBOWSKY ET AL discussed above).

Impact phase: An early paper by BARKAN & TUOHY considered the problem of one-dimensional impact between a four-bar linkage and an external body. The authors presented an approximate solution for cases where the geometry and mass distribution is such that the link concerned is already undergoing rapid

acceleration or deceleration before impact. (In this case the change in velocity from that cause during the finite impact time may be of the same order as the change due to impact itself, so that the effective "approach velocity" to use is not obvious).

FUJITA & HATTORI reported excellent agreement by various criteria between theory and experiment for the case of repetitive impact between spherical and plane bodies. The damping law used was similar to that of HUNT & CROSSLEY, described above (p62). BRACH treated 2 d-o-f oblique impact.

SCHOLES & STROVER described a finite-element method for determining the elastic rigidity of a pin and journal connection.

ROGERS & PICK simulated the motion of a heat exchanger tube constrained by a circular baffle, but without good agreement with the measured behaviour.

Acoustic effects: The study of ludodynamic effects has been extended to another stage by PERREIRA & DUBOWSKY, who developed a method for predicting the acoustic radiation generated by a linkage mechanism with clearance and flexibility, taking the foundation as rigid. A significant conclusion was that not only reduced clearances, but also increased link flexibility or joint compliance led to useful reductions in the predicted noise levels.

CHAPTER 4

AN APPROXIMATE THEORY OF THE LUDODYNAMIC BEHAVIOUR OF A REVOLUTE JOINT IN A GENERAL LINKAGE

Most of the material in this Chapter has been published as Reference HAINES(c). Section E has not been published before, and additionally Section A is modified, equation 77·b is corrected, and significant new material is included at pages 87, 88.

Nomenclature for this chapter is given below and overleaf: this also applies to the related Appendices, namely 10H to 10L.

Symbols	Meaning
$A_0\, A_1\, A_2\, A_3$ } $B_0\, B_1\, B_2\, B_3$ }	Coefficients in equations defining trajectory after contact loss (equations 84·f).
E	Coefficient of restitution between joint members.
e	Radial clearance at joint.
$H_1\, H_2\, H_3$	Dimensionless parameters governing a 'standard' flypast (equations 78·d-78·f).
$\tilde{I}$	Dimensionless index of impact severity, $\equiv (1-\varepsilon^2)\, V_N \,/\, (1+\varepsilon \cos(2\gamma + 2\beta_i))$
J_r	Moment of inertia of link 'r.'
M_r	Mass of link 'r.'
$M_u\; M_u''\; M_{uu}\; M_{uv}$	Generalised inertia terms, see equations 75·f – 75·i. } [M_{uu}, M_{uv}, M_{vv} are elements of the "generalised inertia tensor".]
M_{vv}	Generalised inertia term analogous to M_{uu}.
M_o	Generalised effective inertia, defined by equation 77·a.
$R;\; R_u\, R_v$	Magnitude and components of contact force vector.
$S_u\, S_v$	Components of the contact force under static conditions.

Symbols	Meaning
t	Time: $t=0$ when $R_v^*=0$ in a "standard Flypast" (78·a).
u } $v(=v)$ }	Cartesian coordinates of the pin displacement within the journal.
$\tilde{V}_N$ } $\tilde{V}_T$ }	Normal and transverse components of relative velocity of approach, in *dimensionless form.*
X_r Y_r	Global Cartesian coordinates of the centre of mass of link 'r'.
α	Angle by which <u>actual</u> force vector lags <u>nominal</u> ($\equiv \vartheta^* - \vartheta$).
ϑ	Inclination of contact force vector.
ε	Eccentricity of inertia tensor, equation 77·c.
η	Inclination of major axis of inertia tensor, equation 77·b.
θ	Crank angle.
λ_r	Inclination of link 'r' (arbitrary datum).
τ	Reduced (dimensionless) time; $\equiv \tan\vartheta^*$
$\delta\tau_i$; $\delta\tau_1$	$\delta\tau_i \equiv \tau_i - \tau_\ell$ (see below); $\delta\tau_1$ is a first approximation to $\delta\tau_i$.
Σ	Summation for every link 'r' in the mechanism.
Φ_r	Virtual work done by link 'r' against spring & gravity forces.
Ψ_r	Virtual work done by link 'r' against d'Alembert forces.

<u>Subscripts etc.</u>

i	Value at instant of recontact between pin and journal.
ℓ	Value at instant of loss of contact between pin and journal.
$*$	Indicates applicability to the nominal (no clearance) mechanism.
$'$	Indicates a dummy variable which may or may not correspond to the actual variable.
r	Index of link concerned.

4. AN APPROXIMATE THEORY OF THE LUDODYNAMIC BEHAVIOUR OF A REVOLUTE JOINT IN A GENERAL LINKAGE

4A: AIMS & ASSUMPTIONS

In the preceding chapter the detailed simulation techniques developed for design analysis were contrasted with simple heuristic models suitable for guiding the initial stages of design synthesis. The aim of this chapter is to improve upon the latter models, in the case (as before) of two-dimensional ludodynamic behaviour at revolute joints. To achieve results of maximum generality, it is necessary to adopt a full set of reasonably plausible simplifying assumptions. These may be stated formally as follows:

.a The nominal mechanism* has one degree of freedom, associated with a crankshaft drive running with constant speed or other fixed motion.

.b The mechanism is perfectly planar, with coplanar dynamic and static loads.

.c All links and bearing surfaces are rigid.

.d Friction is light, and may be ignored except insofar as any oscillations that appear are assumed to be moderately damped. There is insufficient liquid lubricant present (if any) to cause hydrodynamic effects.

.e The behaviour at the joint in question is not affected by backlash elsewhere.

.f The clearance at the joint in question is very small compared with any dimensionally similar expression associated with the nominal mechanism.

.g Whether contact is lost or maintained is determined by the conditions obtaining at 'flypasts' (see Section 3B). There is no overlap between the transient effects of such incidents.

.h The coefficient of restitution is constant and known.

.i The forces associated with momentum exchange during impact are large by comparison with the nominal contact forces at the same instant, the impact being quasi-instantaneous.

Each of these assumptions has been made or implied in at least one of the previous investigations surveyed, but no investigation incorporated them all. Moreover, assumption (72.g) will be interpreted here in a novel fashion. In view of the relative brevity of the 'flypast' incidents, the values of certain governing variables (identified later) will be assumed not to change

*: i.e. with clearance neglected.

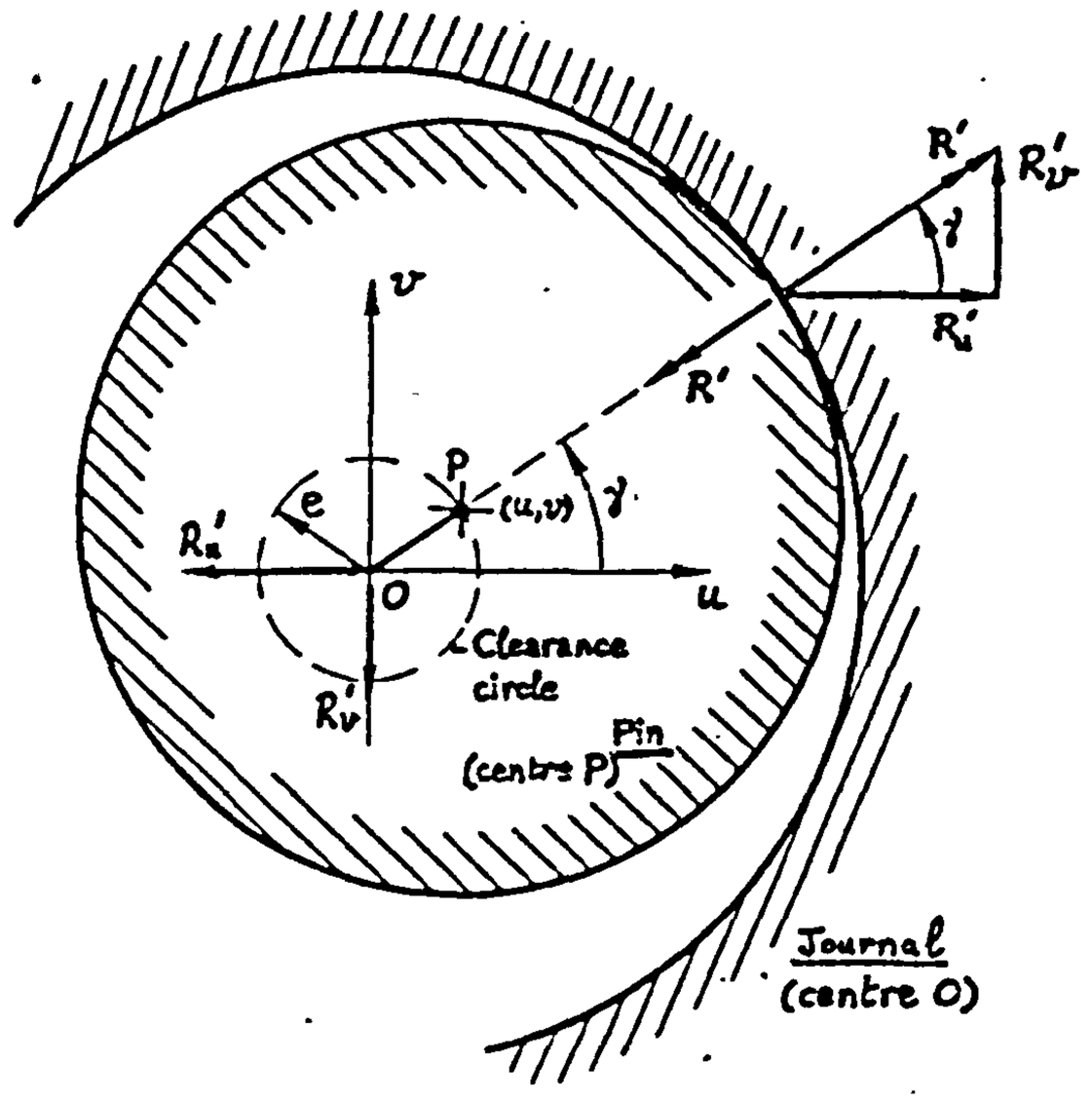

74.a: Typical revolute joint (clearance exaggerated)

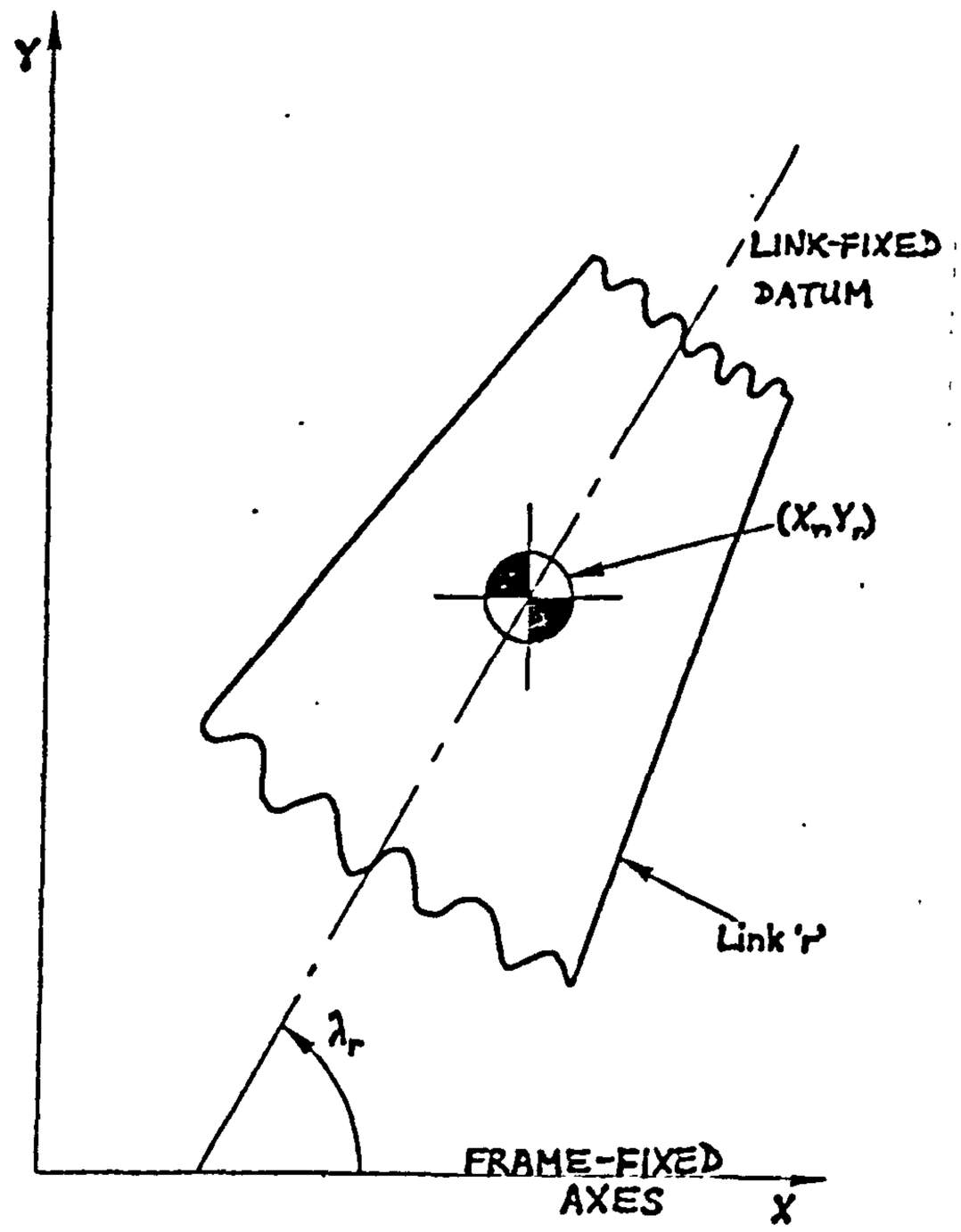

74.b: Typical link

4B: DEVELOPMENT OF THE GENERAL THEORY

Derivation of equations of motion: Fig. •a illustrates the nomenclature for the joint in question, shown in the 'following' mode, and Fig. •b that for a typical link 'r'. The system with clearance included has in general three degrees of freedom, which may be identified with three fundamental coordinates. The chosen coordinates are the crank angle (θ) and the (arbitrarily oriented) coordinates of the relative pin displacement (u, v). The inclusion of a fixed-motion drive eliminates the degree of freedom associated with θ, which becomes a predetermined time-varying parameter. The additional constraint present in the "following" mode, which eliminates another degree of freedom, will not be taken into account until later in this section.

In order to determine the influence of the entire mechanism on the clearance joint, we consider the effect of a pair of equal and opposite external forces, one applied to the pin and one to the journal, acting through O with components R_u', R_v' as shown in Fig. •a. For any given constant value of (u, v, θ) there will be certain values (S_u, S_v) of these dummy external forces which would be necessary in order to maintain the mechanism in equilibrium with any static (spring and gravity) forces that apply. Then according to the principle of virtual work, $-S_u \delta u + \Sigma \delta \bar{\phi}_r = 0$, where $\delta \bar{\phi}_r$ is the work done against static forces by link r due to a small virtual increase δu in u. (The Σ sign indicates summation for every link r). The principle of virtual work can also be extended to the dynamic case if d'Alembert forces are included: thus $-R_u' \delta u + \Sigma(\delta \bar{\phi}_r + \delta \bar{\psi}_r) = 0$, where $\delta \bar{\psi}_r$ is the corresponding work done against d'Alembert forces by link r. Comparing the two equations, we obtain $-R_u' \delta u + S_u \delta u + \Sigma \delta \bar{\psi}_r = 0$, which expanded gives

$$-R_u' \delta u + S_u \delta u - \Sigma[M_r \ddot{X}_r (\partial X_r/\partial u) \delta u + M_r \ddot{Y}_r (\partial Y_r/\partial u) \delta u + J_r \ddot{\lambda}_r (\partial \lambda_r/\partial u) \delta u] = 0 \qquad \text{•c}$$

since the displacement against the d'Alembert force $-M_r \ddot{X}_r$ is $(\partial X_r/\partial u)\delta u$ and similarly. Likewise

$$-R_v' \delta v + S_v \delta v - \Sigma[M_r \ddot{X}_r (\partial X_r/\partial v) \delta v + M_r \ddot{Y}_r (\partial Y_r/\partial v) \delta v + J_r \ddot{\lambda}_r (\partial \lambda_r/\partial v) \delta v] = 0 \qquad \text{•d}$$

The total derivatives $\ddot{X}_r$, $\ddot{Y}_r$, and $\ddot{\lambda}_r$ above may be expanded in terms of the partial derivatives with respect to the fundamental coordinates. Thus, taking $\ddot{X}_r$ for example,

$$\ddot{X}_r = (\partial X_r/\partial\theta)\,\ddot{\theta} + (\partial^2 X_r/\partial\theta^2)\dot{\theta}^2 + (\partial X_r/\partial u)\ddot{u} + (\partial X_r/\partial v)\ddot{v}$$
$$+ (\partial^2 X_r/\partial u^2)\dot{u}^2 + (\partial^2 X_r/\partial v^2)\dot{v}^2 + 2(\partial^2 X_r/\partial u\,\partial\theta)\dot{u}\dot{\theta} + 2(\partial^2 X_r/\partial v\,\partial\theta)\dot{v}\dot{\theta}$$
$$+ 2(\partial^2 X_r/\partial u\,\partial v)\dot{u}\dot{v}. \qquad \cdot a$$

By virtue of Assumption (72·f), as shown in Appendix 10H, the last five terms may be neglected; and the derivatives in the first three (sometimes termed "influence coefficients") may be replaced by their nominal values. Thus we obtain

$$\ddot{X}_r = (\partial X_r/\partial\theta)^*\,\ddot{\theta} + (\partial^2 X_r/\partial\theta^2)^*\,\dot{\theta}^2 + (\partial X_r/\partial u)^*\,\ddot{u} + (\partial X_r/\partial v)\,\ddot{v}. \qquad \cdot b$$

Similarly

$$\ddot{Y}_r = (\partial Y_r/\partial\theta)^*\,\ddot{\theta} + (\partial^2 Y_r/\partial\theta^2)^*\,\dot{\theta}^2 + (\partial Y_r/\partial u)^*\,\ddot{u} + (\partial Y_r/\partial v)^*\ddot{v}; \qquad \cdot c$$

$$\ddot{\lambda}_r = (\partial\lambda_r/\partial\theta)^*\,\ddot{\theta} + (\partial^2\lambda_r/\partial\theta^2)^*\,\dot{\theta}^2 + (\partial\lambda_r/\partial u)^*\,\ddot{u} + (\partial\lambda_r/\partial v)^*\ddot{v}. \qquad \cdot d$$

This approximation is equivalent to the 'perturbation' method of DUBOWSKY & GARDNER(a,b).

Substituting in Equation (74·c) and dividing by δu, we obtain

$$-R_u' + S_u^* - M_u\,\ddot{\theta} - M_u''\,\dot{\theta}^2 = M_{uu}\,\ddot{u} + M_{uv}\,\ddot{v} \qquad \cdot e$$

where

$$M_u \equiv \Sigma[M_r(\partial X_r/\partial u)^*(\partial X_r/\partial\theta)^* + M_r(\partial Y_r/\partial u)^*(\partial Y_r/\partial\theta)^* + J_r(\partial\lambda_r/\partial u)^*(\partial\lambda_r/\partial\theta)^*] \qquad \cdot f$$

$$M_u'' \equiv \Sigma[M_r(\partial X_r/\partial u)^*(\partial^2 X_r/\partial\theta^2)^* + M_r(\partial Y_r/\partial u)^*(\partial^2 Y_r/\partial\theta^2)^* + J_r(\partial\lambda_r/\partial u)^*(\partial^2\lambda_r/\partial\theta^2)^*] \qquad \cdot g$$

$$M_{uu} = \Sigma[M_r(\partial X_r/\partial u)^{*2} + M_r(\partial Y_r/\partial u)^{*2} + J_r(\partial\lambda_r/\partial u)^{*2}] \qquad \cdot h$$

$$M_{uv} = \Sigma[M_r(\partial X_r/\partial u)^*(\partial X_r/\partial v)^* + M_r(\partial Y_r/\partial u)^*(\partial Y_r/\partial v)^* + J_r(\partial\lambda_r/\partial u)^*(\partial\lambda_r/\partial v)^* \qquad \cdot i$$

(the summation in each case being for every link 'r') and where S_u is approximated by S_u^* in accordance with Assumption (72·f). (See Appendix 10H).

Equation 75·e and the corresponding equation for the 'v' direction define the dummy force (R_u', R_v') necessary to produce <u>any</u> given motion as described by $\ddot{u}, \ddot{v}$. Two cases can be considered. If $\ddot{u} = \ddot{v} = 0$, then (R_u', R_v') corresponds to the force that would exist between pin and journal in the absence of clearance, (R_u^*, R_v^*). If $(\ddot{u}, \ddot{v})$ describes the actual relative motion around or across the clearance circle, then (R_u', R_v') corresponds to the actual contact force (R_u, R_v), where this is zero in the absence of contact. Thus we can see that

$$R_u^* - R_u = M_{uu}\ddot{u} + M_{uv}\ddot{v}. \qquad \cdot a$$

Similarly, with M_{vv} defined analogously to M_{uu}, we can write

$$R_v^* - R_v = M_{uv}\ddot{u} + M_{vv}\ddot{v}. \qquad \cdot b$$

Equations ·a and ·b are the basic equations of motion for a general revolute joint with clearance. To the best of the author's knowledge, they have not be established before.

<u>Restriction to following mode</u>: In the 'following' mode, two additional conditions can be invoked. The first is that the magnitude of the displacement vector (u, v) is equal to e, and the second is that, by virtue of the neglect of friction (Assumption 72·d), the inclination of this vector may be taken as equal to the inclination of the (actual) contact force vector.

It is convenient to use polar coordinates, and to solve for α, the angle by which the actual contact force vector lags its nominal counterpart. Then after some trigonometrical manipulation (outlined in Appendix 10I), it is found that

$$\ddot{\alpha} = \ddot{\gamma}^* + [\varepsilon(\dot{\gamma}^* - \dot{\alpha})^2 \sin(2\alpha - 2\gamma^* - 2\gamma) - (R^*/eM_o)\sin\alpha] \times [1 + \varepsilon\cos(2\alpha - 2\gamma^* - 2\gamma)]^{-1} \qquad \cdot c$$

and also that

$$R = R^*\cos\alpha + eM_o[1 - \varepsilon\cos(2\alpha - 2\gamma^* - 2\gamma)](\dot{\gamma}^* - \dot{\alpha})^2 + eM_o[\varepsilon\sin(2\alpha - 2\gamma^* - 2\gamma)](\ddot{\gamma}^* - \ddot{\alpha}) \qquad \cdot d$$

where

$$M_o = (M_{uu} + M_{vv})/2 \; ; \qquad \cdot a$$

$$\eta = (\tfrac{1}{2}) \arctan (2 M_{uv}/(M_{vv} - M_{uu}))^{\circledast} \qquad \cdot b$$

and angle 2η lies in the same quadrant as a point with coordinates $(M_{vv} - M_{uu}, 2M_{uv})$;

$$\varepsilon = (M_{uv}/M_o) \operatorname{cosec} 2\gamma = ((M_{vv} - M_{uu})/2 M_o) \sec 2\eta \qquad \cdot c$$

Equation 76·c is the basic equation of motion for the following mode.

Properties of the equation of motion: Some important features of equation may be established by inspection. Although the following deductions may not appear rigorous, they are all consistent with the numerical simulations described later.

For small amplitudes of α, it is seen that equation 76·c approaches a linear second-order differential equation with both "parametric" and "forcing" excitations. The square of the instantaneous circular natural frequency is given by $\dot{\theta}^2 [(R^*/M_o e \dot{\theta}^2)/(1+\varepsilon \cos(2\alpha - 2\gamma^* - 2\gamma))]$, where the bracketed term is, according to Assumption (72·f), much larger than unity. This indicates that the effective natural frequency is typically well above all significant harmonics of $\dot{\theta}$ in the exciting functions. Thus with light damping the system will rapidly approach a state where α is negligibly small; that is, γ follows γ^* very closely.

A "flypast", however, provides an untypical case. The rapid change in γ^* forces the system at an unusually high rate while the simultaneous reduction in R^* leads to a depression in the natural frequency, as well as an unusually severe parametric excitation. In these circumstances α may depart considerably from zero, subsequently oscillating in pendulum fashion until the light damping assumed restores it to a small value. Near the extremes of the early swings the contact force given by equation 76·d may become negative, indicating that in fact contact is lost, rather as a ball will lose contact with the bottom of a bucket that is swung some way above the horizontal.

$\circledast$ Note, equation 77·b was given incorrectly in HAINES(c).

This picture provides theoretical support for the hitherto intuitive assumption that contact loss is a function of conditions at "flypasts", that is Assumption (72·g). The picture is complicated by two further effects which assume significance later. Because of the terms involving ε, the contact force may drop more at one extreme of the oscillation that at the other; and because of the rapidly changing value of ϑ^* in these terms, the reduction may be greater after the second or third swings than after the first.

Response to a "standard" flypast: With Assumption (72·g) now resting on a secure basis, it will be introduced into the analysis explicitly: that is, it will be assumed that the values of the governing variables $\dot{R}_u^*$, $\dot{R}_v^*$, M_o, ε and η remain effectively constant during the period under consideration. ·a
A flypast for which this is the case will be termed a "standard" flypast. The inclusion of $\dot{R}_u^*$ and $\dot{R}_v^*$ in the list implies that the locus of the nominal contact force can be taken as a straight line during the brief period under consideration. Although this is not invariably the case, it is likely to be true for a usefully large number of cases, and it is with these that the remainder of the analysis is concerned.

The direction of the 'u' axis, hitherto arbitrary, will now be fixed as parallel to the nominal contact force vector at the instant at which it reaches its minimum magnitude. The effect is that R_u^* becomes constant, and $\tan(\vartheta^*)$ ·b changes linearly with time and may be used instead of time as the independent variable (written as τ). The resulting dimensionless equation of motion, derived in Appendix 10J, is

$$d^2\alpha/d\tau^2 = -2\tau(1+\tau^2)^{-2} + [H_3(d\alpha/d\tau - 1/(1+\tau^2))^2 \sin(2\alpha - 2\vartheta^* - H_2) - H_1^3(1+\tau^2)^{1/2}\sin\alpha] / [1 + H_3\cos(2\alpha - 2\vartheta^* - H_2)] \quad \cdot c$$

where the dimensionless governing variables H are given by

$$H_1 \equiv R_u^* / (\dot{R}_v^{*2}\, e\, M_o)^{1/3}; \quad \cdot d$$

$$H_2 \equiv 2\gamma; \quad \cdot e$$

$$H_3 \equiv \varepsilon. \quad \cdot f$$

H_1 might be termed the 'standard flypast severity index', and H_3, H_2 respectively the eccentricity and attitude of the generalised inertia tensor.

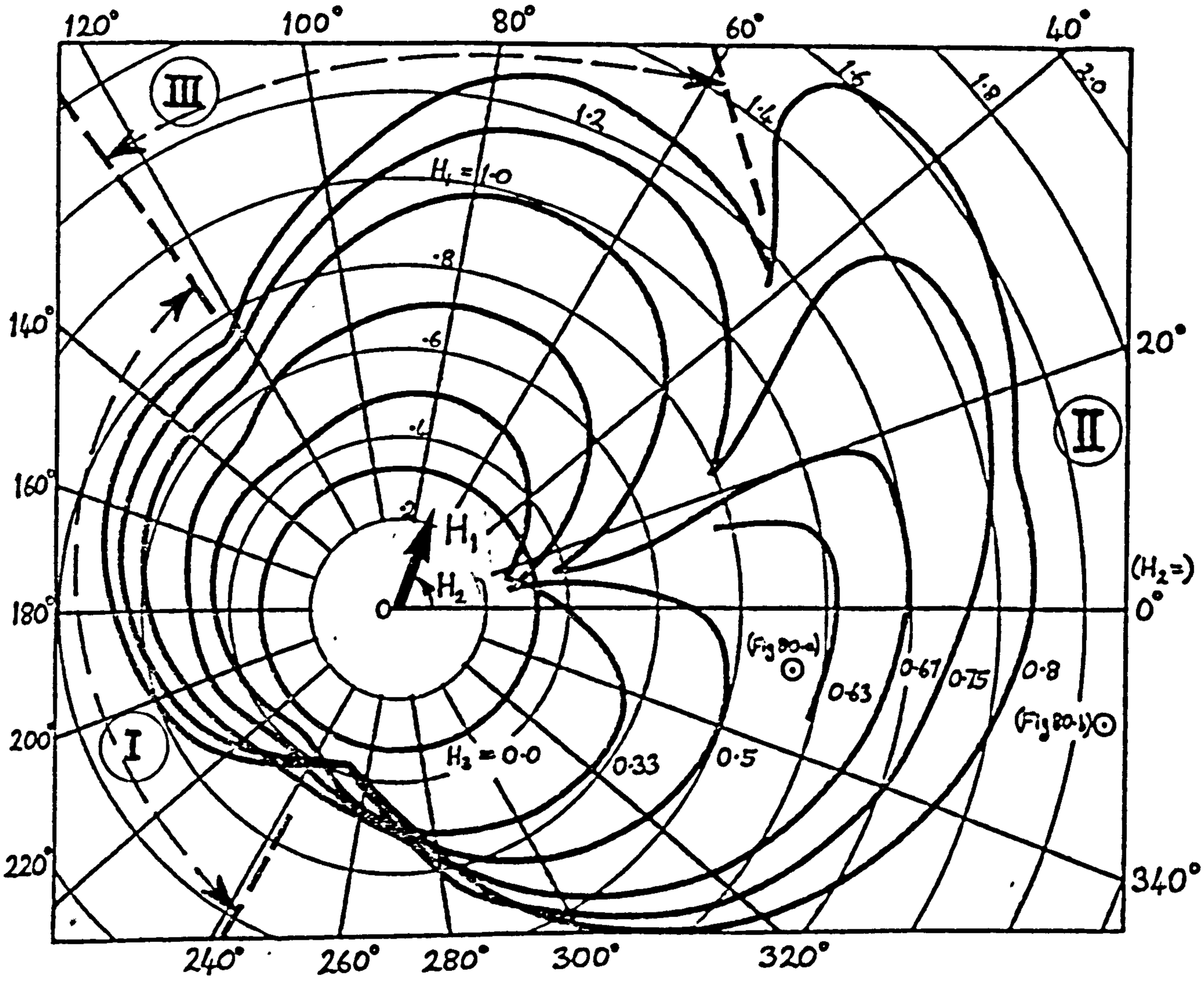

79.a: 'Design chart' – contact lost if design point is inside the relevant contour.

It may be seen that H_1^3 is identical to the group obtained by dimensional analysis in Section 3B (53b).

The corresponding contact force equation is

$$R/R_u^* = (1+\tau^2)^{1/2}\cos\alpha + H_1^{-3}\left[(d\alpha/d\tau - 1/(1+\tau^2))^2(1-\varepsilon\cos(2\alpha-2\beta-H_2))\right.$$
$$\left. - H_3(2\tau(1+\tau^2)^{-2} + \ddot{\alpha})\sin(2\alpha-2\beta-H_2)\right] \qquad \text{.b}$$

This system has been solved numerically for a range of values of H_1, H_2 and H_3 in combination. Appendix 10K gives details of the procedure used. The results enable the (H_1, H_2, H_3) space to be divided into two regions, one containing the values for which contact is lost at some time during the standard flypast, the other containing the values for which contact is maintained throughout. The threshold surface between these two regions is shown in Fig. .a in the form of a contour map, with H_1 and H_2 as polar coordinates, and contours joining equal values of H_3; in each case contact is lost on the inside of the contour and maintained on the outside.

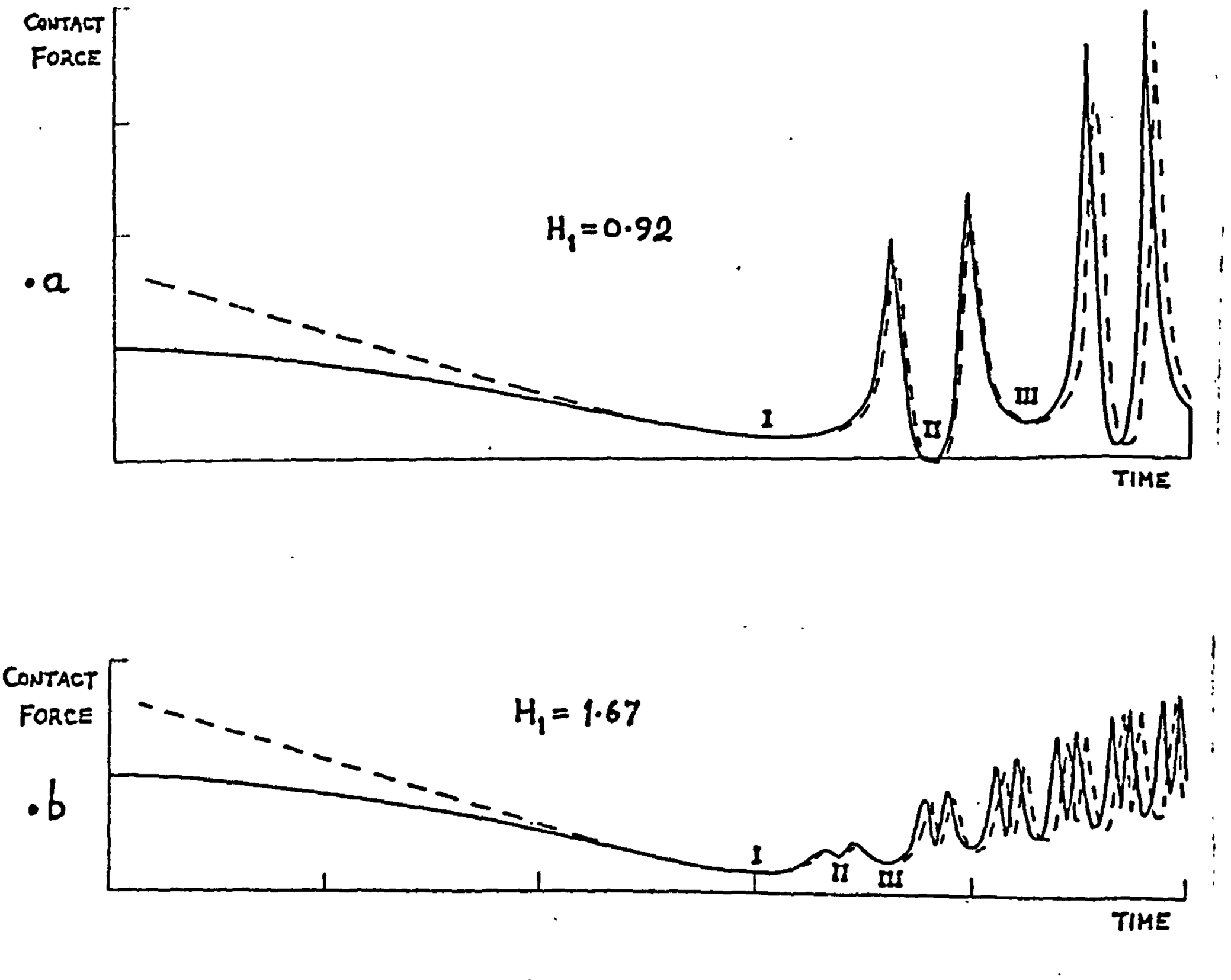

KEY: ——— simulated flypast for linkage

– – – – corresponding standard flypast

80.a/.b: <u>Comparison of actual and standard flypasts for a four-bar linkage.</u> [$H_2 = -6.5°$, $H_3 = 0.625$]

4C: PRELIMINARY TESTING OF THEORY

A preliminary assessment of the theory described above may be made by comparing it with established theories and experimental results. EARLES & WU(a) and GRANT have performed numerical simulations, reviewed in Chapter 3, of the conditions leading up to contact loss in specific mechanisms. In both cases assumptions equivalent to Assumptions (72·a) to (72·e) of this chapter were adopted, and in both cases quite good agreement with experimental results was reported. GRANT also showed that his theory could be simply modelled by the use of CHACE's general purpose program 'DRAM'.

The full lines in Figs (·a, ·b) show the results of some sample simulations carried out by the author, using DRAM in the same way as Grant. Curve (.a) includes a period of negative contact force in the simulation, indicating contact loss in practice. In order to test the effect of the simplifications following from the assumption of small clearance size (Assumption 72·f), parallel simulations were performed* using equations (78·c) and (79·b) in conjunction with a kinetostatic analysis: the results of these simulations were virtually indistinguishable from the previous results on the scale of Figs ·a, ·b. Assumption (72·f) is therefore strongly supported.

The broken lines in Figs.(·a, ·b) show the effect of replacing the actual flypast with a corresponding standard flypast, thus testing the effect of adopting Assumption (72·g). Since it is assumed that the oscillations are in practice progressively reduced by damping effects not included in the simulations, the successful prediction of contact loss depends on the accurate simulation of the first few oscillations. In this respect agreement with the previous results is seen to be good.

This evidence suggests that the general results embodied in Fig. 79·a are likely to be of comparable accuracy to the specific results obtained by the simulations of Earles and Wu and of Grant.

Further relevant evidence is found in the experimental work of Earles and his co-workers. As discussed in Chapter 3, they concluded that, as a broad trend, contact was maintained in their experiments if $\dot{\vartheta}^*/R_u^*$ at each flypast was less than 1 radian/second/Newton. This no-loss condition can also be

*: using program FAB, written by the author and forming Annexe 1

written as $(R_u^*/\dot{R}_v^{*\frac{1}{2}}) > 1\,(N-s)^{\frac{1}{2}}$, for easy comparison with equation 78·d.

It would not be expected that a relationship as complex as that shown in Fig. 79·a would be revealed by an empirical approach in which the inertia terms are not considered. What the Earles et al. results do indicate, however, is that contact loss is to a large extent a function of low values of R_u^*, and to a lesser extent a function of high values of $\dot{R}_v^*$, at flypast points in the cycle. Such a conclusion is fully in accordance with the theory presented here.

4D: USE OF THE GENERAL THEORY IN DESIGN

Figure 79·a provides the designer with an approximate guide as to whether contact loss is or is not likely to occur at a real flypast in a real mechanism. Note that the evaluation of the H-parameters requires an analysis only of the nominal mechanism, and that the generalised inertia terms M_0, ε and η need to be calculated only at the flypast points in the cycle.

Fig. 79·a can also be used to synthesize a bearing design in which contact is maintained. The simplest method would be to use the "Force-form closed bearings" proposed by FAWCETT. In this design a spring element exerts an effectively constant force between the pin and journal, in a direction chosen so that the value of R_u^* is increased. This device has no effect on any of the variables in the above analysis other than R_u^*, and hence H_1. The effect in the design chart (Fig. 79·a) is thus to move the design point radially outwards, in direct proportion to the change in R_u^*. By projection outwards until the appropriate contour is cut, it is possible to determine the value of H_1, and thus the value of R_u^*, necessary to prevent predicted contact loss.

Another possible way to avoid contact loss is to reduce the magnitude of the clearance, e. This technique, like the first, implies changes of H_1 at constant values of H_2 and H_3. However, whereas H_1 varies in proportion to R_u^*, it only varies in proportion to the inverse cube root of e, so that this technique is seen to be far less powerful: indeed, in most cases for which the theory is applicable it will probably not be possible to eliminate loss of contact merely by varying the clearance within a realistic range of values. (This does not rule out the use of small clearances to control the magnitude of the ensuing impact in cases where a loss of contact is accepted as inevitable).

It is also possible in principle to control contact loss by the addition of counterweights to the linkage. Since this would affect all three dimensionless parameters, the selection of a suitable counterweight size and position for this purpose presents a difficult problem, which will be considered further in Chapters 8 and 9. For the present, trial-and-error is the only method available. Nevertheless, it appears that this may well be justified in some cases because of the prominent and unexpected feature in the first quadrant of Fig. 79·a, where (for intermediate values of H_3) the region for which contact loss is avoided is seen to extend inwards to quite low values of H_1. If this "sector of sanctuary" can be attained by a small change in

the value of H_2, the need for a much larger change in H_1 may be avoided.

A further unexpected feature of the first quadrant in Fig. 79·a is that for the higher values of H_3 there is a small range of values of H_2 within which a radial line intersects the contour at <u>three</u> points. In this region it is implied that contact loss can sometimes be eliminated by a suitable <u>reduction</u> in H_1 : for example, a reduction from 1.3 to 1.0 when $H_2 = 35^o$ and $H_3 = 0.75$.

4E: EXTENSION TO 'FREE FLIGHT' & 'IMPACT' PHASES

Basis: While the emphasis in this chapter is on the prediction and control of contact loss, it is worth pointing out that the theory can readily be extended to cover the motion after loss of contact up to the first impact, and the momentum exchange during impact.

We begin by noting that this 'free flight' phase (in Miedema & Mansour's terminology) can be expected to occupy a very small time by comparison with the cycle time. Thus it is reasonable to extend Assumption 72·g one stage further, and assume that the values of $R_u^*, \dot{R}_v^*, M_o, \varepsilon$ and η conform to a standard flypast - i.e. remain constant - between the loss of contact and the first ensuring impact. Thus during the free flight phase we can write $R_v^* = t\dot{R}_v^*$ where $t=0$ at the flypast point.

Trajectory: Since by definition the actual contact forces R_u and R_v are zero during this phase, the equations of motion (76·a & 76·b) become

$$\left.\begin{aligned} R_u^* &= M_{uu}\ddot{u} + M_{uv}\ddot{v} \\ t\dot{R}_v^* &= M_{uv}\ddot{u} + M_{vv}\ddot{v} \end{aligned}\right|_{t\geq t_\ell} \qquad \begin{matrix} \cdot a \\ \cdot b \end{matrix}$$

where subscript (ℓ) refers to the instant when contact is lost. Eliminating $\ddot{u}$ and $\ddot{v}$ in turn, integrating, and converting to dimensionless form as before, we find that

$$u/e = A_o + A_1\delta\tau + A_2\delta\tau^2 + A_3\delta\tau^3 \qquad \cdot c$$

$$v/e = B_o + B_1\delta\tau + B_2\delta\tau^2 + B_3\delta\tau^3 \qquad \cdot d$$

where $\delta\tau \equiv \tau - \tau_\ell$ ·e

$$\left.\begin{aligned} A_o &= \cos\vartheta_\ell & A_1 &= -(d\vartheta/d\tau)_\ell \sin\vartheta_\ell \\ A_2 &= \tfrac{1}{2} H_1^3 (1 + H_3\cos H_2 - \tau_\ell H_3 \sin H_2)/(1-H_3^2) \\ A_3 &= \tfrac{1}{6} H_1^3 H_3 \sin H_2/(1-H_3^2) \\ B_o &= \sin\vartheta_\ell & B_1 &= (d\vartheta/d\tau)_\ell \cos\vartheta_\ell \\ B_2 &= \tfrac{1}{2} H_1^3 (-H_3\sin H_2 + \tau_\ell - \tau_\ell H_3\cos H_2)/(1-H_3)^2 \\ B_3 &= \tfrac{1}{6} H_1^3 (1 - H_3\cos H_2)/(1-H_3^2). \end{aligned}\right\} \cdot f$$

The working is given in Appendix 10L.

The intersection of this trajectory with the clearance circle gives the end of the free flight period; that is it ends at a reduced time $\tau_i = \tau_\ell + \delta\tau_i$

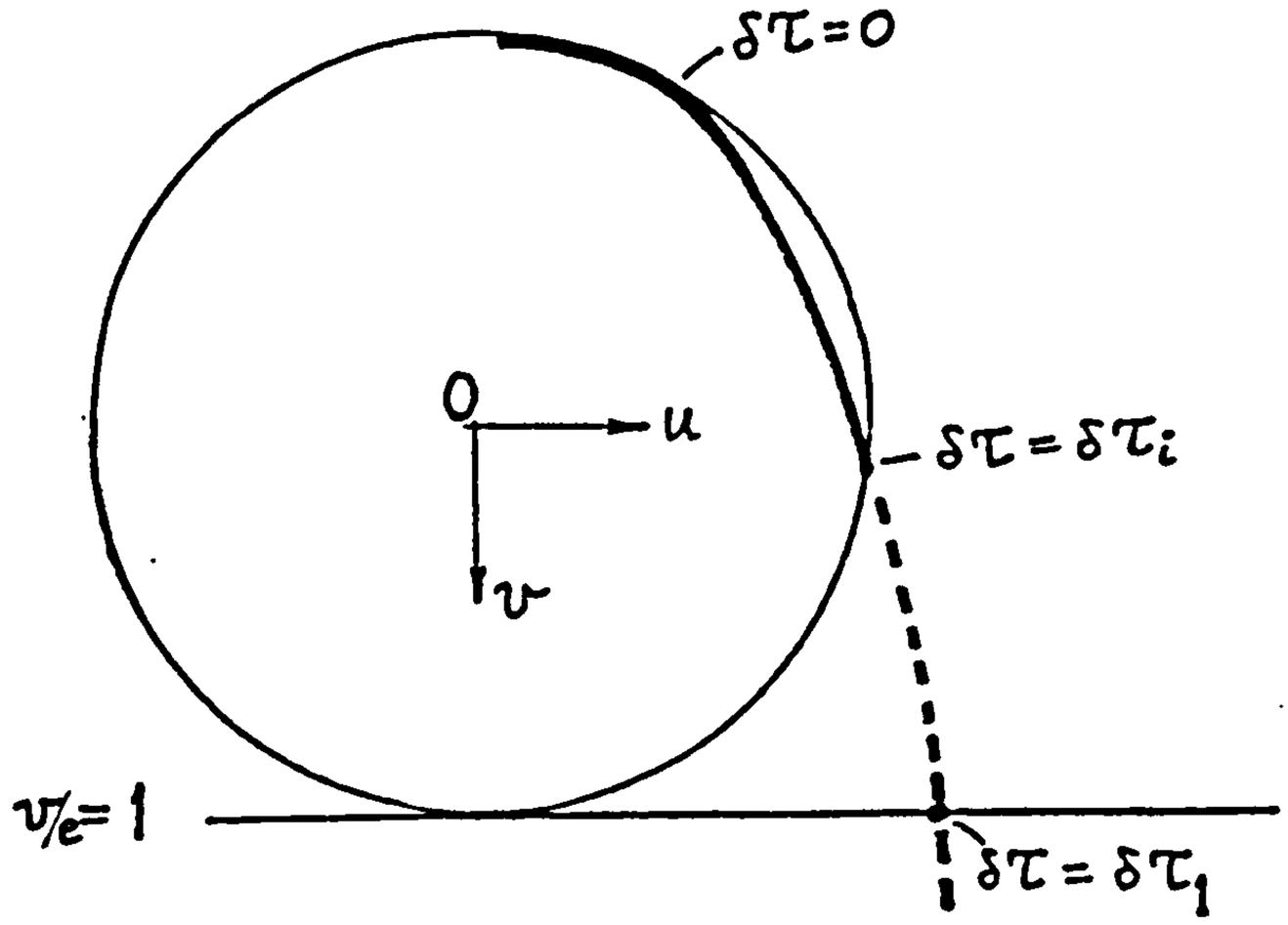

85.a: Start of iterative procedure for finding impact time

given by the equation

$$(1_o + A_1 \delta\tau_i + A_2 \delta\tau_i^2 + A_3 \delta\tau_i^3)^2 + (B_o + B_1 \delta\tau_i + B_2 \delta\tau_i^2 + B_3 \delta\tau_i^3)^2 = 1 \qquad \cdot b$$

This equation can readily be solved for $\delta\tau_i$ by Newton's method provided that a suitable 'initial guess' is used so that the process converges to the relevant root. Such a value can be obtained by finding where the trajectory cuts the line $v/e = 1$ which is shortly after the moment of re-contact (see Fig. $\cdot a$) $\delta\tau$ is then equal to $\delta\tau_1$, the solution of

$$B_o + B_1 \delta\tau_1 + B_2 \delta\tau_1^2 + B_3 \delta\tau_1^3 = 1 \qquad \cdot c$$

Since only an approximate value of $\delta\tau_1$ is required, it is adequate to solve this equation by one iteration of Newton's method with a starting value

$$\delta\tau_1 = [(1-B_o)/B_3]^{1/3} \qquad \cdot d$$

After solving equation $\cdot b$, the value of $\delta\tau_i$ can be substituted into 84$\cdot c$–$\cdot d$ to find the inclination of the contact vector at the point of impact, that is $\vartheta_i = \arctan(v/u)$. Likewise, the derivatives of equations 84$\cdot c$–$\cdot d$ with respect to τ can be used to find the tangential and radial components $\tilde{V}_T$ and $\tilde{V}_N$ of the reduced relative velocity,* and hence the angle of approach

$$\psi = \arctan(\tilde{V}_T/\tilde{V}_N) \qquad \cdot e$$

—

Impact phase: According to the assumption of negligible friction (72$\cdot d$), the tangential component of the contact force is zero during the impact phase; moreover by the assumption that the impact is impulsive (72$\cdot i$) the nominal contact force can be neglected. Then with a coefficient of restitution E, the momentum exchanged can be shown (see Appendix 10L) to be

$$[M_o \dot{R}_v^* e/R_u^*][(1-\varepsilon^2)\tilde{V}_N/(1+\varepsilon\cos(2\gamma+2\vartheta_i))][1+E] \qquad \cdot f$$

Thus a dimensionless index of impact severity $\tilde{I}$ is provided by the term in the middle brackets.

* : defined as $d/d\tau$(displacement /e)

Results: The calculations described above were in fact carried out at the same time as the calculations used to produce Figure 79·a; that is, for each value of (H_1, H_2, H_3) in the 'contact lost' region the reduced approach conditions and reduced impact severity index were determined and stored on file. $\tilde{I}$ and V_N are also tabulated as Annexe 4. Since four dimensions are involved, the graphical presentation of these results is not simple. It may be possible to find an approximate function of only two parameters that adequately describes the results, but the effort needed to find such a function would be considerable and does not seem justified while the validity of the theory is uncertain.

The results for impact need to be treated with reserve for another reason. It is only the severity of the first impact that is recorded. Thus for example in Figure 80·a a small impact will correctly be recorded at the second minimum in the force curve; as H_1 is reduced the impact will become larger and larger until contact is lost at the first minimum, when again only a small value will be recorded at the first impact, although it seems likely that this will be followed by a far larger impact at about the time of the second minimum.

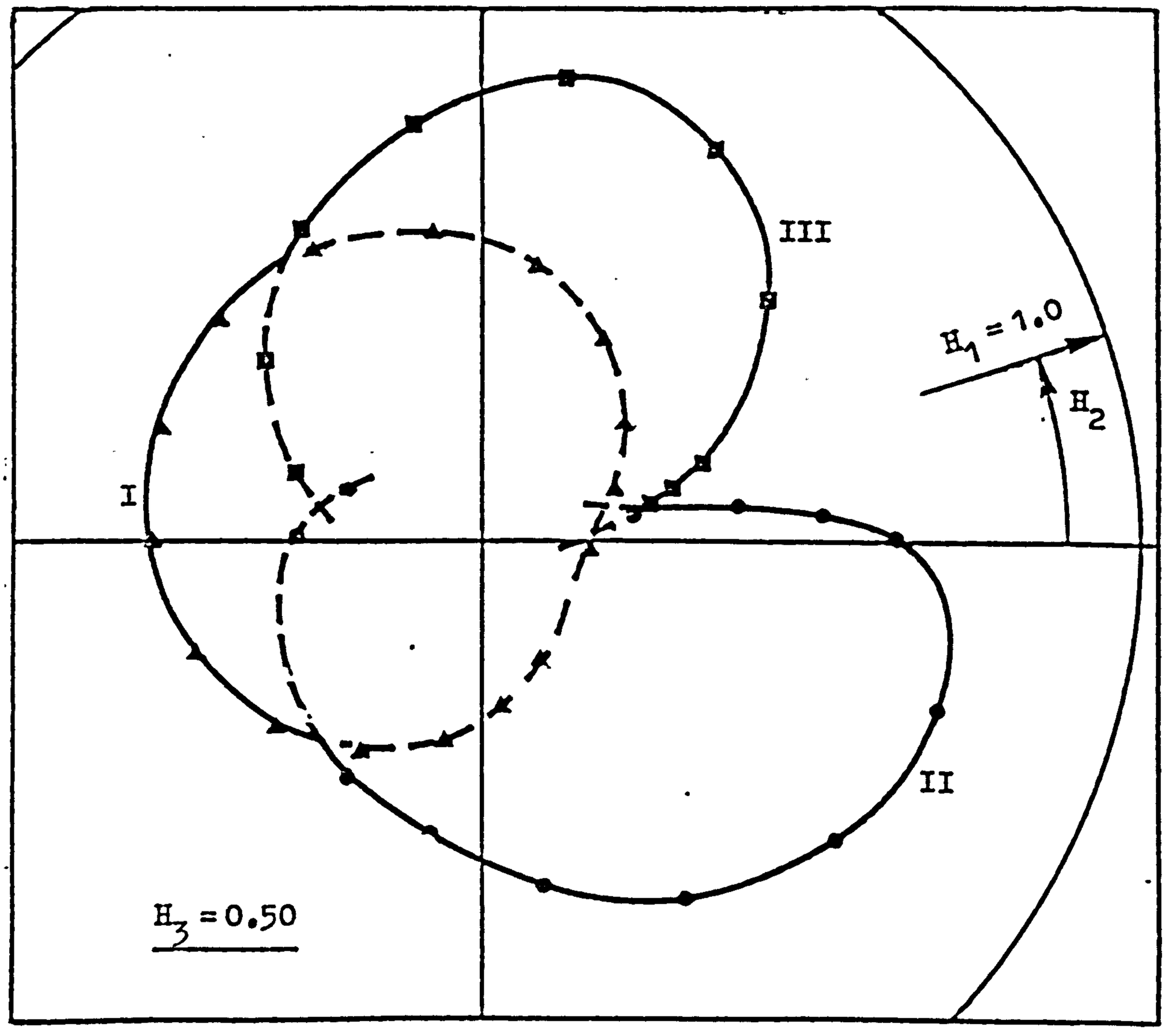

87.a: Construction of a single contour

4F: FEATURES & LIMITATIONS OF THE THEORY

It has been shown that the theory described in Section 4B can give results similar to those of previously published theories, which in turn are known to be supported by experimental results in some cases. The predicted criterion for contact loss has been shown to be qualitatively consistent with Earles' empirical criterion; it has the advantage over the latter of being in dimensionless form. What is now required is to establish the limits of applicability of the theory. This task is itself made easier by the use of Fig. 79·a: firstly, since tests by simulation or experiment of the contact loss criterion need be performed only for values of the H-parameters close to the threshold surface, and secondly, since it assists the selection of "representative" test values near the surface.

Zones: A feature of the threshold surface that must be considered at this point is its division into a number of zones, separated by directional discontinuities in the contours. The explanation for this is apparent in Fig. ·a, in which H_3 has a constant value, and the curves marked I, II and III show the range of values of H_1 and H_2 within which the simulated contact force goes negative at the first, second and third local minima respectively. The corresponding contour in Fig. 79·a is in fact the envelope of all such curves; the inclusion of minima later than the third does not affect the shape very greatly. Thus zones I, II and III in Fig. 79·a are defined, according to which of the three curves provides the effective threshold at any point.

"Passage impact" and "Terminal Impact": The successive minima of the contact force and their associated zones can be related to the angular movements of the nominal force vector (R_u^*, R_v^*) and the displacement vector (u, v). A typical sequence of events is shown schematically at Figs. 88·a to 88·e. Note that, in accordance with equations (76·a – ·b), the relative displacement is always 'pulled' roughly in the direction of the nominal force vector; not exactly, unless $\varepsilon = 0$ so that $M_{uu} = M_{vv}$ and $M_{uv} = 0$.

The first contact force minimum occurs when the nominal force vector is changing direction so rapidly that the displacement vector gets left behind (88·b). This is almost at the flypast point ($R_v^* = 0$). 'Zone I' contact loss may follow, as shown at 88·c, the ensuing trajectory being deflected concave to the clearance circle as R_v^* increases.

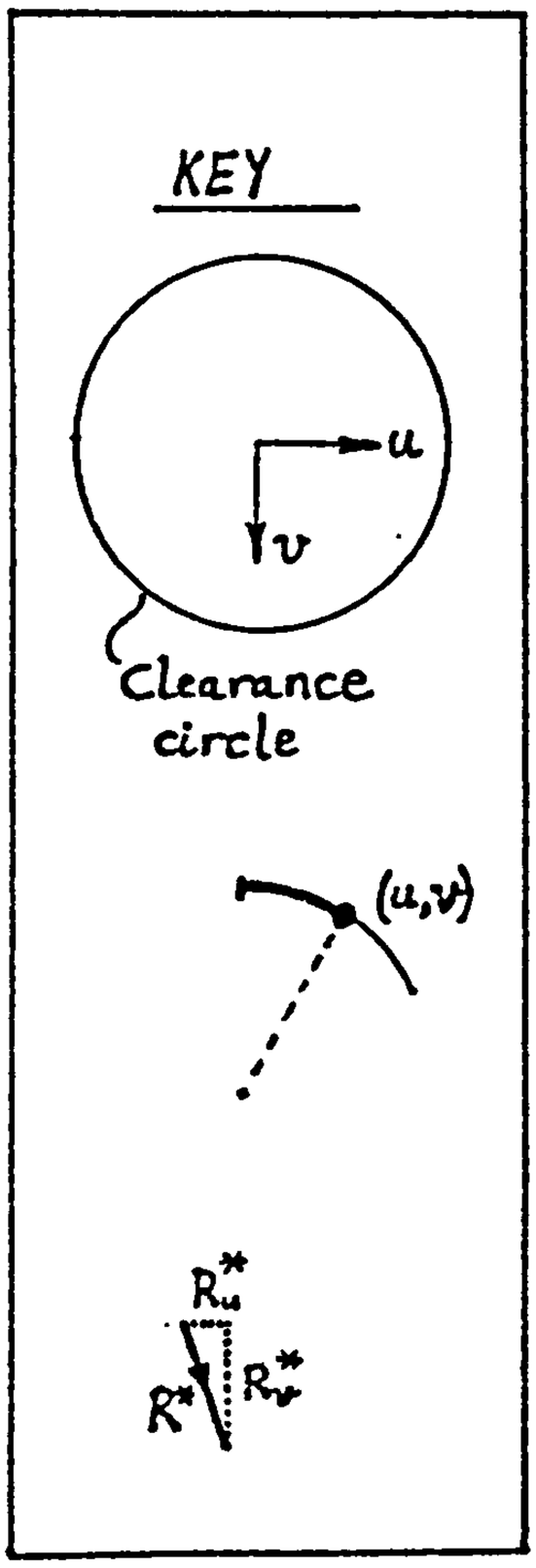

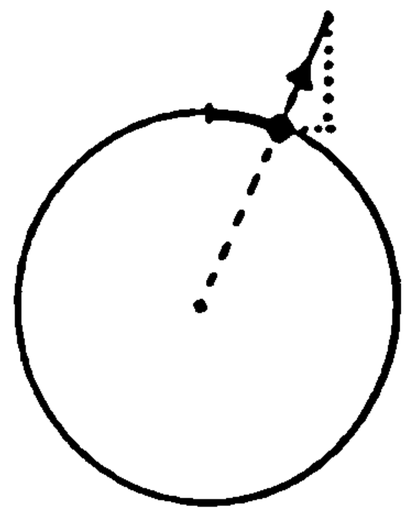

.a

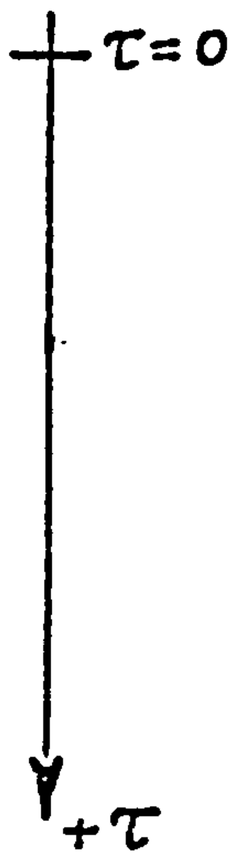

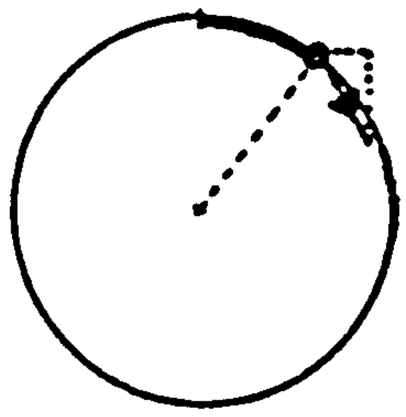

.b

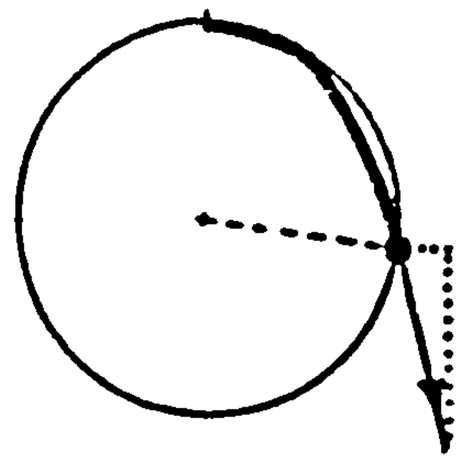

.c

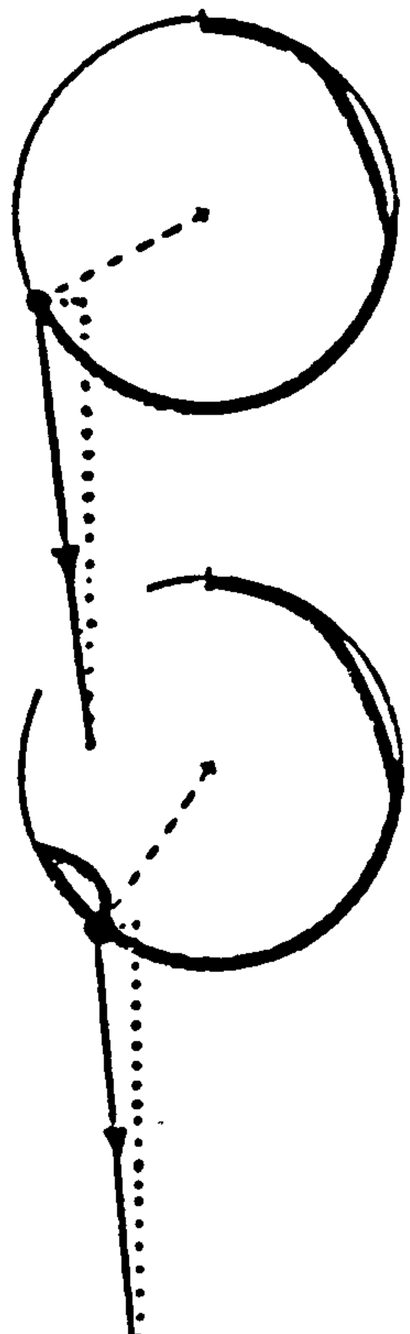

.d

.e

Fig.88 .a - .e

Typical flypast sequence.

The displacement vector, now changing direction rapidly, soon catches up and overshoots the nominal force vector (88·d). If the overshoot is sufficient, a 'zone II' contact loss may occur (88·e), this event being somewhat after the flypast point. Since R_v^* is now much larger, the impact is likely to be much more severe in relation to the degree of separation. 'Zone III' impact bears a similar relationship to the second overshoot.

It may be helpful, considering these figures, to refer to impact in zone I as "passage impact", and that in zones II and III as "terminal impact". Whereas the former appears to be well understood in the literature, terminal impact has apparently not been explained before, although impact answering to the above description has certainly been recorded: consider the results of FUNABASHI ET AL(a,b) and of HAIN, noted on page 70 above. Figure 79·a shows that terminal impact is very much dependent on the values of the inertia terms ε and η, and here it should be noted that the joint in the mechanism studied by Hain has the property that $\eta \neq 0$, and ε is very large if the sliding block is light by comparison with the driven link, so severe terminal impact in this case is entirely to be expected.

Limitations: Since in general each successive oscillation will be simulated with greater error, a general result is that the I contours are likely to give the most accurate, and the III contours the least accurate predictions. "Representative" test values should therefore be chosen near each zone of the surface to obtain a full picture. It also follows that the prediction of the "sector of sanctuary" cannot be made with great confidence at present, as it corresponds to the transition between zones II and III.

The limits upon the validity of some of the assumptions introduced in Section 4A could be tested adequately by simulation alone; for example the effect of departures from the assumed straight-line nominal contact force locus could be tested in this manner. By contrast, experimental tests are probably the only reliable way to establish what degree of misalignment can be tolerated without the theory becoming inapplicable.

4G: CONCLUSIONS OF CHAPTER

.a By the adoption of sufficient simplifying assumptions, it has proved possible to establish a model of the "following" mode of behaviour of a revolute joint with clearance, that is independent of the type of planar linkage in which the joint is incorporated. This model provides a firm theoretical basis for the hitherto intuitive "flypast" approach.

.b In general, the new theory gives results closely similar to those of an established theory that requires a full simulation of each design, and is qualitatively consistent with an established empirical relationship. It breaks down, however, in cases where the nominal contact force locus cannot be represented adequately by a straight line at the points of closest approach to the origin.

.c The predictions of the new theory regarding loss of contact at the joint are embodied in Fig. 79·a. This can be used as a design chart for purposes of both analysis and synthesis. An important and novel feature of this chart is the "sector of sanctuary" apparent in the first quadrant.

.d Force-form closed bearings are predicted to be much more effective than reduced clearances as a measure for eliminating contact loss. In rare cases, the usual effect of these measures is predicted to be reversed. In some cases the addition of counterweights may be the most effective measure, but the choice of suitable parameters for these counterweights poses a difficult problem.

.e The model also makes it possible to predict the severity of the first impact after contact is lost, where this is the case, as in Annexe 4.

.f The major requirement now is to test the new theory to its limits. On theoretical grounds, zone I of the chart is expected to be the most accurate, and zone III the least accurate.

CHAPTER 5

RIG DESIGN & DEVELOPMENT

None of the material in this chapter has been published before.

Nomenclature (also applies to Chapter 6 and Appendices 10M & 10N)

I, II, III, IV: displacement transducer channels, see Fig. 94.b.

$R_u^*, R_v^*, M_{uu}, M_{vv}, M_{uv}$: as for Chapter 4.

/BUILD VARIANTS & CONDITIONS/

Term	Description	See
/Aa/(etc.)	Inertial build (added masses etc., as 97.a)	Appendix 10N
/Ball-pivots/	Ball bearings at zero-clearance pivots	Fig.92 .k/.l
/Clamped/	Journal clamped to pin by screw	Fig. 97.c
/ ry/	Bearing surfaces degreased	p. 97
/Flexible-pivots/	Modular crossed flexures at zero-clearance pivots	Fig. 92.j
/Floated/	Journal /suspended/ or /top-sprung/ and adjusted so as not to touch pin anywhere	p. 96
/Held/	Vertical link pulled against adjustable stop	Fig. 97.d
/Isolated/	Journal housing detached from link	Fig. 97.c
/Oiled/	Trace of oil on bearing surfaces	p. 97
/Propped/	Journal supported by screw jack	Fig. 97.b
/Side-sprung/	Tension spring applied to vertical link	Fig. 96.m
/Suspended/	Horizontal link hanging on hook	Fig. 96.j/k
/Top-sprung/	Horizontal link hanging on tension spring	Fig. 96.l

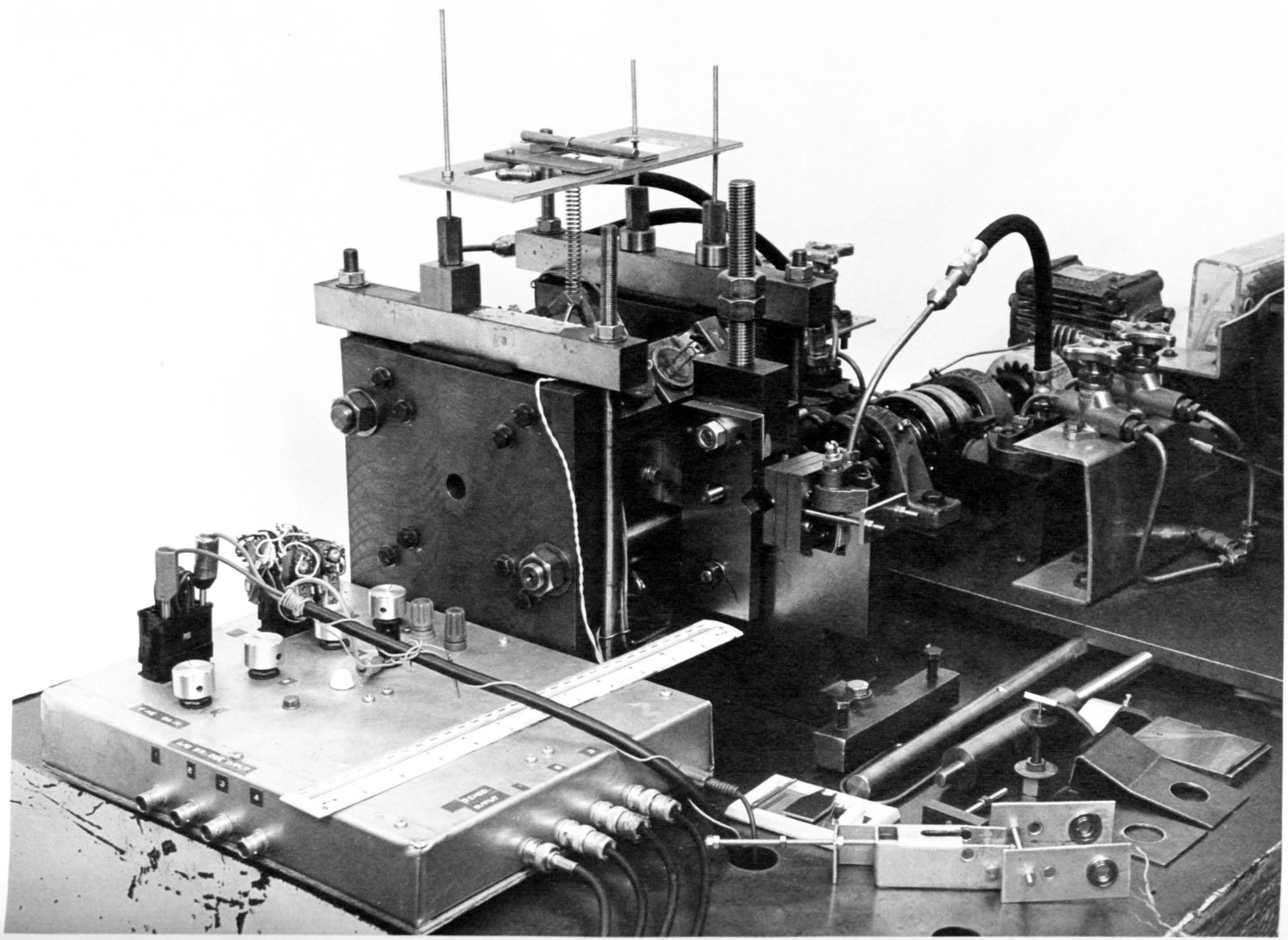

90.a-.t: General view of experimental apparatus

References for details of part or assembly

.a: 96.	.h: 96	.o: A25.b
.b: 94.b	.i: 92.g,96	.p: 97,A24.a
.c: 92.e/.h-.	.j: 94.c-.l,99	.q: 108.a
.d: 96.g/.i	.k: 96.h	.r: A25.c
.e: 92.d	. : 97.a,A22.e	.s: 97.d
.f: 93.k,98.a-.e	.m: 97.b	.t: 96.m
.g: 93.c-.f	.n: 96, A24.h	

Key to tools and accessories

- .k Mandrel
- .ℓ Stem for offset masses
- .m Screw jack and lever
- .n Screwdriver (grub screw)
- .o Spanner (exciters etc.)
- .p Displacement transducer adjusting tool
- .q Bridge assembly
- .r Inspection mirror
- .s Screw jack (horizontal)
- .t Assembly for side-sprung variant

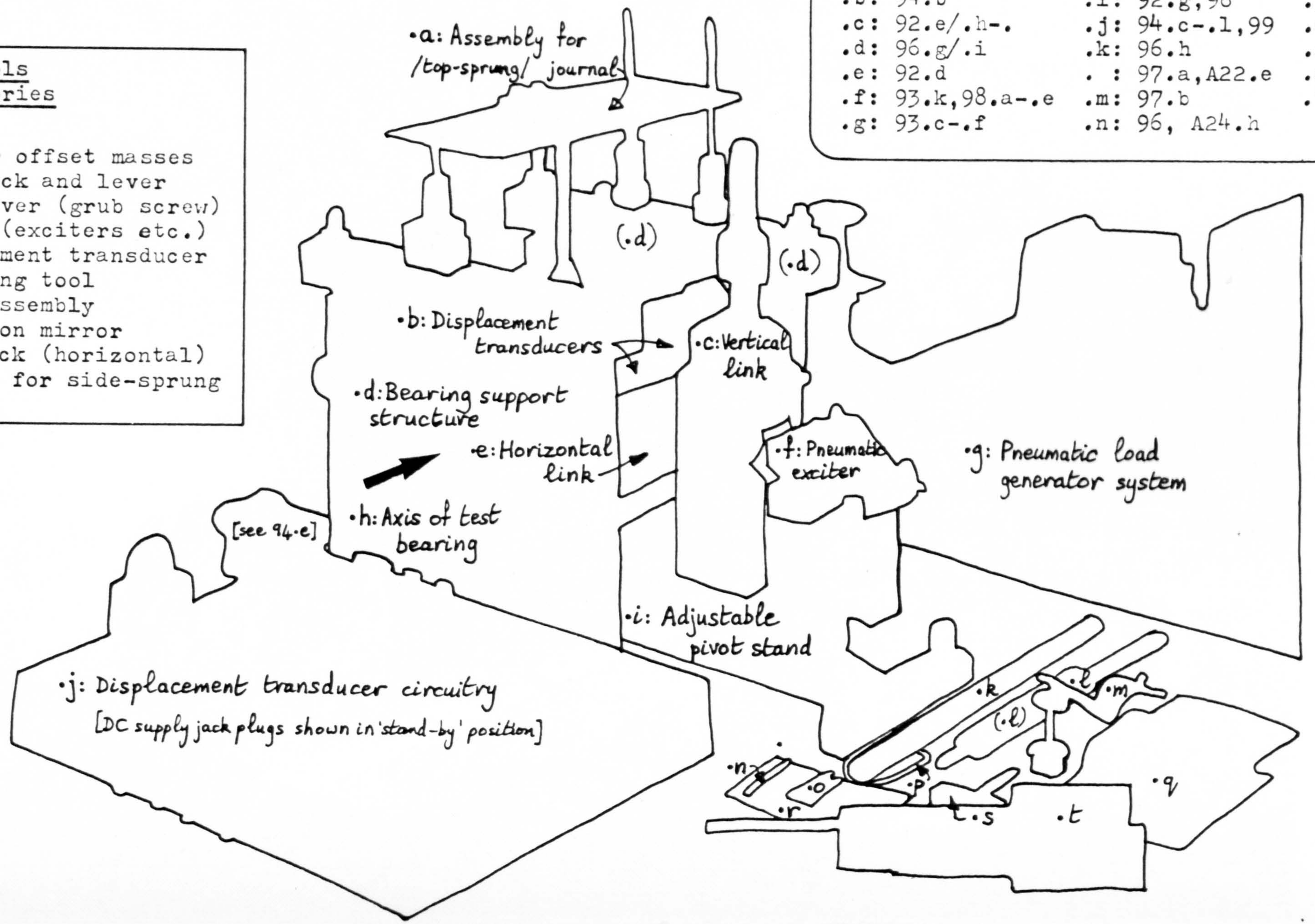

⌣: General view of experimental apparatus

References for details of part or assembly

.a: 96.	.h: 96	.o: A25.b
.b: 94.b	.i: 92.g,96	.p: 97,A24.a
.c: 92.e/.h-.	.j: 94.c-.l,99	.q: 108.a
.d: 96.g/.i	.k: 96.h	.r: A25.c
.e: 92.d	. : 97.a,A22.e	.s: 97.d
.f: 93.k,98.a-.e	.m: 97.b	.t: 96.m
.g: 93.c-.f	.n: 96, A24.h	

Key to tools and accessories

.k Mandrel
.ℓ Stem for offset masses
.m Screw jack and lever
.n Screwdriver (grub screw)
.o Spanner (exciters etc.)
.p Displacement transducer adjusting tool
.q Bridge assembly
.r Inspection mirror
.s Screw jack (horizontal)
.t Assembly for side-sprung variant

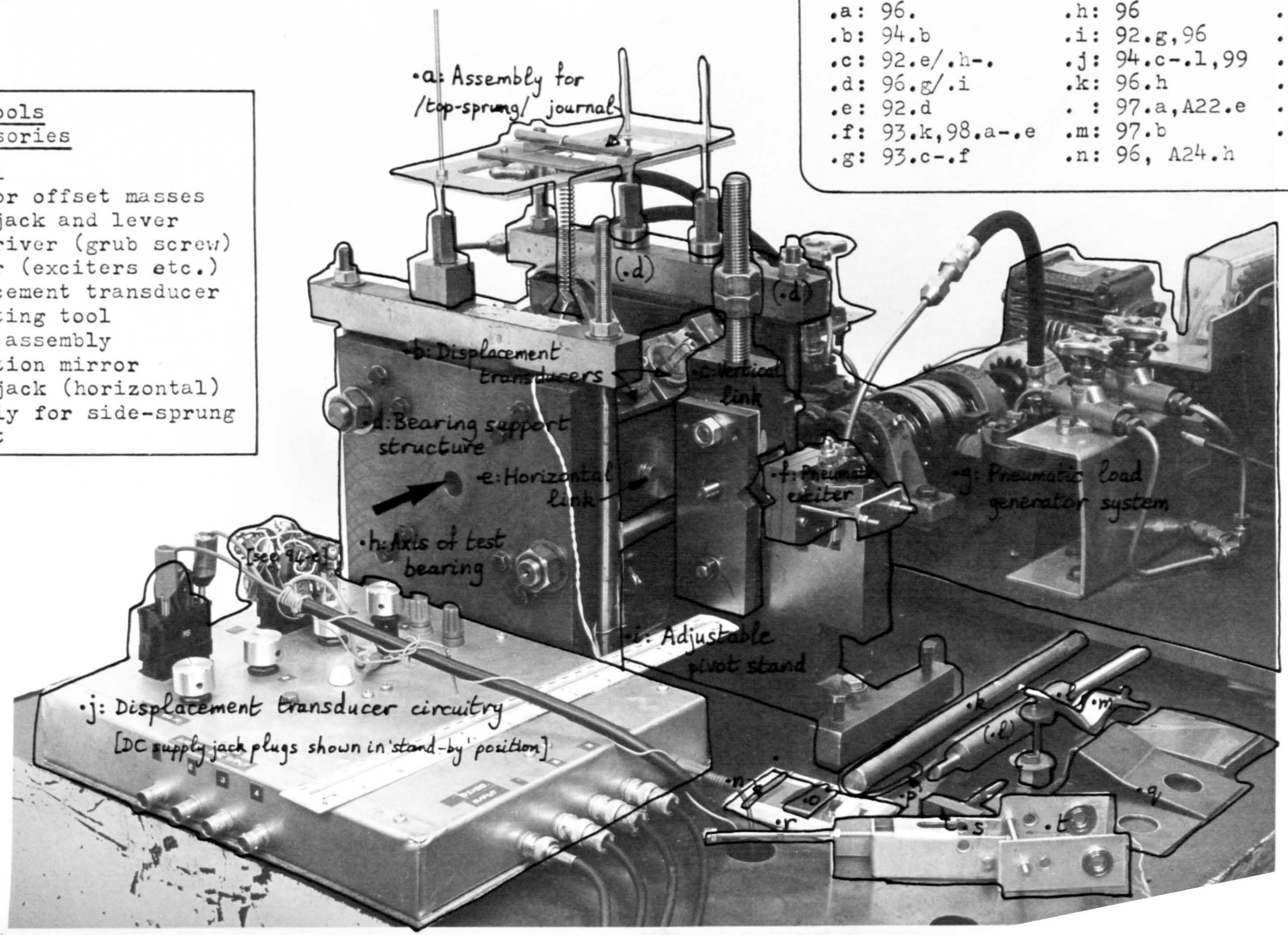

5. RIG DESIGN AND DEVELOPMENT

5A: INTRODUCTION

In the previous two chapters, a need for experimental investigation of the ludodynamics of revolute joints was identified on three counts. Firstly the simplified theoretical predictions of Chapter 4 need to be tested both under conditions approximating as closely as practical to those assumed and under controlled departures from those conditions. Secondly, a more thorough qualitative understanding of the phenomena involved is necessary in order to determine which effects ought to be taken into account in specific numerical simulations. Thirdly, quantitative data on specific matters such as laws of restitution under the conditions pertaining is needed for the same purpose.

In this chapter it is reported in Sections B to F how a rig was specified and designed that should when fully developed by capable of answering most of the above questions. The build and state of the rig can be varied in a number of ways. For brevity, the different variants and conditions are given names enclosed by slashes (/example/). The full range of variants and conditions is listed on the title page of this chapter. A general view is shown opposite.

The large number of systems involved and the rather ambitious specification were reflected in a need for considerable development and testing before the aims of the investigation could be reasonably achieved. The technically significant parts of this development process are described in Sections G and H, and the performance tests applied to the systems in their developed form are described in Sections I to K.

A significant contribution to the work described in this chapter was made by Dr. R. Godlewski, a Visiting Fellow with a particular interest in instrumentation. Dr. Godlewski's specific contributions are described in separate paragraphs prefaced thus:[RG].

5B: REQUIREMENTS

For a fundamental investigation of this kind, "realism" of the test joint is not necessarily desirable. Certainly, the design should as far as possible avoid introducing phenomena not found in practical joints, but it may be advantageous to exclude some of the phenomena usually present, so that the remaining phenomena may be observed more clearly.

The literature survey and theoretical investigation have revealed that loss of contact may be a function of a variety of parameters, here listed:-

.a The joint load locus, specifically R_u^* and $\dot{R}_v^*$ at a flypast, departures from the 'standard' flypast form, and the interval between flypasts;

.b the clearance;

.c the elements of the generalised inertia tensor (M_{uu}, M_{vv}, M_{uv});

.d out-of-plane assymetry of load or inertia distribution;

.e relative angular motion between pin and journal and associated friction forces; and

.f the dimensions and elastic/hysteretic properties of the bearing surfaces.

The rig should as far as possible be capable of independent variation of each of these parameters. It should also have provision for detecting the consequent behaviour in its various aspects, namely the making and loss of contact, the relative motion and the transmission of load. In particular, any deviation from symmetry of loading or motion about the nominal plane of symmetry should be detectable, this possibly significant aspect having been neglected in previous experiments.

A load range of at least 200 N at up to at least 5 Hz is thought desirable for comparability with S. J. Grant's rig. A frequency range of at least 0 to 3 kHz is considered to be highly desirable for the transducers, in order to obtain a reasonably unambiguous picture of all phases of the motion.

For practical relevance it is desirable to be able to study the effects of diametral clearances as low as 20 to 60 μm, and also clearances of an order of magnitude greater size, for comparative purposes.

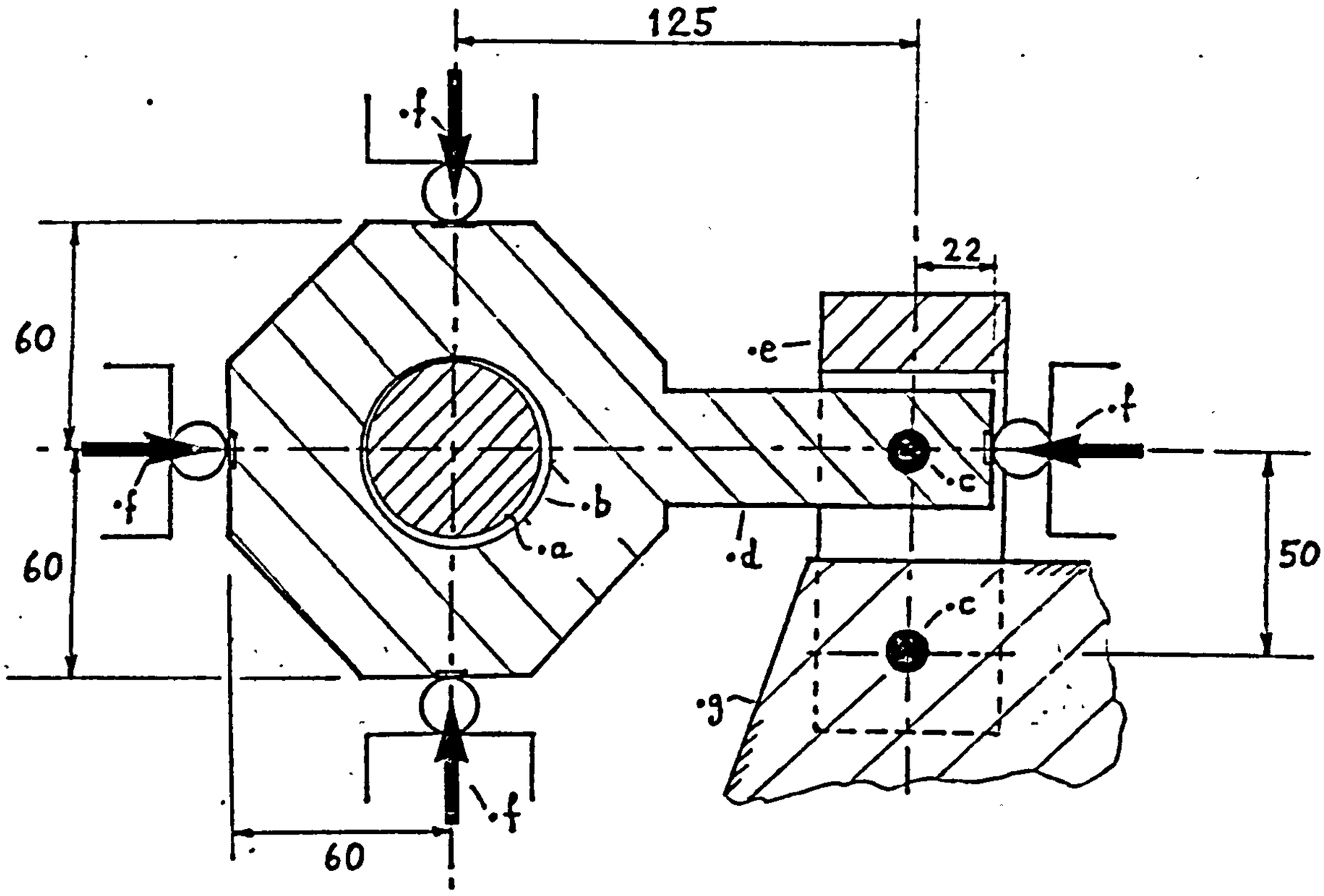

KEY

·a Test bearing pin (fixed to ground)
·b Test bearing journal (clearance exaggerated)
·c Zero clearance pivots
·d Horizontal link and journal housing
·e Vertical link (forked)
·f Exciters for external loading
·g Frame pivot support

92·a–·g: Mechanical arrangement

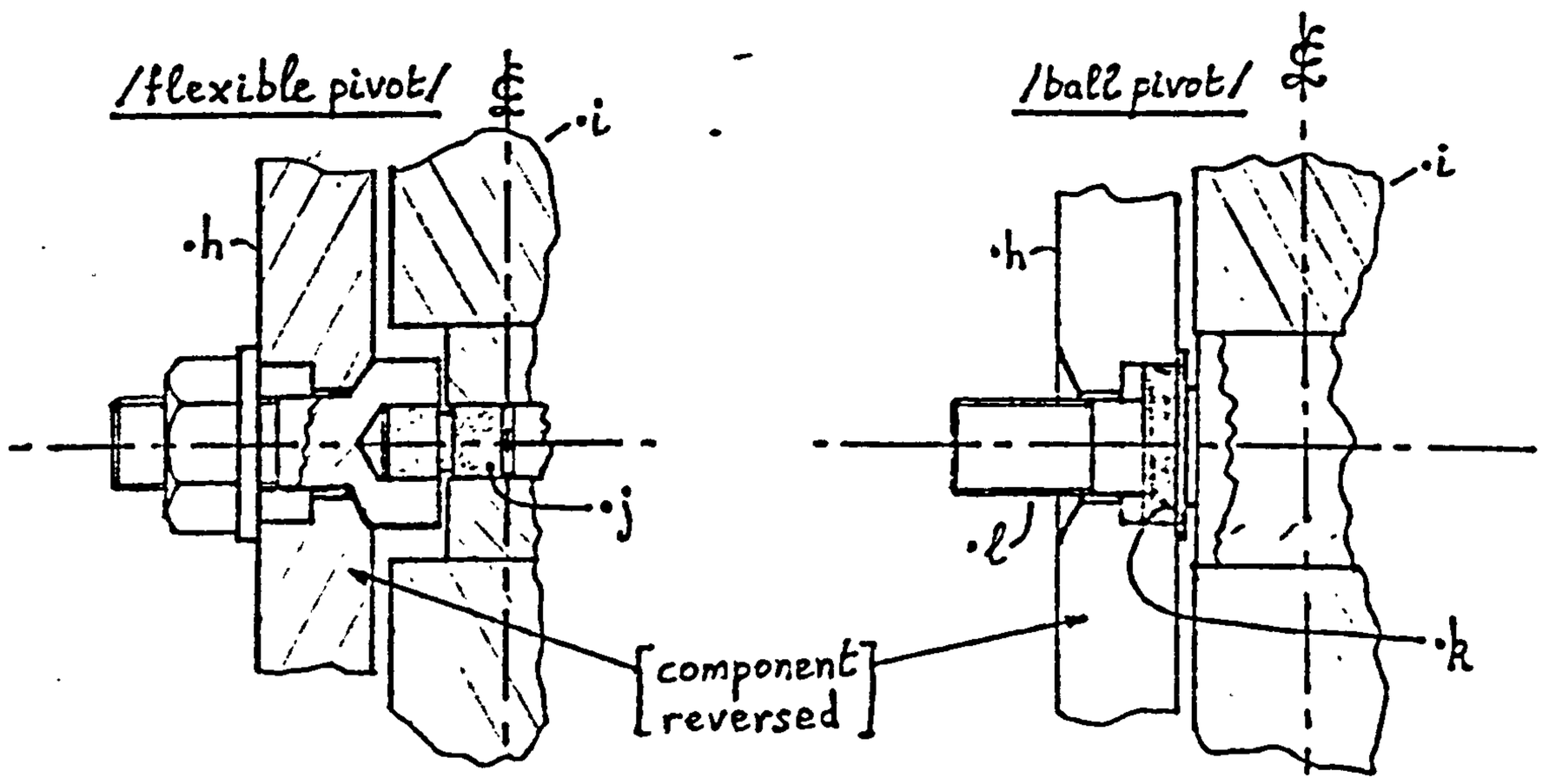

KEY

·h Vertical link fork
·i Horizontal link (or frame pivot support)
·j Modular flexural pivot
·k Instrument class flanged ball bearing
·l Stub shaft (nut and washer to be screwed on during assembly only)

92·h–·l: Zero clearance pivots

5C: BASIC CONFIGURATION

In most previous investigations in this field the joint has been incorporated in an actual linkage, so that the joint loads are generated inertially. Although this has the merit of realism there are two drawbacks with this arrangement for a fundamental investigation into the behaviour of joints per se. Firstly, the crucial parameters cannot be varied independently, since variation in the mass distribution also affects the load locus. Secondly, inertia-generated polar load loci tend to be complex, and difficult to 'tailor' to any chosen form, so that it is not possible to disentangle the effects of different changes to the locus with any certainty.

These problems can be avoided if some form of external excitation is applied to a kinematically stationary linkage or isolated joint (as for example in DUBOWSKY & YOUNG's investigations into one-dimensional ludodynamic behaviour). This also facilitates full instrumentation of the joint.

Dubowsky & Young's arrangement does not provide for a difference between the effective inertias in different directions, which the theoretical investigation has shown to be a potentially very significant factor. A dyad, on the other hand, can be made to represent any effective inertia tensor. Thus the basic configuration adopted for the rig was a single dyad attached to the ground at each end to form a right-angled triangle, having a revolute joint with clearance between one link and the ground and two zero-clearance revolute joints at the other two vertices.* Two types of joint are provided for the latter purpose. In the /flexible pivot/ variant, pairs of Bendix 'Free flex' modular crossed-flexure pivots are used, whereas in the /ball pivot/ variant, pairs of flanged ball bearings are used (see Figure ·g-·i). The latter variant provides a greater rigidity to out-of-plane deflections.

*: see Figure ·a-·g

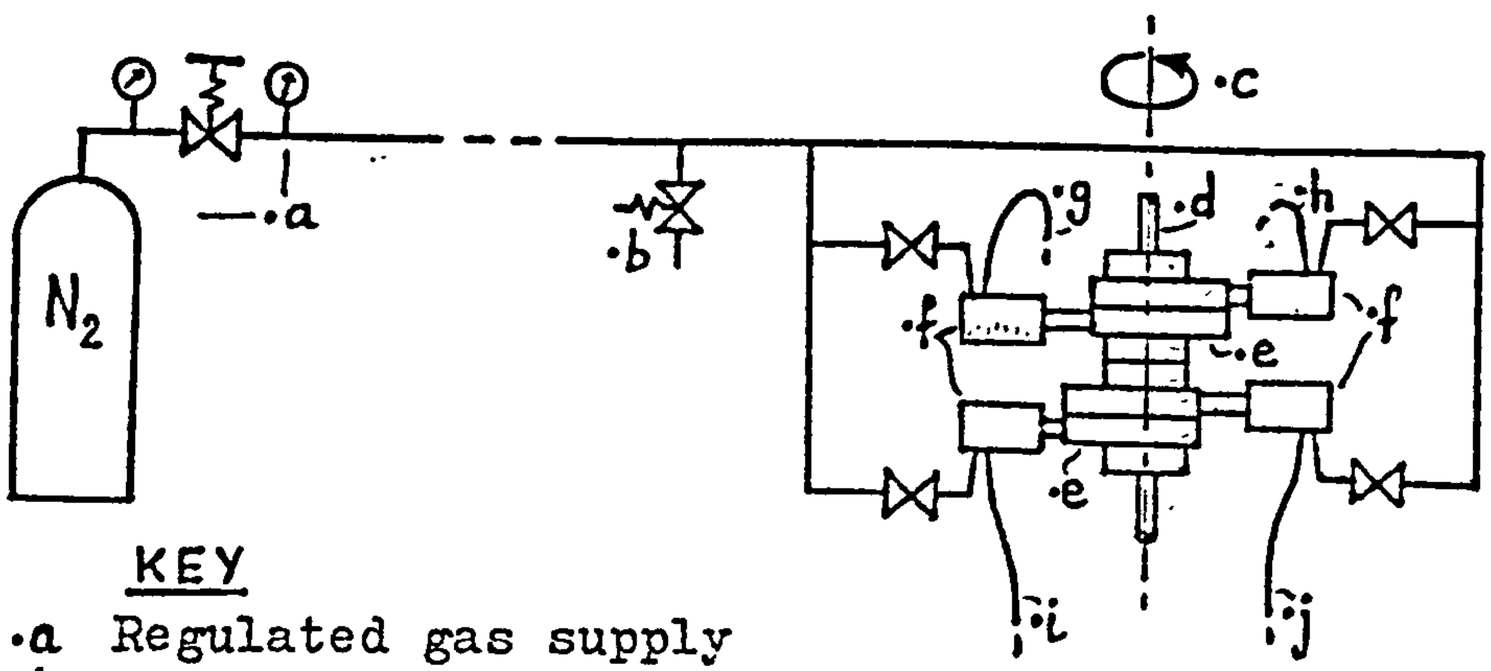

KEY

- ·a Regulated gas supply
- ·b Safety valve
- ·c Variable speed drive
- ·d Drive shaft
- ·e Variable throw eccentrics
- ·f Master cylinders
- ·g, ·h, ·i, ·j } Flexible pipes
- ·k Slave cylinders

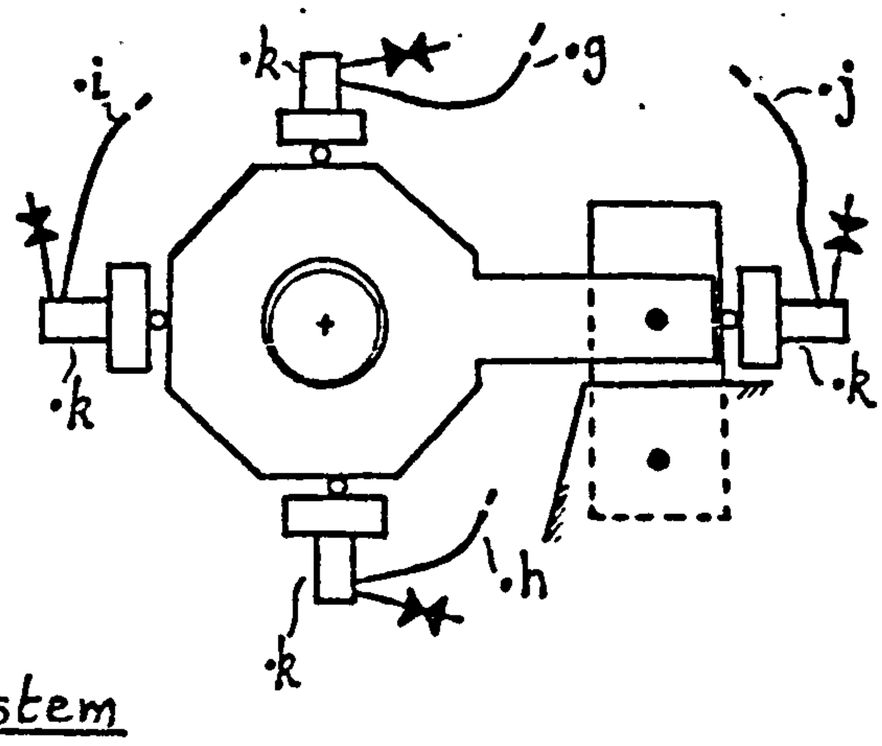

93 ·a–·k: Pneumatic system (schematic)

5D: EXCITERS

External excitation being adopted, it is important that the exciter does not significantly modify the response: i.e. the exciter must have very low mechanical impedance and friction. Pneumatic excitation in principle has this characteristic, whereas hydraulic exciters would be more prone to damp out the high frequency component of the response. Pneumatic or hydraulic excitation scores over electromagnetic excitation in that the exciter can be smaller for the load generated, so the problem of added inertia is minimised and load paths can be kept much shorter. Pneumatic excitation was therefore adopted.

The requirements for the exciting system implied in the previous sections are that it can produce approximately linear and non-linear load vector loci at variable orientations, magnitudes, frequencies and distances from the origin. This can be achieved by using two opposed pairs of unidirectional exciters mounted on orthogonal axes, each generating more or less harmonically varying loads at the same (variable) frequency, with amplitude and phase separately controllable for each pair and mean load separately controllable for each exciter.

[RG] This specification was achieved very quickly and simply by using two variable throw eccentrics driven by a variable speed motor to generate the harmonic signal, and four pairs of automobile brake cylinders (Girling type 390313 W), with compressed nitrogen taking the place of the hydraulic fluid, to transfer the load to the joint. The nitrogen is introduced into each of the lines in turn at a regulated pressure(up to 35bar maximum), then adjusted if necessary by means of the bleed screws on the cylinders until the intended load variation is observed. (Considerable modifications to the slave cylinders proved necessary, as described in Section G). The complete excitation scheme adopted is shown schematically in Figure ·a-·k

The maximum displacement at the master cylinder end is 12mm peak-to-peak, which is so much greater than the displacement at the slave end (the diametral clearance of the joint under test) that the effect of the latter on the gas pressure variation is negligible.

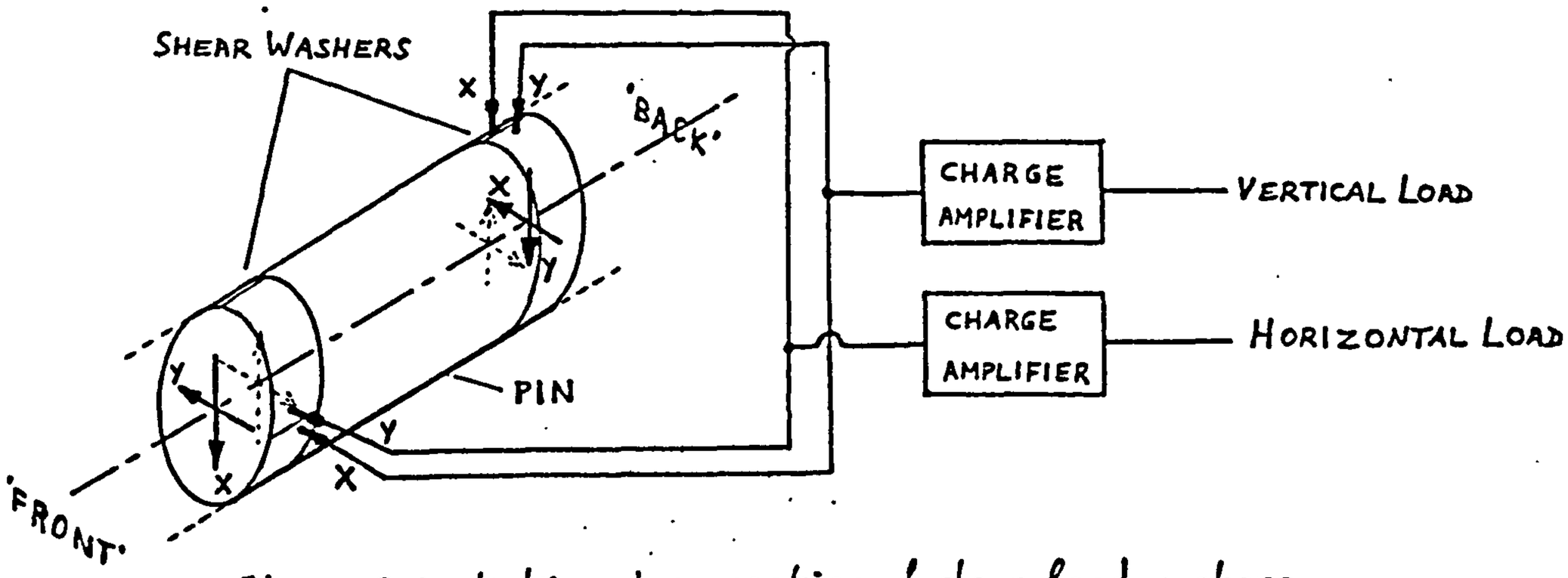

94.a: Orientation & connection of shear load washers

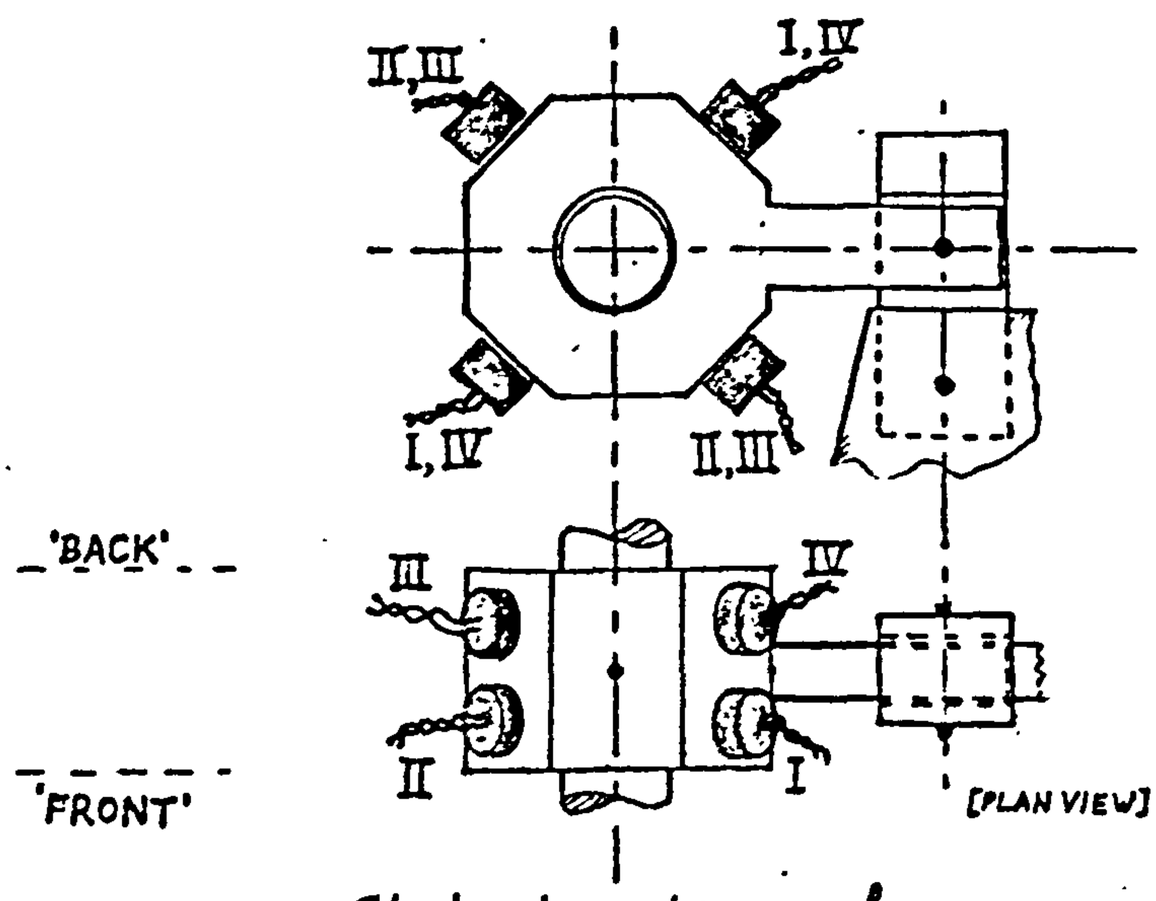

94.b: Location of displacement transducers

.c Carrier wave generator	[Channels II,III,IV similar to I.]	.d 1:1 DC decoupler	.e Bridge: passive arms	.f Bridge: active (transducer) arms	.g Anti-distortion	.h Input impedance compensation	.i Variable gain preamplifier	.j Demodulator/ smoother	.k First stage filter	.l Second stage filter

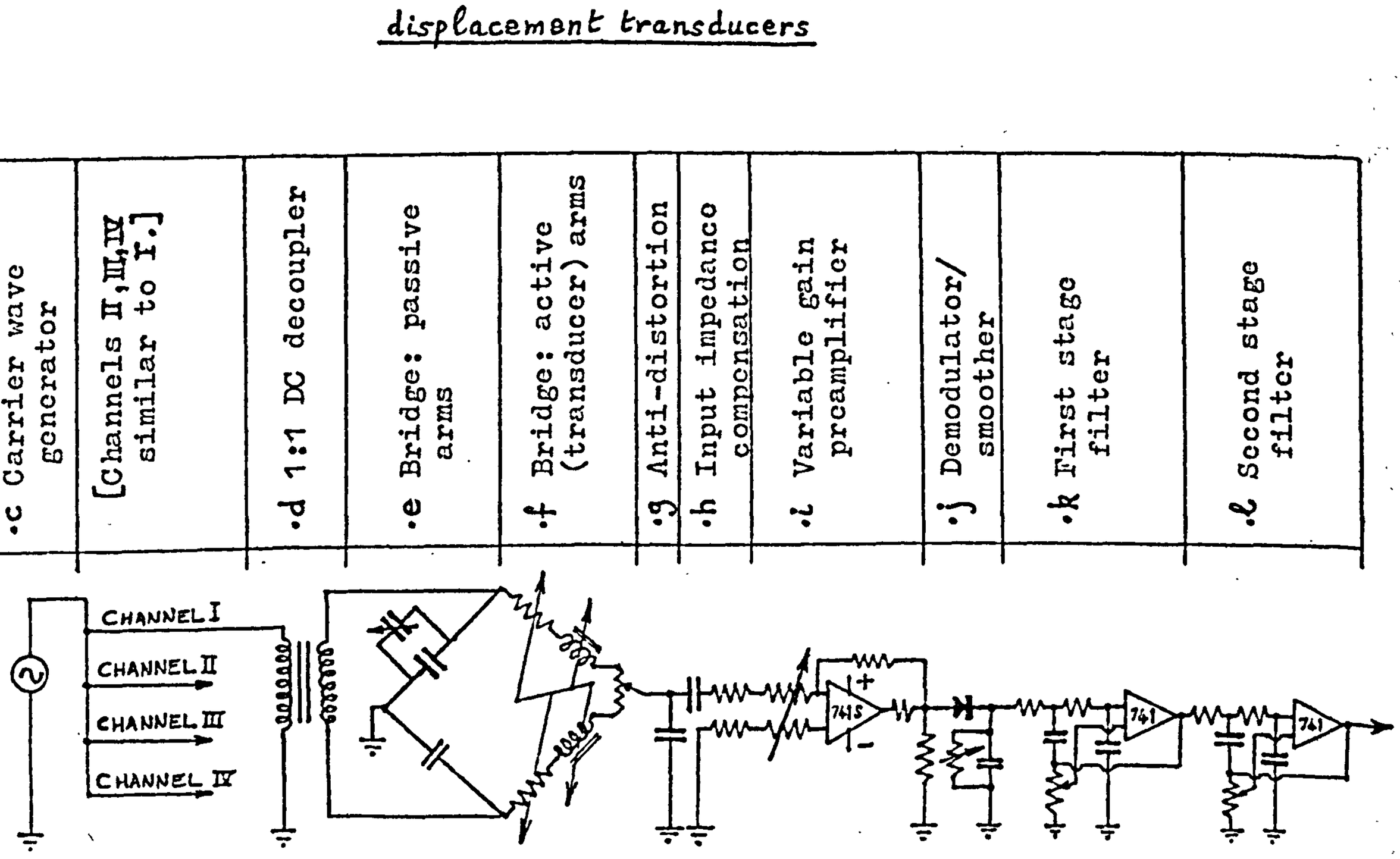

94.c — .l: Circuit diagram for displacement transducers

5E: TRANSDUCERS

Piezo-electric load transducers, offering both high sensitivity and excellent frequency response, seemed highly suitable for recording both continuous and impact loads. A pair of Kistler type 9063 2-component shear load washers were available, having a measuring range of ± 10 kN, resolution of 10 mN, and resonant frequency of 40 kHz (manufacturer's "tentative" data). By clamping the bearing pin between the two load cells, and summing the outputs separately in the horizontal and vertical directions, a sure indication of the total load in these directions is obtained. The orientation and connection of the load cells for this purpose are shown schematically in Figure ·a. With this arrangement, the practical limit on the frequency response is of course the resonant frequency of the pin/load cell assembly (see p.104).

A means of measuring the displacement is also desirable: firstly, in order to follow the trajectory after loss of contact, and secondly, to provide a broader base for diagnosis of any unexpected phenomena. Two side-by-side transducers were specified so that non-coplanar movement could be detected, along each of two orthogonal axes. Spatial considerations led to the axes selected being mid-way between the axes of the exciters (as shown in Figure ·b).

[R.G.] This requirement was met by the use of an opposed pair of inductances for each measurement. These were constructed for the purpose, and each comprised copper wire wound on a ferroxide core, set in epoxy resin and cased in a short length of pipe.

[R.G.] Each pair of inductances was incorporated in a Wheatstone bridge driven at 28.5 kHz (10 V peak-to-peak). The unbalanced signal from each bridge was pre-amplified, demodulated and filtered using a purpose-built circuit (Fig.·c.-·ℓ). Operational amplifiers were used for the preamplifiers and active filters, a high slew-rate type proving to be necessary for the former.

Since neither of the above transducer sets provides a wholly unambiguous indication of whether contact is lost, it was also decided to try to record contact loss by the breaking of two separate electrical circuits, one through each half of the joint (Fig.96·a-·f), so that it is possible to detect occasions when contact is lost from one edge of the bearing only. Accordingly the pin was made in two halves and sandwiched between three discs of insulating material.

Data recording: A particular problem is posed in this investigation by the fact that the incidents of major interest are of brief duration both in absolute terms and in relation to the cycle period, while at the same time it is desirable to study a sequence of such incidents and relate them to the cyclic load waveform.

[RG] This difficulty was met in part by obtaining a four channel F.M. instrumentation tape recorder (Bruel & Kerr type 7003) whose twin operating speeds of 1.5 and 15 inches per second provide a slow motion replay facility. At the higher speed the specified frequency range is 0 to 10 kHz.*

Other recording instruments used were a (Bradley type A2) differential oscilloscope, two (Telequipment types DM53A & DM64) storage oscilloscopes and a (Gould type OS 4000) digital storage oscilloscope with playback, the last being coupled to a (Farnell type RW 11) X-Y pen plotter.

* In practice the recorder was found to generate intermittently an unexpectedly high level of noise in the fractional kiloHertz range, possibly due to a faulty tape transport. Where this is visible on the traces reproduced in this thesis it is marked 'tape noise'.

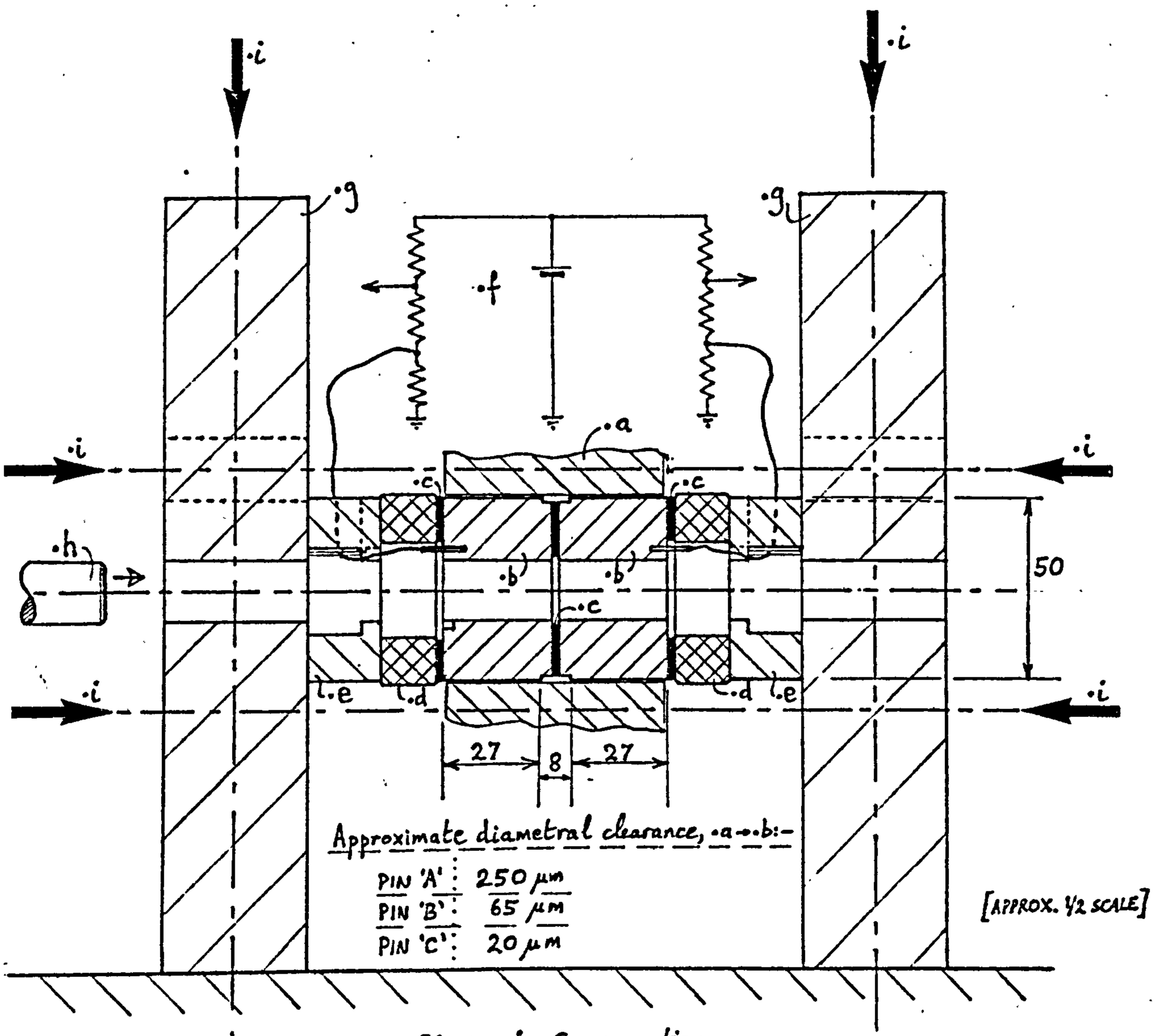

Approximate diametral clearance, ·a→·b:-

PIN 'A'	250 μm
PIN 'B'	65 μm
PIN 'C'	20 μm

[APPROX. ½ SCALE]

96·a–·i: Cross-section through test bearing

KEY:

- ·a Journal
- ·b Pin halves
- ·c Insulating discs
- ·d Load cells
- ·e Spacing collars
- ·f Contact-loss circuit
- ·g Side plates
- ·h Mandrel
- ·i Clamp stud location

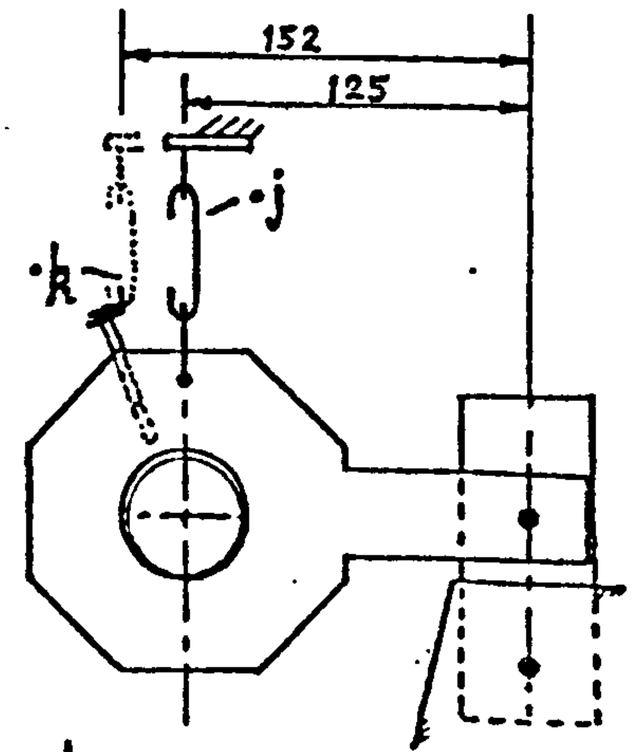

96·j, ·k: alternative positions of hook for /suspended/ journal

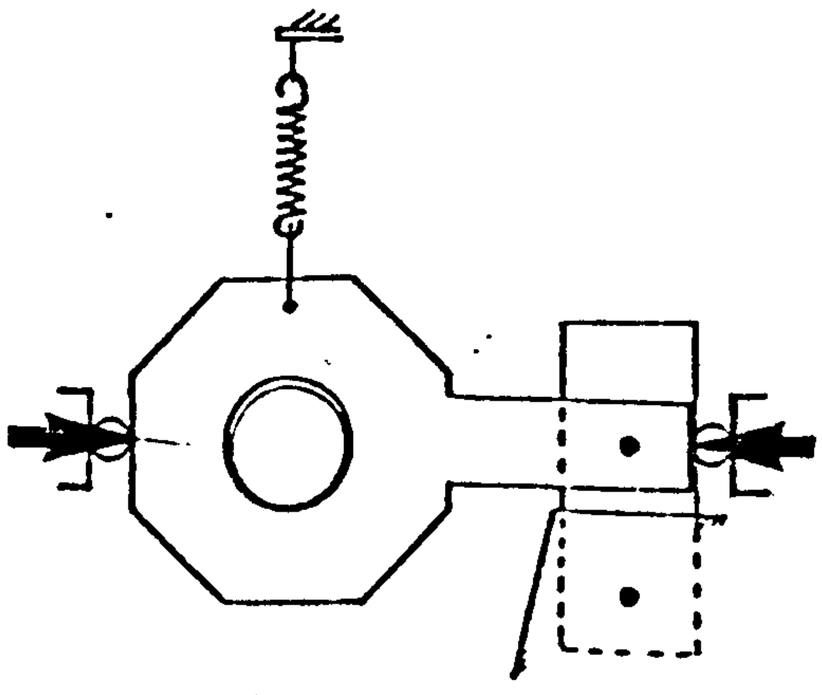

96·l: /top-sprung/ arrangement

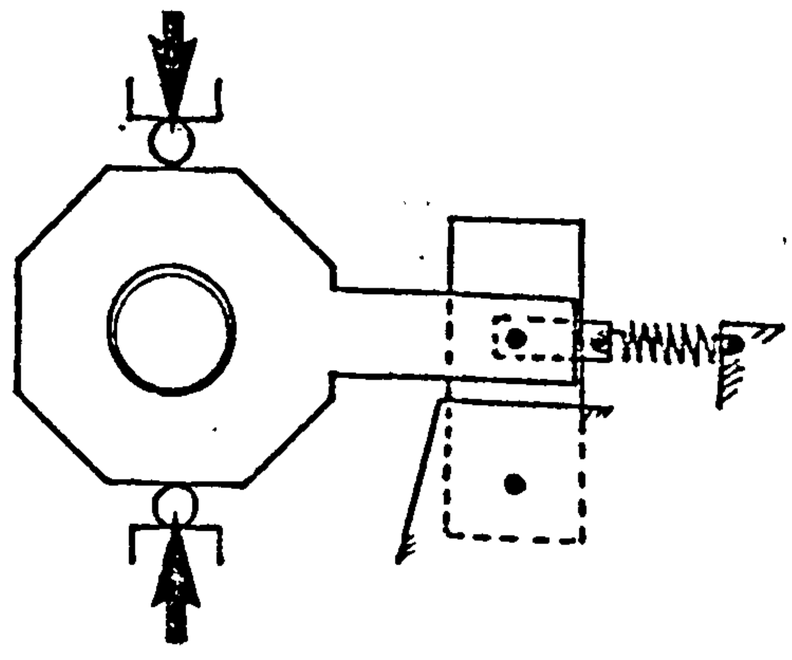

96·m: /side-sprung/ arrangement

5F: ALIGNMENT & ADJUSTMENT FEATURES

The design incorporates a number of features to facilitate correct alignment, and convenient alteration of the parameters listed in section 5B, as follows.

Clearance joint members: The aluminium alloy bearing pin, sandwiched between the two load transducers, is clamped between two heavy side-plates, with a removable mandrel passing through this assembly during the setting-up procedure. The side-plates are in turn clamped to the cast iron block that serves as a base. A selection of different sizes of bearing pin can be used, up to 50 mm diameter,* and the steel journal can also be exchanged, being a taper fit in the cast iron housing. With the mandrel inserted and the clamping nuts slackened the pin can be re-oriented to distribute the wear more evenly. (A grub-screw in the mandrel is engaged in a notch in the pin for this purpose.) The arrangement of the pin is shown in Figure .a-.i.

Joint alignment: The grounded zero-clearance pivot is located in a 'pivot stand' which is attached to the base plate by means of two clamping screws through oversized holes and two levelling screws on a cross bar(90-1). This permits adjustment of the journal axis direction relative to that of the pin in two planes. For this adjustment, and for some of the tests, the bearing housing is /suspended/ by a hook from a point above the assembly, the top exciter being removed if necessary (see Figure .j-.k). By careful adjustment of the suspension point location, the journal can be /floated/ so that it does not touch the pin at any point. By observation of the moment when the journal makes contact with each half of the pin when the linkage is gently disturbed from this position, parallel alignment can be checked to a very high accuracy.

Spring loading: In the /top-sprung/ variant, a small vertical preload is applied by means of a suitable tension spring in place of the hook referred to above. In the /side-sprung/ variant a load is similarly applied to the upper zero-clearance pivot, after removal of the exciter from that side (see Figures .ℓ, .m).

* For the experiments described hereunder, three pins of nearly 50mm diameter were used, identified as A, B and C in order of decreasing clearance.

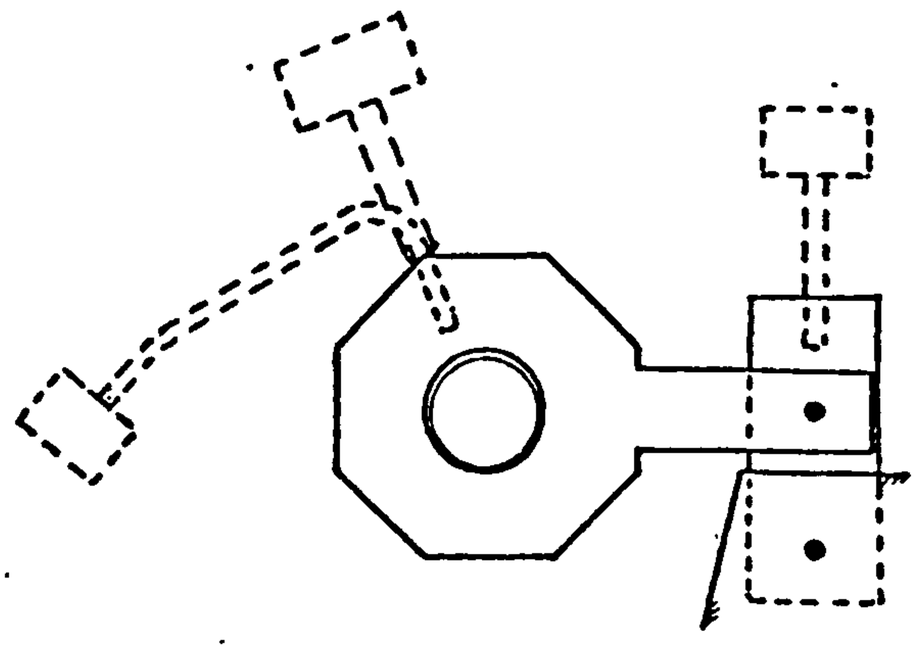

97·a: locations for attached 'counterweights'

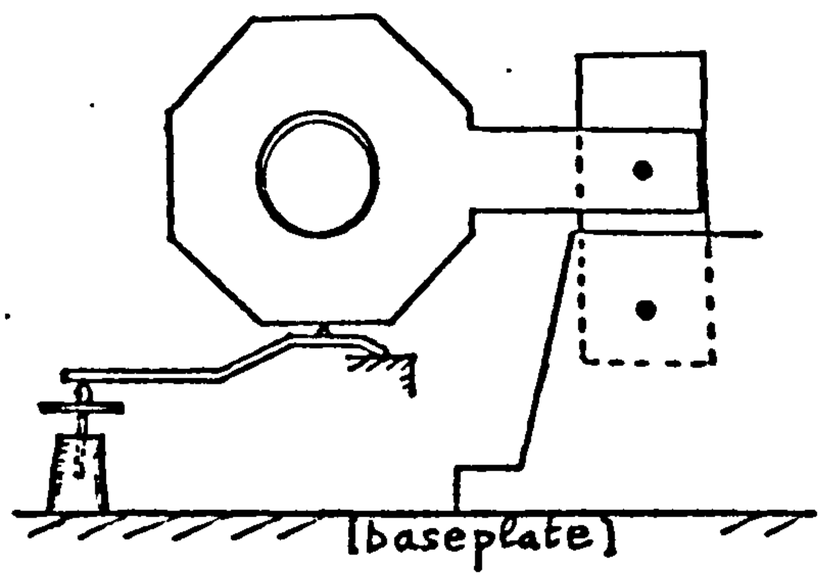

97·b: Journal /propped/ on jack.

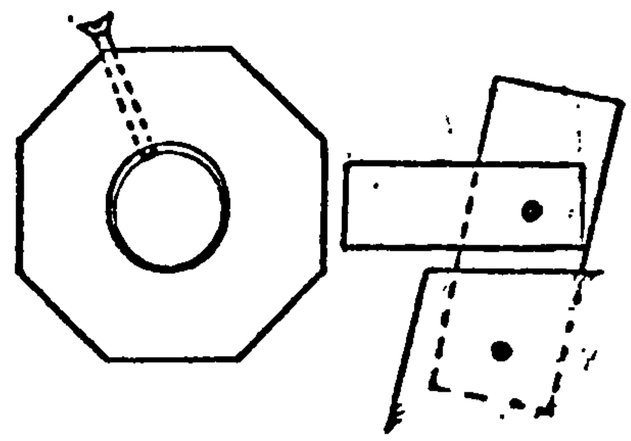

97·c: Journal /clamped/ to pin and /isolated/ from links.

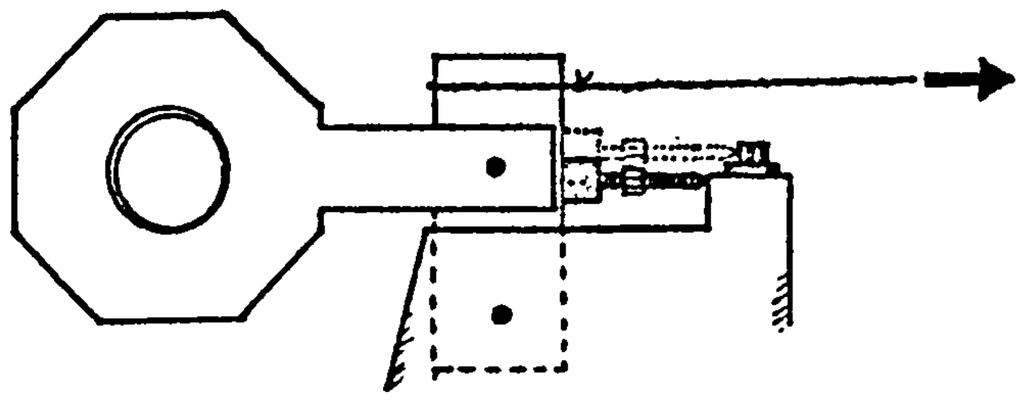

97·d: Vertical link /held/ against side jack.

Inertia: The inertial characteristics of the linkage can be changed by attaching massive components where shown by the broken lines in Figure .a.

Exciters: The throw and phase of both eccentrics can be adjusted by hand after releasing a single clamping nut on the drive shaft. The master cylinder pistons can be instantly removed for checking, lubrication with silicon grease or replacement at any time, after lifting out a spacer block that separates the piston from the eccentric. The slave cylinders are attached to supports with oversized holes for all the screws.

[R.G.] The load from the slave pistons is applied through 16 mm diameter steel balls, to minimise constraint in the transverse directions, and plane-faced tool steel load-pads. The balls are readily removed, for example to align the journal in the /floated/ condition.

Displacement transducers: The inductances are attached by brackets to the side plates; the axial position of each inductance can be adjusted after release of a clamping screw in its bracket.

Screw jacks: A light screw jack and lever arrangement can be inserted under the journal to lift it very slightly out of contact with the pin (Figure .b). In this /propped/ condition the load transducers can be zeroed. Another screw jack can be used to provide an adjustable stop against which the vertical link can be /held/ (by a tensioned cord) to eliminate one degree of freedom (Figure .d).

Clamp screw: The journal housing can be /isolated/ from the dyad and /clamped/ to the pin in its central plane, as shown in Figure .c.

Lubrication: To provide a /dry/ condition, the pin and journal surfaces were degreased with acetone. Alternatively, a few drops of light machine oil were applied and then the excess removed with a tissue, leaving a minimal film of oil: this will be termed the /oiled/ condition.

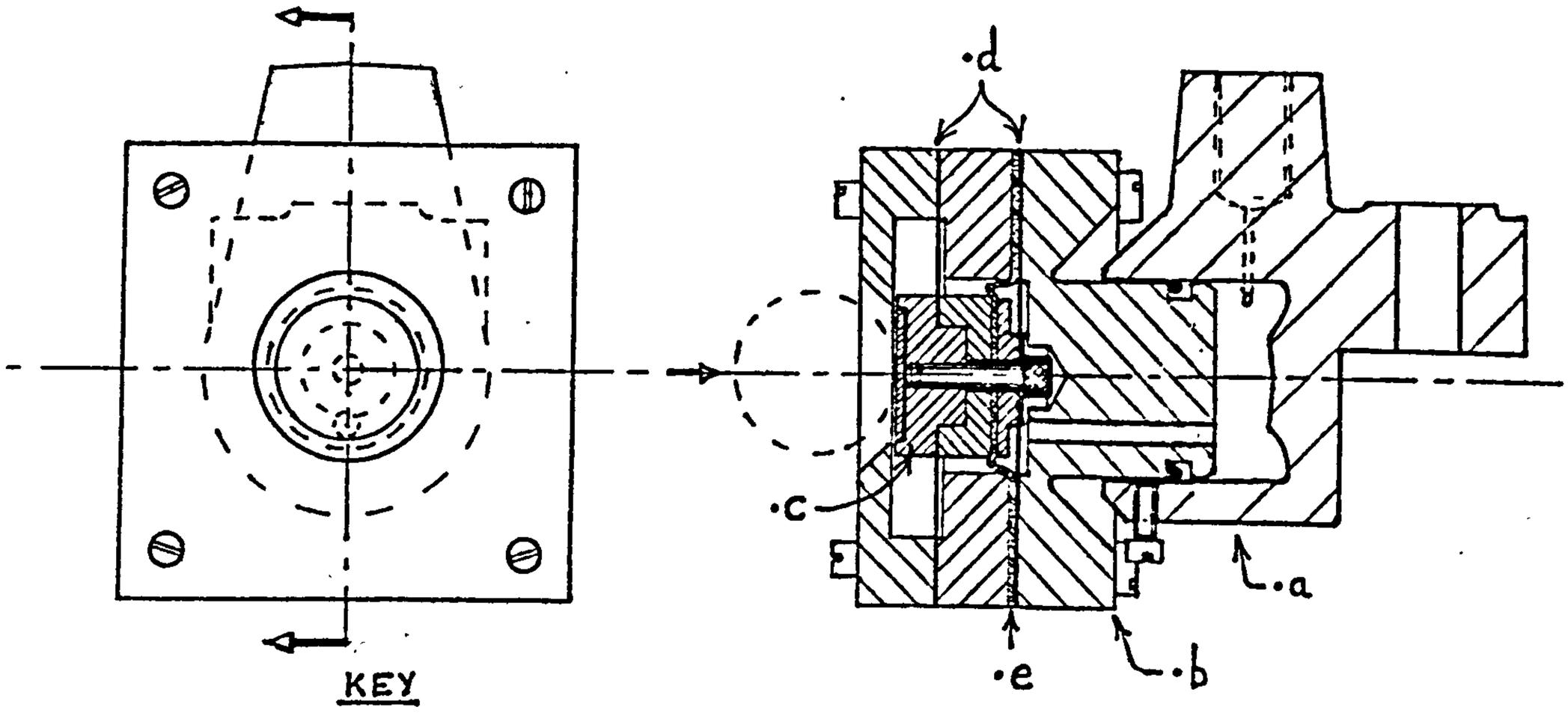

KEY

- a Slave cylinder rump
- b Slave cylinder extension
- c Piston
- d Spider springs
- e Convoluted diaphragm seal

[FULL SIZE]

98.a--.e Modified pneumatic slave cylinder

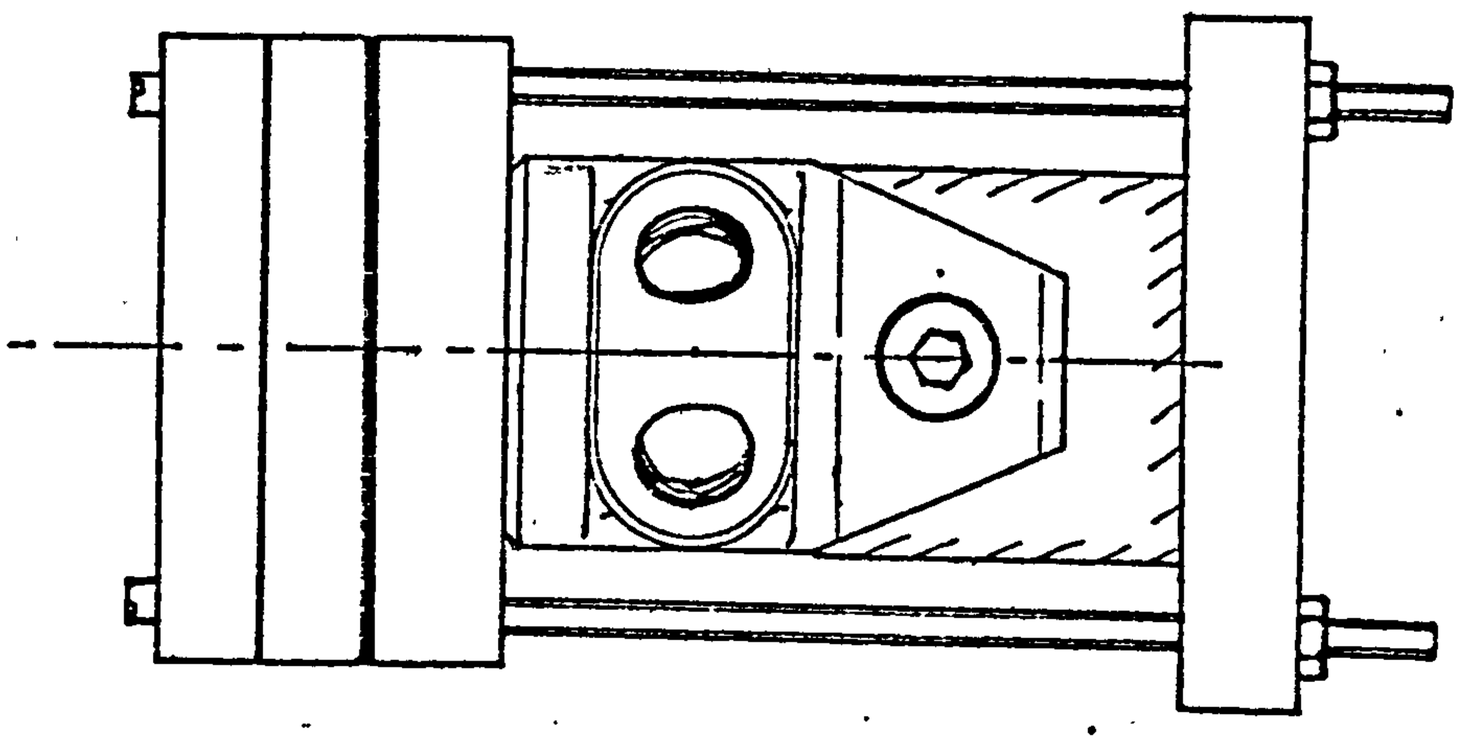

98.f: Typical arrangement of adjustable stops for extension

5G: DEVELOPMENT OF EXCITER SYSTEM

Initially a single exciter unit was tested by mounting the slave cylinder in series with a compression load transducer (piezo-electric type) in a bench vice. It was observed that the amplitude of the recorded load variation fell off rapidly, being restored if the whole assembly was disturbed. This was attributed to binding of the lip seals incorporated in the piston supplied with the cylinder. A new piston was made incorporating an O-ring seal. This appeared to eliminate the problem in the bench assembly, but in the main rig it was found that seal friction was still a significant proportion of the applied load.

Accordingly a completely new actuator assembly was designed. This is shown in Figure ·a-·e. As can be seen, an extension cylinder sealed by an O-ring can be moved and clamped in the rump of the brake cylinder to provide setting-up adjustment. The piston is supported in this extension cylinder by two spider springs to eliminate sidewall contact, and sealing is effected by a 'Bellofram' preconvoluted diaphragm seal. The effect is that Coulomb friction is eliminated entirely. The price for this benefit is the introduction of the force variation associated with the varying deflection of the spider springs. This may well be significant by comparison with the exciting force in the direction of minimum force. It was therefore decided to use only one pair of exciters (vertical or horizontal) at a time, the load on the normal axis being applied by means of soft tension springs (/top-sprung/ or /side-sprung/ variants).

It was found that, because the effective area of the moving piston is slightly less than that of the piston clamped in the cylinder rump, there was a tendency for the extension assembly to be worked outwards at high gas pressures. The clamping screw was therefore supplemented by an adjustable stop limiting the outward movement. Details differed at each exciter position, but Figure f shows a typical arrangement. (See also 90.f).

5H: DEVELOPMENT OF DISPLACEMENT TRANSDUCER SYSTEM

[R.G.] Transducer casings: Short pieces of steel pipe were used in the first place as the casing for the displacement transducers. The capacitance between the casing and the windings was thought at the time to be contributing to circuit balancing problems so a new set was made using plastic piping. These were less robust and one was damaged by overtightening of the clamping screw. A pair of the first set was therefore reinstated, and this time gave no trouble.

Second order imbalance: For a long time the signal from the Wheatstone bridge was highly distorted, mainly due to the presence of a harmonic at twice the carrier frequency. The cause was never found but by trial and error it was discovered that a 10 pF capacitance between the output and the earth (as in Figure 94·g) effectively eliminated the problem.

Bridge balancing: The bridge circuit was originally designed on the assumption that the transducer functions as a variable reactance. In fact at this frequency the hysteresis losses in the cast iron are such that the resistance is both greater ($\approx$1500Ω) and varies more rapidly than the reactance ($\approx$ 700Ω).

As a consequence the bridge must include separate facilities for balancing the resistance and the reactance. As shown (Fig. 94·e-f) this was achieved by means of a potentiometer between the transducers to balance the resistance and a trimming capacitor in one of the passive arms to balance the overall impedance. A "balanced" circuit in this context means one in which the output signal varied in the range 0.05 to 0.25V (peak) without changing phase as the journal was moved across the clearance circle, with a driving carrier signal of 5V peak.

A consequence of the mixture of reactance and resistance balancing is that the output from each of the four channels was at a different phase, so that they could not be added or subtracted until after the demodulation stage.

Linearity: The linearity of the preamplifier/demodulator circuitry in earlier tests was poorer than expected. After extensive investigation, three contributory factors were identified. Firstly, the gain depended on

the combined impedance of the bridge, which varied slightly from maximum to minimum signal. The addition of a 47kΩ resistor in series with the bridge reduced this problem to negligible proportions. Secondly, as noted in Section E, the slew rate of the type 741 operational amplifiers in the pre-amp stage was found to be inadequate for amplified signals of more than 2V: the rate was actually 0.4V/μsec, though nominally 1V/μsec. The replacement amplifiers (type 741S) have a nominal rate of 20V/μsec. Thirdly, the forward voltage drop of the demodulator diode distorted the output unless the modulated amplitude was maintained at no less than 0.5V peak.

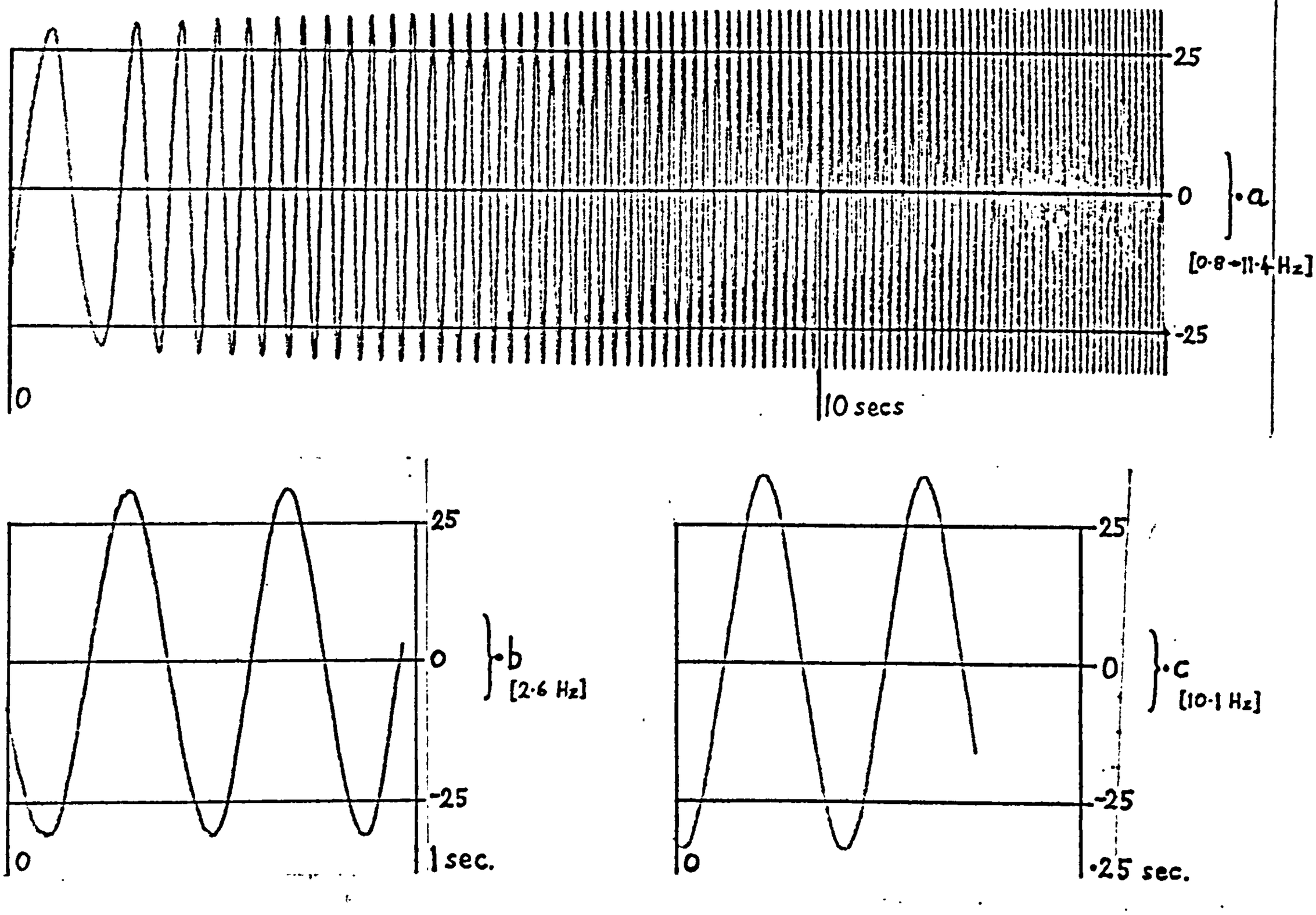

101 ·a--·c: Effect of cycle frequency on waveform & amplitude of load generated by a pair of exciters

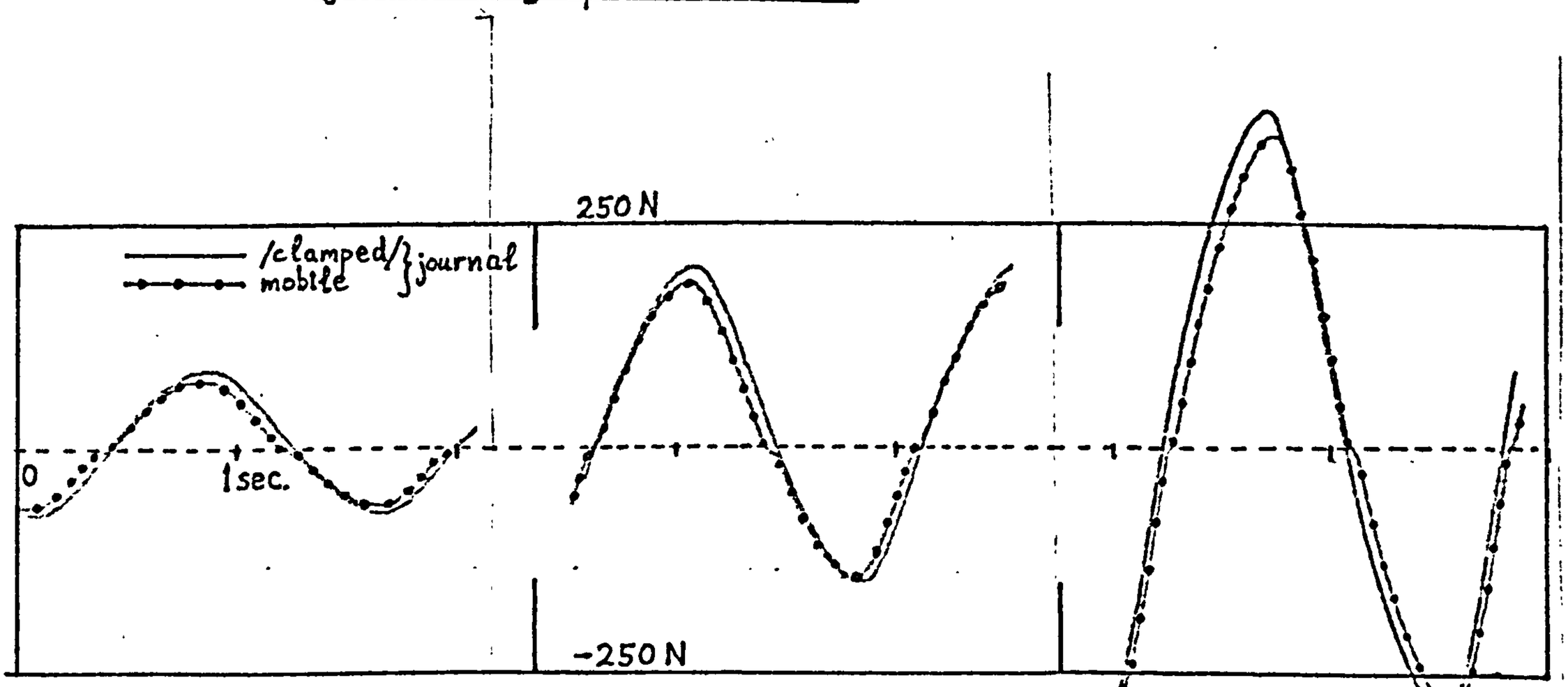

101 ·d--·f: Effect of journal displacement on exciting loads

5I: PERFORMANCE TESTS: EXCITERS

Cyclic pressure variation: The horizontal pair of exciters were filled to approximately 27 bar* and operated (with the eccentrics at maximum throw) at varying frequencies from near the minimum to the maximum obtainable. The journal was /clamped/ to the pin to eliminate dynamic effects, and the summed output of the horizontal load transducers was recorded. Figure .a shows the variation of the cyclic load amplitude with time as the frequency was increased, and Figures .b and .c show the waveform and amplitude at two different frequencies.

A variation of load amplitude with frequency would be expected for two reasons: firstly, the transition from near-isothermal to near-adiabatic conditions, and secondly increasing viscous losses in the pipes (which were threaded with wire to minimise the dead space). The figures suggest that the second effect is negligible while the first causes a peak load variation of about 11% over the speed range. The variation of load with time near the zero load points shows a reasonable approximation to the linear variation assumed, at both the test frequencies. The greatest deviation occurs at the lower frequencies, due to cyclic variation in the motor speed.

A test similar to the above with only one exciter operating showed the ratio of maximum to minimum load generated by a single exciter under nearly isothermal conditions to be about 1.65, with maximum stroke at the master cylinder. It is deduced that the trapped volume is varied between about 5300 and 8800mm^3.

Effects of motion of driven element: With the motor running at the minimum stable speed, the load waveform with the journal /top-sprung/ and free to move in a 250 μm clearance circle (under the action of a moderate net vertical load as well as the cyclic horizontal load) was compared with that when the journal was /clamped/. The difference between the two can be attributed to the spider springs in the slave cylinders and the spring effect of the compressed gas, since inertial effects are very small under these conditions - as was evident from the displacement transducer signals. Figures .d, .e, .f show the comparison at three different pressures. It may be deduced that the spider springs alter the horizontal load by ± 9 N approx. at maximum deflection, the isothermal

*All pressures quoted are line pressures and normally correspond to the master cylinder pressure at mid-stroke.

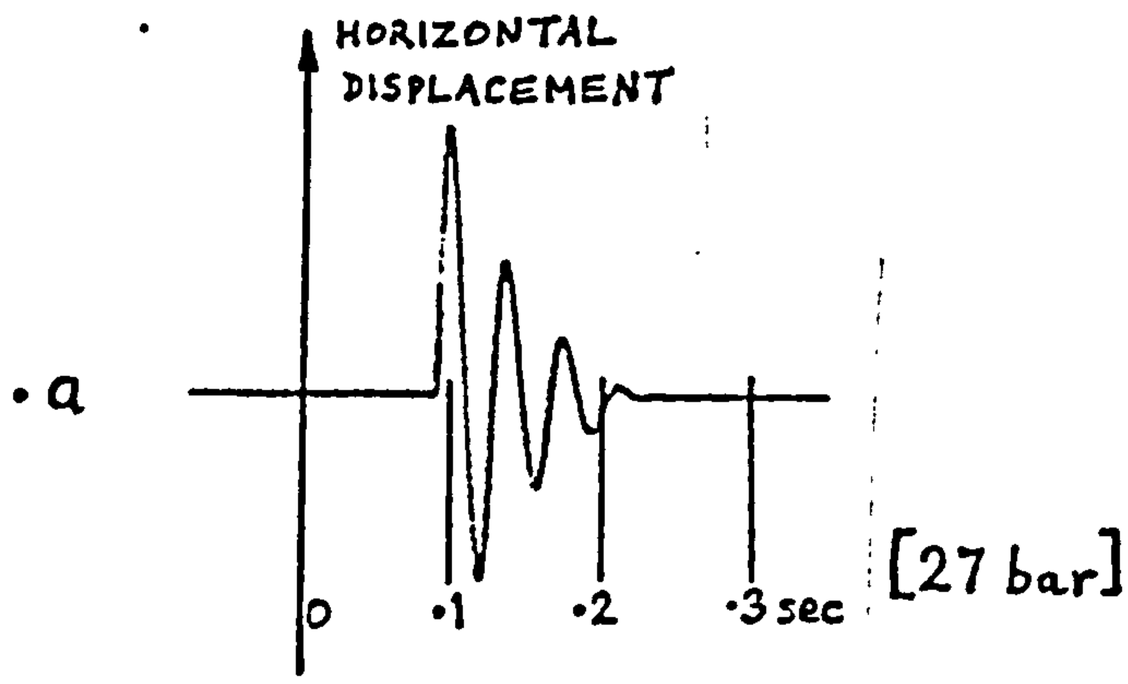

·a

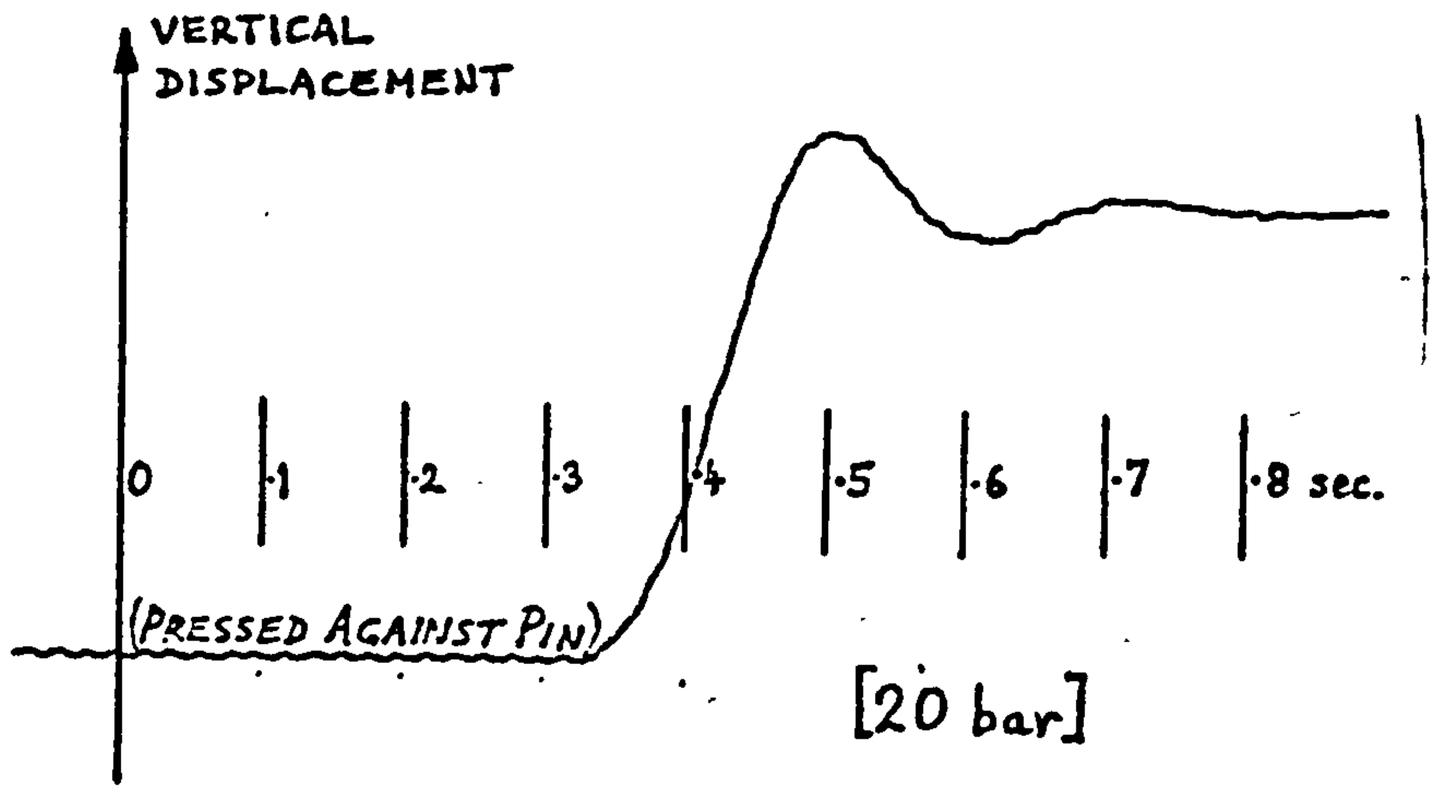

·b

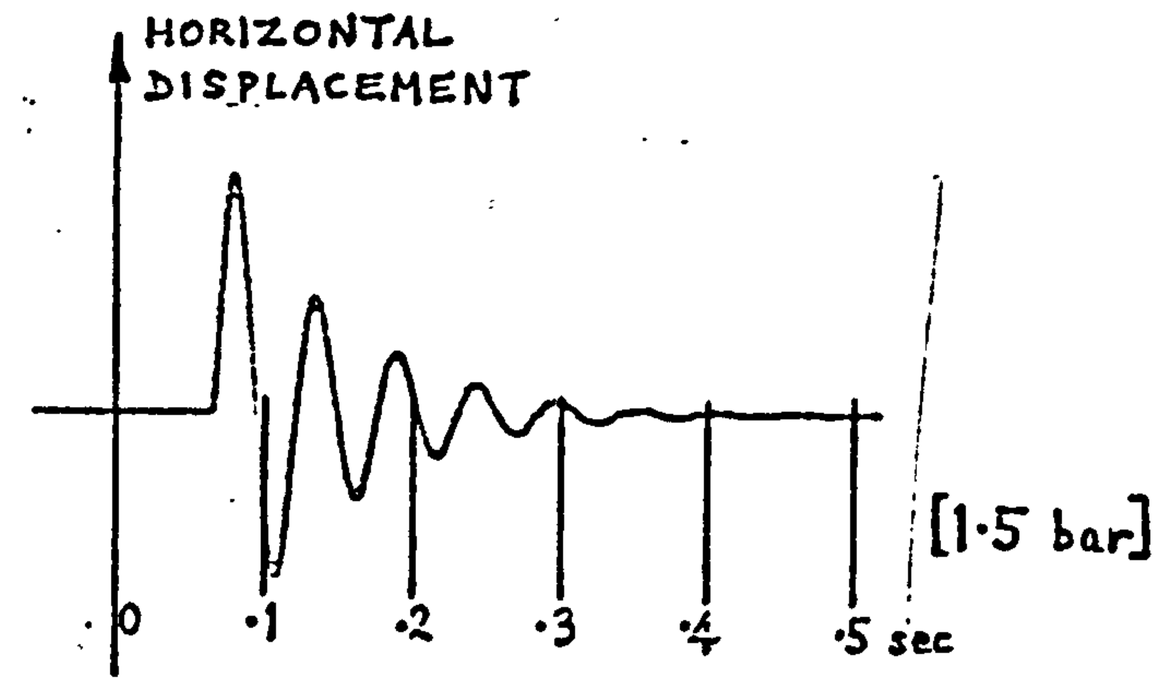

·c

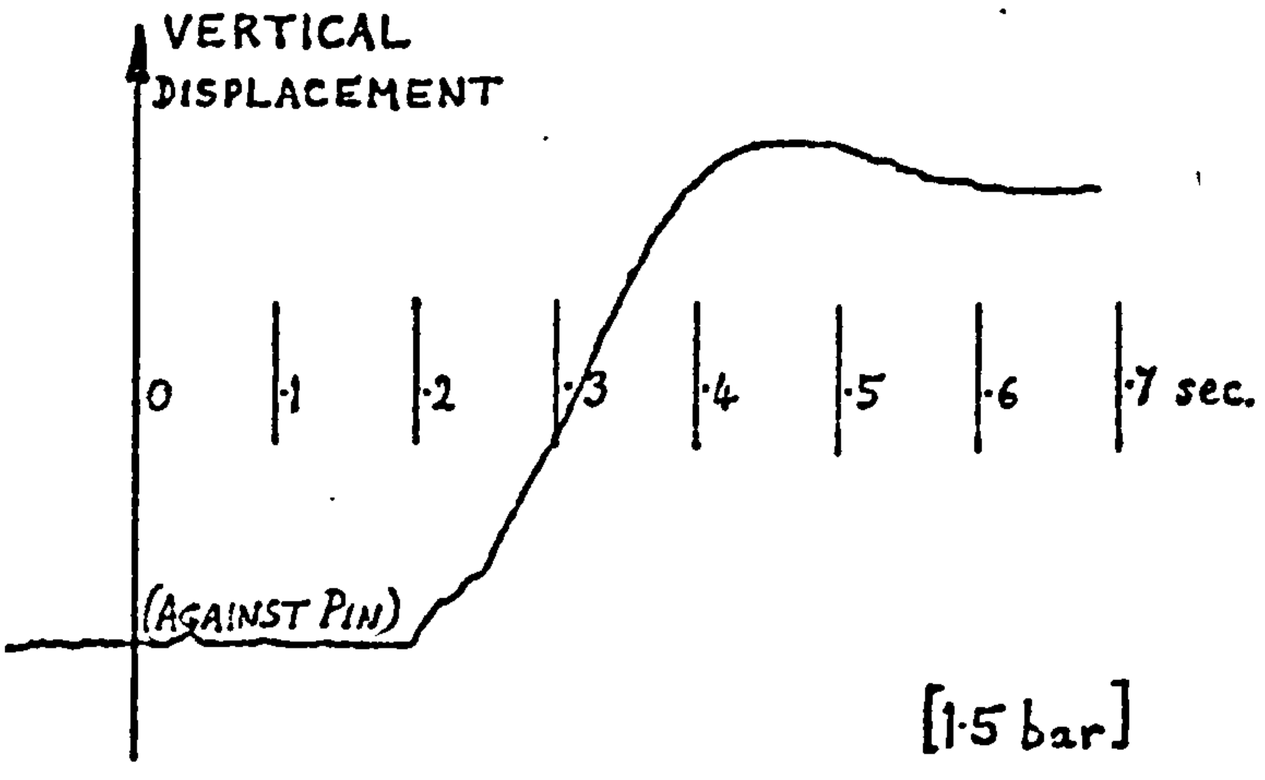

·d

102 ·a – ·d: <u>Free oscillations of journal with horizontal exciters in place</u>

effect of the gas being no greater than this at line pressures up to 30 bar. Both effects should be proportionally reduced when smaller clearances are used.

From similar tests at different times it was observed that in some circumstances the apparent stiffness of the spider springs was greatly increased towards the end of their stroke, probably due to some form of misalignment in the slave cylinder assembly. The effect of this on the results is unpredictable.

For a final test, an equal, constant pressure was applied to the two horizontal exciters and the apparatus was adjusted until the /top-sprung/ journal was in equilibrium in the centre of the clearance circle. Displacement measurements were combined and recorded to show the horizontal displacement after a horizontal blow to the vertical link, and the vertical displacement after the sudden removal of a vertical load. These are shown, for both high and low gas pressures, in Figures .a to .d opposite.

It is estimated that the natural frequency of the horizontal vibrations at low pressure (.c) is consistent with the spider spring stiffness determined statically, and the increased frequency at high pressure (.a) is consistent with the expected adiabatic spring effect of the gas. The level of damping is evidently well below critical. The vertical displacements (.b,.d) show low frequency oscillations associated with the tension spring supporting the journal. The reason for the increased frequency at the high pressure (.b) is obscure, but in any case the magnitude of the effect is not considered to be significant. More importantly, the level of damping of the disturbance in Figure .b is seen to be quite modest, and similar to that in Figure .d. Since the vertical displacement is associated with rolling of the balls over the load pads, this observation rules out any significant Hertzian stress overload at the balls or pads under the high pressure.

Conclusion: The author's evaluation of the performance of the exciters is that it is close enough to the intended performance to yield results of some value, but in view of the known shortcomings - principally the large variation in the apparent spider spring stiffness - a wide margin of uncertainty around quantitative results must be recognized, particularly in the case of relatively large clearances (pin A) and relatively small external loads.

a

b

c

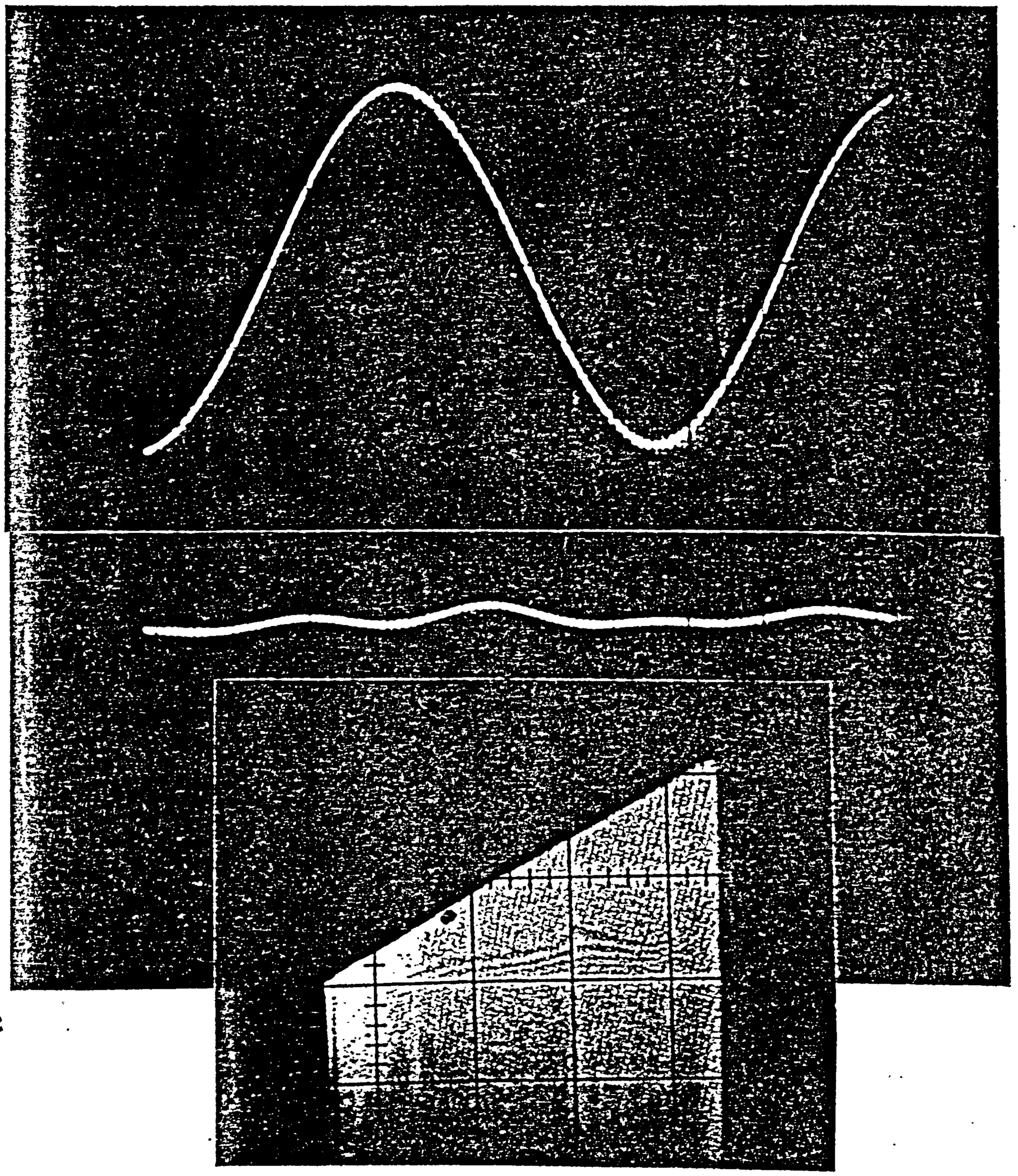

103·a--·c : Modulated displacement transducer signal:-

(·a) Normal (·b) Minimal (·c) Varying, vs. demodulated signal

d

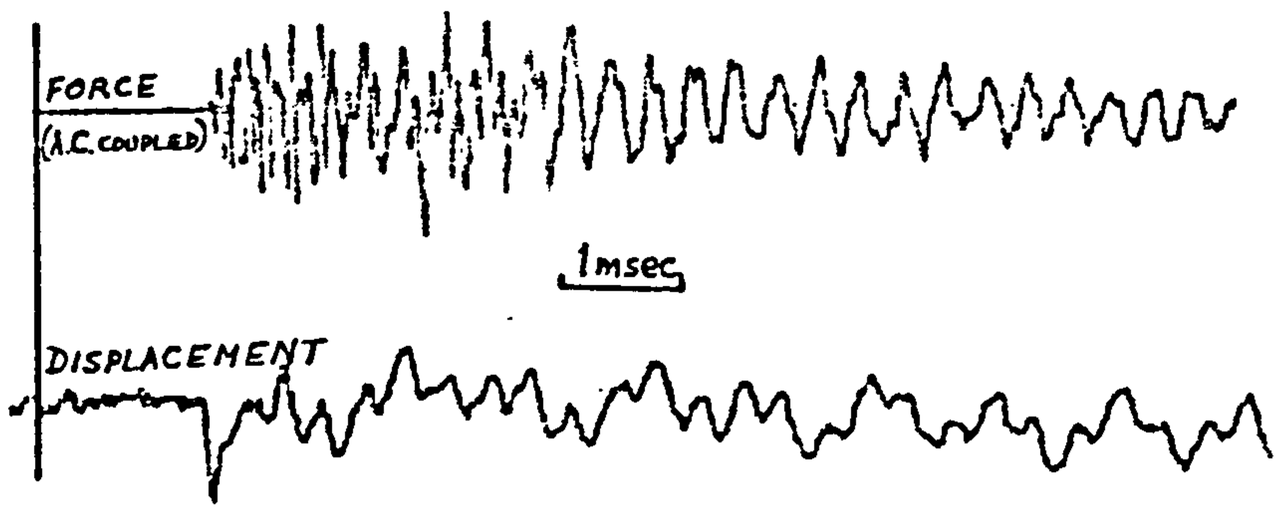

103·d : Response of transducers to high-frequency vibration

5J: PERFORMANCE TESTS: INSTRUMENTATION

Displacement transducers: Figures •a, •b are photographed storage oscilloscope traces showing the performance of the impedance bridge. Figure •b shows a typical signal from the bridge in the 'balanced' condition while •a shows the signal in the normal operating range at the same scale, for comparison. A residual signal at twice carrier frequency is visible in •b, but is seen to be insignificant.

In order to test the linearity of the demodulation, amplification and filtering circuitry, storage oscilloscope traces such as that shown in Figure •c were used. The input (AC bridge output) was applied to the 'Y' plates and the final output signal to the 'X' plates, while the bearing journal (aligned in the /suspended/floated/condition) was rocked to and fro across the clearance circle. The straight top edge of the bright area shows the linearity of these stages.

The frequency response of these stages was checked with the aid of a modulated carrier signal. It was found that with a depth of modulation of 50%, the gain was constant to within 20% (1dB) at modulation frequencies up to 3 kHz, falling off rapidly thereafter: and the output lagged the input by about 100 microseconds.

In order to check the responsiveness of the transducers themselves to high frequency movements, measurements of load and displacement were recorded following a sharp blow on one of the horizontal clamping screws. As seen at •d, a 3 kHz component is clearly present in both traces.

The overall linearity of the response to in-plane motion was checked by the construction of Figures 104 .a - .b. These record the output from the four channels when the journal axis was constrained to move in vertical chords separated by 25.4 μm; then in horizontal chords separated by 20.3 μm; then around the clearance circle, with firm journal/pin contact maintained. (Appendix 10M details the procedure used). Some deviation from the ideal grid pattern is evident, but this is not judged to be significant for present purposes.

In principle it should be possible, by suitably combining the outputs of the four displacement transducer channels, to measure displacements about two axes as well as along two axes. In practice, however, the response to out-of-plane motion - that is, rolling or yawing - is rather uncertain, owing to the

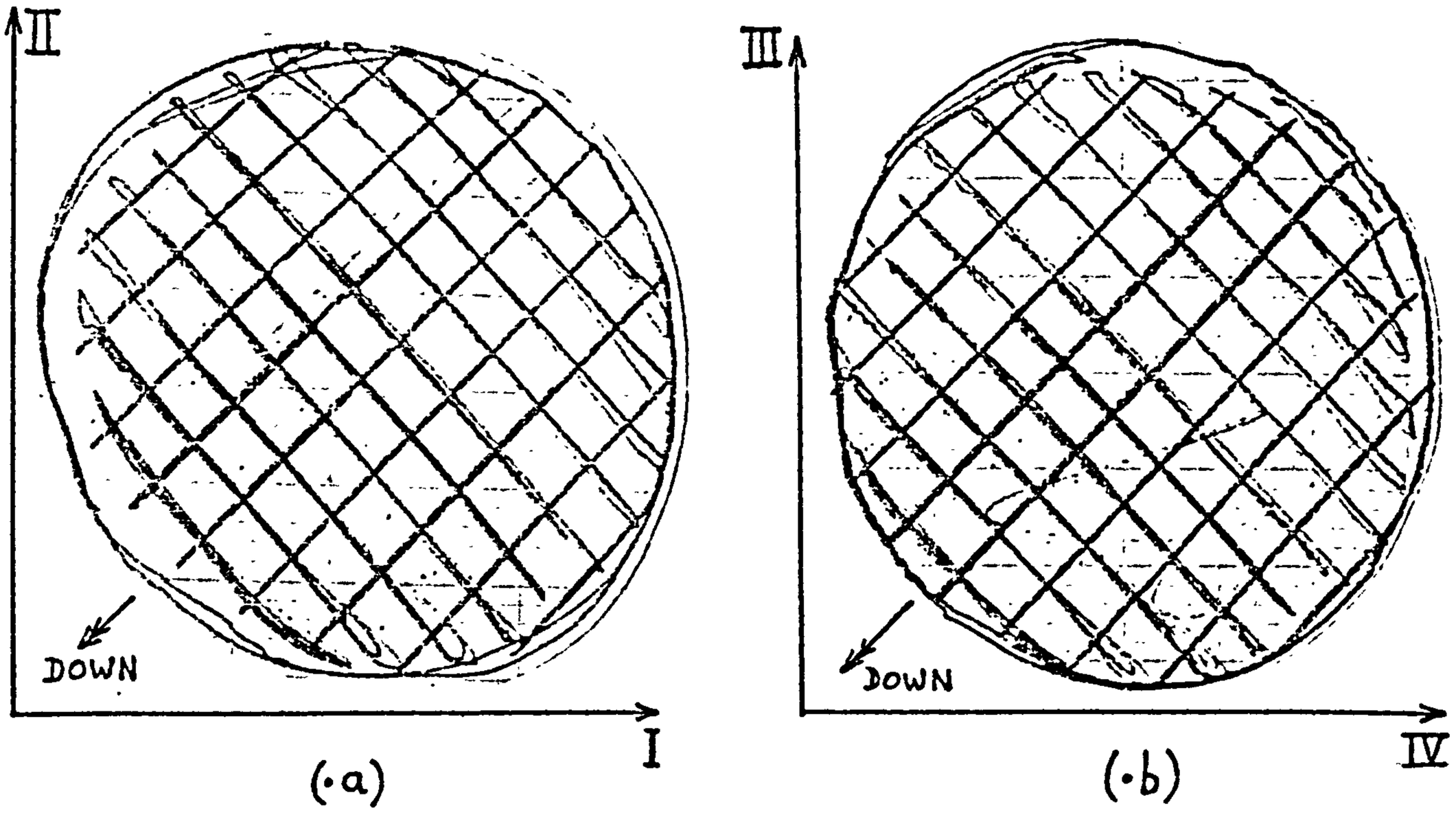

(·a) (·b)

104 ·a--·b : Displacement signals. channels I – IV; 'chord' tests

non-parallelism of the gap being measured in this case, and attempts to calibrate this aspect of the performance were unsuccessful. Nevertheless, considering the similarity between Figures .a and .b, the presence or absence of any significant discrepancy between the signal from the two measurement planes may be taken as a good qualitative indication of the presence or absence of out-of-plane motion.

Load transducers: Since the pin/load-cell assembly is statically indeterminate, the relationship of the separate load-cell signals to the applied load depends on the effective rigidity of the different load paths involved. Although the structure is nominally symmetrical, tests showed that the precise relationship tended to vary each time the assembly was disturbed. Thus the difference between the signals from the two load cells (associated with the same axis) could only be taken as a rough indicator of out-of-plane moments. However, since the summed loads are statically determinate, and the sensitivities of the two load cells are effectively identical, the sum of the signals for each axis may be taken as an accurate indicator of the applied static load on that axis.

From a record of the transient vibration following a blow to the midpoint of the pin (with the journal removed), the fundamental natural frequency of the pin/load-cell assembly was estimated to be approximately 5 kHz. Thus the measured (summed) load variations can be taken to reflect the pin/journal contact force variation quite accurately up to about 3 kHz, but not above (see also Figure 103-d).

Contact transducers: The contact detection system did not perform satisfactorily in that apparent momentary contact loss was recorded when the journal was rocked slowly while mechanical contact with the /dry/ pin was firmly maintained. This suggests a large point-to-point variation in the surface electrical resistance, presumably because of the formation of a non-uniform oxide layer. Naturally, the problem was worse in the /oiled/ condition, when the film of lubricant added to the resistance. The contact transducer system was therefore disconnected for most of the tests reported in Chapter 6.

Conclusion: With the contact transducers excepted, the demonstrated performance of the instrumentation is considered to be adequate for the purposes of this investigation.

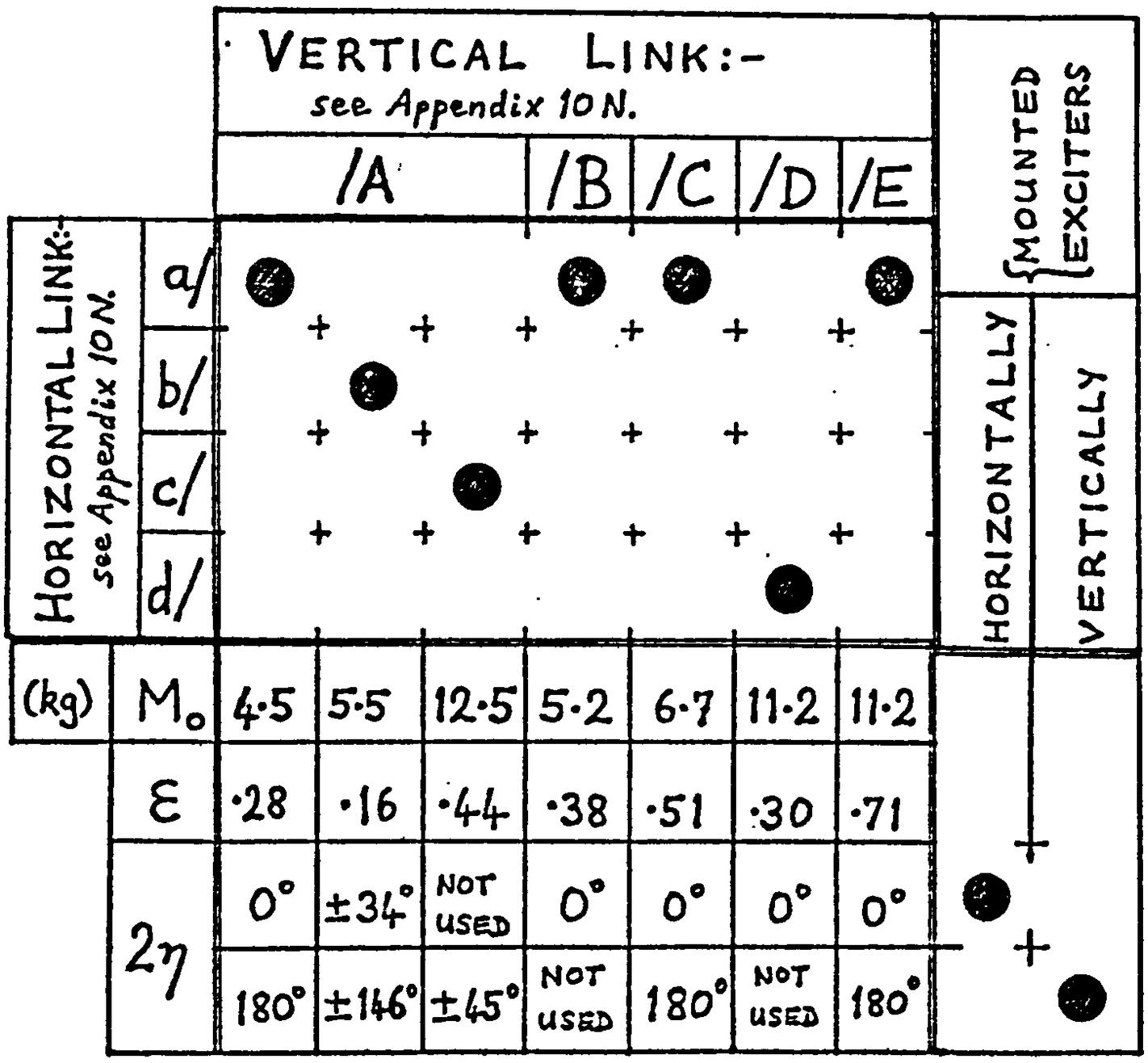

(kg)	M_o	4·5	5·5	12·5	5·2	6·7	11·2	11·2
	ε	·28	·16	·44	·38	·51	·30	·71
	2η	0°	±34°	NOT USED	0°	0°	0°	0°
		180°	±146°	±45°	NOT USED	180°	NOT USED	180°

TABLE 105·a: Inertial parameters of build variants used.

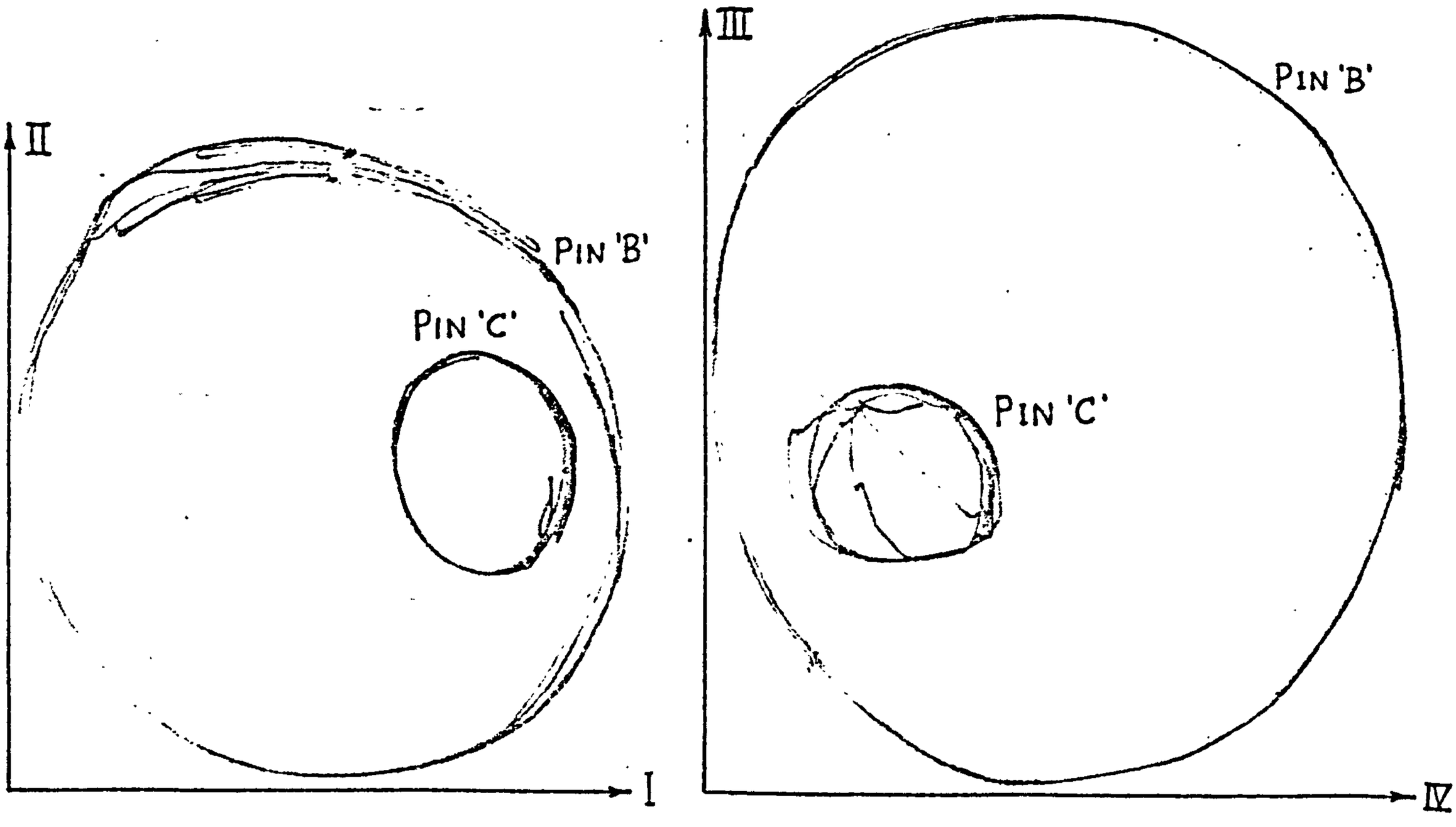

105·b--c: Clearance profiles, Pins 'B' & 'C'

5K: MECHANICAL SYSTEM DIMENSIONS AND PROPERTIES

Dimensions: The most important dimensions of the apparatus are shown in Figures 92·a-·g & 96·a-·k. The clearance diameters quoted were estimated from Figs.104·a/·b,105·b/c, and similar figures traced on the storage oscilloscope but not permanently recorded.

Inertia: The inertial parameters of the moving parts were determined by standard methods, including a compound pendulum method in which the displacement transducer signals were used to establish the natural frequency. The various inertial builds are distinguished by a pair of letters, e.g. /Bc/, where the upper case letter defines the added mass on the 'vertical' link and the lower case letter defines that on the 'horizontal' link. Further details are given in Appendix 10N. The inertial parameters M_0, ε, η are given in Table .a for each combination that was used of horizontal link inertia, vertical link inertia, and direction of the cyclic exciting force.

Profile errors: Inevitably, neither the journal nor the pins were perfect cylinders. Figures ·b, ·c, 106·a show the measured displacements at the perimeter of the clearance 'circle' using three different pins, under conditions of light contact between pin and journal. The gain of the two channels in each figure was balanced so that vertical chords were correctly traced (cf Appendix 10M), and in Figures ·b and ·c the inductances and associated circuit gains were left unchanged while the pins were exchanged, so that the clearance diameters could be compared. The gains for each figure are not the same however.

Departures from circularity of the order of 10μm are evident in all the figures, which is small by comparison with the clearance in the case of pin A but rather significant for pin B and clearly a major factor for pin C. It also became apparent that there was a slight taper in the bore (again about 10μm). One consequence is that at some parts of the profile in the figures shown, contact has occurred at only one end of the bearing, leading to poor repeatability. (It may be observed that these profile errors are probably not untypical for machined parts - the journal was ground, the pin turned; it is the ability to study them in a ludodynamic apparatus that is unusual).

CHAPTER 6

EXPERIMENTAL STUDY OF LUDODYNAMICS

None of the material in this chapter has been published before.

For build variants shown /thus/, see nomenclature for Chapter 5.
Other nomenclature for this chapter and for Appendices 10P - 10R is given below.

Symbol	Meaning	Reference
D	Bearing diameter.	
E_i	Young's modulus of material of component 'i'.	
e	Radial clearance of bearing.	
$H_1\ H_2\ H_3$	Dimensionless parameters governing 'standard' flypast.	78.d-.f
L	Bearing length.	
M_o	Generalised effective inertia	77.a
R	Contact force.	
$R_H\ R_V$	Components of R:	
$R_H^*\ R_V^*$ / $R_u^*\ R_v^*$	Components of force applied to journal:	
δ	Measured displacement.	
$\delta_H\ \delta_V$	Components of δ. (H: mean horizontal, V: mean vertical)	
$\delta_I\ \delta_{II}$	Components of δ (individual transducers).	94.b
ε	Eccentricity of inertia tensor.	77.c
γ^*	Inclination of applied force vector.	
η	Inclination of major axis of inertia tensor.	77.b
ν_i	Poisson's ratio of material of component 'i'.	

H: horizontal (from vertical link)

V: vertical (downwards)

u: direction of minimum applied force

v: direction of increasing applied force

6. EXPERIMENTAL STUDY OF LUDODYNAMICS

6A: INTRODUCTION

Types of test: A variety of types of experiment have been carried out with the apparatus described in Chapter 5, with a view to elucidating various aspects of ludodynamic behaviour. This report will concentrate on three types which have been found to be the most informative. These are 'flypast tests' in which a load variation approximating to a standard flypast is imposed using a pair of pneumatic exciters; 'compliance tests', in which a varying unidirectional load is applied by means of a single exciter; and 'drop tests', for which no exciters are used, the journal simply being allowed to fall under gravity across the diameter of the clearance circle.

Misalignment: For all the experiments reported here, the journal was aligned as nearly as possible parallel to the pin (cf 96.n). Thus the provision of pairs of transducers on either side of the central plane was exploited in this phase of the investigation to facilitate and monitor this parallel alignment, rather than as a basis for regulated misalignment. At this stage a strictly subjective observation might be made on the latter aspect: that in view of the very careful adjustment that proved necessary in order to eliminate clear discrepancies between the measured displacement trajectories at the front and back planes of the bearing, the author would now treat with considerable reserve any results obtained with only a single plane of measurement.

Arrangement of material: The compliance tests and drop tests will be described first, since their results provide a valuable aid to interpreting the complex flypast phenomena. Certain basic procedures common to all the tests are outlined in appendices, namely alignment and adjustment (Appendix 10P), calibration (10Q), and recording (10R).

Doubtful details: The varied and time-consuming nature of the experiments precluded a completely systematic procedure, as improved methods were adopted in the light of what was learnt, and repetition of more than a few tests was impracticable. As a consequence, some details were left unrecorded that were later thought to be possibly significant. These are reported by memory, with a bracketed query (?) to indicate their less certain status.

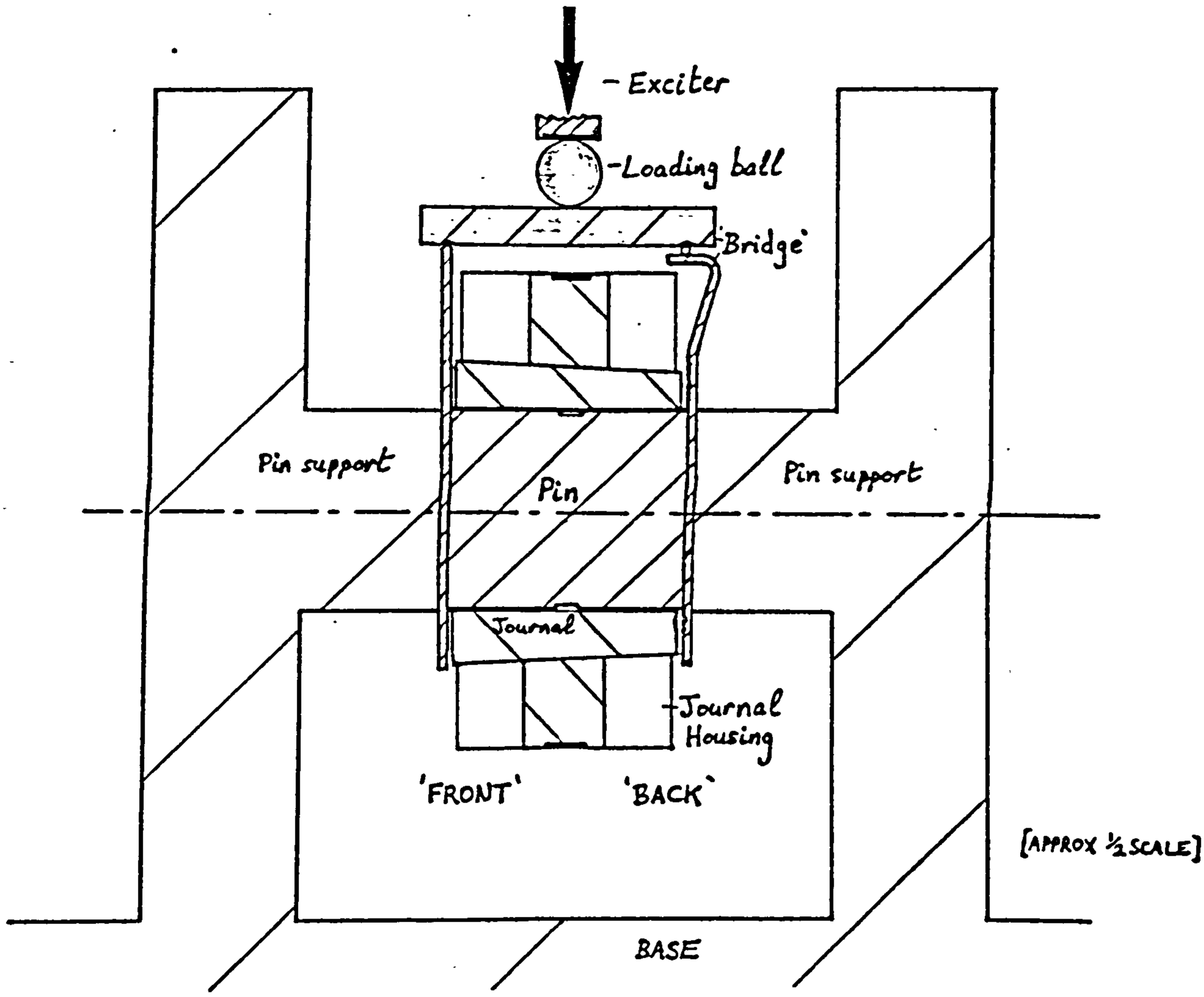

108·a : Arrangement of 'bridge' for testing support stiffness (schematic)

(c.f. 96·a – ·i)

6B: COMPLIANCE TESTS

Theory: A number of theories are available for predicting the pin/journal contact compliance. The formulae quoted in ROARK & YOUNG relate to a quasi-infinitely long pin in a hole in a quasi-infinite solid. A deflection formula is given only for the case of similar materials, but a formula predicting the width of the contact zone is given for the case of dissimilar materials, and by substitution and rearrangement, the following somewhat speculative formula may be obtained:

$$\left.\begin{aligned} \delta &= Q[1 + \log(4e/Q) - 2\log(2.37)] \\ \text{given}\quad Q &= (R/\pi L)((1-\nu_1^2)E_1^{-1} + (1-\nu_2^2)E_2^{-1}) \end{aligned}\right\} .b$$

where δ = deflection, R = load, e = radial clearance, L = length of bearing, and ν_i = Poisson's ratio and E_i = Young's modulus for material 'i'.

DUBOWSKY & FREUDENSTEIN gave a formula apparently relating to a close-fitting short pin in a cylindrical hole in a quasi-infinite plate. In the same notation, this can be arranged to give:

$$\left.\begin{aligned} \delta &= Q[1 + \log(4e/Q) - 2\log(D/L)] \\ Q &\text{ as above} \end{aligned}\right| \quad .c$$

where D is the pin diameter. These formulae will be termed the "long pin" and "short pin" formulae respectively. Both are based on Hertzian theory, which assumes that the contact width is small by comparison with the pin diameter.

ESHWAR gave non-Hertzian numerical results for a short rigid pin in a quasi-infinite elastic plate, but these relate to bearing pressures some orders of magnitude larger than those relevant here. STROVER & SCHOLES described a finite element method for predicting the deflections of a pin in a finite journal. This is certainly relevant, but the method is too lengthy for present purposes and the numerical results are only applicable to the specific case studied. Thus, *faut de mieux*, the formulae quoted above will be tried.

Experimental procedure: The bearing was assembled with two additional components clamped on either side of pin 'B'. These formed the uprights of a bridge which was completed by resting a grooved plate across the top (see Figure .a). The top exciter was positioned so that its loading ball acted on this plate (the other three loading balls being removed). The displacement transducers were suitably adjusted and coupled so that net signals proportional to the

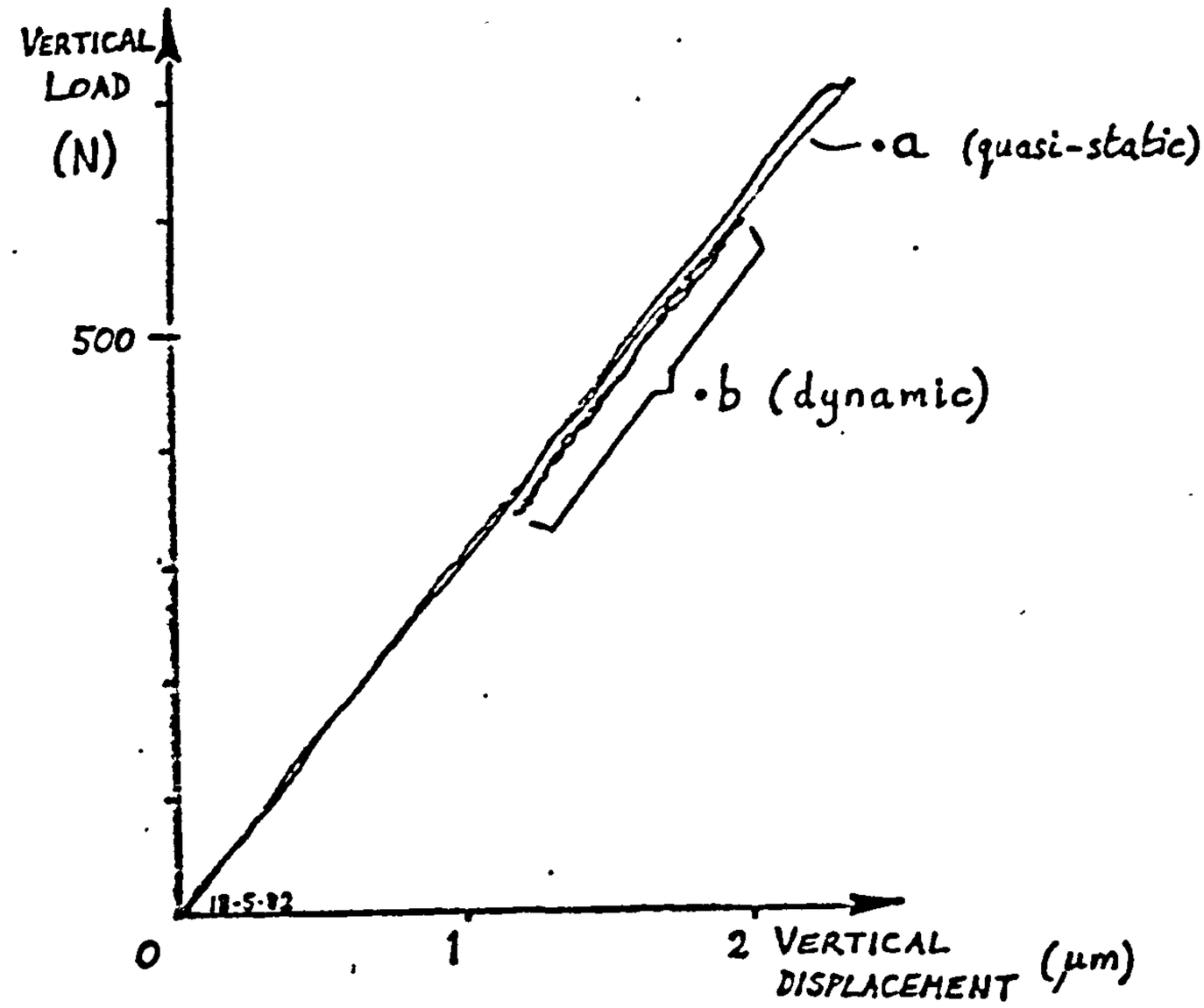

109.a/b: Deflection of journal: load applied via bridge

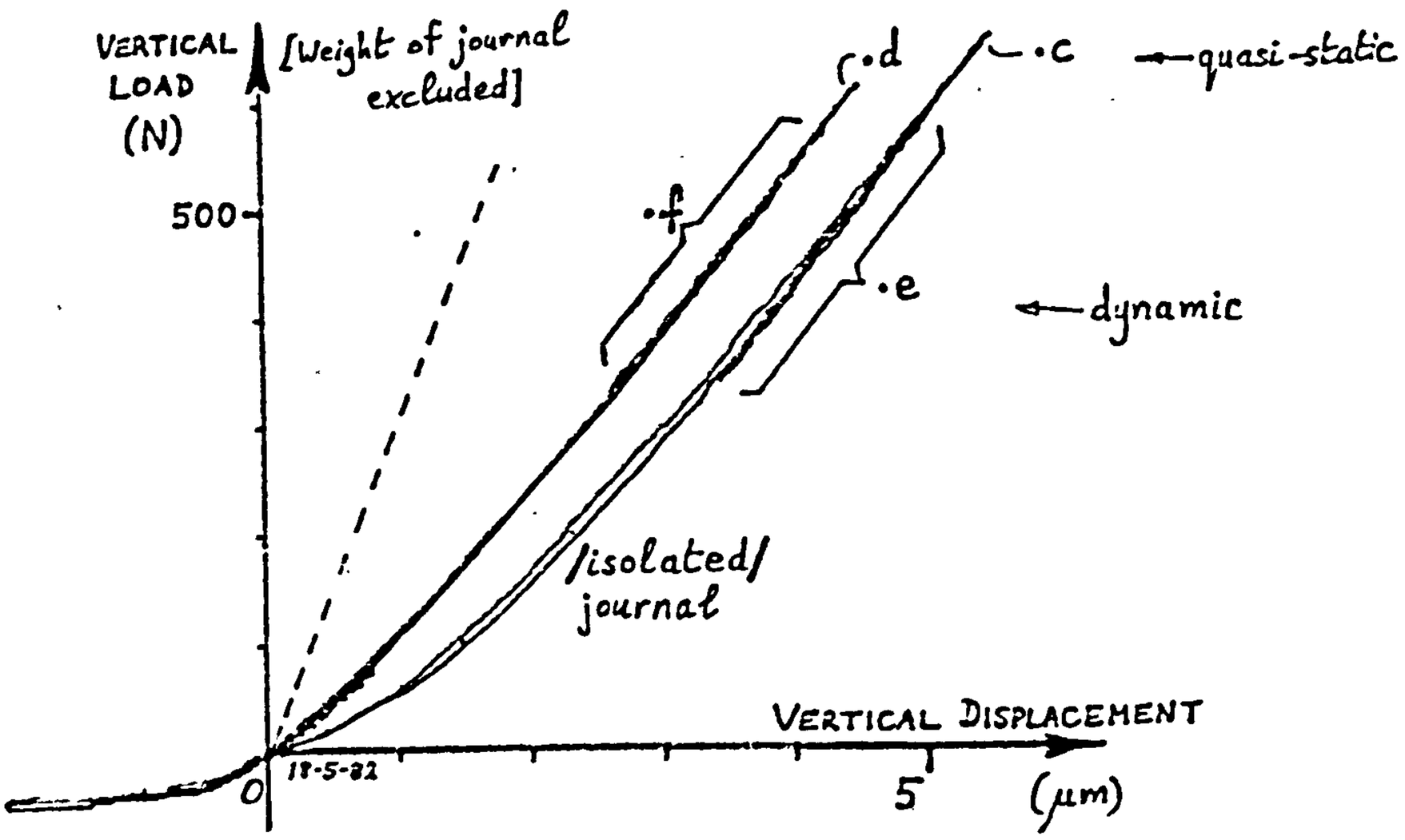

109.c-f Deflection of journal under load: Pin 'B'.

vertical displacements of the journal at the 'back' and 'front' planes of the bearing were obtained (see 10.R). These were highly amplified and displayed separately on the Bradley oscilloscope, and also combined to give the mean vertical displacement. The variation of the combined signal with the vertical load was recorded while divers load variations were applied.

A similar test was performed with the bridging plate removed, the exciter being repositioned so that its loading ball bore on the journal housing in the usual way, both with the journal /isolated/ from the dyad and with the connection restored.* Tests similar to the last, but with a horizontal exciter active rather than a vertical one (?), were performed with pins 'A' and 'C' in turn taking the place of pin 'B'; for these tests, of course, horizontal load and displacements were recorded rather than vertical.*

For the low frequency load variation the exciter system was open to the (N_2) pneumatic line, the line pressure being varied by means of the regulator (93.a). For higher frequency variations the exciter system was filled with gas and closed, and the master piston driven by the eccentric system (93.d-.e).

Results: Figure .a/.b records the tests with the bridging plate in place. Two traces are superimposed. The first (.a) was made with a low frequency variation: from zero to maximum load in 20 seconds, constant for 20 seconds, and back to zero in 20 seconds. The second trace (.b) is of a single load cycle at about 11 Hz. This figure is taken as showing the response to load of the bearing pin supports (see 108.a). It is seen that the load/deflection relationship is linear to a good approximation, and little affected by the rate of loading.

Figure (.c/.f) records the tests with the load applied to the journal (assembled with pin 'B'), both /isolated/ (.c and .e) and attached to the dyad. The cycle time was 45 seconds for the low frequency tests (.c and .d), while the barely distinguishable superimposed curves (.e and .f) record variation at about 11 Hz. The minimum load for .c is that due to the weight of the journal, but for curve .d this load was eliminated by slow jacking up of the journal (cf 97.b) at the end of the cycle. The broken line shows the support flexibility obtained from Figure .b/.c, on the same scale. The differences between this and the solid traces are taken as showing the compliance of the pin/journal contact zone.

* For these tests, the alignment of the journal was very carefully adjusted until the two signals on the Bradley oscilloscope moved together as a small vertical load was applied by finger pressure.

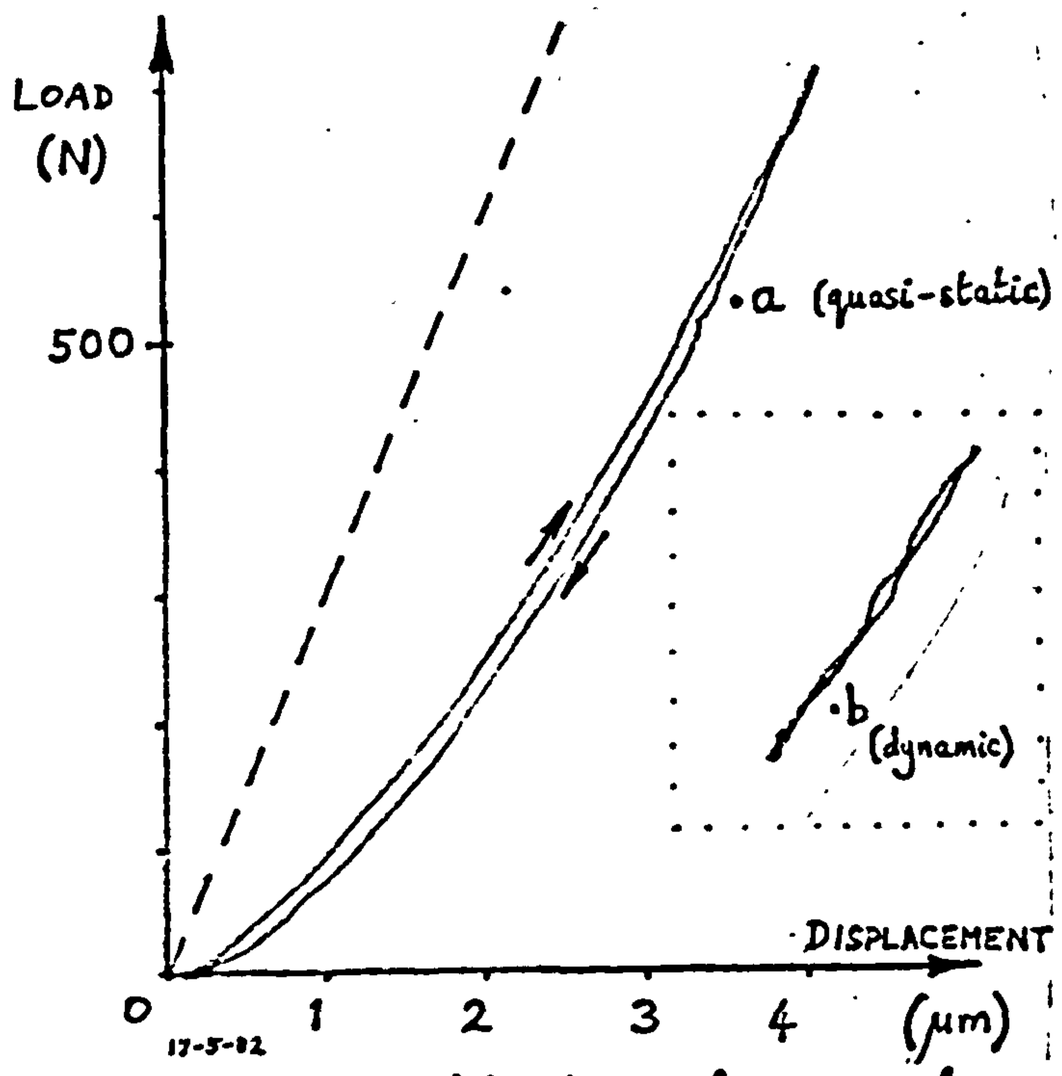

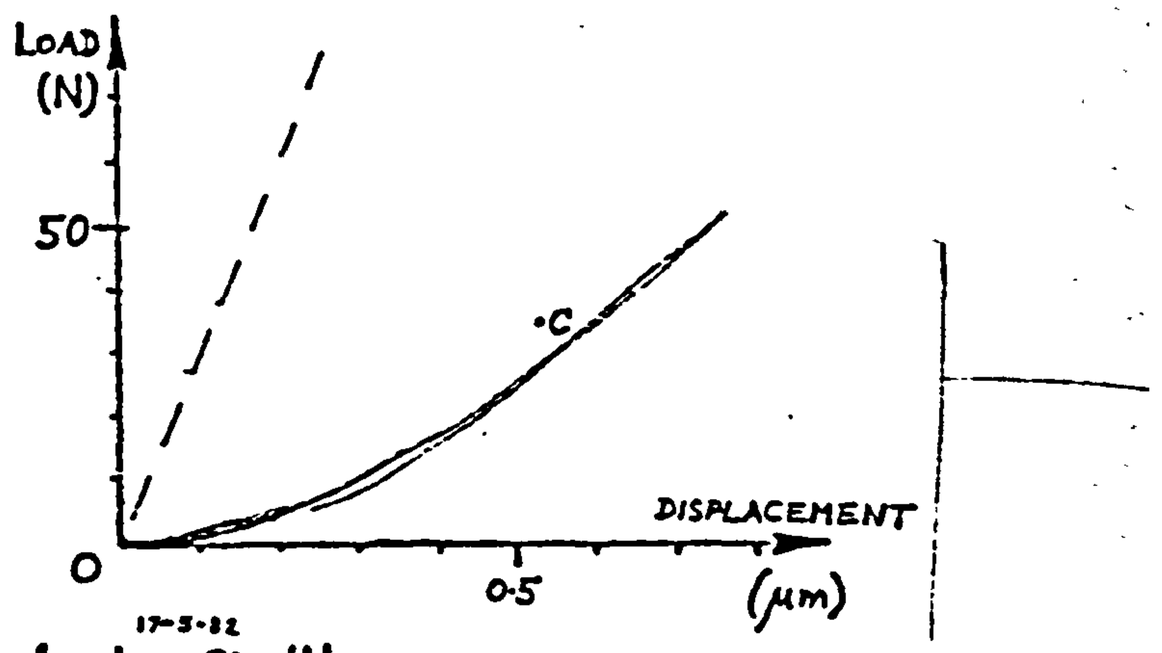

110·a–·c : Deflection of journal under load: Pin 'A'

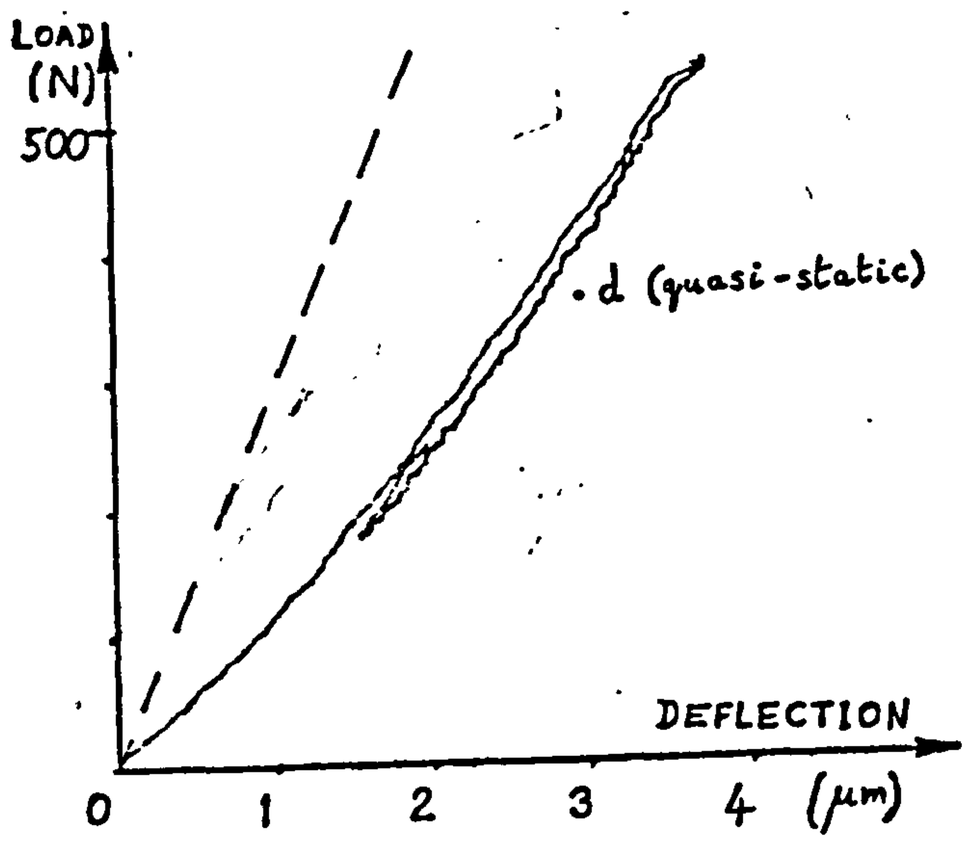

110·d : Deflection of journal under load: Pin 'C'

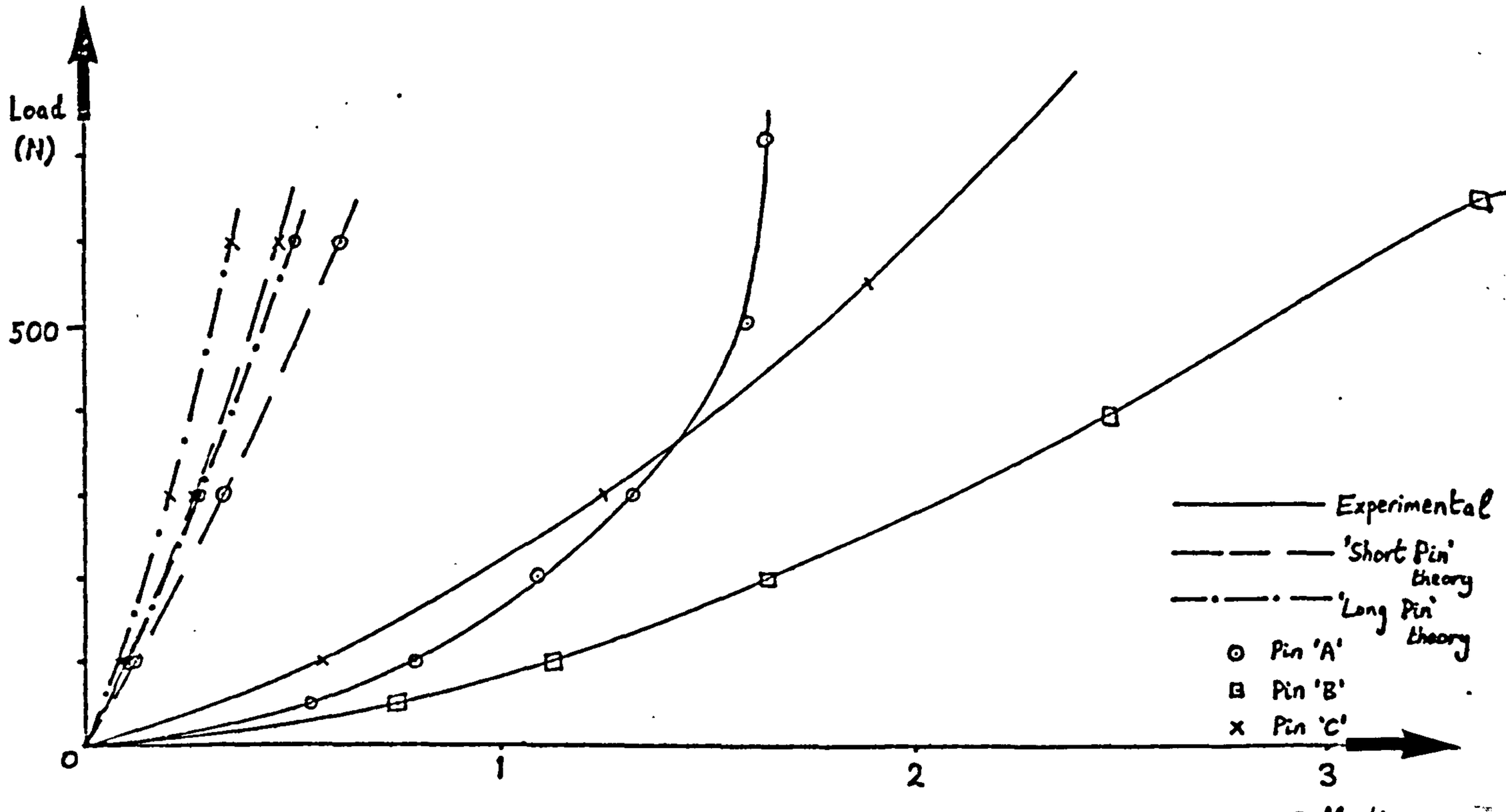

110·e Comparison of theory & experiment for contact compliance

With the dyad attached to the journal housing, any vertical deflection of the journal must be associated either with linear deflections at the zero-clearance pivots (92.c) or torsion of the pin, or slip between the pin and journal. This would explain the greater stiffness shown in curve 109.d by comparison with curve 109.c (The reversibility of curve 109.d suggests that in fact slip does not occur). The cause of the slight irreversibility apparent in curve 109.c is unknown: it does not seem very significant. Hysteresis at the higher frequency is seen to be negligible; thus the load/deflection relationship is seen to be essentially elastic, though far from linear.

Figure (110.a-.b) and Figure (110.c) record the tests with pin 'A', using a horizontal exciter. The problem of constraint by the zero-clearance pivots does not arise in this case. Curve .a is for a low frequency increase and decrease of load over 45 seconds in total; curve .b is for a single cycle at about 12 Hz. (the origin was omitted from this trace); curve .c is for a variation over 5 seconds, with both scales magnified by 5.

The ripple on curve .b is probably due to vibration transmitted from the eccentric drive system. This feature apart, the curves are qualitatively consistent with the previous curves, the non-linearity again being highly visible. The same is true of the test with pin 'C', recorded in Figure .d, the load cycle in this case taking 90 seconds.

Comparison with theory: Figure .e (full lines) combines sketches of curves 109.c and 110.a,.d converted to common scales, with the support deflection from 109.a subtracted in each case on the assumption that this is equal in all directions. The curve for pin 'A' appears anomalous in this figure; it looks very much as if a scale error was made in the calibration. (Because of the large correction for pin support flexibility, this would distort the shape as well as the scale).

Also shown in Figure .e are predicted curves for pins 'A' and 'C', using equations 108.b (chain lines) and 108.c (broken lines). It is seen that they differ markedly from the measured deflections both in magnitude and in degree of non-linearity.

Two factors could contribute to both of these discrepancies. Firstly, the journal is by no means an infinite homogeneous plate, but an irregular two-component ring, and some distortion of the ring may occur. However, although the latter effect could be highly significant if a tensile load was applied to

the bearing, so that the load path passed around the ring, in this experiment the major load is carried in compression directly across the thickness of the ring, so significant distortion seems unlikely.

Secondly, owing to the errors of form of the nominally cylindrical surfaces, the contact area would not be rectangular as assumed: contact would be made initially at local high spots, which must be 'flattened' before the ideal surface stiffness becomes effective. Since the bearing in this case is quite lightly loaded in relation to its size, this effect may well be significant, but the extent of the departure from the theoretical curves remains surprising.

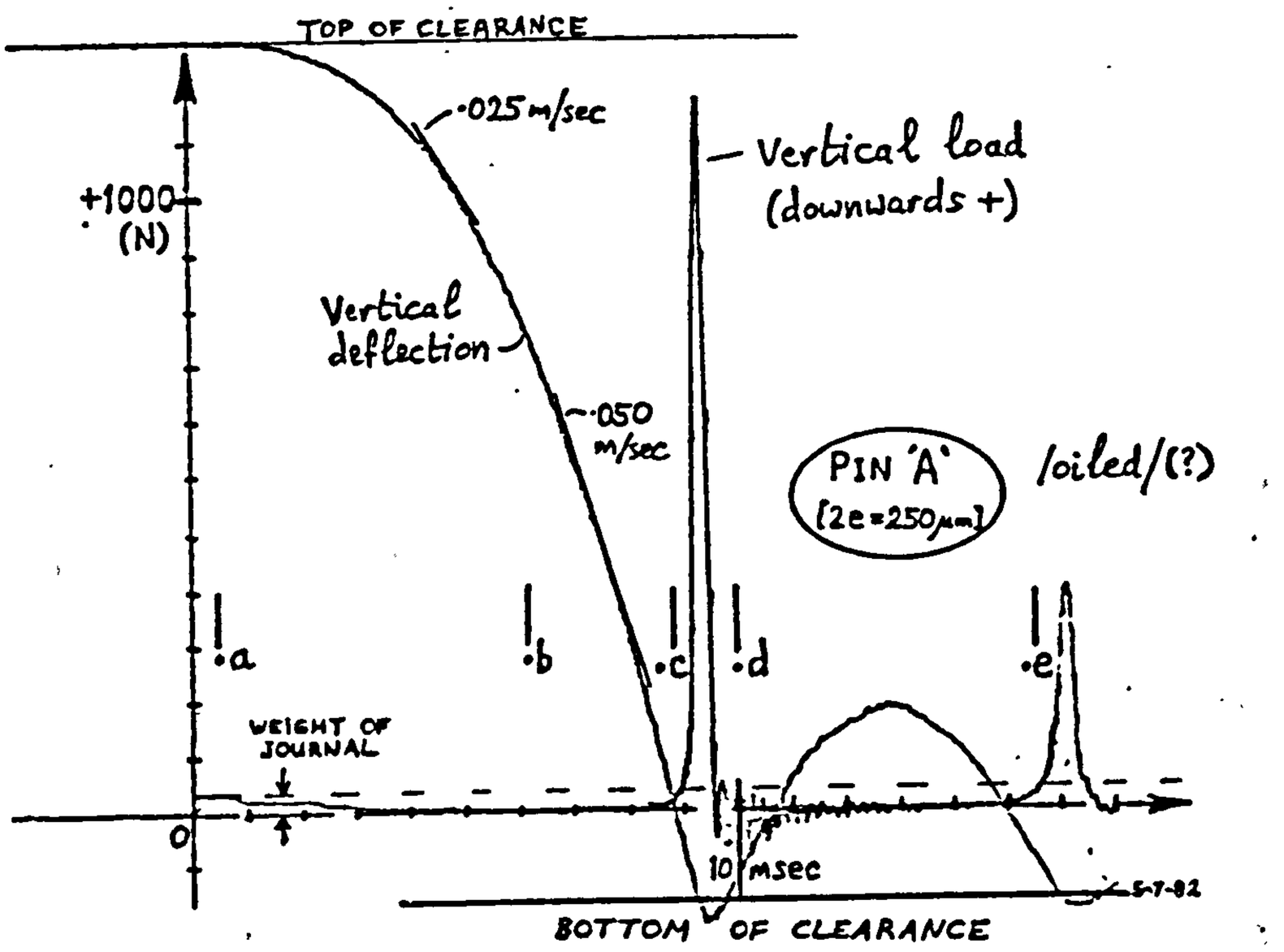

·a—·e

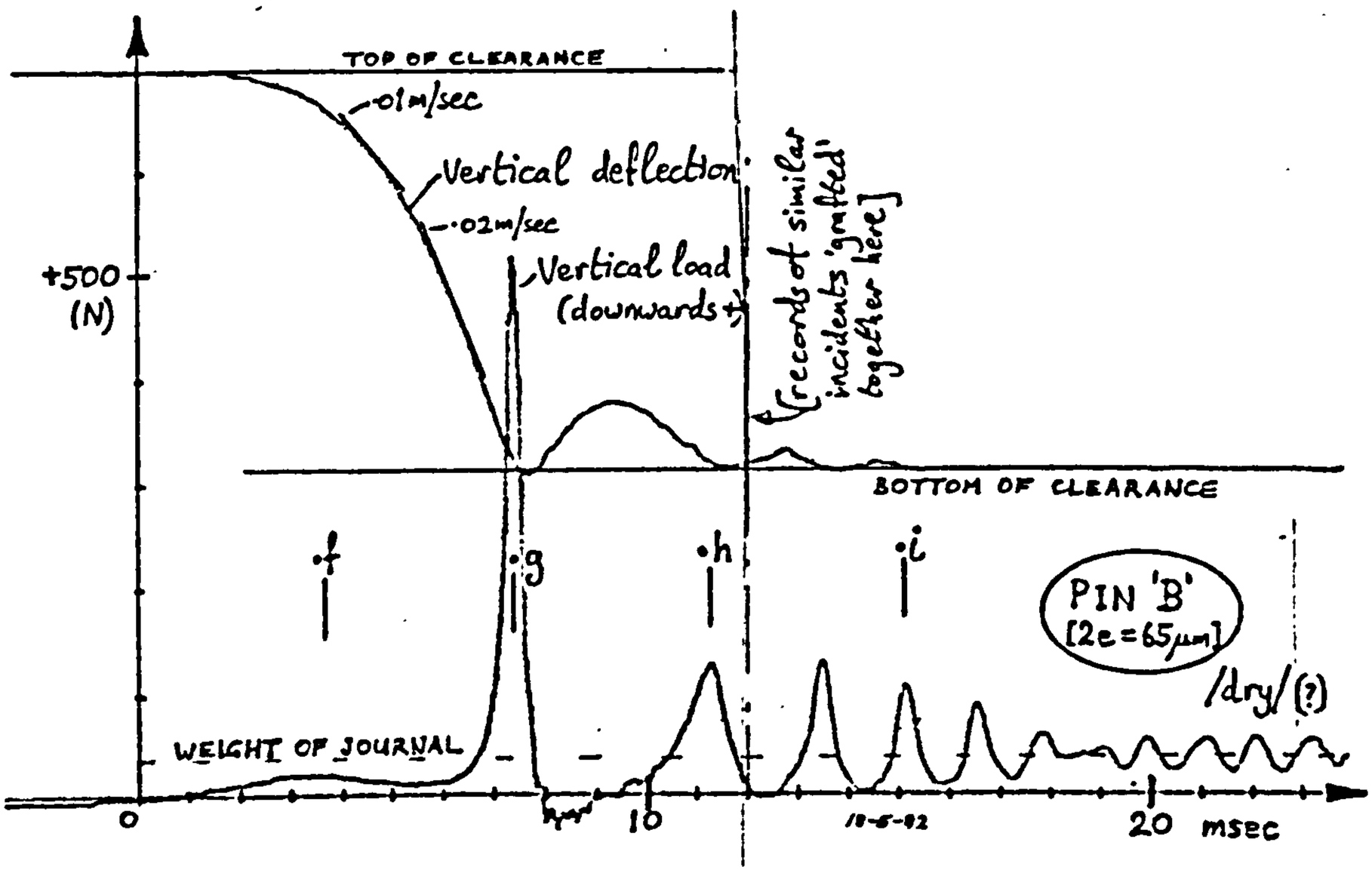

·f—·i

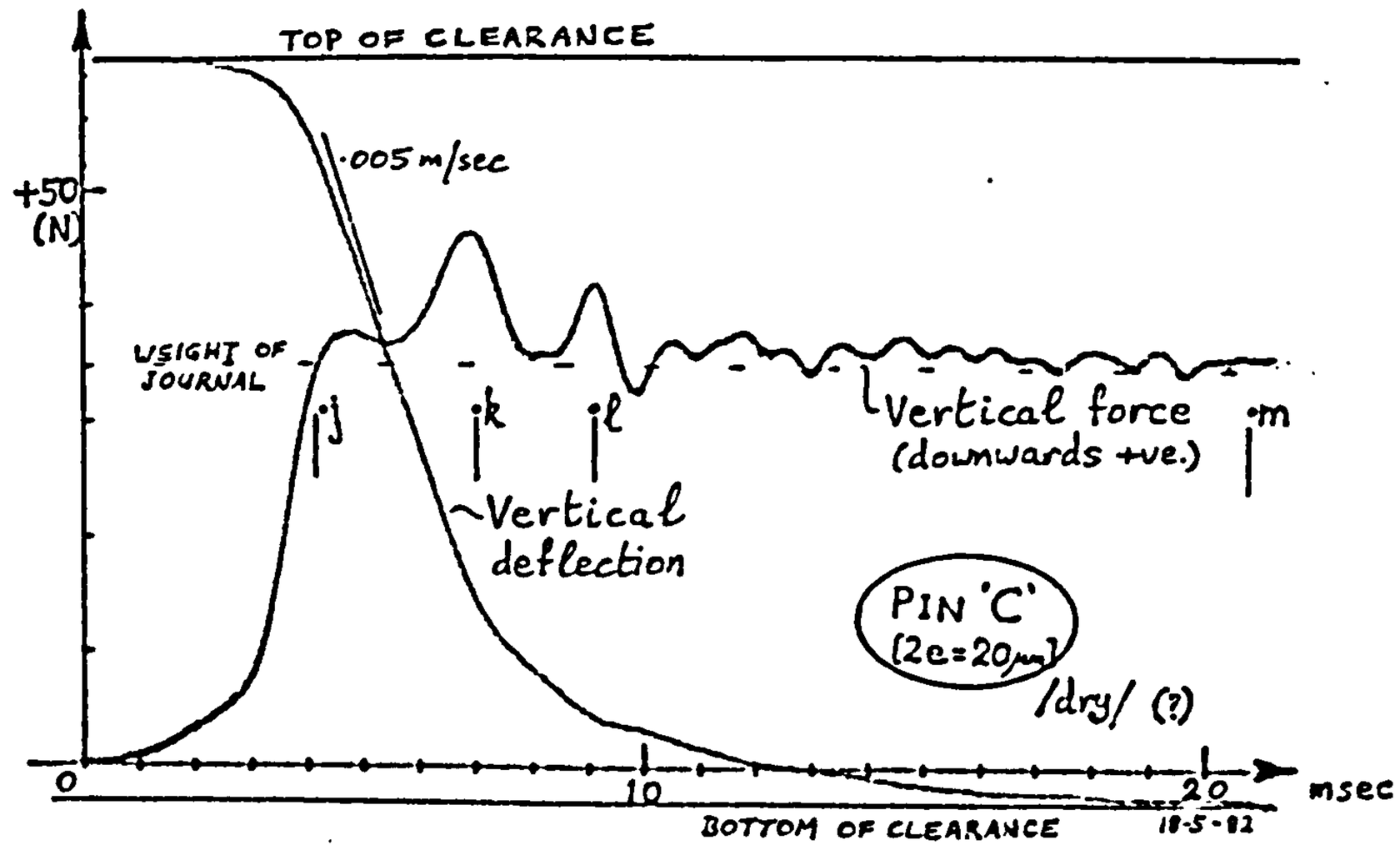

·j—·m

112 ·a—·m: Displacement of journal when dropped across the clearance, and consequent load on pin.

6C: DROP TESTS

Theory: For inertial builds /Aa/ to /Ea/, the effective inertia referred to the journal axis is about 3.25 kg for vertical accelerations. The gravitational load measured at this axis is about 34N. Thus in the absence of any energy dissipation, the journal axis would fall under gravity with an acceleration of about 10.5 m/sec^2.

From Figure 109.d, a linearised first approximation to the flexibility of the effective spring acting on the journal during the impact phase is 10^{-8} m/N for pin 'B'. This would cause an oscillation with a period of about 1 msec. Using the theoretical spring flexibility on the other hand (equation 108.c), the total flexibility is about 4.3×10^{-9} m/N (including 3.4×10^{-9} m/N from the pin supports), leading to an oscillation period of about 0.75 msec.

Experimental procedure: With the loading balls removed from the pneumatic exciters, the journal was /suspended/ from a light cross-beam resting on two supports. The positions of these were adjusted by hand until the journal was just touching the pin at the top of the clearance circle. The vertical link was /held/ against a stop in this position. One of the cross-beam supports was then jerked away, so that the journal dropped under the influence of gravity, the resulting variation in vertical load and displacement being recorded on the digital storage oscilloscope. This test was performed with each pin (A,B,C) in turn installed in the bearing.

Results: The recorded loads and deflections with the three different clearances are shown at .a-.m opposite. Those for pins A and B showed excellent repeatability after the first 3 msecs(?).

At .a it is seen that the weight of the journal is momentarily felt by the pin as the adhesion of the oil film is overcome. At .b the journal is almost unimpeded as it accelerates across the clearance at about 9 m/sec^2. At .c a rapidly increasing load, evidently due to the rapid displacement of the air film, is felt immediately before the moment of impact - at which a severe peak load of over 30 times the weight of the journal is recorded. At .d the pin is left vibrating at about 5 kHz as the journal rebounds. At .e a 'squeeze film' load is again felt just before the second impact.

The oil film adhesion is absent from the second trace, but due to the thinner, more nearly parallel squeeze film, the pin feels a significant proportion of the weight of the journal throughout its drop (112.f), and the acceleration is reduced to about 6 m/sec^2. After the impact at 112.g the rising journal imparts a 'sucking' load of about 20 N to the pin. The second impact 'spike' at 112.h is much broader than that at 112.~~f~~e. After the fourth impact at 112.l the load variation is less than the weight of the journal, so no further contact loss occurs: the pin/journal system vibrates without separation with a period of about 1.4 msec falling to about 1 msec. The shape of the 1.4 msec oscillations is strongly suggestive of a non-linear spring.

In the trace for pin C the air squeeze film is clearly a dominant phenomenon. By point 112.j the journal has reached a terminal velocity of just under 5 mm/sec, and its full weight is transmitted by the air film to the pin. A possible interpretation of the rest of the trace is that owing to the profile errors, impacts occur first at an edge of the bearing, causing the impulses at 112 .k-.~~l~~, after which the journal tilts over until a second point of contact is made at 112.m.*

Comparison with theory: The dramatic increase in the air squeeze film effect with reducing clearance, shown very clearly and consistently in Figs 112.a-.m, was not anticipated; it obviously has major implications for the flypast tests.

The shape and period of the force oscillations after 112.i support the findings of the previous section rather than the theoretical predictions of contact compliance. Another check can be made from the height of the force peaks in the case of pin 'A' (where the squeeze film effect is small). At 112.c the approach velocity is about .065 m/sec, so the kinetic energy is about 7×10^{-3} dyne. Converted to spring energy, a peak force of 1200 N implies a flexibility of about 10^{-8} m/N, supposing the spring to be linear. On the other hand it could be argued that a mean of the approach kinetic energy and the recoil kinetic energy should be used. With a recoil velocity of 0.028m/sec this leads to a flexibility of about 6×10^{-9} m/N. For the impact after ~~110.c~~ 112.e the recoil velocity was not recorded, but the approach velocity of 0.025 m/sec and peak force of 400 N imply a flexibility of about 1.4×10^{-8} m/N. Unfortunately there is no 'reliable' experimental compliance curve for pin A with which to compare these values, but they are certainly more consistent with the order of magnitude of the measured compliance than with that given theoretically, bearing in mind that the load level in the first impact (11~~9~~2.c) is well off the scale of Figures 109.c-.f and 110.a-.d.

* [Nov.'82]: subsequent tests tend to confirm this.

6D: FLYPAST TEST (DETAILED): STANDARD BUILD

The majority of the flypast tests were carried out with inertia build /Ca/,in conjunction with pin 'A' and excitation on the horizontal axis. This is regarded as the 'standard' build. Results from a test using this build are considered in detail in this section. A series of simpler tests using the standard build are considered in Section E, while the effects of changes to the inertia build and of using tighter pins are reported in Sections F and G respectively.

Theory: As given in Table 105.a, the inertial parameters for build /Ca/ are effective inertia (M_o) = 6.7 kg, eccentricity of inertia tensor (ε) = 0.51, inclination of major axis (γ) = 0^o. Quite fortuitously, the value for ε almost corresponds to that (0.5) applicable to Figure 87.a: the difference will be neglected. Thus it is predicted that terminal contact loss and impact (curve II) will occur if H_1 is less than about 0.63, and passage contact loss and impact will occur if H_1 falls below about 0.17. However, even at the latter value the design point is only just inside contours II and III of 87.a, so the terminal contact loss prediction is a very uncertain one.

Using pin 'A', $e = 125 \times 10^{-6}$, so from equation 78.d the predicted threshold relationships between $\dot{R}_v^*$ and R_u^* (in S.I. units) are

$$\dot{R}_v^{*2/3} \doteq 17 R_u^* \qquad \text{(terminal impact - tentative)} \qquad .a$$

$$\dot{R}_v^{*2/3} \doteq 63 R_u^* \qquad \text{(passage impact)} \qquad .b$$

For the test considered in this section, $R_u^* = 4(N)$, so the threshold values of $\dot{R}_v^*$ are 560 and 4000 (N/sec). .c

For comparison, Earles' empirical criterion predicts contact loss above the threshold $\dot{R}_v^{*2} = R_u^{*2}$ for any linkage, i.e. $\dot{R}_v^* = 16$ (N/sec) for this test. .d

Procedure: /Ball-pivots/ were installed in the vertical link. The test bearing was /oiled/. The journal was /top-sprung/ as shown in Fig. 97.1 (with a spring of stiffness 780 N/m), and the spring tension was adjusted until the measured vertical load on the pin was 4.0 N downwards: this corresponds to R_u^*. The loading balls were inserted in the two horizontal exciters, and correctly adjusted as described in Appendix 10P. The exciters were pressurised to about 14 bar, and the eccentric motor set in motion so that an oscillating horizontal

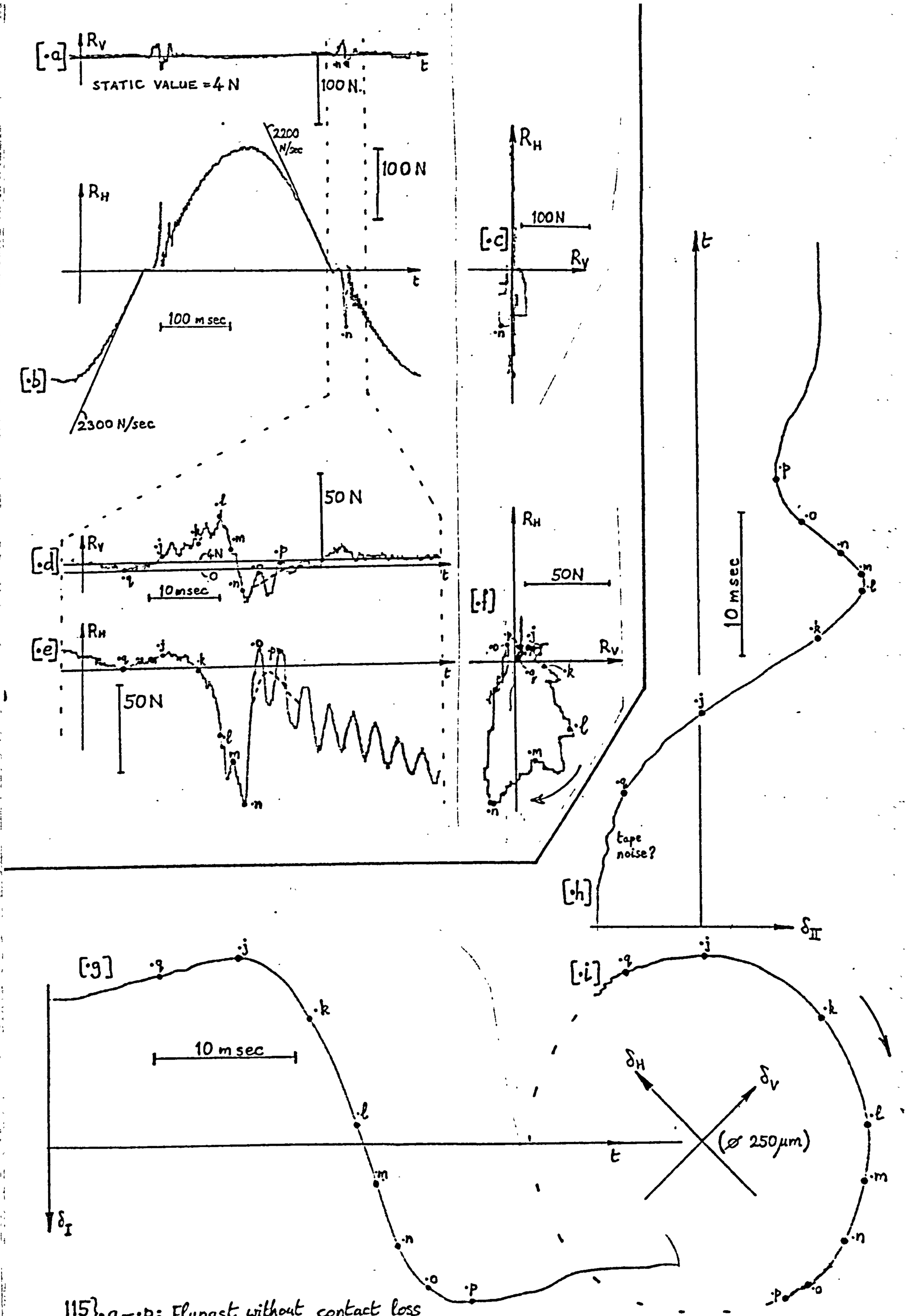

115 } •a–•p: Flypast without contact loss
116 } (standard build)

load (R_v^*) was applied to the journal as well as the small vertical load (R_u^*). Thus two flypasts were generated per cycle, with the horizontal load increasing first in one direction and then in the other.

After a check that the measured motion at the back of the bearing matched that at the front, a tape-recording was made of the two displacement signals for the front of the bearing (δ_I and δ_{II}), along with the net vertical and horizontal loads (R_v and R_H). The eccentric speed was slowly increased until passage contact loss was apparent (in one direction only) in the displayed displacement locus. The system was then disturbed by applying hand pressure to the journal for a second: it was seen that the pattern of the signals before the disturbance was immediately re-established, that is the behaviour was stable. The acceleration of the eccentric drive was then resumed.

A check on the value of R_a^* immediately after this test showed that it was 3.8 N. Checks on the "apparent coefficient of friction" as described on page 106 yielded values of 0.11 before the test and 0.14 afterwards.

Interpretation of a recorded flypast: Details from one cycle of loading are shown in curves [.a] to [.i]. Positive values of R_H and R_v are defined (here and subsequently) as away from the zero-clearance pivot and downwards respectively. In this test R_v corresponds to R_u, while R_H corresponds to $+R_v$ in the first half of the cycle and $-R_v$ in the second. Curve [.a] shows how $\dot{R}_v^*$ for this cycle was estimated by extrapolation from the earlier portions of each flypast, during which the dynamically induced difference between R_v^* and R_v is negligible. Taking a mean value of 2250 N/sec, the theory predicts no passage impact but possible terminal impact; Earles' empirical criterion predicts impact by a considerable margin.

Although curves [.a] and [.b] might seem to indicate impacts, e.g. at instant .n, curves [.d] to [.f] tell a different story. Here the time base is ten times faster - which is still well within the range appropriate to the measuring systems - and it is seen that although the contact force drops momentarily to about zero at .q, the peak at .n does not occur until 17 msec later; moreover, the force vector locus [.f] shows that the direction of the contact force is swinging through about 180^o during this period of growth.

The displacement curves [.g] to [.i] show no sign at all of contact loss between points .q and .n. (As explained in Appendix 10R, labelled points on the curve correspond in time to the similarly-labelled points on the force curves).

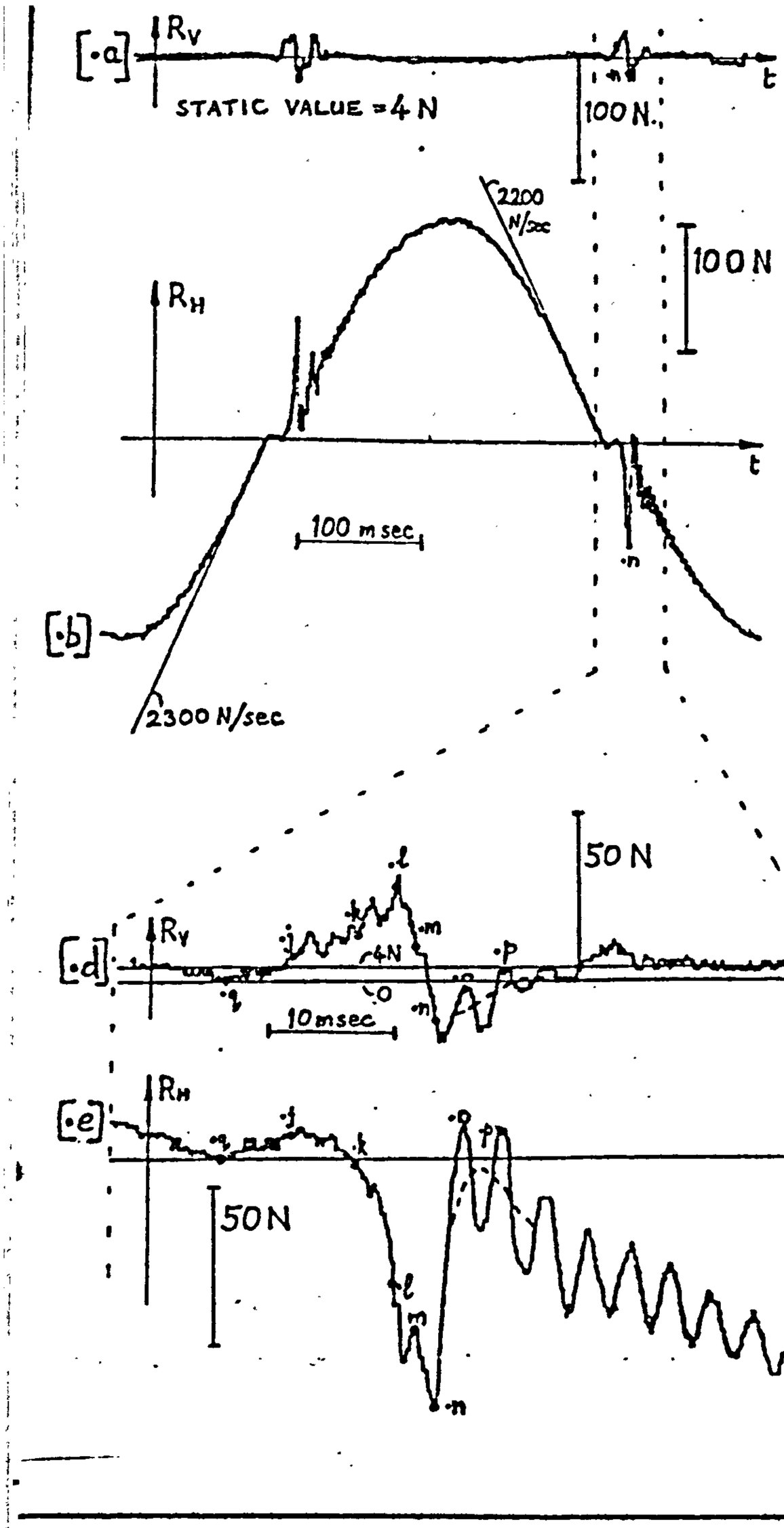

115 / 16 [bis] ·a–·p: Flypast without contact loss (standard build)

Rather, it is seen that the growth in the contact force is associated with the rapid acceleration of the contact point around the clearance circle. The oscillation superimposed on the main loop of the force vector could reflect the unevenness of the contacting surfaces or elastic vibration excited by the (fairly) sudden change in contact load, or both.

The apparent similarity between the force variation after point .o and that in the similar part of the simulated curves, Figure 80.a/.b, is spurious, since in the simulation the force variation is associated with continued oscillations of the displacement vector, whereas in the experimental curves the motion stops after a single overshoot (see curve [.g]), and the continuing force fluctuation is evidently elastic vibration.

It is interesting that the reduction of force after the first peak at .n is much steeper than the preceding increase; that is, the ensuing vibration is mainly attributable to the abrupt deceleration of the journal at the end of its passage. (In fact a plot of the displacement angle in curve [.i] against time -not shown - confirmed that its rate of swing peaks near point .n).

Comparison of the force and displacement vector orientations at each labelled point shows that for points .k to .n the second lags the first by a surprisingly large amount, around 20^{o}. At points .o and .p the orientations are approximately opposed, indicating a tensile contact force. This suggests that terminal contact loss would have occurred at this point, but for the adhesive effect of the oil film. Note that even without the elastic vibration, the contact force would have dropped to near zero around point .p (broken lines in [.d] and [.e]), that is at the point where terminal contact loss is predicted by the approximate theory.

The frequency of the vibration after .n is about 300 Hz. Since the effective inertia on the horizontal axis is about 10.1 kg, the implied stiffness is about 36 N/μm, which is on the low side even by comparison with the results in 6B.

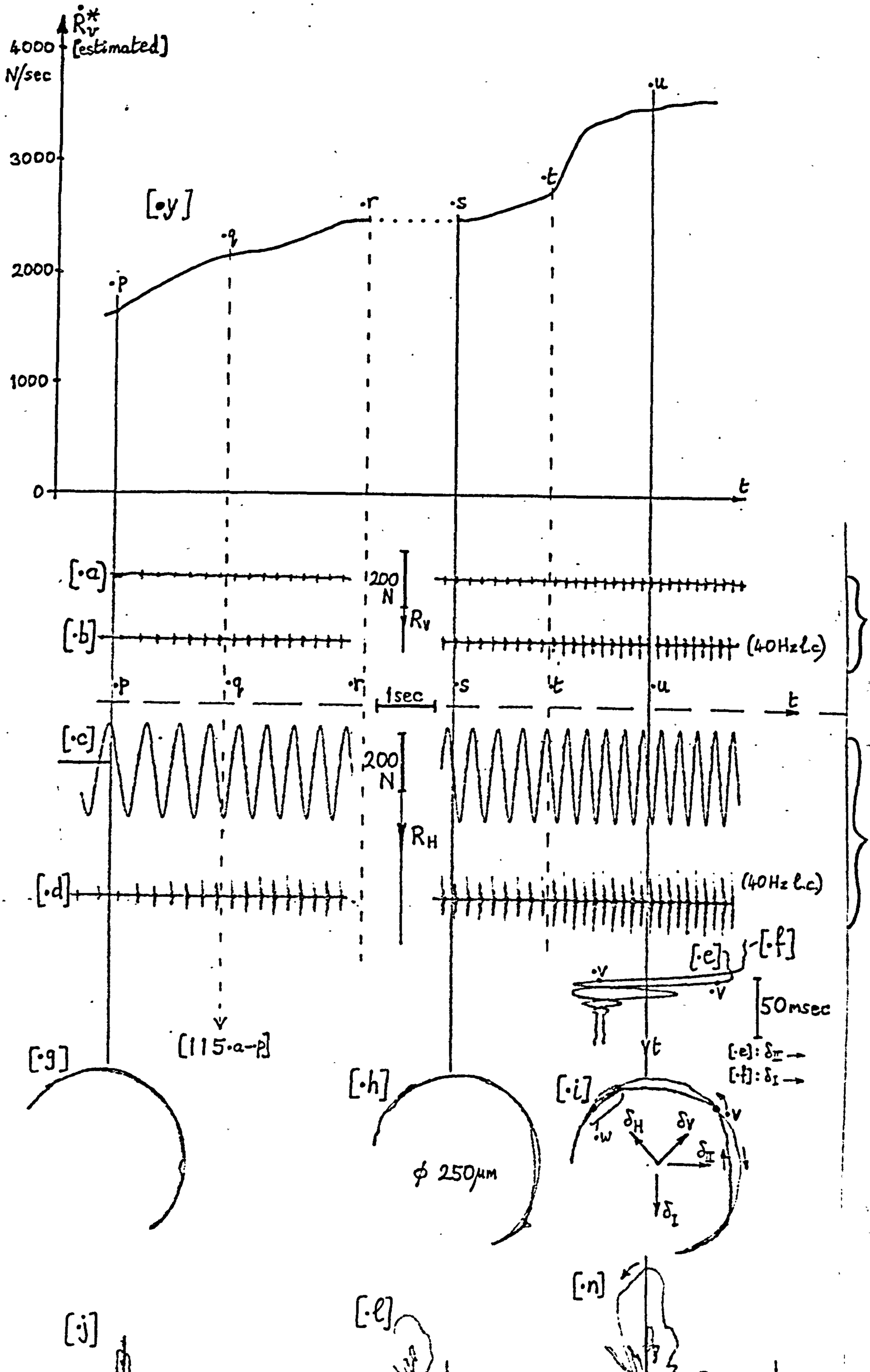

117 ·a–·y : <u>accelerating sequence of flypasts (standard build)</u>

13-4-82

Results for sequence of flypasts: The above close study of a single flypast provides a sound basis for studying the recorded sequence of flypasts at accelerating rates. The main features can be seen in curves [.a] to [.o], opposite. Curves [.a] and [.c] show the components of force, direct from tape to plotter, while [.b] and [.d] show the effect of passing the same signals through a passive filter with low cutoff frequency of 4 Hz (corresponding to 40 Hz at recording speed). The recordings between .r and .s have been suppressed because this is when the system was manually disturbed.

Curves [.g] to [.o] show details of the force and displacement variations near times .p, .s and .u; the flypast studied in detail above was also taken from this sequence, near time .q. The displacement trajectories [.g] to [.u] each show a complete cycle, but for the force vector plots [.j] to [.o] the two flypasts have been separated for clarity. The axes and scales for [.j] to [.o] are as shown for [.n].*

The top curve [.y] shows the estimated variation in $\dot{R}_V^*$, on the assumption that it varies in proportion to the frequency of the external force variation (curve [.c]). The rather sudden acceleration after .t merely shows clumsy speed control.

Interpretation: Displacement trajectory [.h] shows the marginal unidirectional passage contact loss at .s, re-established after the disturbance. By time .u passage contact loss is seen to be well established in both directions (curve [.i]). The main new feature in the load vector loci is the large spike in the $+R_V$ direction (e.g. point .v in [.o]), which is the birth-mark of passage impact. The direction of the load spike is very close to the direction of the displacement vector at this time.

Curves [.e - .f] show that after contact is regained at .v the displacement vector overshoots three times before coming to rest. At .w in curve [.i] there is plausible evidence of terminal contact loss between the first and second overshoot. From a study of larger scale traces including force/time traces, there is almost certainly terminal contact loss after the flypast in the other direction too, although the maximum separation appears to be no more than 5 μm. Thus the oblique load spikes on curves [.n] and [.o] can also be identified as impact spikes.

* Note that the handing is reversed relative to the displacement axes.

The major peak load associated with the flypasts throughout the sequence is seen to be the continuous-contact load 'loop', e.g. at .x in [.o], rather than the impact loads. Presumably this would cease to be the case at higher values of $\dot{R}_u^*$, when contact is lost by a larger margin. Even in the case shown, the impact loads must have a major influence on the high frequency content of the loading. Curves 117[.b] and 117[.d] show that the 40 Hz+ load increases markedly just after .p and again after .t. Curve 117[.a] on the other hand shows a steady increase, with no abrupt transitions.

Comparison with theory: In the displacement curves, loss of contact in the passage phase becomes apparent in one direction at about 2500 N/sec, and in both directions at about 3000 N/sec. The mean value corresponds to a value of $H_1 = 0.21$ (for $R_u^* = 3.9$), that is 25% above the value predicted by the simplified theory, and to a value $\ddot{\delta}^*/R_u^* = 160$ radians/N-sec, that is 160 times greater than the value predicted by the empirical criterion.

Curves 117[.b/.d] suggest that there is a terminal load spike, if not actual contact loss, from about 2000 N/second upwards. Since the theoretical prediction for terminal impact is not a clear-cut one, however, no conclusions can sensibly be drawn from this.

6E: SERIES OF FLYPAST TESTS: STANDARD BUILD

Object: The purpose of the four groups of tests reported in this section is to determine how the threshold of passage contact loss varies, if at all, with R_u^* and with peak load, and its repeatability from one test to the next.

The detailed interpretation of recorded measurements as in the previous section is too time-consuming to apply to a large series of tests. Thus a variety of cruder methods of evaluating the threshold value were employed. Before these methods are outlined, some inevitably impressionistic observations on qualitative aspects of the revealed behaviour may be appropriate.

Spurious or irrelevant contact loss: Ideally, it should be possible to interpret any departure of the displacement trajectory from the trajectory established at very low speeds as indicating loss of contact. In practice, however, owing to form errors the latter trajectory is itself not exactly repeatable, so that small deviations may occur due to changes in the precise point of contact rather than due to actual loss of contact. The oil-film 'flats' described on page 106 should also be discounted for our purposes. In general these two effects can be distinguished from 'true' contact loss in that their magnitude remains effectively constant over a range of speeds, whereas once passage contact-loss proper occurs, the free-flight trajectory extends progressively as the speed is increased further.

Repeatability: Despite the approximate symmetry in the applied load variation (cf 101.a/.c), the measured displacements and loads sometimes varied quite a lot between the two halves of a cycle, presumably due to variations in the friction and local radius of relative curvature from point to point around the journal.

In the great majority of cases, the oscillations of the journal following a flypast ceased before the next flypast began. In these cases, though not in the contrary cases, the pattern of both load and motion showed good repeatability from one complete cycle to the next - apart from variation in the height of the terminal load spike, if any; equally, the pattern showed good stability when disturbed.

Over a period of tens of seconds, however, repeatability was poorer. In particular, the tendency to lose contact sometimes distinctly decreased, and

sometimes increased. This could well be due to changes in the condition of the metal surfaces, if /dry/, or of the temperature of the oil-film, when present. Over the longer term, the development of surface damage and jerky 'stick-slip' motions has already been noted (p 106).

Procedure: Except as stated overwise, the procedures used for the tests considered in this section were as described in the previous section.

/Flexible pivots/ were installed in the vertical link. For the first group of tests, the spring tension was adjusted to give a net static load on the pin of 2N, upwards. Tape recordings were made with the drive slowly accelerating and then decelerating, with the exciter systems charged to mean pressures of approximately $3\frac{1}{2}$ bar (twice), then 7 bar, then 14 bar.

Each recorded sequence was repeatedly played back with the displacement trajectory displayed on one oscilloscope and R_H displayed against a time base on another. (R_V was found to be over-recorded). Four points were thereby identified in each sequence: firstly, the highest speed at which contact loss was not apparent in the displacement trajectory during the flypast with R_H increasing; secondly, the lowest speed at which it was clearly apparent; and likewise for the flypast with R_H decreasing. The value of $\dot{R}_V^*$ at each point was estimated from the second oscilloscope trace, by the methods described in the previous section; thus upper and lower bounds to the threshold speeds were established.

For the next group of tests, the tape recorder was not used. The static vertical contact force was set to a series of different values in turn, from 1.5 to 12 N in the $+R_V$ direction (?), and then 5N in the opposite direction. In each case the eccentric was accelerated and decelerated a number of times, and upper and lower bounds for $\dot{R}_V^*$ at the threshold speed were estimated directly from the displayed signals.

The third group of tests followed the same procedure as the second, except that the bearing was /dry/. A final untaped test was performed with /flexible pivots/ and an /oiled/ bearing.

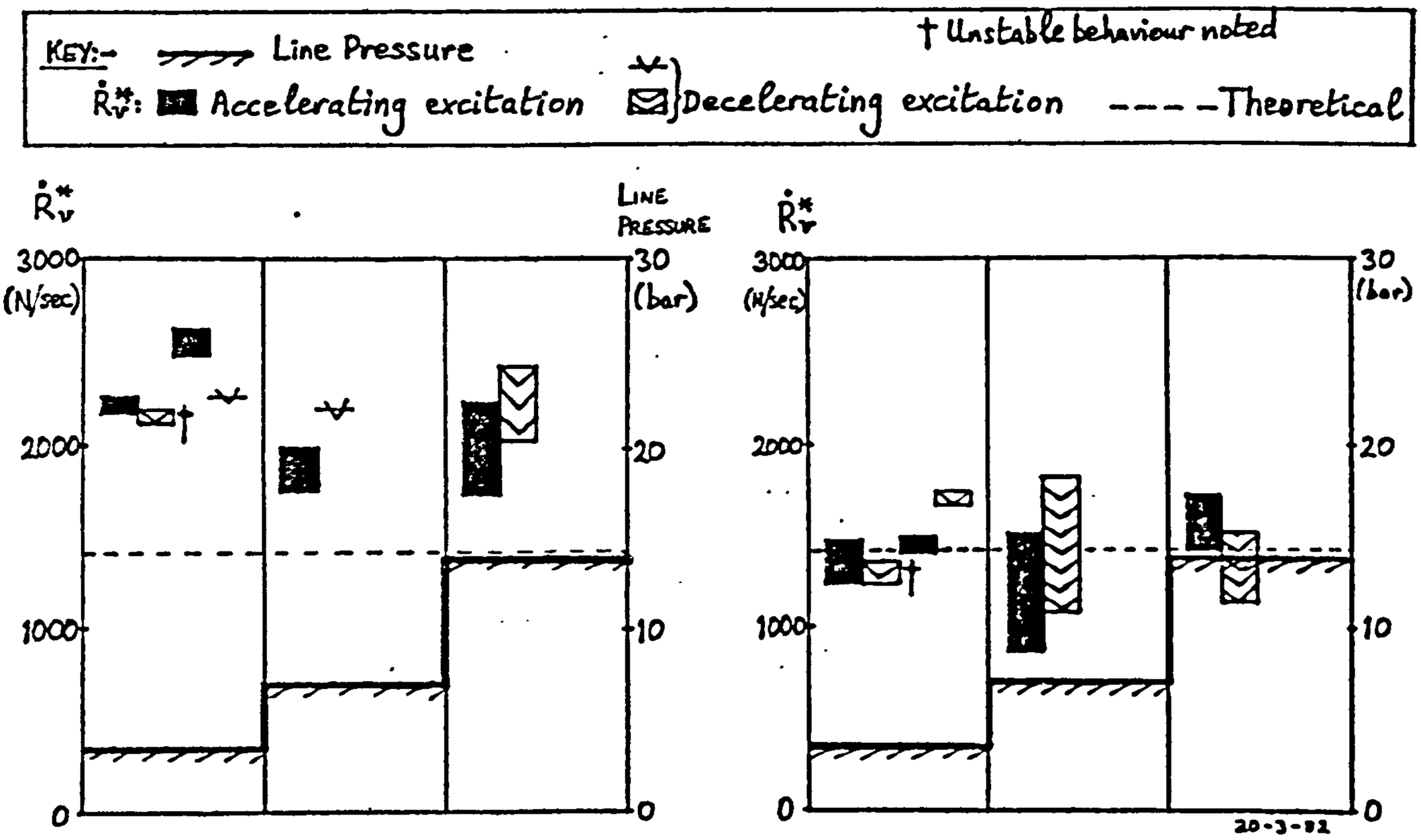

[•a]: Flypast with R_H increasing

[•b]: Flypast with R_H decreasing

121•a–•b: <u>Consistency of passage contact-loss threshold (standard build).</u> [$R_4^* = 2N$]

Results: Figures [.a] and [.b] show in bar-chart form the estimated threshold values for $\dot{R}_v^*$ from the first group of tests. It is seen that the margin of uncertainty is quite large in some cases, as is the variation between the pairs of repeated results ($3\frac{1}{2}$ bar case).

The effect of changing the gas pressure is to increase the peak contact force between flypasts, and (more importantly) to increase the interval between them for a given value of R_u^*. Comparing the three boxes in each figure, it is seen that this variation has no significant effect - consistently with the theory. However, in one case at the lowest pressure (marked †) some interference between successive flypasts was visible - so that, as noted previously, there was a lack of repeatability in the displacement trajectory.

No consistent difference is shown between the sequences with the eccentric drive speed increasing (solid bars) and those with it decreasing (chevron bars). However, a consistent difference is certainly visible between the two figures, suggesting that one side of the bearing has surface features more favourable to contact loss than the other. Nevertheless, the difference is no greater than the scatter in either figure, so in view of the arbitrary nature of the presumed cause there seems little point in pursuing the matter.

Referring to equations 114.b/.d, the predicted threshold value of $\dot{R}_v^*$ is about 1400 N/sec by the simplified theory and $\frac{4}{\pi}$ N/sec by the empirical criterion. It is seen that the former value falls within the range of measured values.

The results of the second group of tests are shown, using double logarithmic axes, in Figure 122[.a]. The overall range of the results from the first group has also been transferred to this figure.

All the results in this figure were taken 'blind', in the sense that the inertial measurements necessary for making a theoretical prediction were not taken until after the second group of tests, in an attempt to exclude subjective bias. The theoretical prediction is in fact shown as a band, taking into account the estimated uncertainty in the value of $M_o^{1/3}$ (5%/3), in the value of $e^{1/3}$ (15%/3) and in reading from Figure 87.a (10%). An error in the value of ε has <u>not</u> been allowed for: this could well double the width of the band.

It is seen that the trend of the results (subjectively approximated by the chain line) is broadly consistent with the theory, the discrepancies being of the same order as the scatter in the experimental results.

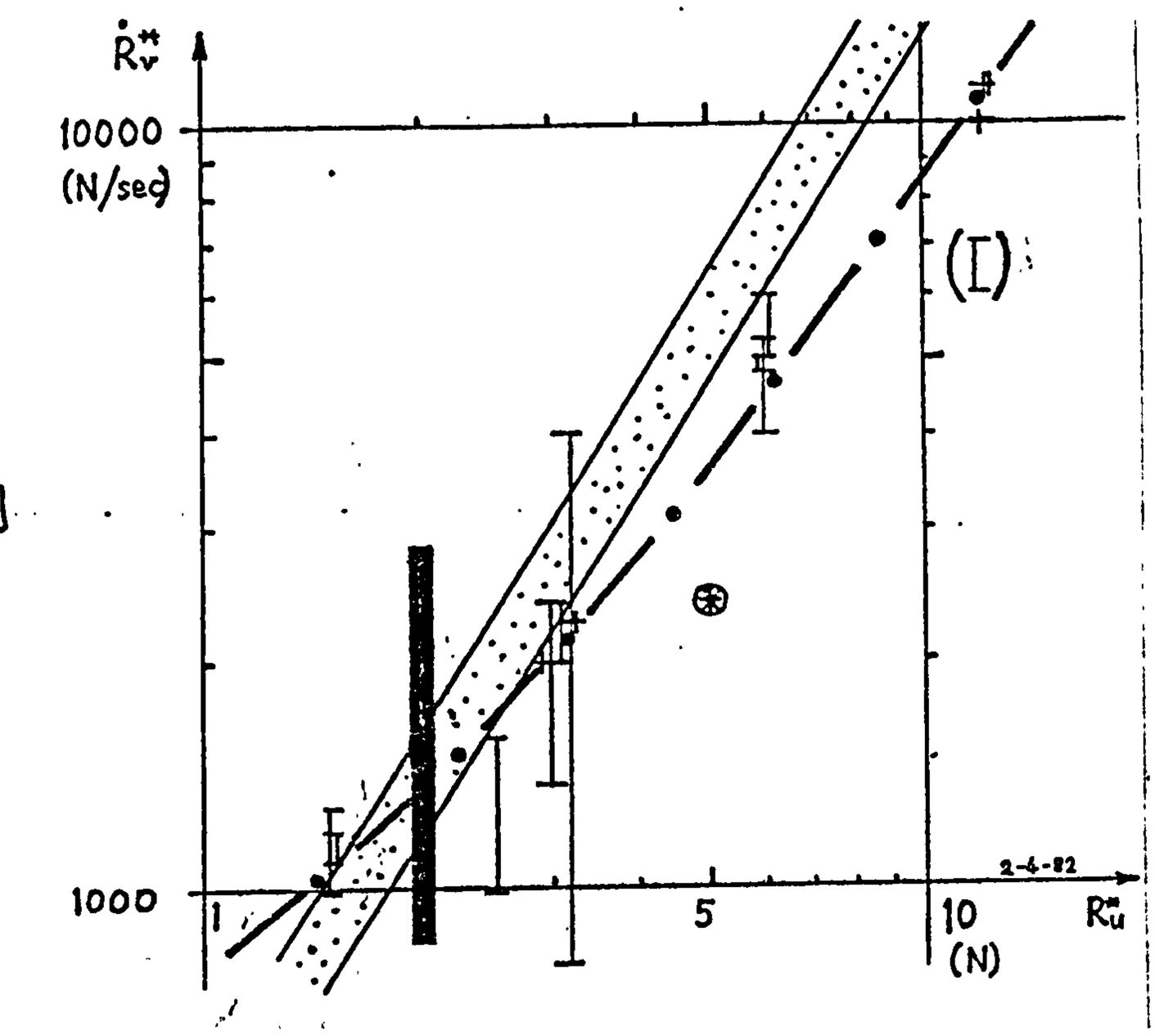

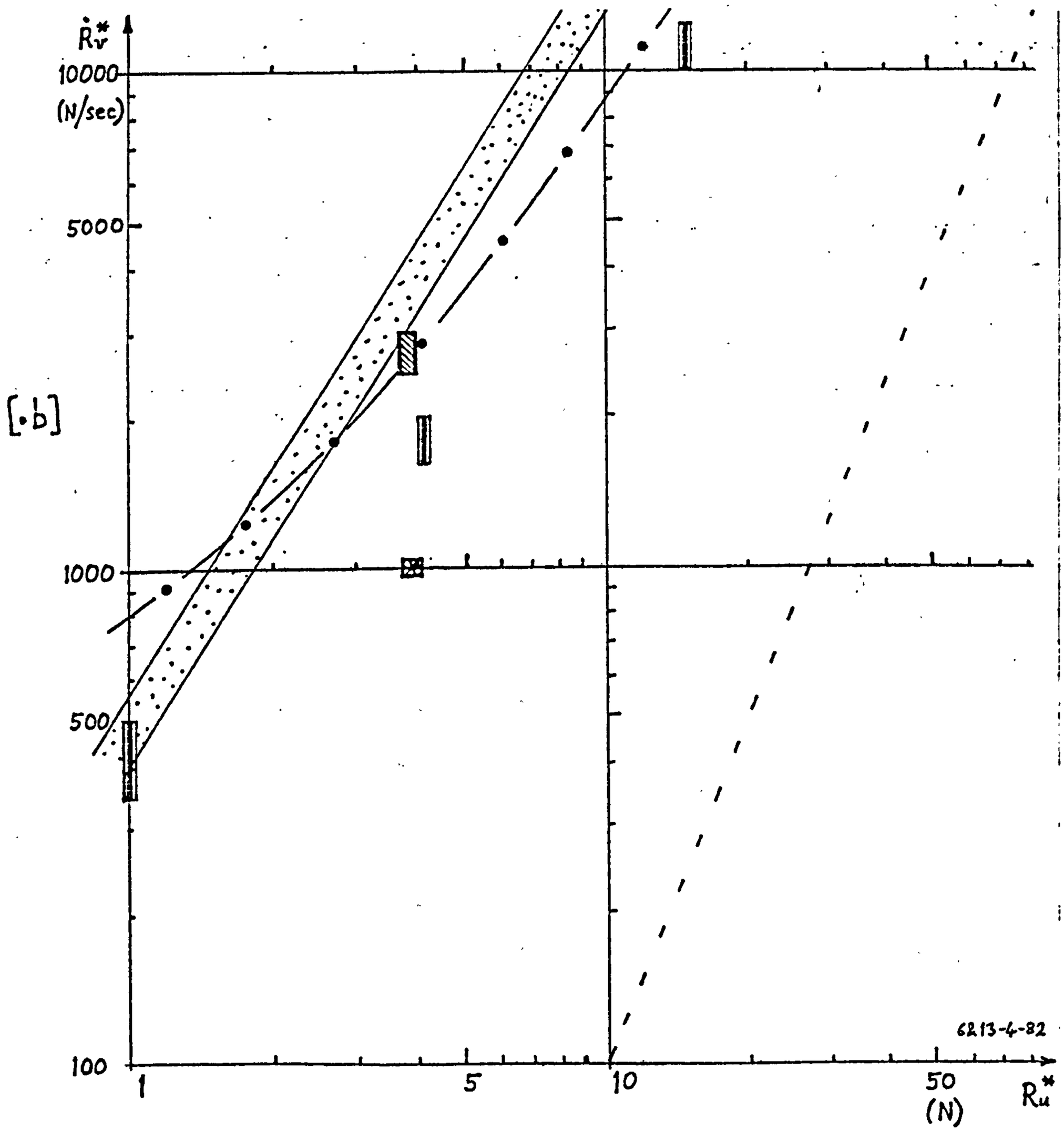

122 ·a --·b : Relationship between $\dot{R}_{vr}^*$ and R_u^* at threshold of passage contact loss (standard build)

The subjective trend line is copied onto Figure [.b] for comparison with the later results. The sequence studied closely in Section D was among these, and the threshold values for the two halves of the load cycle, shown by the limits of the hatched bar, are seen to straddle the trend line. The results with the bearing /dry/ (striped bars) seem to follow a similar trend but at a generally lower level.

A few of the results are seen to depart quite considerably (by a factor of two or more) from the general trend. This is most probably because the alignment was poorer in these cases: definite asymmetry of the displacement trajectories was noted, for example, in the case indicated by paratheses in [.a].

Departures from the theory: Apart from the uncertainty of alignment and form errors, there are three obvious respects in which the apparatus departs quite significantly from the assumptions of the theoretical model.

Firstly, the stiffness of the diaphragm springs in the pneumatic exciter has the effect (see 101.d-.f) that R_v^* momentarily 'hesitates' as the journal displaces across the clearance. This may be expected to inhibit loss of contact, that is raise the threshold value of $\dot{R}_v^*$ - particularly at lower values of R_u^*, in which case the exciter spring force is larger relative to the other forces.

Secondly, friction in the bearing must hold back the initial rotation of the displacement vector so that it lags the nominal load vector more, with the result that contact loss is more likely in the passage phase. This would be expected to lower the threshold curve, particularly with the bearing /dry/.

Thirdly, when the bearing is /oiled/ the adhesion of the oil film would be expected to raise the threshold curve. This applies particularly when R_v^* is negative (as in the first group of tests), since then the contact occurs in the lower half of the bearing, where the oil film would tend to be thicker.

It may be seen that insofar as a pattern is discernible in the departures from the theory, it conforms to the above expectations. This tends to support the view that the cited factors are the main shortcomings of the theory in the present application.

[a]

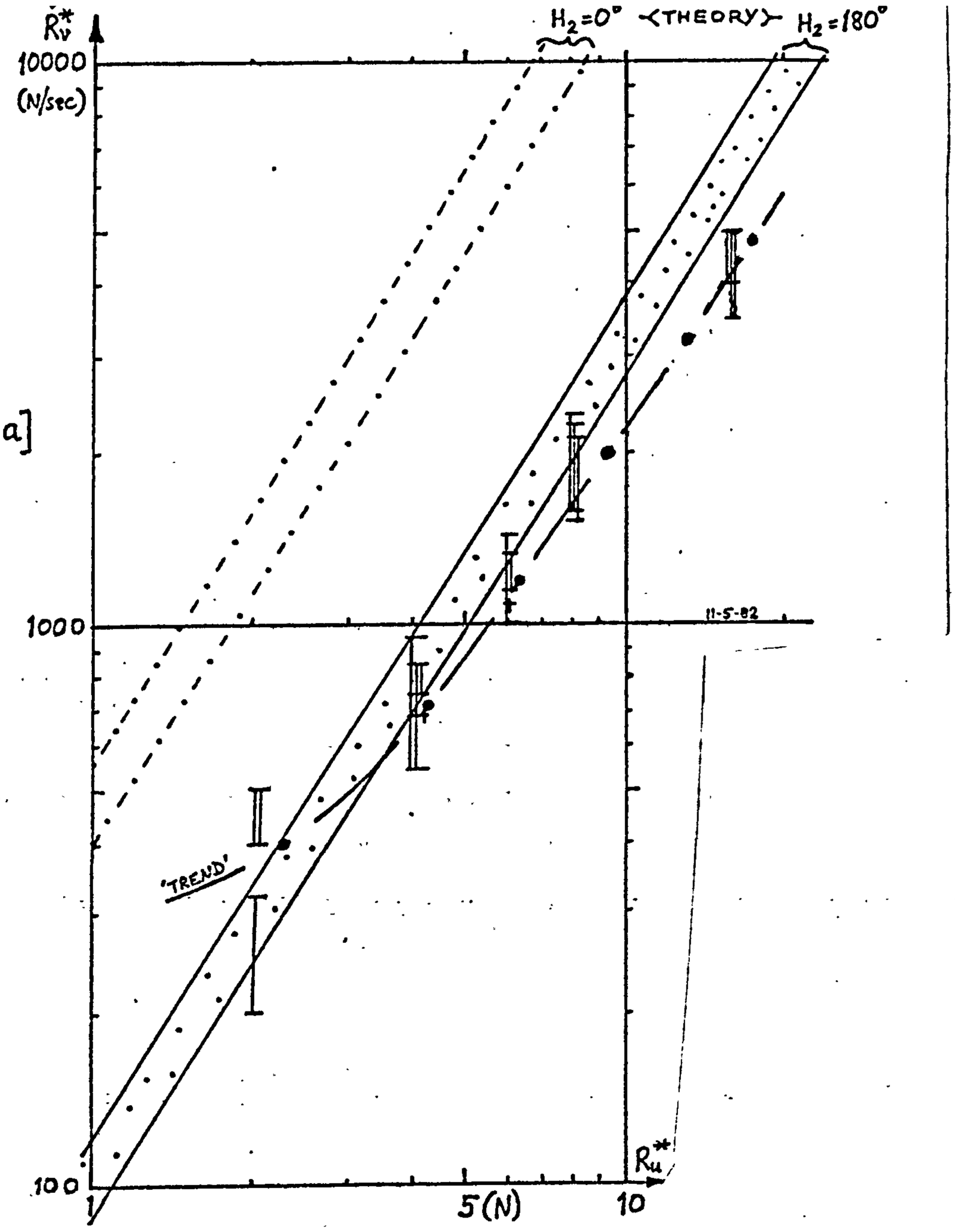

123·a: $R_u^*/\dot{R}_v^*$ threshold relationship with axis of exciters vertical ($H_2=180°$)

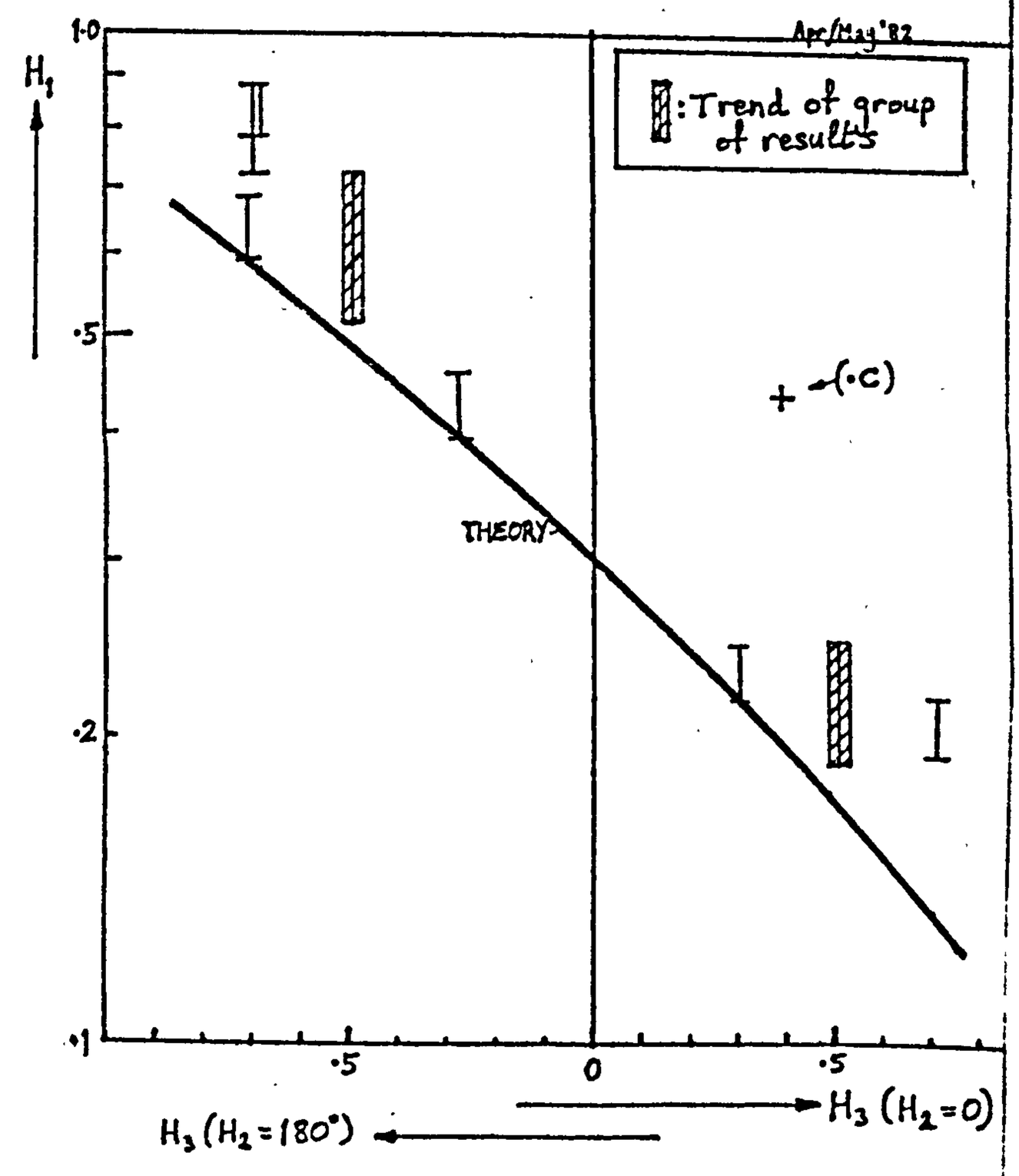

123·b: Variation of H_1 with H_3 at passage contact-loss threshold

6F: EFFECT OF VARYING INERTIA PARAMETERS

The results in this section test the predicted effect of changing H_2 and H_3, that is 2η and ϵ. It is not practicable to change M_o to a sufficient degree to provide a useful test of the weak influence predicted for this parameter. The former parameters can be changed either by adding or subtracting masses (see 97.a) or by transferring the excitation from the horizontal to the vertical axis, which has the effect of changing H_2 by 180^o. It should be noted that when an offset mass is added to the horizontal link the values of H_2 associated with each of the two flypasts in the load cycle are of opposite sign.

Procedure: In general, the procedures described in the two previous sections were followed, with masses added or subtracted as appropriate. With excitation in the vertical plane, the journal was /side-sprung/ to provide the force component R_u^*, and the weight of the horizontal link was balanced by a top spring and/or by charging the lower exciter to a slightly higher pressure than the upper one.

Passage contact-loss: $\dot{R}_v^*/R_u^*$ law for $H_2 = 180^o$: For $H_3 = 0.5$, the theory predicts passage contact-loss at a value of $\dot{R}_v^*$ about five times lower for $H_2 = 180^o$ than for $H_2 = 0^o$. The results shown in Figure .a bear this out. Indeed, considering that these measurements were carried out with an apparent coefficient of static friction of 0.2, and visible jerkiness in the sliding motion, it is quite surprising how well the results conform to the predictions, even to the extent that the trend of the discrepancies matches that observed in the previous results.

Passage contact-loss: effect of changing H_3: According to the theory in Chapter 4, changing H_2 by 180^o is equivalent to changing the sign of H_3. Thus the results of tests with $H_2 = 0^o$ and with $H_2 = 180^o$, for a range of values of H_3, can be conveniently combined as shown in Figure .b. The ordinate logarithmically represents the value of H_1 corresponding to the threshold of contact loss as determined from the displacement signals. The series of results for $H_3 = 0.5$ are summarised by the hatched bars, which record the range of values on the subjective trend lines in Figures 122.a and 123.a, for $R_u^* = 4$ to 10N.

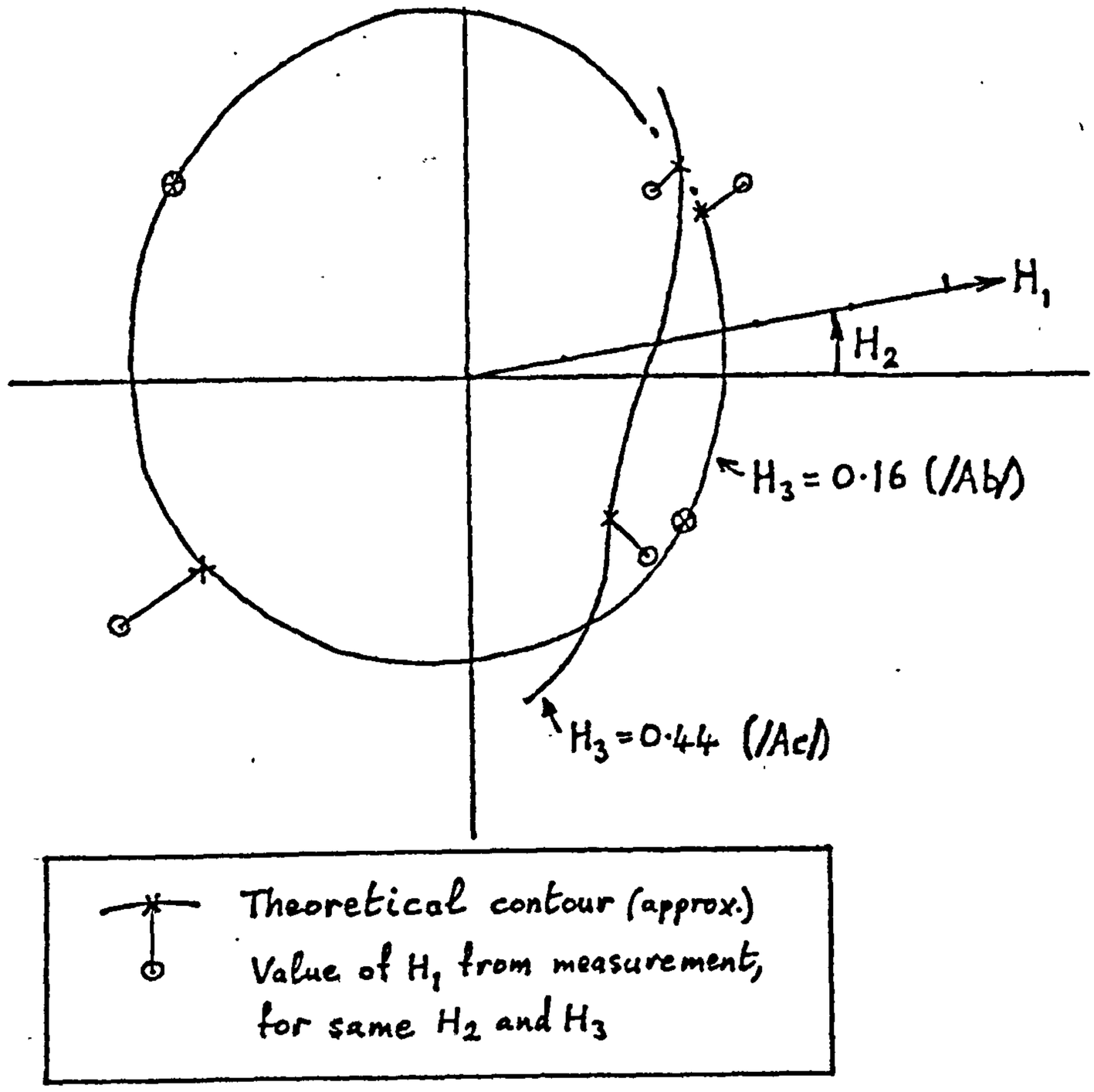

124·a: Passage contact-loss threshold with offset masses

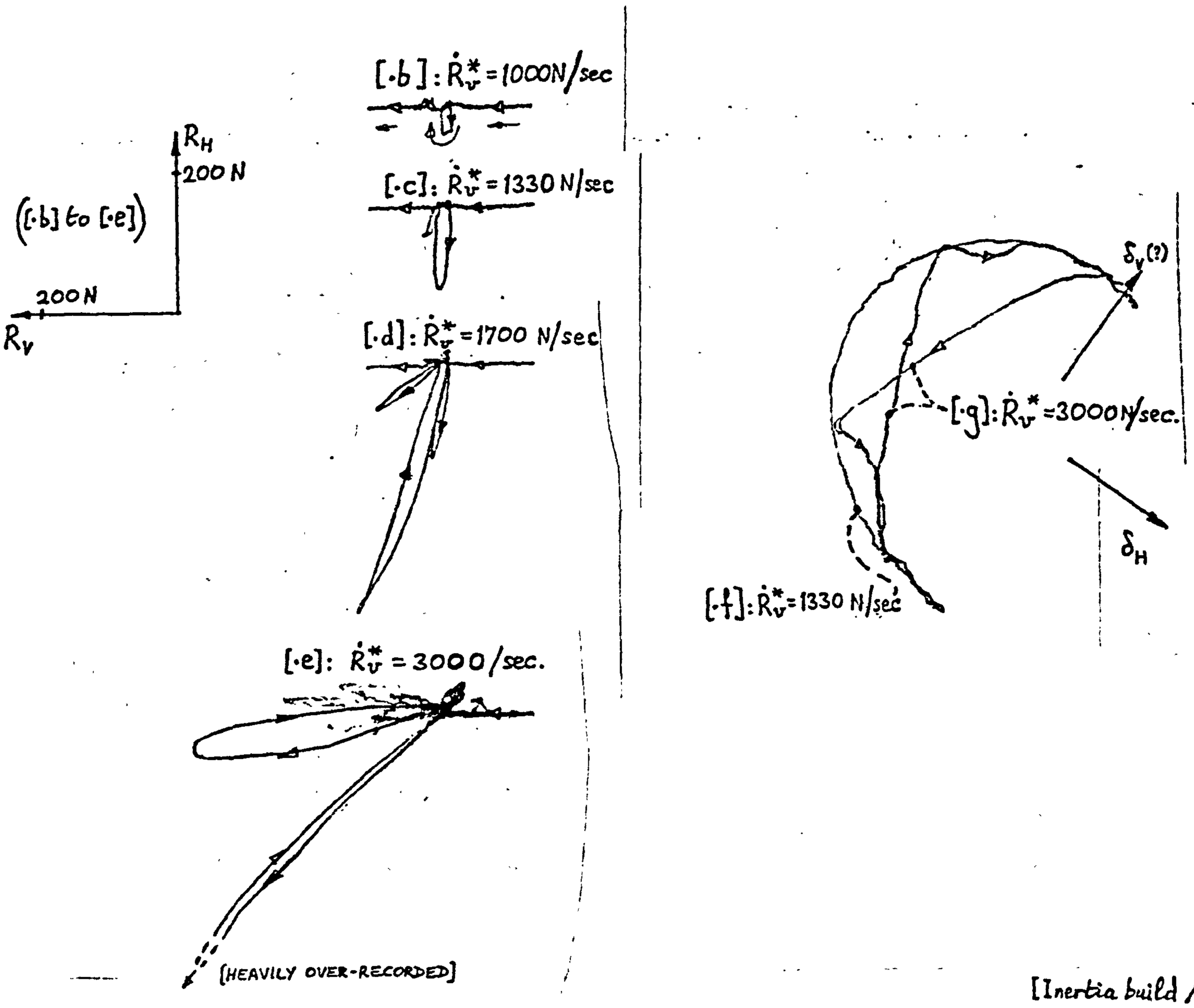

[Inertia build /Aa/]

124·b–·g: Accelerating sequence of flypasts, $H_2 = 180°$, $H_3 = 0·28$, $R_u^* = 4N$, Pin 'A'.

11-5-82

The other points are calculated from upper and lower estimates (where necessary) of the threshold $\dot{R}_v^*$ for a particular value of R_u^*, namely 16 N for '$H_3 = -0.71$' and 4N for the other cases. /Ball-pivots/ and /oiled/ bearing surfaces were used in each case.

It is seen that the main trend of the theoretical curves is clearly reflected in the results, with a consistent bias on the high side. The exceptional result (.c) was taken immediately after the result marked '⊠' in 122.b, adding to the suspicion that an unnoticed loss of alignment had occurred at this time.

Passage contact loss: effect of changing H_2: Figure .a opposite shows results from three runs with offset masses on the horizontal link. Again R_u^* was set to 4N and /ball-pivots/ and /oiled/ surfaces were used. The theoretical passage contact-loss threshold contour for two values of H_3 (interpolated from results for $H_3 = 0$, 0.33 and 0.5) is sketched in (H_1, H_2) polar coordinates, in the same manner as Figure 87.a. The corresponding points from the test runs are seen to agree, subject to the usual scatter for single readings.

Vector loci: $H_2 = 180^o$: The characteristics of the force and displacement vector loci recorded with the modified inertia parameters differ in some significant respects from those for the standard build, considered in Section D. Curves [.b] - [.g] show extracts from an accelerating sequence of flypasts in one case with $H_2 = 180^o$. Contact is maintained up to $\dot{R}_v^* = 1330$N/sec (see curve [.f]). The load vector loop in [.c] associated with the rapid passage of the contact point around the clearance circle has its major diameter along the 'u' axis (contrast 115.f), as might be expected since $M_{uu} > M_{vv}$. At higher speeds contact is lost, and impact loads rapidly become the dominant feature of the load curves; in curve [.g], rebounds are clearly apparent.

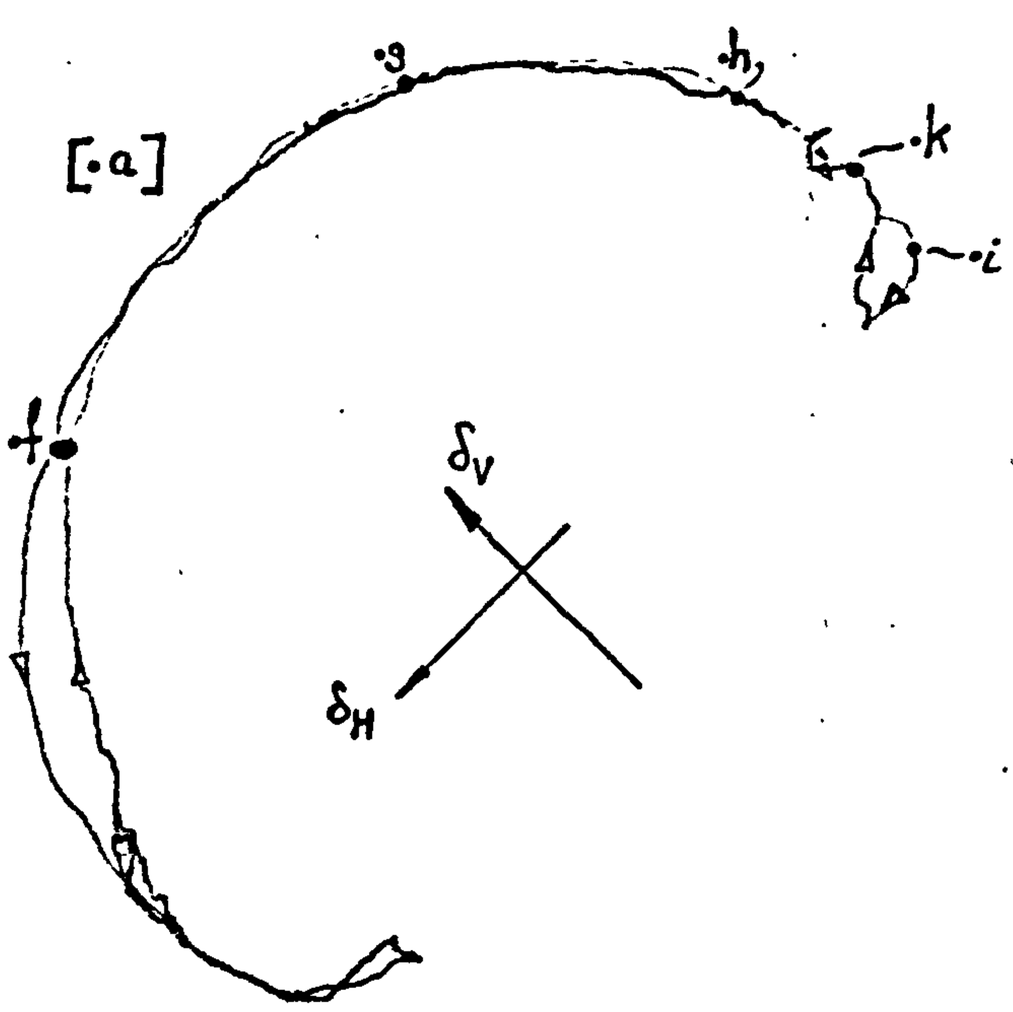

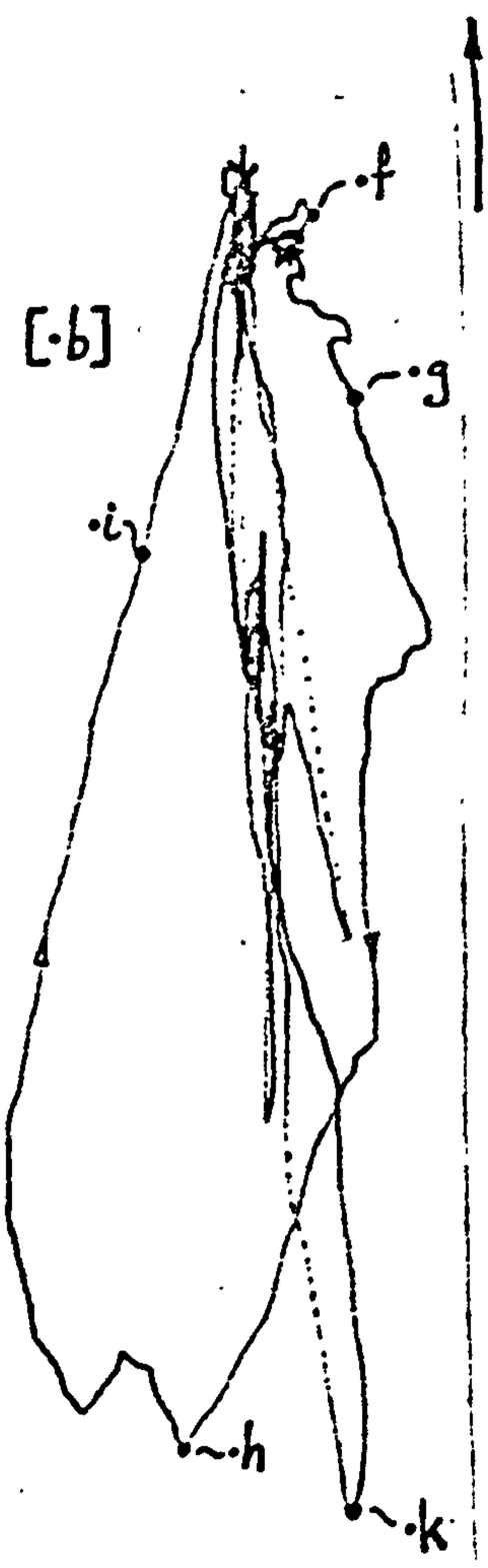

[Inertia build /Ea/]

125·a--·b: Flypast with terminal impact; $H_2 = 0°$, $H_3 = 0.71$, $R_4^* = 4N$, Pin 'A'

13-4-82

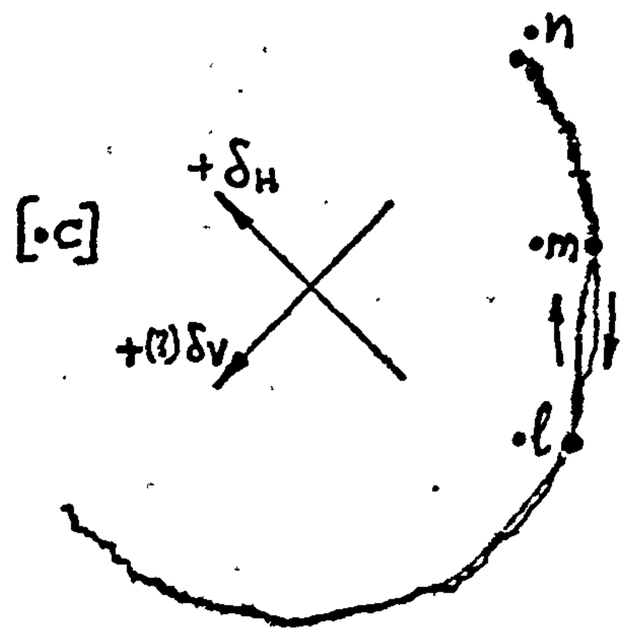

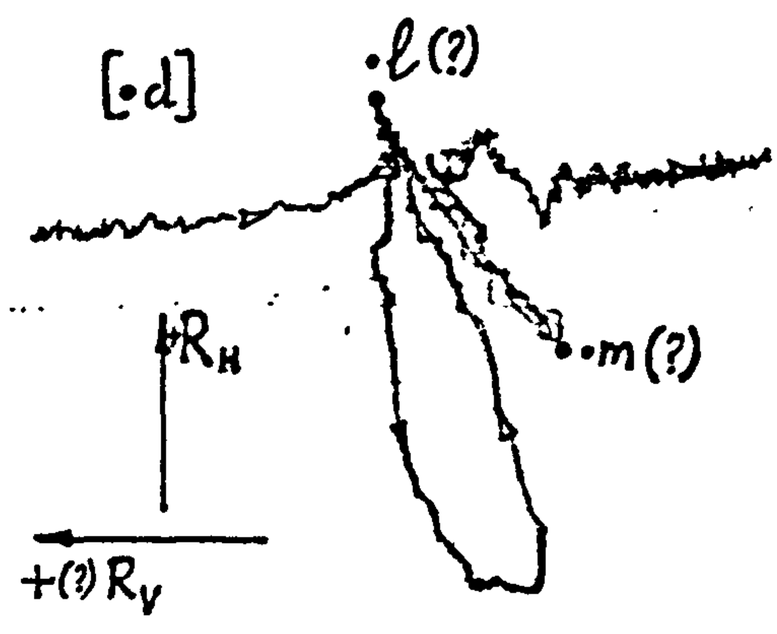

[Inertia build /Ea/]

125·c--·d: Flypast with (early) terminal impact; $H_2 = 180°$, $H_3 = -0.71$, $R_4^* = 16N$, Pin 'A'

12-5-82

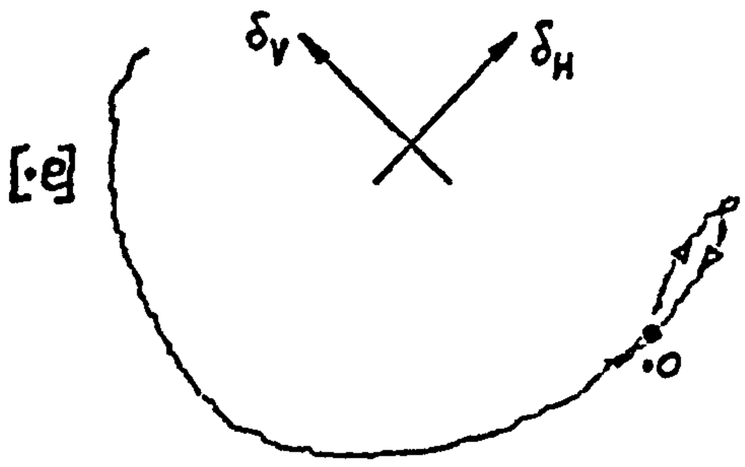

[Inertia build /Ac/]

125·e: Flypast with terminal impact; $H_2 = 45°$, $H_3 = 0.44$, $R_4^* = 4N$, Pin 'A'

7-5-82

Terminal contact loss: Curves [.a] - [.e] opposite show displacement and load vector loci, for part or all of one cycle, for three other inertia builds. In each case contact loss in the terminal phase of the flypast can be seen.

Studying corresponding curves [.a] and [.b], the passage contact loss is seen to give rise to a small impact at instant .f, dwarfed by the subsequent continuous-contact load loop (.g - .i), but the first terminal impact load (.k) is slightly larger still.

Curve [.c] shows a very significant difference: contact is seen to be lost (.ℓ) and regained (.m) well before the displacement vector reaches the end of its swing at .n - yet still in the 'terminal' phase of the flypast. (It should be explained that the free-flight 'arc' .ℓ - .m, although small, was stable and repeatable). The corresponding load vector locus [.d] suggests the explanation for this behaviour: the initial increase in contact force as the contact point accelerates is followed by an elastic recoil that momentarily reverses the sign of the contact force.

As the mechanism of terminal contact loss considered in the simple theory of Chapter 4 is quite different to that noted above, the relevant threshold values for $\dot{R}_v^*$ would not be expected to agree with those predicted, and indeed they did not. The crucial test is that with build /Ac/ ($H_2 = \pm 45^o$, $H_3 = 0.44$). According to Figure 79.a, as the flypast severity is increased contact should be lost firstly at stage II (first overshoot) in the half of the cycle for which H_2 is negative, then at stage III (second overshoot) in the other part of the cycle, before passage contact loss intervenes in both parts of the cycle. By contrast, the first contact loss in practice occurred in the positive-half of the cycle, just before the first overshoot of the displacement vector (at .o in curve [.e]), whereas no terminal contact loss was observed in the other part of the cycle, up to the speed at which passage contact loss occurred. In no case was contact loss observed at stage III.

The phenomenon of elastically mediated terminal contact loss is obviously governed by factors other than H_1, H_2, H_3 : such as the natural frequencies of elastic vibration (in proportion to $\dot{R}_v^*/R_u^*$, say). In this connection, it is worth noting that all of the cases in which the phenomenon was observed involved added masses attached to one link or both by stems. This would both introduce a new mode of vibration (associated with stem flexure) and reduce the natural frequency associated with bearing compliance, so that the half-period of the vibrations corresponds more closely to the pulse-width of the contact force during the passage phase, and therefore the mass-elastic system would be

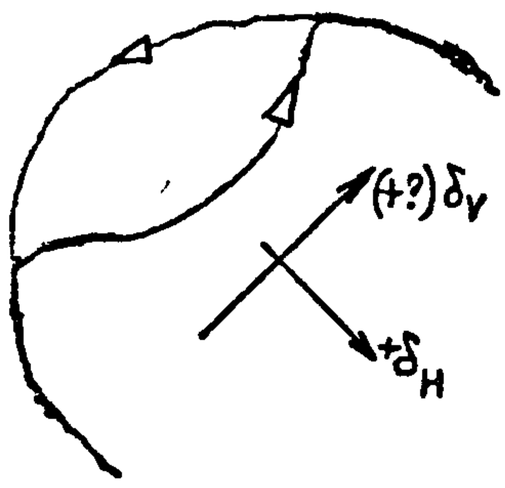

(Build /Dd/)

126.a: Displacement locus at a 'resonant' speed for build with flexibly mounted mass.

13-5-82

excited by the contact force pulse to a greater degree. The consequence, in the critical case of build /Ac/, is that vibration at a fundamental frequency of about 75 Hz is continuously visible in the force records (not shown), and indeed the force vector locus is barely intelligible for this reason.

Resonance effects: For one test, an attempt was made to modify the inertia parameters by attaching an overhung mass to the horizontal link by means of a long curved stem (see 97.a). In the event, this was found to vibrate at about 30 Hz with considerable amplitude and a low decay rate, so that the 'rigid body' values of H_2 and H_3 ceased to be very relevant even in the passage phase of the flypast. However, this unintended phenomenon had an interesting effect on the joint behaviour. As the excitation frequency was increased, a series of five 'resonant' speed bands was observed at which severe passage contact loss occurred, as shown for example at Figure .a, separated by four bands of speeds at which no loss occurred in the passage phase; terminal contact loss occurred in the last of these four bands. The highest value of $\dot{R}_v^*$ at which no passage contact loss occurred was about 3 (?) times as high as that expected according to the theory (that is with elasticity disregarded), indicating that the vibration positively inhibits contact loss in the favourable speed bands.

A further illuminating observation in this test was that the number of complete cycles of vibration during the parts of the cycle when the journal was at rest was approximately integral for the unfavourable speeds (4, 3, 2, 1, $< \frac{1}{2}$) and half-integral for the favourable speeds ($3\frac{1}{2}$, $2\frac{1}{2}$, $1\frac{1}{2}$, $\frac{1}{2}$).

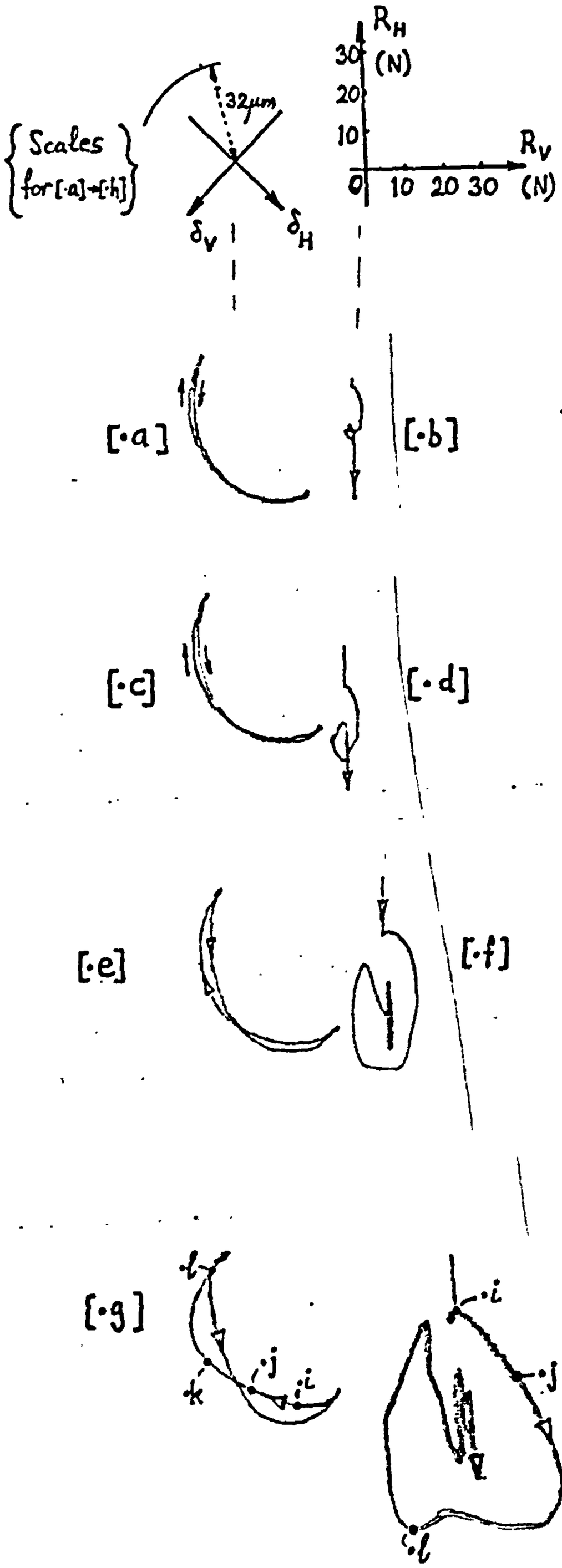

$R_u^* = 15\,N$

[·a]

[·b]

$\dot{R}_v^* = 350$ N/sec

[·c]

[·d]

$\dot{R}_v^* = 440$ N/sec

[·e]

[·f]

$\dot{R}_v^* = 620$ N/sec

[·g]

[·h]

$\dot{R}_v^* = 1050$ N/sec

(Build /Ca/)

127·a–·h: Displacement & Load vector loci at flypasts using pin 'B' (/dry/); $H_2 = 0°$, $H_3 = 0{\cdot}5$

15-4-82

6G: EFFECT OF REDUCING CLEARANCES

The replacement of pin 'A' by the smaller clearance pins 'B' and 'C' might be expected to have the following effects:-

.m In accordance with the theory, a relatively weak increase in the threshold values of $\dot{R}_v^*$;

.n reduction in the effects of the exciter springs: that is, improved linearity in the logarithmic $\dot{R}_v^*/R_u^*$ threshold curve;

.o increasing sensitivity to errors of form;

.p reduced contact compliance;.

.q in accordance with the results of Section C, a strong increase in the influence of the 'air squeeze film'.

The actual behaviour with these pins was tested using the same procedures as previously, for the 'standard' inertia build, that is $H_2 = 0^o$, $H_3 = 0.5$, so that theoretically $H_1 = 0.17$ as before at the threshold of passage contact loss. /Ball-pivots/ and /oiled/ surfaces were used in the first place; in the case of pin 'B', tests were also carried out with the bearing /dry/.

Profile error problems: The problem of 'spurious contact loss' noted in Section E was increased with pin 'B', and still more so with pin 'C', so that there was an increasing degree of arbitrariness in the identification of the threshold speed for 'true' contact loss. In particular, the displacement trajectories associated with the two halves of the cycle were always distinct, as in [.a] opposite, even at the lowest speeds; presumably, this is because they involved contact at slightly different high-spots, due to slight changes in alignment between the two flypasts.

With pin 'C', contact loss only occurred in one half of the cycle in many of the tests. This is believed to have been due to the variation in the local radius of curvature of the clearance locus.

Vector loci: Curves [.a] to [.g] illustrate the behaviour observed, for the example of pin 'B' in the /dry/ state. Contact loss in the clockwise direction (+ R_H^* decreasing) can be seen marginally in curve [.c], and to an increasing extent in curves [.e] and [.g]. By contrast, the force vector curves for the same flypasts show a continuous development with no qualitative transition: one implication of this is that load recordings alone are quite unsuitable for identifying cases of contact loss with these clearance dimensions.

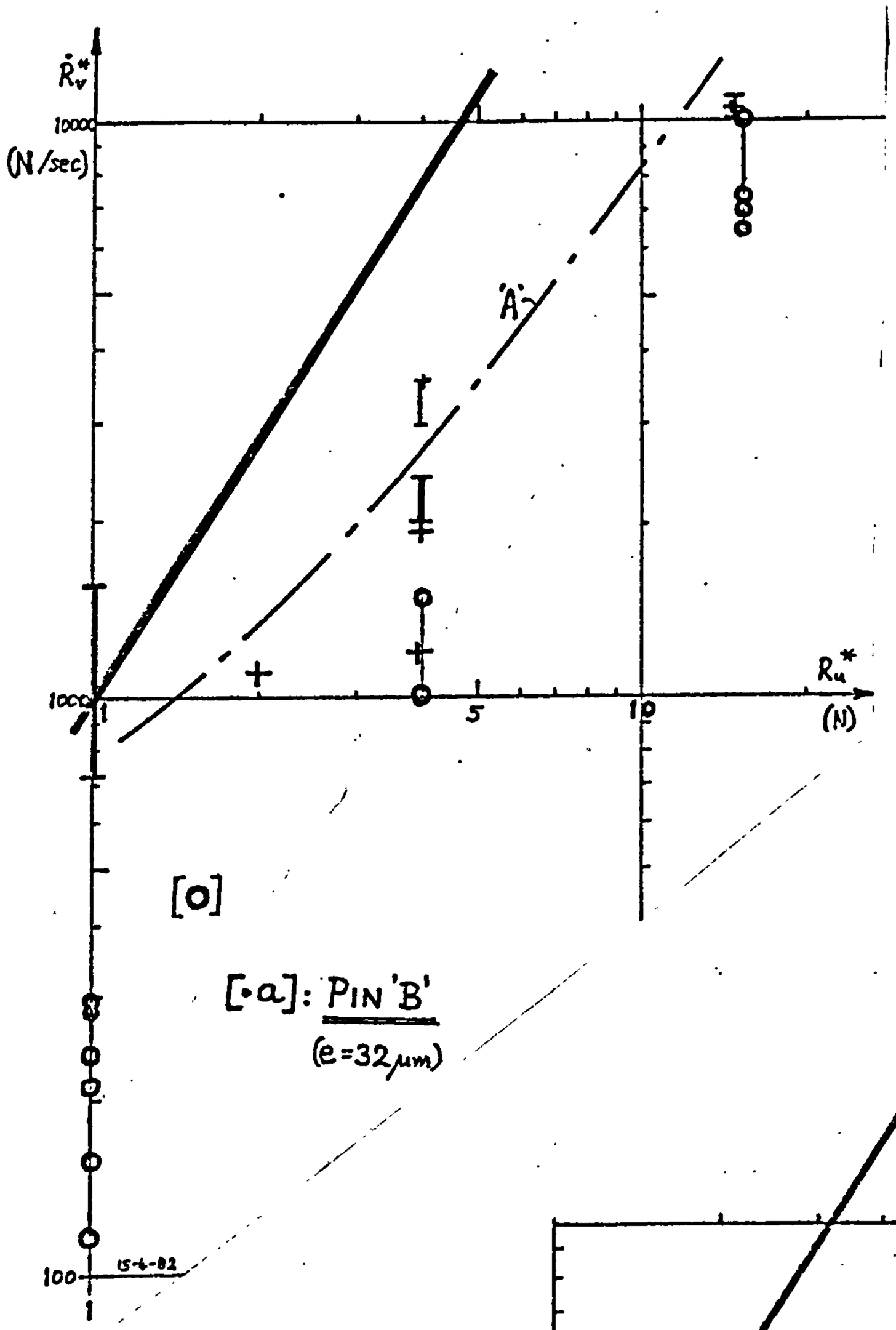

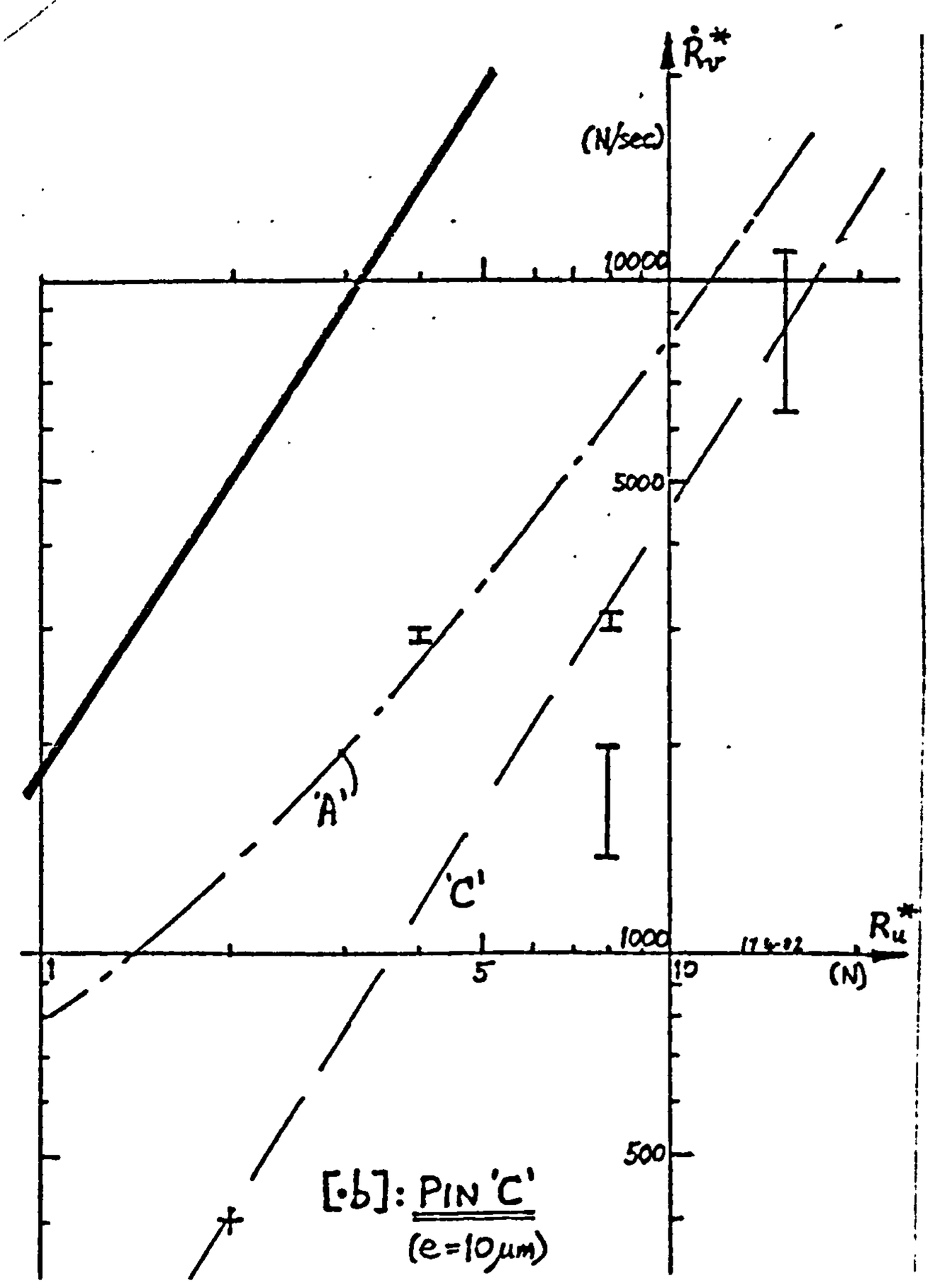

KEY:

I, + } Experimental values for pin concerned: /oiled/ bearing.

o Experimental values for pin concerned: /dry/ bearing.

— Experimental trend line

-·- Experimental trend line for pin 'A' for comparison.

━ Theoretical values for pin concerned.

128·a—·b: 'Passage' loss threshold relationship with reduced clearances; $H_2 = 0°$, $H_3 = 0{\cdot}51$ (Build/Ca/)

Curve 127[.h] is remarkable for the lack of any impact spike, such as would be expected given the clear contact loss visible in 127[.g]. Indeed, the pin load is seen to increase continously during the period of free flight (points 127 • i to •k), providing dramatic evidence of the effects of the air film. The smooth curve in the displacement trajectory as contact is resumed just after point 127 • k is consistent with this.⊛

It may be recalled that in the 'drop tests' reported in Section C, an air film effect as dominant as this was not found until pin 'C' was used. However, considering that the displacement trajectory in the present test is nowhere very far from the contact circle, an effect of greater magnitude than for diametral motion is not altogher surprising. Unfortunately, owing to a fault in the tape recorder, vector loci for the flypast tests with pin 'C' cannot be shown.

Threshold curve: Although, as noted above, the threshold of contact loss was very indeterminate in many cases, a representative speed for passage contact loss was judged as well as could be for a selection of values of R_u^* using the two pins in turn: in the case of pin 'C', this related to the half of the cycle in which contact loss did always eventually occur, the other being disregarded. Results are shown in Figure .a (for pin 'B') and .b (for pin 'C').⊛ The predicted relationships for the relevant values of e are shown by the full lines. The experimental trend line for pin 'A' is shown as a chain line in both figures, for comparison.

The trend of the relationship in both figures is seen to agree well with the theoretical line in respect of gradient, and for the /dry/ tests at least, the non-linearity at low values of R_u^* appears to be less significant than before. The effect of the profile errors no doubt accounts for the large scatter, particularly for pin 'C'.

The most striking feature of the graphs, however, is the large gap between the theoretical line and the experimental trend: indeed, the threshold values of $\dot{R}_v^*$ are in most cases actually lower for these tighter pins than for pin 'A',

⊛: Owing to a slow gas leak from one of the exciters in the test with $R_u^* = 1.5$ N, the positive peak value of R_H^* was considerably less than the negative peak. This should not affect the qualitative features of the behaviour recorded in 127.a - .h, but the quantitative results are put in question, particularly for the case of R_H^* increasing.

not higher as predicted. One tentative explanation that immediately offers itself is that the highly conformal surfaces, stationary under load between flypasts, produce a 'limpet' effect that greatly increases the effect of friction at the start of the flypast, and thereby amplify the downward shift of the trend line already attributed to friction.

6H: CONCLUSIONS OF CHAPTER

Substantiated predictions: For the conditions and within the parametric ranges applicable to the apparatus used, the following distinct and previously unanticipated theoretical predictions have been critically tested and substantiated, subject to a margin of variation commensurate with the irreducible variation of like measurements:-

.a Loss of contact between pin and journal can occur in either the passage or the terminal phase of a flypast.

.b For a given clearance and mass distribution, the threshold of contact loss in the passage phase occurs at a constant value of $\dot{R}_v^{*2/3}/R_u^*$, for different values of R_u^*

.c For the 'standard' build of the apparatus, the value of the dimensionless flypast severity index H_1 at the passage contact loss threshold is given to a first approximation by the relevant point in Figure 87.a.

.d For the builds without offset weights on the horizontal link (that is, with $M_{uv} = 0$), H_1 at the aforementioned threshold varies with H_3 in the manner predicted by the curve in Figure 123.b.

A further substantiated prediction, which cannot be said to provide a sharply distinct test of the theory, is as follows:-

.e The values of H_1 at the threshold in question for the tests with offset masses are also consistent with the corresponding predicted values.

Falsified predictions: Under the conditions described, several predictions have been clearly shown to be false, thus:-

.f For reduced clearances the (passage contact loss) threshold values of H_1 are not increased, but slightly reduced.

.g The threshold values of H_1 for contact loss in the terminal phase differ markedly from the values given in the contours in zones II and III of Figure 87.a.

.h Contact loss was not found to occur at the second or subsequent overshoots of the contact point (relative to the direction of the nominal joint force vector).

.i The values of $\dot{\vartheta}^*/R_u^*$ at the threshold of contact loss are not of the order of $1N^{-1}$ sec^{-1}, nor are they constant with respect to variations in R_u^*.

.a The elastic compliance between the pin and journal is much ~~lesser~~ greater, and less linear, than predicted.

Further observations: The following hypotheses may be advanced, on the basis of the observed behaviour, as qualitative modifications of the simplified theory advanced in Chapter 4:-

.b The value of H_1 at the threshold of passage contact loss is increased due to the presence of friction. This effect is reduced by the addition of a trace of oil, but substantially increased in the case of relatively tight clearances.

.c Contact loss in the terminal phase is provoked by the elastic recoil following the sudden inertial loading associated with the rapid acceleration and deceleration of the contact point during the passage phase.

.d The air film between the pin and journal reduces the severity of the impact following contact loss, very considerably in the case of relatively small clearances.

CHAPTER 7

THE STEADY-STATE RESPONSE OF FORCED HILL'S EQUATIONS

None of the material in this chapter has been published before.

Principal nomenclature for this chapter and for Appendices 10.S, 10.T is given below.

Symbol	Meaning
$c\ (\equiv C/2)$	Equivalent damping ratio.
$D;\ \bar{D}$	Frequency ratio; mean frequency ratio in normalised form.
f	Fractional variation of effective inertia (single harmonic).
f^*	Mean effective inertia of coupler and rocker, relative to total.
$g(x)$	Dimensionless instantaneous effective inertia.
J_r	Moment of inertia of link 'r' about its centre of mass.
J_ϕ	Effective inertia of mechanism at crank angle ϕ.
$J_o;\ J_d$	Mean of J_ϕ; inertia of drive link;
$J_{cr}(\phi);$	Effective inertia of coupler and rocker together at crank angle ϕ;
$\bar{J}_{cr},\ \overset{*}{J}_{cr}(\phi)$	mean value of $J_{cr}(\phi)$; variation in $J_{cr}(\phi)$.
S	Torsional stiffness of drive system.
$\mathbf{T}$	Transfer matrix relating $y(2\pi)$ to $y(0)$ in free vibrations.
$\underline{t}$	State vector at $x=2\pi$ when $\underline{y}(0) = (0,0)^T$ (forced).
x	Independent variable in normalised Hill's equation.
y	Dependent variable in normalised Hill's equation.
$\underline{y}, \underline{y}(x);\ \underline{y}_p(x)$	State vector: $\equiv (y,\ dy/dx)^T$; periodic solution.
$Z_1,\ Z_2$	Dimensionless factors of inertial loading $[\ddot{\theta}/\dot{\phi}^2,\ (\dot{\phi}+\dot{\theta})^2/\dot{\phi}^2]$.
θ	Torsional deflection of drive system.
ϕ	Angular position of prime mover ($\dot{\phi}$ = constant).
ζ	Damping coefficient for drive vibrations.
$\Omega_i;\ \bar{\Omega}$	Instantaneous frequency ratio; mean of Ω_i (in general form).
$\dot{}\ ,\ '$	Differentiation with respect to time; with respect to x.

7. THE STEADY-STATE RESPONSE OF FORCED HILL'S EQUATIONS

7A: INTRODUCTION

The investigation presented in Chapter 2 raised two cases which were governed by effectively linear second order differential equations with periodic coefficients: the flexible coupler with end-load varying to a significant degree by comparison with the critical end-load, and the flexible drive system driving a mechanism with varying effective inertia. The latter in particular was thought likely to be of practical significance in some cases, particularly in combination with non-rigid links.

It appears that the majority of studies of such "Hill's equations" (including the special case of Matthieu's equation) have concentrated on stability and thus on the homogeneous form of the equation. In practice, it is quite possible that the inhomogeneous 'forcing' term may give rise to serious vibrations even if the system is stable. It is therefore desirable to establish as generally as possible the nature of the steady state response of an inhomogeneous Hill's equation, whose parameters have values appropriate for the two applications referred to above.

In this chapter a numerical method for finding the steady-state response will be outlined, and results relevant to each application will be presented and analysed in turn.

7B: METHOD

The most general form of Hill's equation can be written as

$$(d^2y/dx^2) + H(x)\,(dy/dx) + \Omega^2 Q(x)\,y = \Omega^2 P(x) \qquad \cdot a$$

where H, Q and P are periodic functions of x with period 2π, and $\int_0^{2\pi} Q(x)\,dx = 1$. The state of the system at any value of x can be defined by a state vector $\underline{y}$ with elements $(y,\ dy/dx)$. The system can be shown to have the following properties:-

- Since the system is linear and periodic, the value of $\underline{y}$ at $x = 2\pi$ is related to the value at $x = 0$ by the linear equation

$$\underline{y}_{2\pi} = \underline{\underline{T}}\,\underline{y}_0 + \underline{t} \qquad \cdot b$$

  where the transfer matrix $\underline{\underline{T}}$ is determined by the homogeneous part of the equation alone and $\underline{t}$ arises from the forced transient with null initial conditions. The elements of $\underline{\underline{T}}$ and $\underline{t}$ may be determined from numerical integrations over one cycle from each of three independent initial states.

- The system is stable if ~~(1 + determinant ($\underline{\underline{T}}$)) is greater than the absolute magnitude of trace ($\underline{\underline{T}}$).~~ the absolute magnitudes of the eigenvalues of ($\underline{\underline{T}}$) are both less than unity. $\cdot c$

- If in a stable case $\underline{y}_{2\pi} = \underline{y}_0$, the solution is periodic, and therefore constitutes a steady-state solution. The latter condition suffices to determine $\underline{y}_{0s}$, the initial state of the dynamic steady state solution:

$$\underline{y}_{0s} = [\underline{\underline{I}} - \underline{\underline{T}}]^{-1}\,\underline{t} \qquad \cdot d$$

  where $\underline{\underline{I}}$ is the unit matrix. Thus by numerical integration over one cycle from this initial state, the complete steady state solution can be found.

- If the periodic function $P(x)$ is expressed as a Fourier series, the corresponding steady state solution can be expressed as the sum of the steady state solutions corresponding to each term of the series acting on its own.

The formal proofs of these properties are given in Appendices 10S and 10T. The method for finding the stability and steady initial conditions has been incorporated by the writer in a FORTRAN subroutine SSICS, which is reproduced with Appendix 10S.

This routine has been utilised in two related programs, to suit the two applications. In each case the time-varying terms are first evaluated at regular intervals through the cycle, and stored. Then the steady state initial

conditions are found by the subroutine SSICS, using a Runge-Kutta fourth-order algorithm. Finally the Hill's equation is integrated from these initial conditions and relevant aspects of the response are determined.

7C: APPLICATION TO FLEXIBLE DRIVE - GENERAL STUDY

Previous work: MAYER-ZUR-CAPELLAN studied the behaviour of rigid-linked four-bar mechanisms with a flexible shaft at the input and/or output, using an analogue computer as well as an approximate numerical method for comparison. For the former method the periodic functions were approximately synthesized from their principal harmonics. If the problem of predicting damping levels is discounted, the results were well supported by experimental measurements. The results presented for input/output flexibility apply to a different model from that used for studying output-only flexibility, so the effect of the flexible input shaft on the output vibrations cannot be distinguished.

Since Mayer-zur-Capellan's work the topic seems to have received little attention, but recently WIEDERRICH studied a scotch-yoke mechanism with flexible drive, utilising an approximate (two harmonic) analytic technique related to Hill's original 'infinite determinant' method. Results of numerical integrations were also given for comparison, with the "transient" supposedly eliminated by taking the sixth cycle of the response. However, since damping is not included, the complementary function cannot decay, so the latter results cannot be taken as reliable.

TAMURA reported on an incomplete investigation into this class of problem, conducted at Newcastle, with the emphasis on efficient techniques for digital computation. He obtained the steady-state solution by adjusting the starting conditions to obtain periodicity.

Choice of technique: Although analogue computers can provide rapid solutions to Hill's equation problems, they cannot be satisfactorily integrated into a package of programs covering other aspects of mechanism behaviour; therefore digital techniques will be used here. The infinite determinant method involves rather complicated manipulations and it is not obvious where the determinant should be truncated in cases where the periodic terms have several significant harmonic components, particularly when the high-frequency content of the response is of interest. By contrast, a method based on numerical integration can exploit available subroutines for all the more complex steps, and the accuracy can easily be increased or checked by reducing the step-size of the integration stage. An appropriate variant of the latter method will therefore be employed, as outlined in the previous section. It is of interest both to identify the resonant conditions and to establish whether the peaks are likely to be significant, with particular regard to the frequency content.

Specialised form of equation: The approximate (linearised) governing equation for a rigid linkage driven by a flexible drive system was derived in Chapter 2 (42.b) as follows:-

$$\ddot{\theta} + [(\dot{J}_\phi + F)/J_\phi]\dot{\theta} + [(S + \tfrac{1}{2}\ddot{J}_\phi)/J_\phi]\theta = -\tfrac{1}{2}[\dot{J}_\phi/J_\phi]\dot{\phi} \qquad \cdot a$$

(This agrees with the equations derived by the authors cited.) It is seen that in this application the periodic coefficients and the forcing term are each dependent on the variation of the effective inertia J_ϕ with the crank angle ϕ. In this section it will be assumed that it takes the form:

$$J_\phi = J_o[g(2\phi)] = J_o[1 + f\sin 2\phi]. \qquad \cdot b$$

Since the effective inertia for a simple mechanism with oscillating components (e.g. crank-slider or crank-rocker, but not crank-follower) typically reaches a maximum twice per cycle, this function provides a first approximation to the actual variation for many mechanisms of that class: indeed, in the case of a scotch yoke mechanism it holds true precisely. A more exact study of a mechanism with a multi-harmonic variation of J_ϕ will be reported in the following section.

To simplify the equation that results from the relationship assumed above, 2ϕ is written as x (which becomes the independent variable), 2θ as y, $(S/4J_o\dot{\phi}^2)$ as D^2, and $\xi(SJ_o)^{-\frac{1}{2}}$ as C. Then we obtain

$$d^2y/dx^2 + [(g'(x) + CD)\,dy/dx + (D^2 + \tfrac{1}{2}g''(x))y]/g(x) = -\tfrac{1}{2}g'(x)/g(x) \qquad \cdot c$$

where $g'(x) = f\cos x$ and $g''(x) = -f\sin x$. Comparison with equation A30 ·a then shows that C corresponds to $2c(1-f^2)^{\frac{1}{2}}$.

Mean frequency ratio: In the form (·a), the coefficient of θ is $(S + \tfrac{1}{2}\ddot{J}_\phi)/J_\phi$. The square root of this may be written as $\dot{\phi}\Omega_i$, where Ω_i is termed the instantaneous frequency ratio; then the mean value of Ω_i over $\phi = 0$ to 2π will be termed the mean frequency ratio, written $\bar{\Omega}$. The hypothesis will be advanced that, to an adequate approximation, unstable speed bands (if any) will be centred on integral or half-integral values of $\bar{\Omega}$, and resonant speeds will correspond to integral values of $\bar{\Omega}$. (Since the complementary solutions associated with half-integral values oscillate with period 4π in ϕ, they should not interact with the forcing term, and therefore should not give rise to resonance). In the non-dimensional form (·c), Ω_i becomes $2D[(1 + \tfrac{1}{2}g''(x)/D^2)/g(x)]^{\frac{1}{2}}$. As the term involving $g''(x)$ is normally relatively small, D may be obtained for a specified $\bar{\Omega}$ by iterating

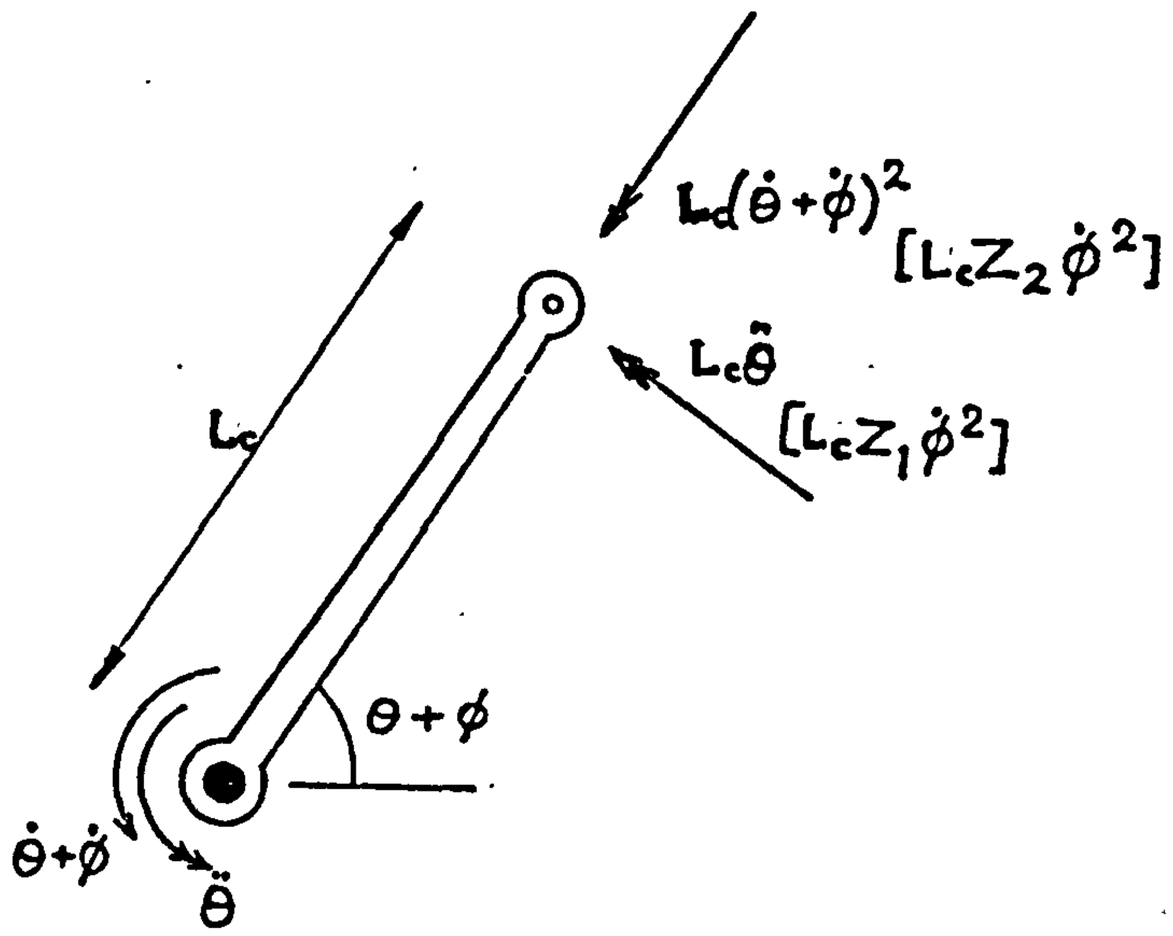

137·a: Coefficients of components of acceleration at end of crank

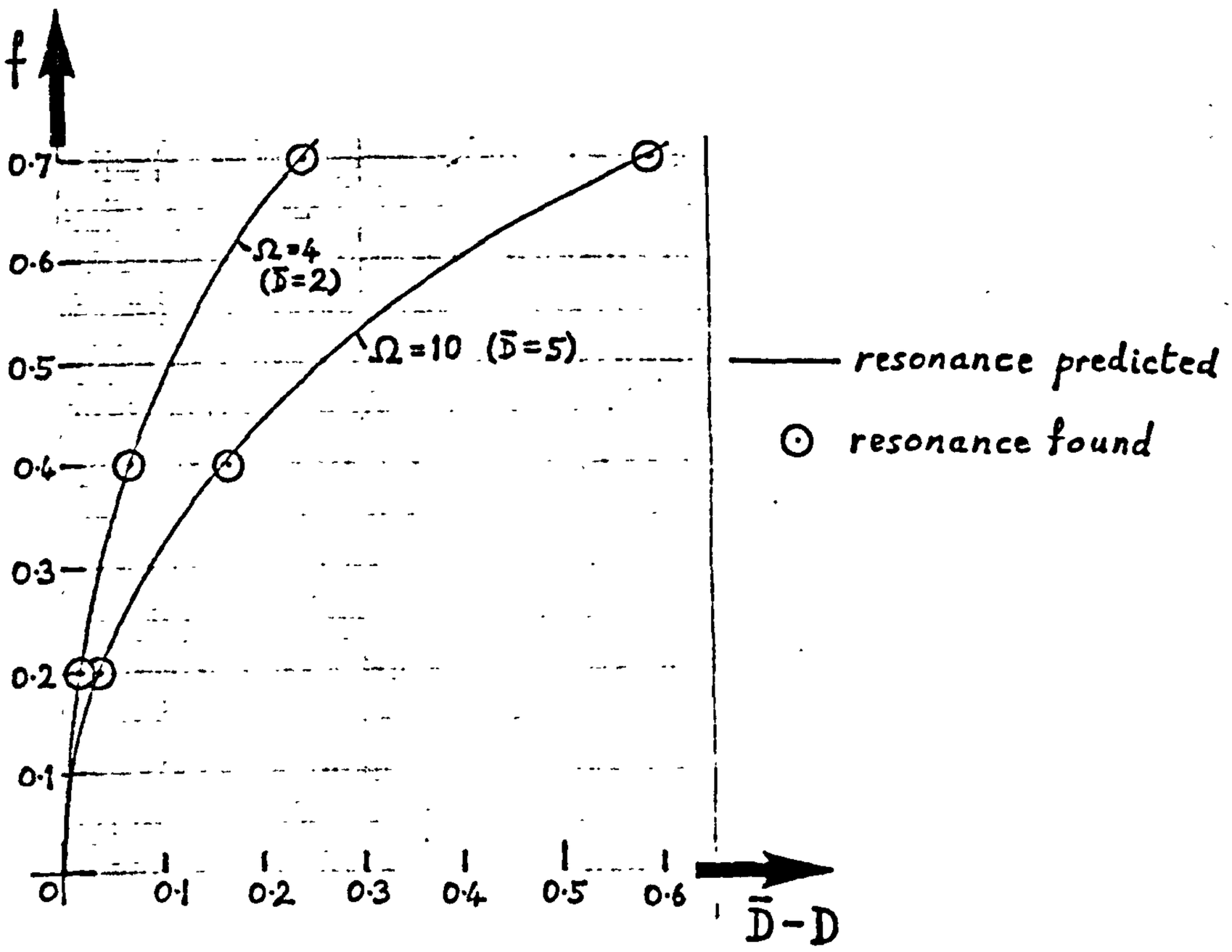

137·b: Test of critical speed approximation

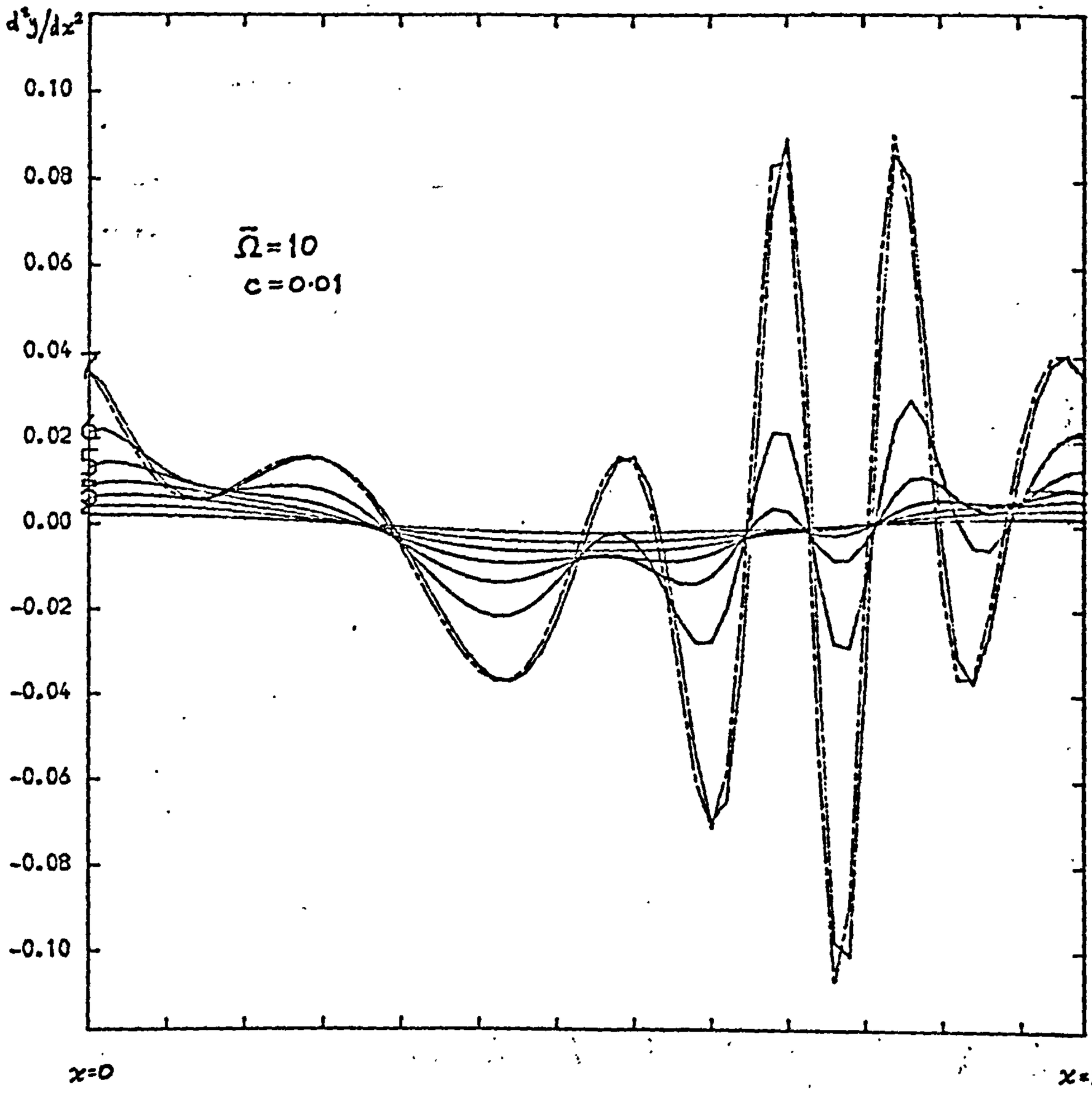

138·a: Steady-state variation of d^2y/dx^2 with x ('Scotch yoke' case)

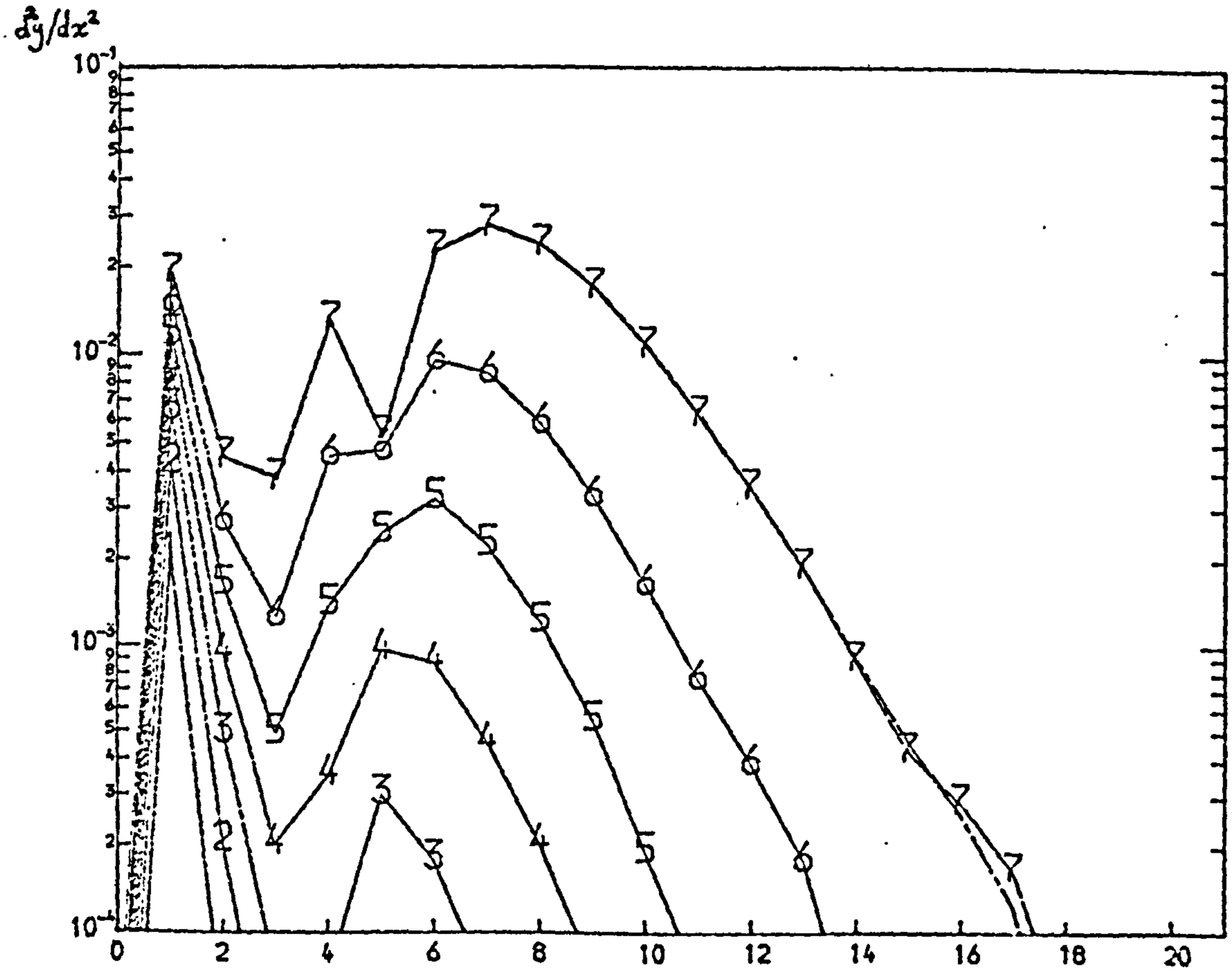

138·b: Harmonic composition of curves in 138·a

$$D = \bar{D} / \text{Mean}\left[(1 + \tfrac{1}{2} g''(x)/D^2)/g(x)\right]^{1/2} \qquad \cdot c$$

where $\bar{D} = \bar{\Omega}/2$ and D is initially set to equal $\bar{D}$. Since the assumed form of J_ϕ has no terms of odd order, only integral and half-integral values of $\bar{D}$ are of interest.

Basis for evaluation of amplitudes: According to GOODMAN's* analysis the instantaneous acceleration at any point in a rigid crank-driven linkage is a linear function both of the crank acceleration and of the square of the crank speed. The same must apply to the inertial loads and reactions generated. Since $\dot{\phi}$ is assumed to be constant, the two factors may be expressed in dimensionless form as $Z_1 \equiv [\ddot{\theta}/\dot{\phi}^2]$ and $Z_2 \equiv [1 + 2(\dot{\theta}/\dot{\phi}) + (\ddot{\theta}/\dot{\phi})^2]$: then if R is some rigid-body inertial load we can write $R = b_1 Z_1 + b_2 Z_2$. The coefficients b_1 and b_2 will vary with ϕ in a manner that depends on the mechanism and load in question, but in general may be assumed to be of equal orders of magnitude. (Consider for example the acceleration at the end of the crank, Figure $\cdot a$). $\cdot d$

If the drive system is rigid, $Z_1 = 0$ and $Z_2 = 1$, so the relative significance of vibrations in a non-rigid drive system may be measured by the magnitudes of Z_1 and $(Z_2 - 1)$ compared to unity. In terms of the normalised variables, we therefore seek the magnitudes of $[2\, d^2y/dx^2]$ and $[2\, dy/dx + (dy/dx)^2]$, and more particularly the harmonic composition of each. The maximum value of y is also of interest since the theory assumes that $\theta \ll 2\pi$, that is $y \ll 4\pi$.

Program details: The program written for this application typically takes $\bar{D}$, f and C as data items, determines D, finds the steady-state response $y(x)$ with the aid of routine SSICS, prints out the peak value of y and records the variation over the cycle of either (d^2y/dx^2), or $(dy/dx + \tfrac{1}{2}(dy/dx)^2)$ as desired. Fast Fourier Transforms are then performed on the recorded values, the results being both tabulated and plotted on logarithmic scales. One variant of this program constitutes Annexe 5 to this thesis.

Results, stability and resonance: Figure $\cdot b$ (full lines) shows the variation of $(\bar{D} - D)$ with f as determined by a single iteration of equation $\cdot c$, for $\bar{\Omega} = 4$, 10 respectively. The nearest resonant values for $f = .2$, $.4$, $.7$ are shown by circles. These values are established by the iterative use of

*: GOODMAN, T.P: "An Indirect Method of Determining Accelerations in Complex Mechanisms", ASME Paper 57-A-108 (Dec. 1957).

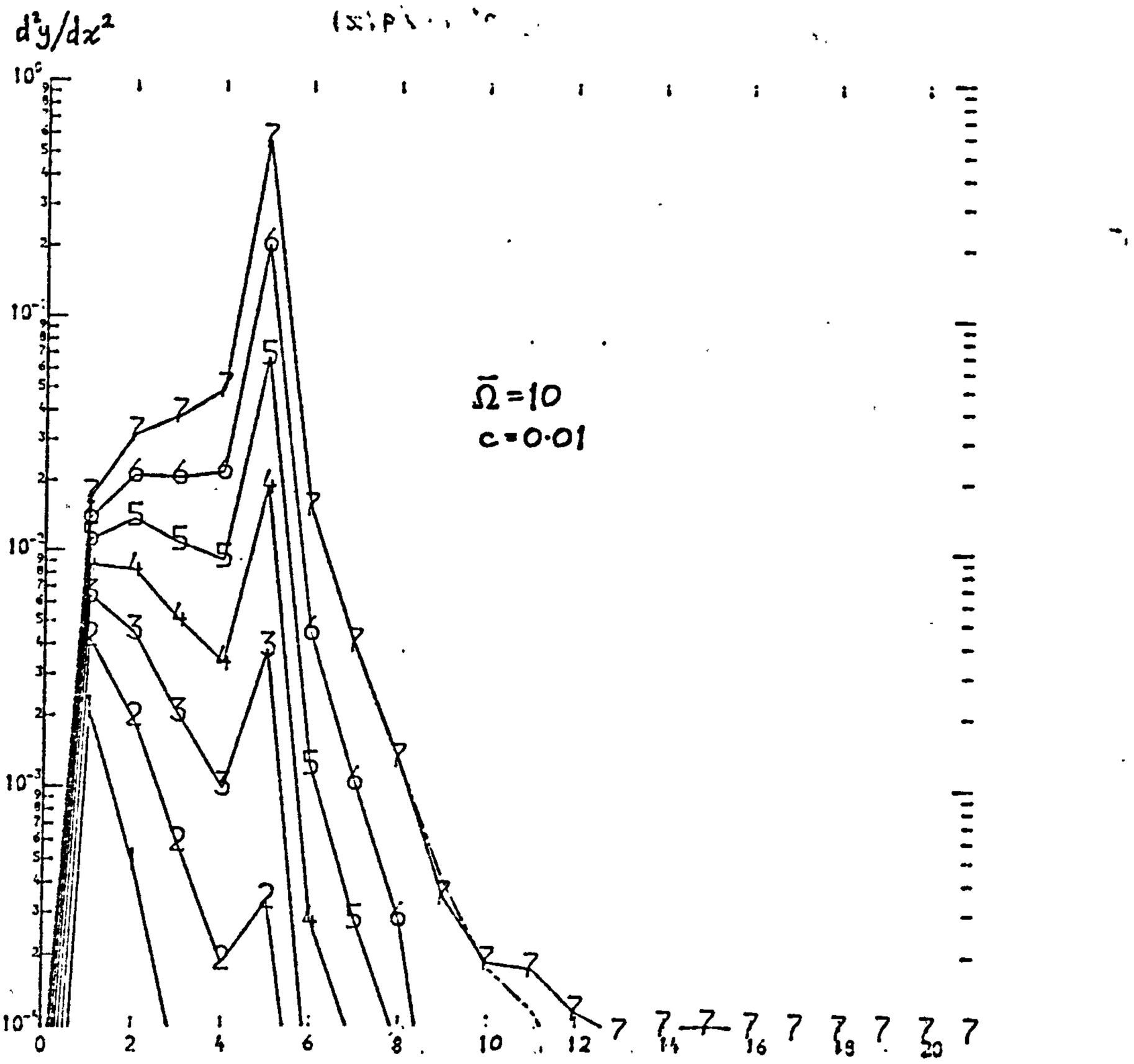

139.a: Harmonic composition of d^2y/dx^2 without parametric variation

function was used but the frequency variation was eliminated: that is to say the equation solved was

$$d^2y/dx^2 + CD\,dy/dx + D^2y = -\tfrac{1}{2}g'(x)/g(x) \qquad \text{.b}$$

It can be seen that although the resonant harmonic is amplified far more in the constant frequency case, the much broader spectrum of the response in the variable frequency case has the effect that from the 6'th harmonic (12 x crank speed) upwards it is increasingly the latter case that shows the greater amplitude.

Significance threshold: Suppose, for example, that the linkage contains a flexible link whose natural frequency is 20 x crank speed. If $f = 0.7$, Figure (138·a) shows that the corresponding (10th) harmonic of Z_1 is of magnitude about 2 x 0.011. This suggests that the flexible link experiences an excitation whose resonant component is between one and two orders of magnitude smaller than the low frequency component. Taking into account the dynamic magnification in the flexible link, this could lead to a dynamic error of the same order as the quasi-static deflection. Such a result is certainly not obtained if the frequency variation in the drive system is neglected, since then, as can be seen in Figure 139·a, the 10th harmonic of Z_1 is only about 2 x 0.0002 for $f = 0.7$.

There is an apparent inconsistency in the argument as presented above, since the linkage was assumed to be rigid in deriving Figs. 138·a--b, 139·a, but flexible in evaluating them. The argument should more properly be understood as follows. If there were not significant vibrations in the flexible link, it could be treated as rigid when analysing shaft vibrations. Such an analysis leads to the prediction of conditions at the link inconsistent with the lack of significant vibrations: thus a reductio ad absurdum has been achieved, and it follows that significant vibrations of the link may be expected, although a more complete simulation involving coupled equations would be necessary to predict their magnitude in a quantitative sense for a particular application.

According to this reasoning, it may be concluded that further analysis is warranted if a harmonic of (d^2y/dx^2) or $(dy/dx + \tfrac{1}{2}(dy/dx)^2)$ close to a resonant frequency of the driven linkage exceeds about 0.001, or if any harmonic of either term exceeds about 0.05.

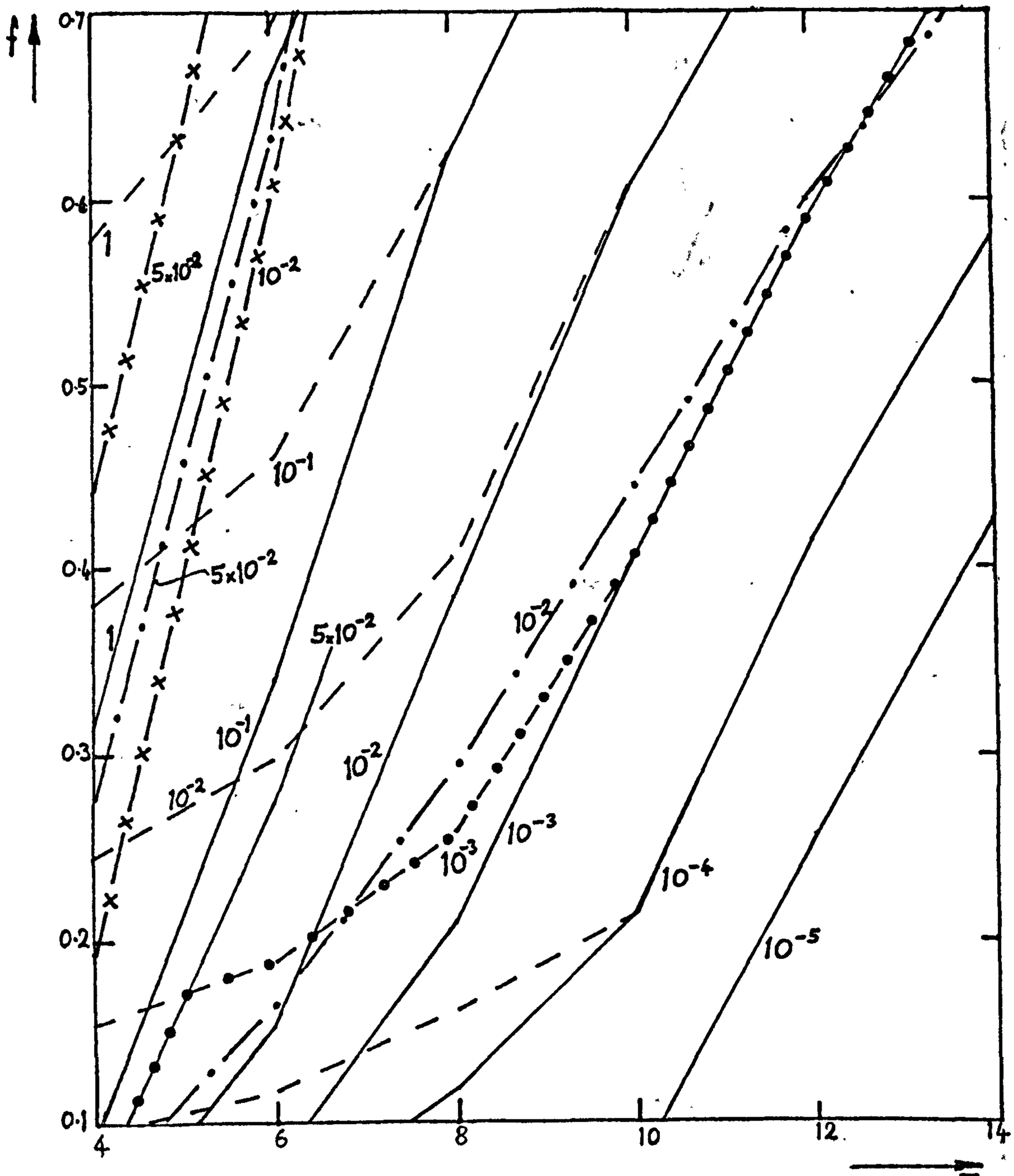

140·a: Contours of comparable vibration in $(\bar{\Omega}, f)$ space

CRITERION:-
- ——— MOST MAGNIFIED HARMONIC OF y''
- — ·— MOST MAGNIFIED HARMONIC OF y'' EXCLUDING HARMONICS BELOW 10× CRANK SPEED
- ·—·—· FUNDAMENTAL OF y''
- ● ● ● 'SIGNIFICANT' VIBRATION THRESHOLD
- —x—x PEAK VALUE OF $y/4\pi$

Results for $\bar{\Omega}$ = 4 through 16: It was argued in Section 2C that although frequency ratios below 10 were unlikely to be of practical interest for flexible links, the same considerations did not apply to flexible shafts. Accordingly lower frequencies should be considered, so the program was run with $\bar{D}$ given integral values of 2 through 8, corresponding to $\bar{\Omega}$ = 4 through 16, keeping ~~$\zeta = 0.01$~~ $\zeta = 0.02$. With this level of damping, stable solutions were found in every case. For $\bar{D} > 5$, 512 steps per cycle were found to be necessary.

A concise presentation of some of the information from these runs of the program may be seen in the form of Figure ·a, which is a contour map in ($\bar{\Omega}$, f) space, constructed by interpolation from the tabulated results. Full lines connect equal values of the most magnified harmonic of d^2y/dx^2. Since it is assumed that all the links vibrate at frequencies no less than (10 x crank speed), however, it seems more appropriate to consider the largest harmonic excluding harmonics below that frequency. The effect is to replace the full lines by the broken lines in the lower left portion of the figure. Thus if (as suggested above) a value of 0.001 is taken to be the threshold of significance for the potentially resonant frequency range, and 0.05 below that range, "significant" crank vibration is indicated for values above and to the left of the line marked with dots (•••) in the figure. In the region below and to the right of this line, that is where $[d^2y/dx^2]$ was below the threshold, the values calculated for $[dy/dx + \frac{1}{2}(dy/dx)^2]$ were also below the threshold.

The chain lines in the same figure show the value of the first harmonic (fundamental) of d^2y/dx^2, which would also be taken as significant if it exceeded 0.05. It is seen that this threshold is less critical than that already considered. The 'cross chain' lines (-x—x—x-) in the figure are contours showing equal values of $(y_{max}/4\pi)$. It can be seen that the assumption made, that $y_{max} << 4\pi$, is fully justified for the region of interest.

Effect of damping level: For $\bar{\Omega}$ = 8, the program was rerun with ζ reduced to ~~0.01~~ 0.005 (ie ~~$\zeta = 0.01$~~ $\zeta \approx 0.005$). As might be expected, the effect was to increase the fourth harmonic of d^2y/dx^2 by a factor of very nearly 2. The amplitudes of the higher harmonics were increased by virtually the same factor, those of the second and third harmonics were increased to a lesser extent (increasing with f), while the amplitude of the first harmonic was virtually unchanged.

Non-harmonic inertia variation: In practice, the periodic variation of J_ϕ with ϕ will not in general be of the simple harmonic form given by 136·b. The effects of significant higher harmonics in the variation are complex, since as well as the forcing term, the parametric excitation is modified, and the latter has a very non-linear influence on the response. Qualitatively, it can be argued that just as the introduction of a single harmonic in $g(x)$ enriches the harmonic content of the system by comparison with the constant frequency case, so the presence of significant higher harmonics is likely to enrich it further, so that the 'threshold' of significant vibration is more likely to be breached.

Thus Figure 140·a is non-conservative for other forms of $g(x)$, and is therefore not suitable in its own right as a design tool. Its utility, rather, is to help to define an area in which further research is needed. This will be illustrated in the next section.

7D: APPLICATION TO FLEXIBLE DRIVE - CASE STUDY

The method illustrated in the previous section will now be applied to a particular mechanism, namely a crank-rocker mechanism, for which the precise variation of J_ϕ with ϕ is not a simple function, although the harmonic variation (136·b) is valid as a first approximation.

Determination of J_ϕ : A separate program was written to determine the variation of J_ϕ and J'_ϕ with ϕ for this class of mechanism. This proceeds in three stages at each value of ϕ, for 1024 points in the cycle. Firstly the linear and angular displacements, velocities and accelerations of the reference axes are calculated for the coupler and rocker, using an existing kinematic analysis subroutine with $\dot{\phi}$ set to 1 radian/unit time and $\ddot{\phi}$ set to zero. Secondly, these values are all referred to axes through the centre of mass for each link, again utilising an existing subroutine. Thirdly, $J_{cr}(\phi)$ and $J'_{cr}(\phi)$ are found from

$$J_{cr}(\phi) = \Sigma_r^{(cr)} [M_r \dot{X}_r^2 + M_r \dot{Y}_r^2 + J_r \dot{\lambda}_r^2] \qquad \cdot a$$

$$J'_{cr}(\phi) = \Sigma_r^{(cr)} [M_r \dot{X}_r \ddot{X}_r + M_r \dot{Y}_r \ddot{Y}_r + J_r \dot{\lambda}_r \ddot{\lambda}_r] \qquad \cdot b$$

and written to file. Here M_r, J_r are the mass and moment of inertia about the centre of mass of link 'r'; X_r, Y_r λ_r are as shown in Figure 74.b, and (cr) indicates that the sum is taken over the coupler and rocker only.

The values $J_{cr}(\phi)$ may be expressed as $\bar{J}_{cr} + \check{J}_{cr}(\phi)$, where $\bar{J}_{cr}$ is the mean value over the cycle and $\check{J}_{cr}(\phi)$ the variation from the mean. Then the total effective inertia including a drive link of inertia J_d may be expressed as

$$J_\phi = (J_d + \bar{J}_{cr})(1 + f^* \check{J}_{cr}(\phi) / \bar{J}_{cr}) \qquad \cdot c$$

for $f^* \equiv \bar{J}_{cr} / (J_d + \bar{J}_{cr})$. Also, $J'_\phi \equiv J'_{cr}(\phi)$. $\cdot d$

Standardisation of equation: In this case ϕ is written as x, θ as y, $\frac{1}{2} S^{-\frac{1}{2}} (J_d + \bar{J}_{cr})^{-\frac{1}{2}}$ as C which is again ~~equivalent~~ approximately equal to $2c$, $S\dot{\phi}^{-2}(J_d + \bar{J}_{cr})^{-1}$ as D^2 and $[1 + f^* \check{J}_{cr}(\phi)/\bar{J}_{cr}]$ as $g(x)$; then $[f^* J'_\phi / \bar{J}_{cr}] \equiv g'(x)$, $[f^* J''_\phi / \bar{J}_{cr}] \equiv g''(x)$. Equation 136·a then reduces to the form (136·c) that suits the program already described.

ITEM	LENGTH (m)	MASS* (kg)	MOMENT OF INERTIA ABOUT (1) C/MASS* (2) GROUND PIVOT ($kg-m^2$)	RIGIDITY: (1) EI or (2) GJ_2 ($N-m^2$)
Drive shaft	0·13	(steel bar, 0.01 diameter)		(2) 77.
Frame link	0.25	-	-	-
Crank	0.05	-	(2) 0.00011	(1) 1400. (steel strip, 0.01×0.02)
Coupler	0.20	0.332	(1) 0.00128	
Rocker	0.275	0.474	(1) 0.00405	
O/put compnt⊖	-	-	(2) 0.02	-

Mean effective inertia of complete linkage found to be 0.00158 $kg-m^2$.

Crank speed = 600 revs/minute, ie $\dot{\phi} = 62.8$ rad/sec

Thus $D^2 = 77. / (0.13 \times 0.00158 \times 62.8^2) = 9.74^2$

$c = 0.01$

Natural frequency of rocker/output system: neglecting distributed mass of rocker, $(1/2\pi)(1400. \times 3/0.275 \times 0.02)^{\frac{1}{2}} = 139$ Hz $\doteq 14 \times$ crank speed.

* Centre of mass of each link located at mid-length

⊖ Output component attached to end of rocker

Table 143·a: Data for example linkage

Program details: Two modifications were made to the program described in the previous section to meet present requirements. Firstly, $g(x)$ and $g'(x)$ are calculated for a given f^* from the values of $J_{cr}(\phi)$ and $J'_{cr}(\phi)$ stored on file as described above; $g''(x)$ is then estimated from the increments in $g'(x)$. Secondly, the 'output' value that is plotted and harmonically analysed is the dimensionless angular acceleration at the rocker, that is $[\ddot{\lambda}_{rocker}/\dot{\phi}^2]$. This is calculated using the kinematic analysis routine referred to above, with $\dot{\phi}$ set to $[1 + dy/dx]$ and $\ddot{\phi}$ to $[d^2y/dx^2]$.

It may be added that any other mechanism could be treated in just the same way.

Mechanism details: Table ·a gives the values assumed for the mechanism parameters. The mechanism is essentially that referred to in the next Chapter (156·a), with the addition of an assumed 0.02 kg-m^2 driven component attached to the rocker and a shaft flexibility chosen to make $\bar{\Omega} = 10$ at 600 revs/minute.

Comparison with simplified case: For comparison with the results in the previous section, an equivalent value of f must be estimated. The calculation of J_ϕ for this mechanism revealed that $J_d + \bar{J}_{cr} = 0.00158$, and the semi-range of $\breve{J}_{cr}(\phi)$ is 0.00075 (unit = kg-m^2). For $0.00158\times(1 + f \sin 2\phi)$ to have that semi-range, $f \doteqdot 0.48$. An alternative estimate can be made in a similar way from the semi-range of $J'_{cr}(\phi)$; this gives $f \doteqdot 0.65$. Consultation of Figure 140·a shows that for $\bar{\Omega} = 10$, the value $f = 0.48$ lies somewhat inside the 'threshold' of significant acceleration at the crank, and $f = 0.65$ lies well inside, so this is a suitable case for further study.

Results: By one iteration of equation 137·c with $\bar{\Omega} = 10$ it was predicted that resonance occurs for $D = 9.738$.† From a series of runs with D near this value it was found that in fact the most magnified (9th) harmonic peaks at $D = 9.732$, and is then only 0.6% higher than at the former value. Thus the mean frequency ratio again proves an excellent predictor of resonance.

Figures(144·a,144·b)respectively show the variation over the cycle and the harmonic composition of the predicted angular acceleration of the rocker, for three conditions of the mechanism. The bold full lines show the effect of using a rigid, constant speed drive as well as rigid links. Consistently with the observations advanced in Section 2D, the frequency spectrum declines very sharply and all harmonics above the sixth are of negligible magnitude.

†: Note, $\bar{D} = \bar{\Omega}$ in this case.

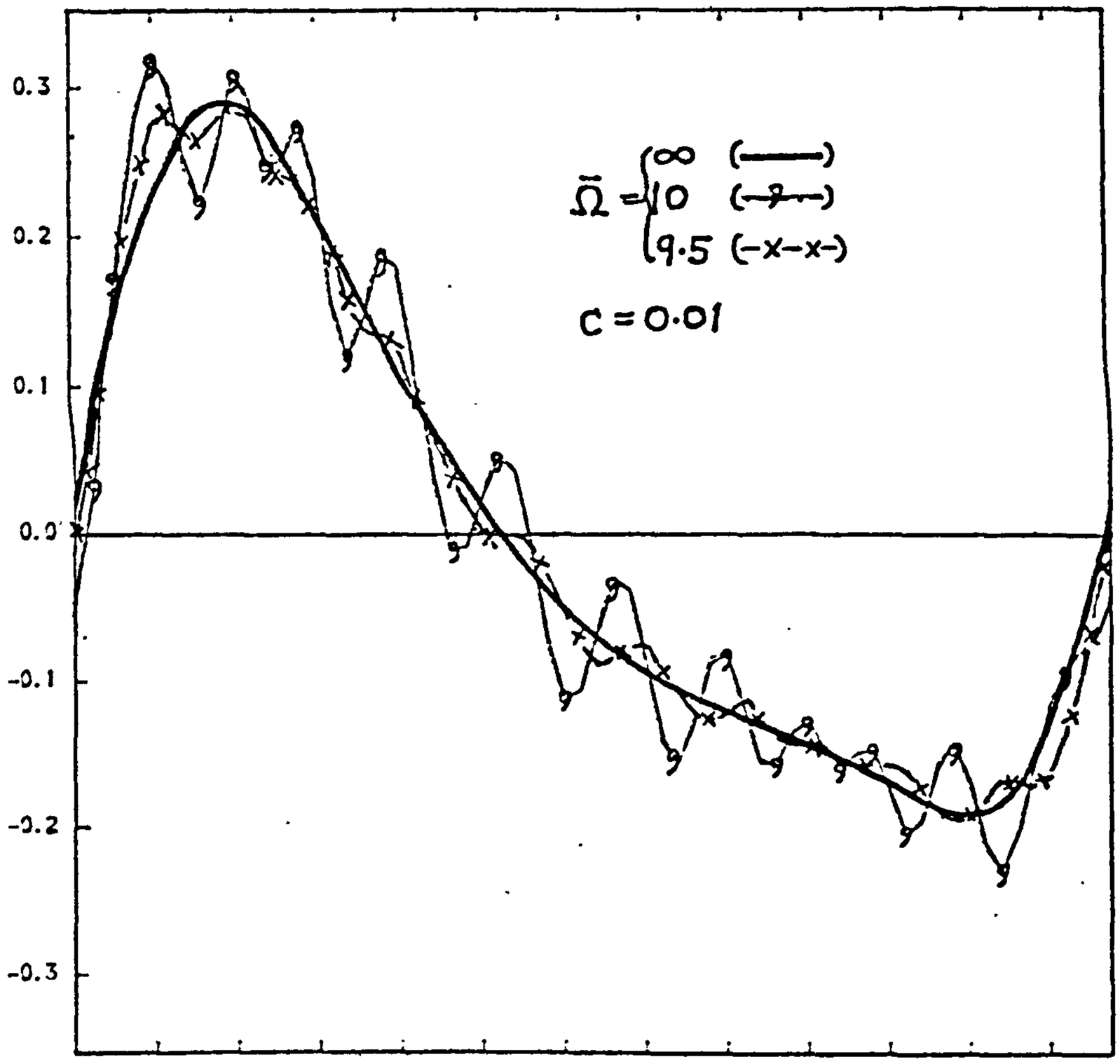

144.a: Steady-state variation of rocker acceleration over a cycle

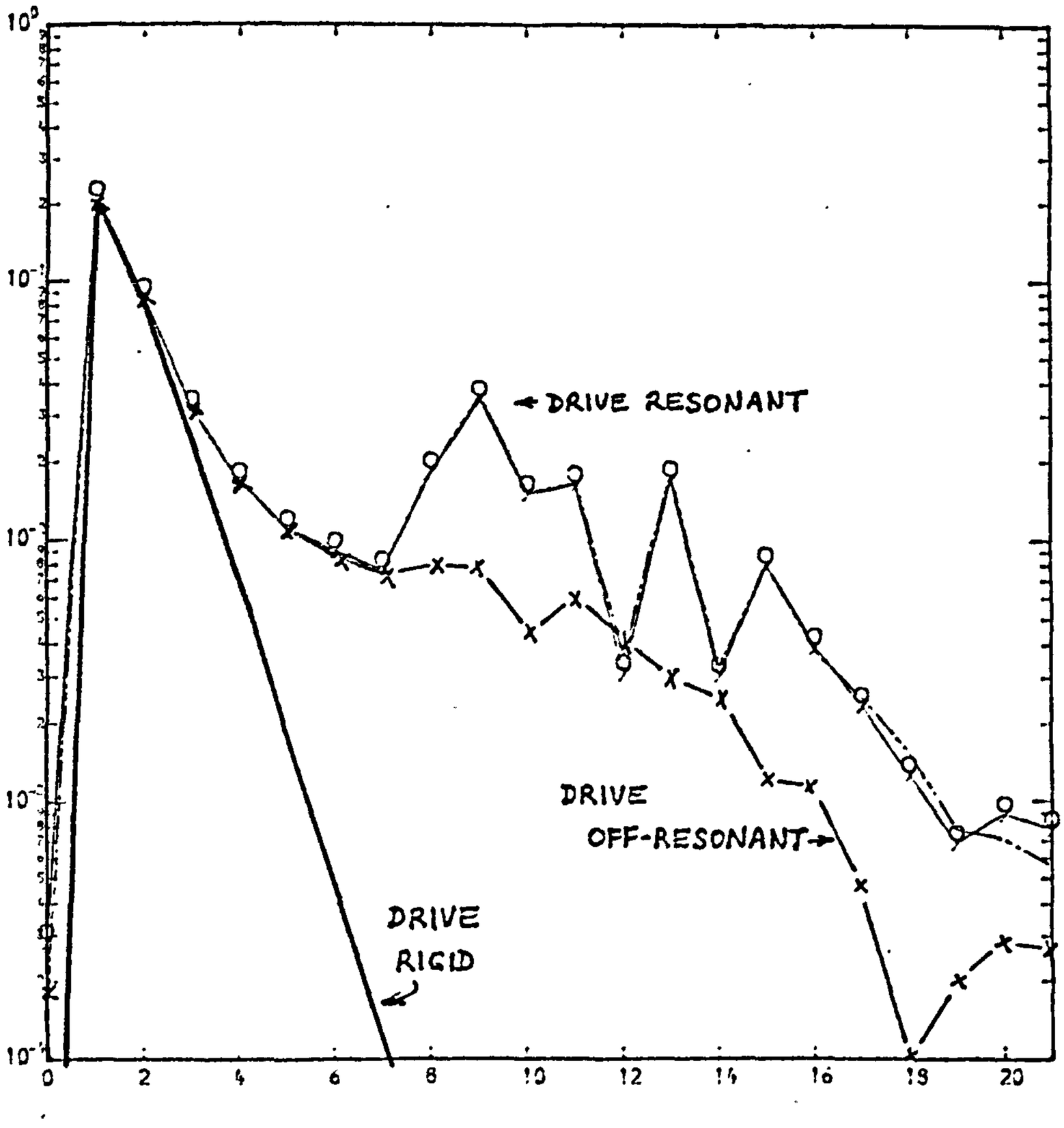

144.b: Harmonic composition of response curves shown in 144.a

The full lines annotated '9' show the effect of the flexible shaft as specified in Table 13.a, using 512 steps in the cycle, and the chain lines likewise using 1024 steps in the cycle. It is seen that the higher harmonics are severely magnified, and coupling with the rocker/output system would be likely in practice to cause vibratory deflections at least as large as the quasi-static deflections at the rocker.

Finally, the cross-chain lines show the effect of doubling the moment of inertia of the driving link, so reducing $\bar{\Omega}$ to 9.5 and also reducing f^* from 0.9 to 0.82. Although the resonance is detuned by this means, and the higher harmonics are thereby reduced by a factor of about four or five, they are seen to be still greatly magnified by comparison with the rigid drive case, so that the deflections of the rocker would probably still be significantly modified.

All cases: $2c = \cdot 02$; 256 steps/cycle.

Case	Parametric variation: $1 + \sum_r (Q_r \sin rx)$ where Q_r is as below:- r=1 2 3 4 5 6 7 8 9 10	Peak error for forcing function: $\cos(nx)$ n= 1	2	3	4	5
a	0.0, 0.0, 0.0.....	·0103	·0417	·0992	·1905	·3335
b	·25, ·05, ·01, ·002, ·0005, 1×10^{-4}, 2×10^{-5}, 5×10^{-6}, 1×10^{-6}, 2×10^{-7}, ...	·0242	·0837	·1985	·3985	·7751
c	·003, ·0015, ·0010, ·00075, ·00060, ·00050, ·00043, ·00038, ·00033, ·00030, ...	·0269	·0601	·1174	·2120	·3621
d	·25, ·05, ·01, ·002, ·00060, ·00050, ·00043, ·00038, ·00033, ·00030, ...	·0346	·0845	·2118	·4045	·7681
Case (b) error − Case (a) error		·0139	·0420	·0993	·2080	·4416
Case (c) error − Case (a) error		·0166	·0184	·0182	·0215	·0286
Case (d) error − Case (b) error		·0104	·0008	·0133	·0060	−·0070

Table 145·a: Dynamic error in coupler link deflection due to varying end-load

7E: APPLICATION TO END-LOADED COUPLER

The only first-order term present in this application is that necessary to model damping. In the absence of an explicit model of the mechanisms of damping involved, it is assumed for simplicity that the damping coefficient varies in the same way as the elastic coefficient: that is, $H(x)$ is assumed to be of the form $2c\Omega Q(x)$ where $2c$ is a data item, 'C'. $Q(x)$ is defined in the data as a finite Fourier series, which is converted to a time-variation by means of an inverse Fast Fourier Transform algorithm. The effect of each harmonic in the forcing function is considered separately. The output of interest is ε_{max}, the maximum dynamic error over the cycle, that is the maximum of $|y - P(x)/Q(x)|$. This was found for four cases.

The cases and results are shown in Table ·a. Case (a) shows the zero end-load dynamic errors as a basis for comparison. In case (b) there is a largely low frequency end-load of up to 26% of the Euler load ($Q_{max} = 1{\cdot}26$). In case (c) there is an impulsive end-load of sufficient magnitude that the tenth harmonic of $Q(x)$ is of amplitude 0.0003 (as considered in Section 2G).

Comparison of case (a) and case (b) shows that the low frequency fluctuation in the end-load causes an approximate doubling of the small dynamic error already present in case (a). Provided that the excitation spectrum shows the typical sharp decline, this error remains negligible, as predicted in Section 2G.

For case (c) the investigation reported in Section 2G predicted a peak dynamic error of $q_j R_{ij}$ where $R_{ij} = 0.0003$ for $j = 10$: that is, the peak error is predicted to be 0.027. This is closely borne out by the numerical results for the response to the first harmonic excitation. For the higher harmonics the error is seen to be less than for case (b), and the combined effect of the impulse and low frequency variation in the end load (case d) is hardly worse than that of the low frequency variation alone.

CHAPTER 8

DEVICE SYNTHESIS

None of the material in this chapter has been published before in this form. Certain of the ideas presented in Section B were presented in a different form in HAINES(d), and the theory described in Section E is described at greater length, and with different examples, in a paper accepted for future publication (HAINES e).

Principal nomenclature for this chapter is given below and overleaf.

Symbols	Meaning
$\underline{A}$	Matrix of linear coefficients relating $\underline{\bar{\xi}}$ to $\underline{\bar{\mu}}$.
$\underline{B}$	Matrix of linear coefficients relating $\underline{\psi}$ to $\underline{\bar{\phi}}$.
$\underline{D}$	Matrix of quadratic coefficients of $\underline{\bar{\mu}}$ in Gaussian objective function.
$\underline{d}; \underline{\bar{d}} (\underline{\bar{d}}^*)$	Vector of desired values: of $\underline{\xi}$; of $\underline{\bar{\xi}}$. ($\underline{\bar{d}} \equiv \underline{P}\,\underline{\bar{d}}$).
E	Stored energy in auxiliary spring.
$\underline{e}; e_i$	Vector of target error magnitudes; element of $\underline{e}$.
$F; F_{xL}, F_{yL}$	Force transmitted to frame by complete linkage; its components.
F_{xi}, F_{yi}	Components of d'Alembert force on link 'i'.
$\underline{f}$	Vector of weighted errors in $\underline{\bar{\xi}}$.
$\underline{G}$	Matrix of coefficients of d'Alembert loads in equilibrium equations.
g	Gravitational acceleration.
$H_t; H'_t$	Linear coefficients relating W_{rs} to q_t: given $\ell_o = 0$; given end locations.
$\underline{H}; H_{tp}$	Matrix of linear coefficients relating $\underline{w}$ to $\underline{q}$; element of $\underline{H}$.
H'_{tk}, H''_{tk}	Linear coefficients relating Fourier components of $\underline{w}$ to q_t ($t = 2$ to 7).
$\underline{H}_t$	Matrix of selected terms from series H'_{tk}, H''_{tk} for $t = 2$ to 6.
$\underline{h}$	Vector of selected terms from series H'_{7k}, H''_{7k}.
$\underline{i}$	Vector with six elements of value unity.
i_1, i_2	Links to which auxiliary spring is attached.
J	Number of joints in linkage.
K_i	Kinetic energy of link 'i'.
k	Proportion of driving torque reacted at motor supports.
$\ell; \ell_o$	Length of auxiliary spring; length in unstressed state (extrapolated).
M, M_L	Total reaction moment at frame in plane of motion.
M_{xi}, M_{yi}, M_{zi}	Component d'Alembert moments on link 'i', about axes through local origi
δm_{hi}	Mass of small element 'h' of link 'i'.
N	Number of moving links in linkage.
$\underline{P}$	Diagonal weighting matrix: i'th diagonal term = e_i^{-1}.
$\underline{\bar{P}}$	Composite diagonal matrix: diagonal terms comprise those of $\underline{P}$ for each point in the cycle.

8. DEVICE SYNTHESIS

8A: AIMS AND SCOPE

It is desirable not only to be able to predict the effects of joint clearance and drive system flexibility, but also to be able to design specifically to avoid or minimise these effects. Since the analyses in previous chapters have shown the effects to be functions of the nominal (rigid link, zero clearance, constant speed) mechanism loads, the design objective can be expressed in terms of suitably modifying these nominal loads.

In accordance with the arguments in Section 1B, the aim of this chapter is to consider how best to use auxiliary devices to modify the nominal dynamic performance of linkages whose geometry and basic structure have already been determined by other considerations. The devices to be considered are firstly, simple counterweights (that is, counterweights integral with existing links) and secondly, springs: these two being the simplest and most widely used devices. The dynamic performance variables to be considered are the joint loads (R); the fluctuating driving load (T), here assumed to be a torque; and the net force (F), in-plane moment (M) and out-of-plane moment (Q) transmitted to the frame.

There are three fairly distinct though interacting problems involved. Firstly, there is the need for efficient and systematic formulations of the relationship between the device parameters and the dynamic performance variables in question (Sections B,D). Secondly, criteria must be established for evaluating performance quality and design practicality. Thirdly, techniques are required for synthesising optimal or improved device parameters in the light of these criteria. The second and third problems will be taken together, specific synthesis techniques being proposed for two classes of problem (Sections C,E). The question of generalising these techniques will be considered in the following chapter.

[Coefficient in equation for:] ↘	ELEMENTS OF $\underline{\Delta}$ [where $C \equiv \cos(\theta)$, $S \equiv \sin(\theta)$]						
$\dot{K}$	$\dot{X}\ddot{X}+\dot{Y}\ddot{Y}$	$(-\dot{X}\dot{\theta}^2+\ddot{Y}\dot{\theta}+\dot{Y}\ddot{\theta})C$ + $(-\ddot{X}\dot{\theta}-\dot{X}\ddot{\theta}-\dot{Y}\dot{\theta}^2)S$	$(-\dot{X}\ddot{\theta}-\ddot{X}\dot{\theta}-\dot{Y}\dot{\theta}^2)C$ + $(-\dot{Y}\ddot{\theta}-\ddot{Y}\dot{\theta}+\dot{X}\dot{\theta}^2)S$	$\dot{\theta}\,\ddot{\theta}$	0	0	0
F_x	$-\ddot{X}$	$\dot{\theta}^2C+\ddot{\theta}S$	$-\theta^2S+\ddot{\theta}C$	0	0	0	0
F_y	$-\ddot{Y}$	$\dot{\theta}^2S-\ddot{\theta}C$	$\dot{\theta}^2C+\ddot{\theta}S$	0	0	0	0
M_z	0	$\ddot{X}S+\ddot{Y}C$	$\ddot{X}C-\ddot{Y}S$	$-\ddot{\theta}$	0	0	0
M_x	0	0	0	0	$\ddot{Y}$	$-\dot{\theta}^2S+\ddot{\theta}C$	$-\dot{\theta}^2C-\ddot{\theta}S$
M_y	0	0	0	0	$-\ddot{X}$	$\dot{\theta}^2C+\ddot{\theta}S$	$-\dot{\theta}^2S+\ddot{\theta}C$
ELEMENTS OF $\underline{\mu}$	$\Sigma[\delta m_i]$	$\Sigma[x_i\delta m_i]$	$\Sigma[y_i\delta m_i]$	$\Sigma[(x_i^2+y_i^2)\delta m_i]$	$\Sigma[z_i\delta m_i]$	$\Sigma[x_iz_i\delta m_i]$	$\Sigma[y_iz_i\delta m_i]$

Table 148.a: Coefficients and constants in dynamic state equation 148.b

The treatment that follows is close to that of Dresig and Schonfeld, but is extended to cover in-plane joint loads and flywheel-controlled drive systems.

The solution: The inertial loads are necessarily obtained in a form that is already linear when the laws of rigid body motion are derived from the superposition of infinitesimal elements.

Thus consider a rigid link "i" in plane motion comprising small elements of mass δm_{hi} at locations (x_{hi}, y_{hi}, z_{hi}) in link-fixed axes with origin o_i and axes $o_i x_i$, $o_i y_i$ in the plane of motion. The position and motion of the link will be characterized by the position (X_i, Y_i, Z_i) of o_i in some global axes $OXYZ$, the anticlockwise inclination θ_i of the x_i axis to the X axis, and the first and second derivatives of these terms. (By convention, o_i will be chosen so that $Z_i = 0$). The dynamic state of the link will be characterized by a column vector $\underline{\phi}_i$ comprising (in this order): the rate of change of its kinetic energy, $\dot{K}_i$; the d'Alembert forces F_{xi} parallel to OX and F_{yi} parallel to OY; and the d'Alembert moments M_{zi}, M_{xi}, M_{yi} about axes through o_i parallel to OZ, OX, OY respectively. Summing these properties for every element, it is found that

$$\underline{\phi}_i = \underline{\Delta}_i \underline{\mu}_i \qquad \cdot b$$

where the elements of $\underline{\Delta}_i$ and $\underline{\mu}_i$ are given in Table $\cdot a$, the subscript 'i' being omitted for simplicity. (Considering equations A5·b, A5·e the derivation of Table $\cdot a$ is elementary and will not be spelt out). If the linkage is in a vertical plane with OY upwards, each term $(\ddot{y})$ in the table may be replaced by $(\ddot{y} + g)$ where g is the gravitational acceleration: then $\underline{\phi}$ represents the resultant of inertial and gravitational effects.

The analysis of a complete linkage requires the application of equation $\cdot b$ to every link, forming a composite equation

$$\bar{\underline{\phi}} = \bar{\underline{\Delta}} \bar{\underline{\mu}} \qquad \cdot c$$

where the overbar indicates a partitioned matrix or column vector whose components are the corresponding link matrices or vectors. The "fundamental inertia vector" $\bar{\underline{\mu}}$ contains all the necessary information about the mass distribution in the linkage. The terms of $\bar{\underline{\mu}}$ will not be recast in terms of the centres of mass in the usual manner, since it is at this stage that the pristine linearity of equation $\cdot c$ is lost.

Overall energy balance and equilibrium: The total kinetic energy of the linkage is given by $K_L = \sum_i K_i$. Neglecting frictional losses, conservation of energy requires that $T\omega = \dot{K}_L$ where ω is the nominally constant shaft speed. Thus $T = (1/\omega)\Sigma\dot{K}_i$

The set of d'Alembert loads recorded in $\bar{\Phi}$ is reacted both at the frame link joints and at the motor supports. The resultant load acting on the foundation can be characterized by a vector Ψ whose elements are:-

the net force terms F_{XL} in the OX direction and F_{YL} in the OY direction;
an in-plane moment $M_L = Q_{ZL} + T_G$, comprising the moment Q_{ZL} transmitted via the frame joints and the moment T_G transmitted via the motor supports;
and out-of-plane moments Q_{XL}, Q_{YL} about axes OX, OY respectively.

For equilibrium of the linkage excluding the drive system, we have:

$$F_{XL} = \sum_i (F_{Xi}) \qquad \cdot a$$

$$F_{YL} = \sum_i (F_{Yi}) \qquad \cdot b$$

$$Q_{ZL} = \sum_i (M_{Zi} + Y_i F_{Xi} - X_i F_{Yi}) + T \qquad \cdot c$$

$$Q_{XL} = \sum_i (M_{Xi}) \qquad \cdot d$$

$$Q_{YL} = \sum_i (M_{Yi}). \qquad \cdot e$$

A factor not considered in the papers cited is that the driving system in practice often incorporates a flywheel, or at least a motor armature or other component with significant flywheel effect. If the presumed near-constant speed of the linkage is mainly attributable to this, rather than to high torque capacity and torque/speed rate of the motor, it follows that the drive system inertia generates a fluctuating inertial torque approximately equal and opposite to T; so that the motor is 'isolated' from the driving torque fluctuations and T_G is largely eliminated, rather than necessarily equal to $-T$ as is usually assumed. It will therefore be assumed here that $T_G = -kT$, where $k = 0$ for a flywheel-regulated system and $k = 1$ for a motor-regulated system. (The $k = 0$ case has recently been treated in another context by WEIDERRICH). For intermediate cases, k cannot be reliably estimated by a purely kinetostatic analysis. (The writer's suggestion elsewhere that intermediate values of k are used - HAINES(d) - is questionable since it does not account for phase changes.) The 'shaking moment' M_L is then given by

$$M_L = \sum_i [M_{Zi} + Y_i F_{Xi} - X_i F_{Yi} + (1-k)\omega^{-1}\dot{K}_i] \qquad \cdot f$$

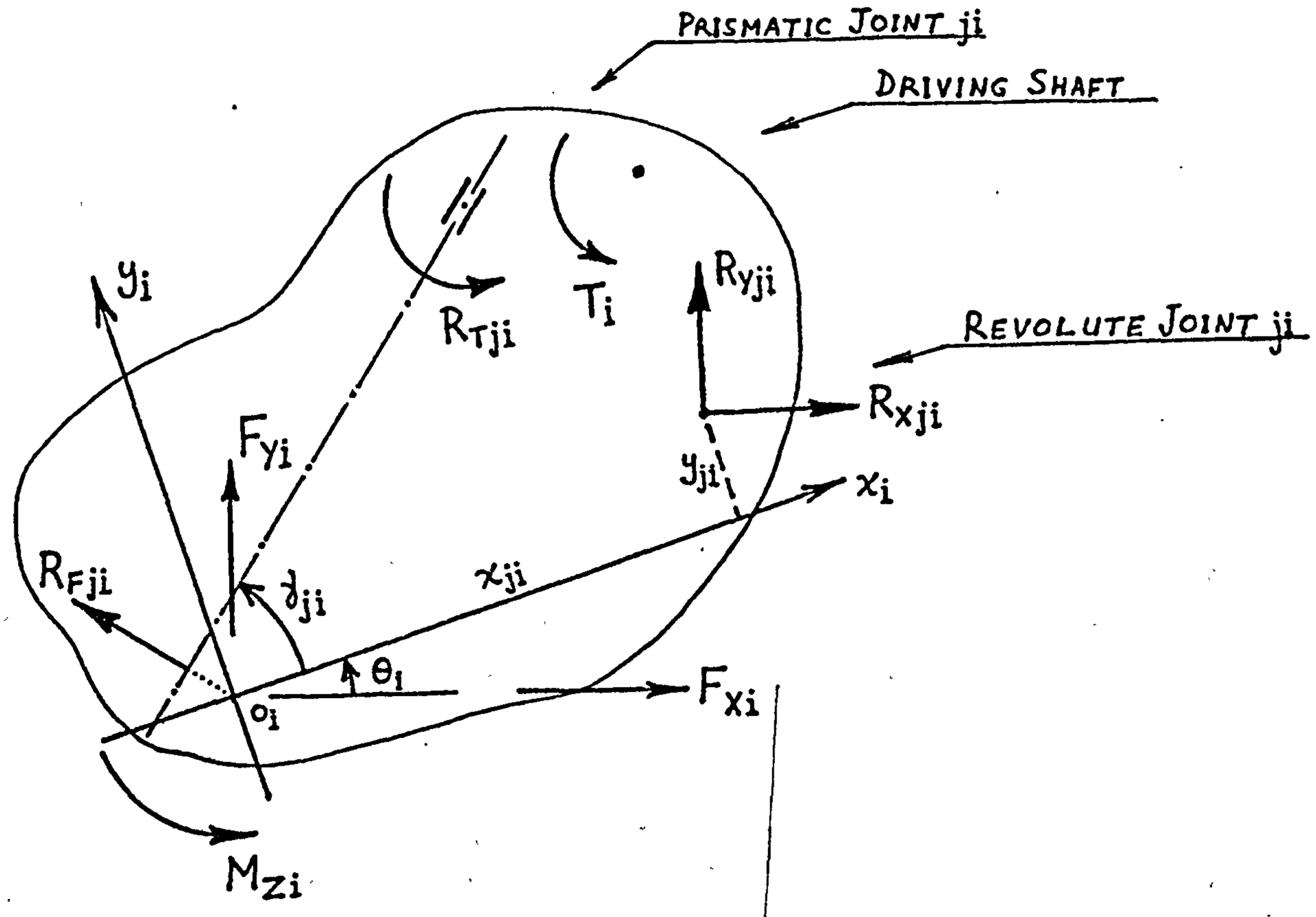

150·a: GENERAL LINK 'i'

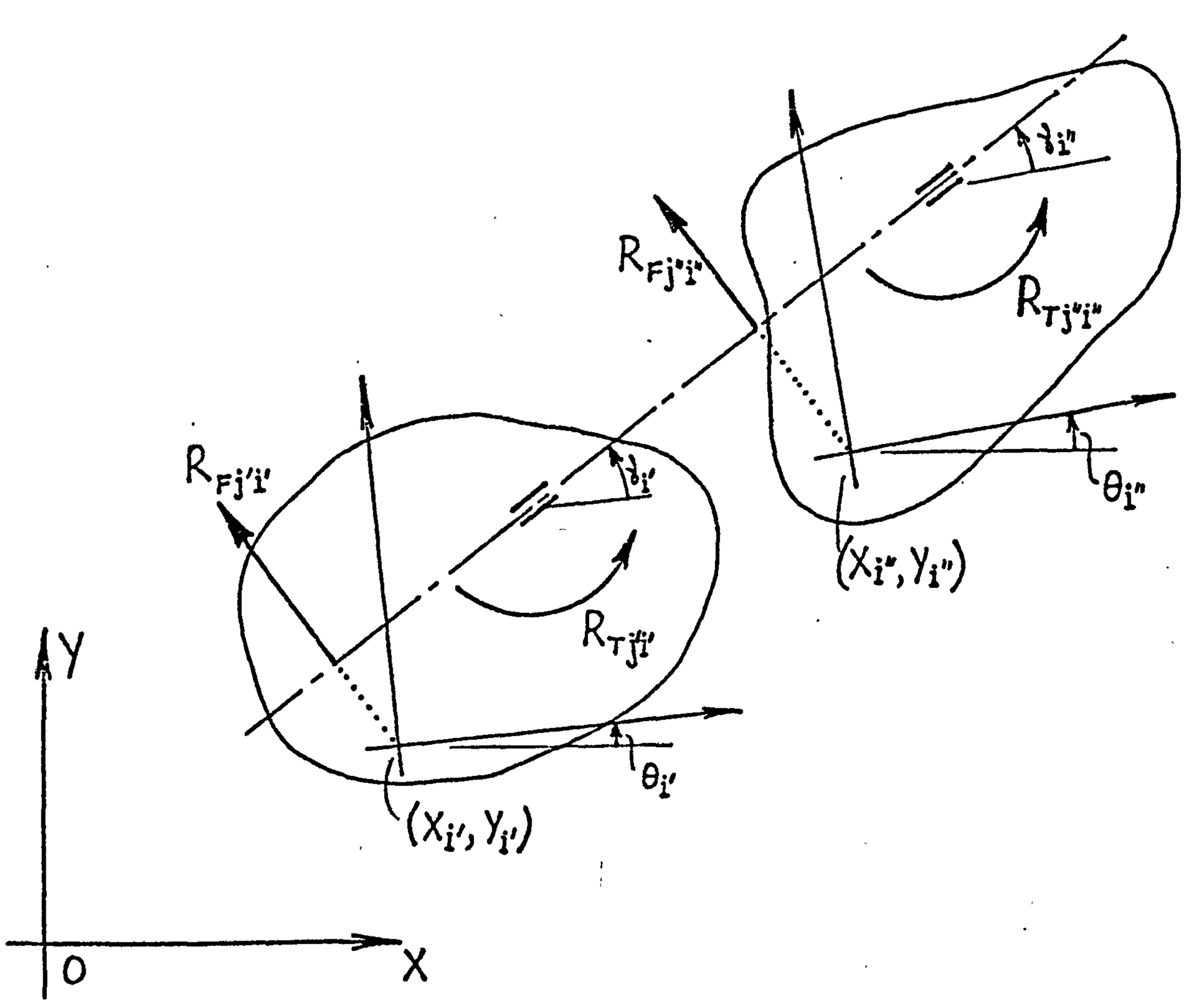

150·b: PRISMATIC JOINT BETWEEN LINKS i' & i"

The set of equations (149.a,b,.d,.e,.f) is linear in the elements of $\underline{\bar{\phi}}$ and can therefore be summarised in the form

$$\underline{\bar{\Psi}} = \underline{B}\,\underline{\bar{\phi}} \quad = \underline{B}\,\underline{\bar{\Delta}}\,\underline{\bar{\mu}}\,. \qquad .c$$

Link equilibrium: Planar linkage mechanisms are typically structurally indeterminate as far as the out-of-plane moments are concerned, so the analysis of joint loads will be confined to in-plane components. Thus let link 'i' have:-

n_{1i} revolute joints at (x_{ji}, y_{ji}), with reaction forces R_{xji}, R_{yji} parallel to OX, OY;

n_{2i} prismatic joints with sliding axes at inclinations γ_{ji} anticlockwise from the x_i axis, with a reaction force R_{Fji} at inclination $(\gamma_{ji} + 90°)$ and reaction torque R_{Tji} about o_i;

and a driving torque $T_i = T$ if the link is a driving link, otherwise $T_i \equiv 0$.

The equations of equilibrium of the d'Alembert and gravitational loads and joint reactions for link 'i' are then, from Figure .a,

$$F_{Xi} + \Sigma_{j=1}^{n_{1i}} (R_{Xji}) - \Sigma_{j=1}^{n_{2i}} (R_{Fji} \sin(\gamma_{ji} + \theta_i)) = 0\,; \qquad .d$$

$$F_{Yi} + \Sigma_{j=1}^{n_{1i}} (R_{Yji}) + \Sigma_{j=1}^{n_{2i}} (R_{Fji} \cos(\gamma_{ji} + \theta_i)) = 0\,; \qquad .e$$

$$M_{Zi} + \Sigma_{j=1}^{n_{1i}} [-(R_{Xji} \cos\theta_{ji} + R_{Yji} \sin\theta_{ji})\, y_{ji} + (R_{Yji} \cos\theta_{ji} - R_{Xji} \sin\theta_{ji})\, x_{ji}]$$
$$+ \Sigma_{j=1}^{n_{2i}} (R_{Tji}) + T_i = 0. \qquad .f$$

Joint equilibrium: Let a joint connecting links i' and i'' be numbered j' in link i' and j'' in link i''. Then equilibrium of the loads acting at this joint is expressed as

$$R_{Xj'i'} + R_{Xj''i''} = 0, \qquad .g$$

$$R_{Yj'i'} + R_{Yj''i''} = 0, \qquad .h$$

for a revolute joint, or (with reference to Figure .b)

$$R_{Fj'i'} + \frac{R_{Fj''i''}}{\cancel{R_{Xj}}} = 0, \qquad \cdot a$$

$$R_{Tj'i'} + R_{Fj'i'}(X_{i'} \cos(\theta_{i'} + \gamma_{j'i'}) + Y_{i'} \sin(\theta_{i'} + \gamma_{j'i'}))$$

$$+ R_{Tj''i''} + R_{Fj''i''}(X_{i''} \cos(\theta_{i''} + \gamma_{j''i''}) + Y_{i''} \sin(\theta_{i''} + \gamma_{j''i''})) = 0, \qquad \cdot b$$

for a prismatic joint.

Matrix solution: It can be seen that the complete set of link and joint equilibrium equations can be expressed by the single matrix equation

$$\underline{\Gamma}\,\underline{\ell} = \underline{G}\,\underline{\dot{\phi}} \qquad \cdot c$$

where $\underline{\ell}$ is a vector comprising all the terms R_{Xji}, R_{Yji}, R_{Fji}, R_{Tji} for every joint j on every link i, together with T. Matrix Γ varies with the crank angle and speed, whereas G is a constant matrix.

The rows of the above equation are in general linearly independent and equal in number to $(3N + 2J)$ where N is the number of moving links and J the number of joints. The number of unknowns is $(4J + 1)$, which is equal to $(3N + 2J)$ since the mechanism has one degree of freedom associated with T. Thus the equation can be solved to give

$$\underline{\ell} = \underline{\bar{\Gamma}}^{-1}\,\underline{G}\,\underline{\dot{\phi}} = \underline{\bar{\Gamma}}^{-1}\,\underline{G}\,\underline{\Delta}\,\underline{\bar{\mu}}. \qquad \cdot d$$

By means of equations 150·c and 151·d, $\underline{\Psi}$ and $\underline{\ell}$ can be determined (for a given crank speed) as linear functions of $\underline{\bar{\mu}}$ at as many crank angles as are desired; that is,

$$\underline{\bar{\Xi}} = \underline{A}\,\underline{\bar{\mu}} \qquad \cdot e$$

where $\underline{\Xi}$ is a composite vector containing all the elements of both $\underline{\Psi}$ and $\underline{\ell}$ and $\underline{\bar{\Xi}}$ contains all the values in $\underline{\Xi}$ at every point of interest in the cycle; $\underline{A}$ is a constant matrix with terms calculated from $\underline{B}\,\underline{\Delta}$ or $\underline{\Gamma}^{-1}\underline{G}\,\underline{\Delta}$ as appropriate, and $\underline{\bar{\mu}}$ is the fundamental inertia vector. This general linear relationship, ·e , is the essential result for the subsequent development.

8C: COUNTERWEIGHT SYNTHESIS

Four-bar linkage example: An important feature of the counterweight synthesis problem is illustrated by the case of a revolute-jointed four-bar linkage whose shaking moment (M_L) is to be optimised by means of addition or redistribution of mass subject to the requirement that the shaking force (F_{XL}, F_{YL}) be fully balanced. BERKOF & LOWEN(b) considered this problem and showed that the formal optimal solution in the absence of constraints on the inertial parameters is worthless, since it implies reducing the links to zero thickness. They therefore proposed finding a partial optimum (by the minimum root mean square criterion) with all the parameters for one link considered as fixed. LOWEN & BERKOF published details of a family of linkages partially optimised in this fashion. CARSON & STEPHENS reported a case study using the same technique in which it was prone to yield unfeasible solutions, and accordingly proposed first changing the dimensions of the "fixed" link. The writer has argued elsewhere (HAINES d) that these two approaches are inappropriate since a solution that is an optimum with respect to only some of the variables has no particular merit unless the unoptimised variables are in fact fixed for practical reasons, or at least close to a practical lower bound.

Constraints: If the unconstrained solution is trivial, it is the constraints that determine the best obtainable solution, and therefore they should be incorporated in the technique in some manner. The exact and full specification of the real constraints in a practical problem would almost certainly be prohibitive in most cases. As a realistic approach to the problem it will be assumed (following WALKER) that the balancing is achieved by adding disc-shaped counterweights, with a positive width subject to a specified maximum, to a link whose inertial parameters are previously established and unaffected.*

Thus any interpenetration of link and disc, or mounting struts for the discs, or necessary stiffening of the basic link is disregarded; in practice such second-order effects could probably be dealt with by a few successive approximations. As a further simplification, out-of-plane effects will be excluded from consideration in the remainder of this section. The restriction to counterweights of disc shape is then reasonable since any other shape can, without exceeding the thickness limit, be replaced by a disc that is dynamically equivalent as regards all in-plane loads.

* Then if the fundamental inertia vector of the original linkage is $\bar{\mu}^o$ and that of the counterweight set is $\bar{\mu}^c$, $\bar{\mu}$ is given by $\bar{\mu} = \bar{\mu}^o + \bar{\mu}^c$.

Matching criterion: A satisfactory match between the desired and achieved variation in the dynamic performance variables may be sought either by forcing an exact match of certain variables at certain points in the cycle, or by minimising the peak error (Chebyshev criterion) or (root) mean square error (Gauss criterion) over a relatively large number of points in the cycle. The first method requires the elimination of linear dependencies between the relevant rows of $\underline{A}$ in equation 15|·e. Although the techniques devised by ELLIOTT appear to be capable of this, their success depends on the order in which the techniques are applied, and an algorithm for the systematic determination of the correct order has yet to be established. Moreover, the constraints suggested above are non-linear in the space defined by the elements of $\underline{\bar{\mu}}^c$, so the incorporation of this essential aspect of the design requirement is no easy task. By contrast, well established techniques are available for constrained numerical minimization, and some of these techniques are <u>not</u> embarrassed by the presence of linear dependencies.

Thus the current state of the art points to the use of a minimum error criterion. This has the further advantage that any number of affected dynamic performance variables may be included in the error calculation.

Weighting factors: If more than one variable is to be taken into account, the relative weights given to the different variables must be specified. A convenient weighting term is the reciprocal of a user-specified target error magnitude. If the ideal value of each term in $\underline{\xi}$ at some point in the cycle is recorded in a vector $\underline{d}$, with target errors $\underline{e}$, then the term to be minimised at this instant is $\underline{P}(\underline{\xi} - \underline{d})$ where $\underline{P}$ is a diagonal weighting matrix with terms $P_{ii} = e_i^{-1}$, or zero if the corresponding term in $\underline{\xi}$ is not be considered.

'Worst error' criterion: Using the Chebyshev criterion, the value of the objective function Ω is the largest element in the vector $\underline{f}$ defined by $\underline{\bar{P}}(\underline{A}\underline{\bar{\mu}} - \underline{\bar{d}})$ where $\underline{\bar{d}}$ is a composite vector containing the ideally desired values $\underline{d}$ at each point of interest in the cycle.* $\underline{\bar{P}}\,\underline{A}$ can be found at the outset as $\underline{A}^*$, and $\underline{\bar{P}}\,\underline{d}$ as $\underline{\bar{d}}^*$. Then the calculation of all the elements of $\underline{f}$, i.e$(\underline{A}^*\underline{\bar{\mu}} - \underline{\bar{d}}^*)$, involves one multiplication for each element in $\underline{A}^*$. For example, suppose the objective involves just F_{xL}, F_{yL}, M_L and T, defined at 36 points in the cycle (every 6^o of crank), and three counterweights are

* $\underline{\bar{P}}$ is defined similarly.

to be optimised, involving 12 terms in $\bar{\mu}$. (The terms $\mu_{i5}, \mu_{i6}, \mu_{i7}$ are of course excluded by the restriction to in-plane effects). Then (4 x 36 x12=) 1728 multiplications are required per objective function evaluation.

Root mean square criterion: For minimization according to the Gauss criterion, the objective function can be taken as the sum of the squares of the weighted errors in every variable of interest at every point of interest in the cycle, that is $\Omega = \underline{f}^T \underline{f}$ where ^{T} indicates the transpose. Expanding and simplifying, this reduces to

$$\left.\begin{aligned} \Omega &= [\bar{\mu}^T \underline{D} - \underline{\sigma}^T]\bar{\mu} + \tau \\ \text{where } \underline{D} &= \underline{A}^T \underline{\bar{P}}^2 \underline{A} = \underline{A}^{*T} \underline{A}^*, \quad \underline{\sigma}^T = 2\,\underline{\bar{d}}^T \underline{\bar{P}}^2 \underline{A} = 2\underline{\bar{d}}^{*T} \underline{A}^*, \quad \tau = \underline{\bar{d}}^T \underline{\bar{P}}^2 \underline{\bar{d}} = \underline{\bar{d}}^{*T} \underline{\bar{d}}^* \end{aligned}\right\} \cdot a$$

If the elements $D_{iji j}$ and σ_{ij} of $\underline{D}$ and $\underline{\sigma}$ are calculated at the outset and stored, only $n_\mu^2 + n_\mu$ multiplications are necessary per objective function evaluation, where n_μ is the number of terms in $\bar{\mu}$; that is, 156 multiplications in the example given above. Thus the Gauss criterion can reduce the calculation time per iteration by an order of magnitude. If joint loads are included in the objective the improvement is still greater, since the sizes of $\underline{D}$ and $\underline{\sigma}$ are unaffected. This has to be set against the large number of multiplications in the initial calculation: 20880 more for the Gauss criterion in the example cited, that is equivalent to 14 iterations.

A further consideration is that the Gauss criterion leads to a continuously differentiable objective function, whereas the Chebyshev criterion leads to a function with discontinuities in the gradient, which pose greater difficulties for the search algorithm.

In view of these observations the Gauss criterion will be adopted for present purposes, while noting that the preference is not conclusive.

Calculation of μ^c from physical dimensions: From the designer's point of view the design variables are the thickness v_{i1}, radius v_{i2}, and cartesian coordinates (v_{i3}, v_{i4}) of the centre of the counterweight, for each link i. These elements may be taken to comprise a vector $\underline{v}_i$ for each link i, or a composite vector $\bar{\underline{v}}$ for the set of moving links. (The densities ν_i may be taken as fixed).

	j = 1	j = 2	j = 3	j = 4
μ^c_{ij}	$\pi \nu_i v_{i1} v_{i2}^2$	$\mu^c_{i1} v_{i3}$	$\mu^c_{i1} v_{i4}$	$\mu^c_{i1} (\frac{1}{2} v_{i2}^2 + v_{i3}^2 + v_{i4}^2)$
$\partial \mu_{ij} / \partial v_{i1}$	μ^c_{i1} / v_{i1}	μ^c_{i2} / v_{i1}	μ^c_{i3} / v_{i1}	μ^c_{i4} / v_{i1}
$\partial \mu_{ij} / \partial v_{i2}$	$2\mu^c_{i1} / v_{i2}$	$2\mu^c_{i2} / v_{i2}$	$2\mu^c_{i3} / v_{i2}$	$2\mu^c_{i4} / v_{i2} + \mu^c_{i1} v_{i2}$
$\partial \mu_{ij} / \partial v_{i3}$	0	μ^c_{i1}	0	$2\mu^c_{i2}$
$\partial \mu_{ij} / \partial v_{i4}$	0	0	μ^c_{i1}	$2\mu^c_{i3}$

155·a: Fundamental inertia parameters of disc counterweight as function of physical parameters, with derivatives

The minimisation problem can be cast in two equivalent ways: as the minimisation in $\underline{\mu}^c$ space of a quadratic function subject to non-linear constraints, and as the minimisation in $\underline{v}$ space of a higher-order function subject to simple bounds. There seems little reason to suppose that either formulation would lead to an easier search. The latter is preferred here as offering rather simpler programming. Thus we require expressions for $\underline{\mu}_i^e$ as a function of $\underline{v}_i$. These are given in Table ·a.

Gradient: For gradient-based optimisation techniques we also need expressions for $\partial\mu_{ij}/\partial v_{ik}$. These are also given in Table ·a. Then the gradient vector may be obtained from

$$\frac{\partial\Omega}{\partial v_{ik}} = \sum_{j=1}^{4}\left[\frac{\partial\Omega}{\partial\mu_{ij}}\ \frac{\partial\mu_{ij}}{\partial v_{ik}}\right] \qquad \cdot b$$

where, from 154·a,

$$\frac{\partial\Omega}{\partial\mu_{ij}} = \sum_{i'=1}^{N}\sum_{j'=1}^{4}\left(D_{iji'j'}\,\mu_{i'j'}\right) + D_{ijij}\,\mu_{ij} - \sigma_{ij} \qquad \cdot c$$

Optimisation algorithm: For the class of problem referred to, the documentation for the National Algorithms Group (NAG) subroutine library recommends the use of a "quasi-Newton" algorithm.* This is a quasi-second-order method using analytically determined first derivatives of the objective function and a positive-definite approximation to the matrix of second derivatives (Hessian matrix). The use of the positive definite approximation to the Hessian makes the-method tolerant of linear dependencies in the true Hessian.

From this information at the start of each iteration, excluding variables that are inactive due to the bounds, a direction of search is chosen; a linear search in that direction establishes a minimum to some specified accuracy, and the gradient vector is recalculated at the new point; the set of active variables and the Cholesky factors of the approximate Hessian are updated in the light of the information obtained in this process; and all is then ready for the next iteration.

*The authors are apparently P. Gill and W. Murray. The algorithm is a cousin of the "Davidon-Fletcher-Powell" algorithm.

Table 156·a: Example linkage, data

i: Link	Length (m)	Mass (kg)	Moment of inertia about (x_i, y_i) (kg-m^2)	Centre of mass* (m) x_i	y_i
1: Frame	0.25	-	-	-	-
2: Crank	0.05	-	large	0.0	0.0
3: Coupler	0.20	0.332	0.00128	0.1	0.0
4: Rocker	0.275	0.474	0.00405	0.1375	0.0
* in local axes shown in Figure 157·a.					
Linkage assumed to act in horizontal plane.					
Constant crank speed = 300 revs/min (Section 8C) 600 revs/min (Sections 8D, 8E)					

Table 156·b: Comparison of CPU times (seconds)

Analysis (DRAM)		Synthesis (MUSCLE)	
Loading program	0.46	Loading program	0.29
Data interpretation & assembly of mechanism	0.21	Data interpretation & other preliminaries	0.67
Simulation phase	0.36	Calculation of A matrix & 1st D matrix 0.68 + 2nd D matrix 0.03	= 0.71
		Optimisation phase: first stage 0.59 + second stage 0.14	= 0.73
Output phases	0.28	Output phases	0.20
Total run time	1.31	Total run time	2.60

Implementation: The technique developed by the writer as described above (with some restrictions and additions noted below) has been programmed by Mr. C.M. Boivin in consultation with the writer. The program is termed 'MUSCLE' for Multicriterion Synthesis of Counterweights for Linkage Enhancement. The version of 'MUSCLE' referred to caters for the class of dyadic linkages with up to twelve links. The objective function uses the Gauss criterion, and may include the driving torque, frame shaking force, in-plane frame moment, and in-plane joint forces: no out-of-plane effects are taken into account. Upper and lower bounds may be specified for any of the variables.

Example: The programming, 'tuning' and use of 'MUSCLE' is not considered to be within the scope of this thesis, but a typical result may serve to support the theory given previously. The aforementioned four-bar example studied by CARSON & STEPHENS provides an interesting case. Following the previous work, the mechanism is assumed to be motor-regulated ($k = 1$). Table ·a gives quantitative details and Appendix 10U shows recorded highlights from one terminal session. The following points are notable:-

The efficiency of the formulation is evident in the CPU times, which are between one and two orders of magnitude better than those of WALKER's program 'MEDIC', for example. Indeed, one complete optimisation run (from a random start) takes only twice as long as a single dynamic analysis of the same mechanism using CHACE's program 'DRAM' (with 72 points in the cycle): see Table ·b. From a practical point of view, this changes the problem radically: from one requiring overnight batch runs, to one in which the user can monitor progress and intervene to change the control parameters or requirements in an interactive manner.

The best three-counterweight solution reduces the root mean square shaking moment to only 35% of that obtained when the mechanism is force-balanced by the usual manual method, which gives counterweights on the crank and rocker alone (see OLDHAM & WALKER for example). This is clearly a valuable improvement. The driving torque fluctuation is virtually the same as for the unbalanced linkage.

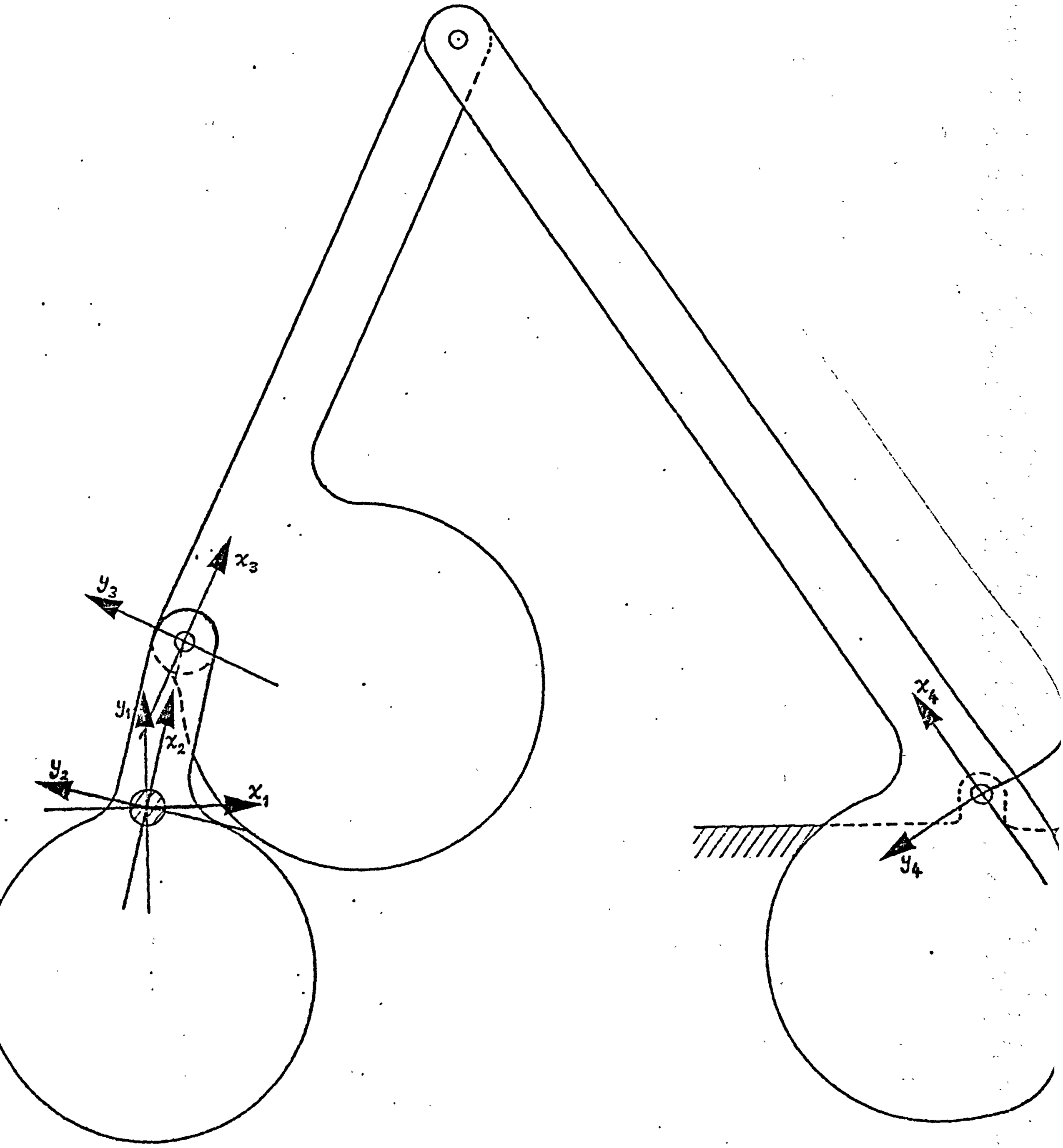

157·a: Linkage for balancing example, showing axes & optimised counterweights

The solution agrees well with that found previously by a method of much more restricted applicability, as reported in reference (HAINES d).

Similar runs from different random starts all converged to the same solution, which strongly suggests that the recorded solution is a true global optimum.

The coupler counterweight is perhaps surprisingly large, and considerably offset from the link centrelines: the proportions can be seen in Figure d. (The advantage of using offset counterweights was previously reported by WEIDERRICH & ROTH, on the strength of an approximate technique).

8D: THE EFFECTS OF SPRINGS

The problem: The addition of nominally massless springs to a kinematically determinate, constant speed planar linkage cannot alter the rate of change of linear momentum or moment of momentum, and therefore cannot alter the net frame force, F; the out-of-plane frame moments, Q; or the in-plane frame moment, M, of a motor-regulated ($k = 1$) system. It can certainly alter the driving torque fluctuation, T, and is usually used for this purpose (or equivalently to alter the speed fluctuation). It can also be used to change the distribution of the joint loads, R. The spring in question may be a torsion spring at a revolute joint, or a line-acting spring at a sliding joint or between two fixing-points on different links i_1, i_2. Thus the design parameters in general may include fixing point coordinates $(x_{S1}, y_{S1}; x_{S2}, y_{S2})$ as well as the spring stiffness S and free length l_o or free angle α_o.

The performance variables T and R are in general highly non-linear functions of the design parameters if the latter are all treated as adjustable. However, if some of the design parameters are provisionally fixed or given special values, and the others are suitably grouped, it is possible to reduce the functions to certain relatively tractable forms. Thus the problem is firstly to derive general expressions for T and R, and secondly to identify the reduceable cases.

Previous work: Fairly comprehensive investigations roughly along the lines described have been carried out by Halter, Carson and others, by Matthew and Tesar, and by Esat in collaboration with the writer.

The work of Halter and his colleagues is reported in references HALTER ET AL., HALTER & CARSON, and HALTER. They considered synthesis of the time response as well as the constant-speed driving load, using a constrained numerical optimisation technique to minimise the mean square error. The configurations they considered were torsional springs at joints and line-acting springs between any two links.

MATTHEW & TESSAR(a,b) only considered synthesis of the driving load (or its integral, or derivatives), using zero free-length line-acting springs between two links not directly joined together. They introduced a quite different synthesis technique, however, by adapting to this problem the method of exact matching to the specified curve at certain 'precision points', separated finitely or infinitesimally.

ESAT & HAINES developed a common framework for the two investigations referred to above, by systematically listing possible spring configurations, design objectives, formulations, reduceable cases and synthesis techniques. By this means it was possible to construct a comprehensive 'catalogue' of spring synthesis design problems and solution methods. That project is too lengthy to reproduce here, but the application of the approach to a particular case will be described, both as an attempt to illustrate and illuminate the whole project and to establish the basis for some further developments.

Example: The four-bar mechanism considered in the previous section provides an interesting case study, since driving torque fluctuation was not taken into account in the reported counterweight synthesis - the counterweights in fact leave the RMS driving torque virtually unchanged, so it is of interest how far this can be balanced by the incorporation of a spring, which does not affect the complete force balance and partial moment balance already achieved. A method for formulation of the joint loads is also of interest.

The configuration considered will be a line-acting spring between the coupler and the frame, since this provides the largest number of independent design variables. An influence coefficient method will be used, since the energy balance method of Matthew & Tesar is not applicable to joint loads.

Formulation: Consider the mechanism, before attaching the spring, as a non-dissipative system described by generalised coordinates u_r associated with generalised forces W_r. If the loads at a joint are to be analysed, two extra generalised coordinates u_r are defined corresponding to the additional degrees of freedom which would be introduced if the joint were broken; then the corresponding generalised forces W_r are the joint load components. According to Lagrange's equation, before attachment of the spring $W_r = W_{ro}$, where for kinetic energy K and potential energy V:

$$W_{ro} = d/dt(\partial K/\partial \dot{u}_r - \partial V/\partial \dot{u}_r) - (\partial K/\partial u_r - \partial V/\partial u_r) \qquad .a$$

If a spring is attached, the potential energy is increased by an amount E, where for a spring with stiffness S and free length l_o, $E = \frac{1}{2} S(l-l_o)^2$ .b

Thus, providing that the input motion is effectively unchanged, the load

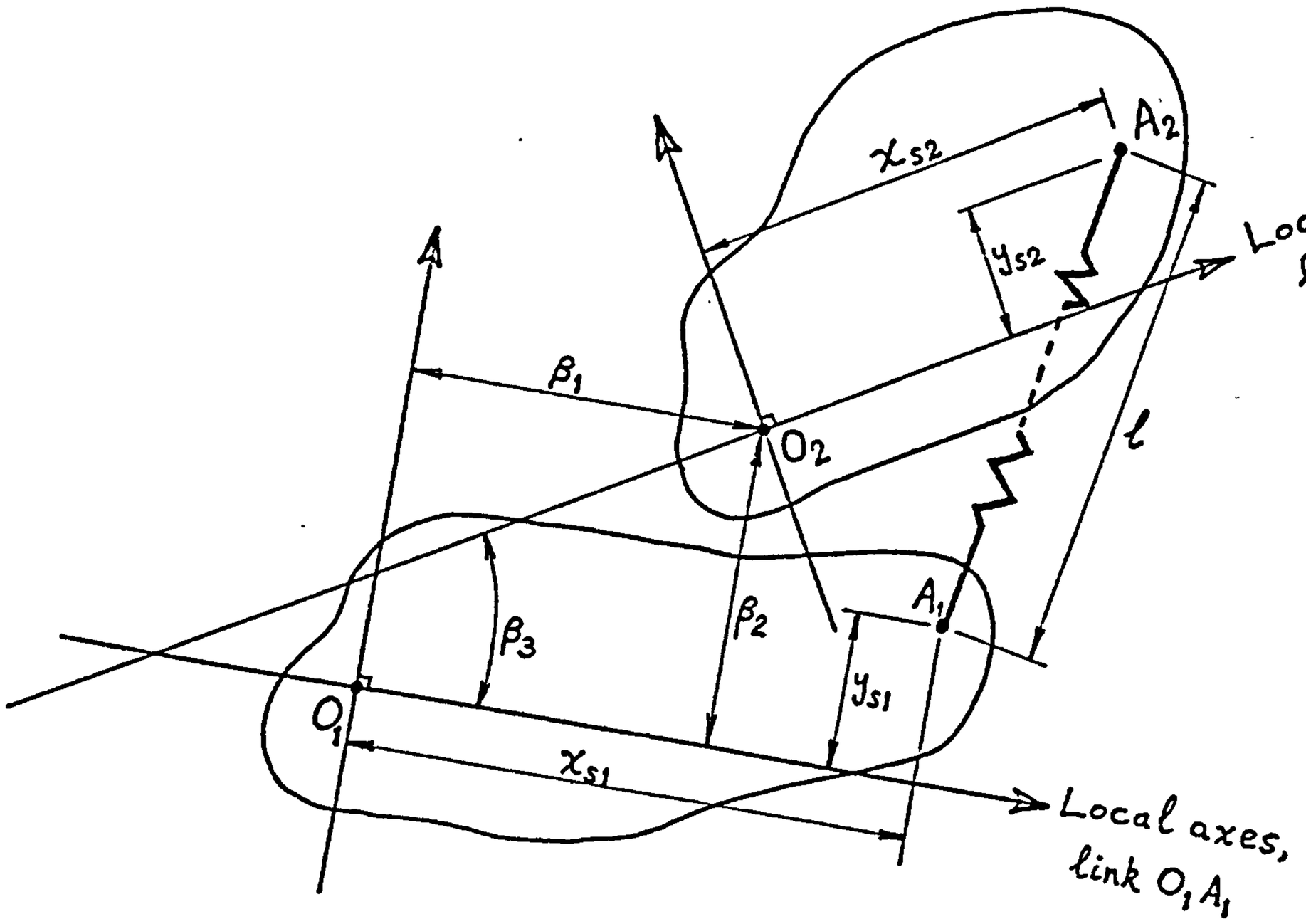

160.a: Nomenclature for tension spring between two links

Coefficients		Parametric groups	
H_1	$\beta_1(\partial\beta_1/\partial u_r) + \beta_2(\partial\beta_2/\partial u_r)$	q_1	S
H_2	$-(\partial\beta_1/\partial u_r)$	q_2	$S\,x_{s1}$
H_3	$-(\partial\beta_2/\partial u_r)$	q_3	$S\,y_{s1}$
H_4	$\cos\beta_3(\partial\beta_1/\partial u_r) + \sin\beta_3(\partial\beta_2/\partial u_r)$ $+(\beta_2\cos\beta_3 - \beta_1\sin\beta_3)(\partial\beta_3/\partial u_r)$	q_4	$S\,x_{s2}$
H_5	$\cos\beta_3(\partial\beta_2/\partial u_r) - \sin\beta_3(\partial\beta_1/\partial u_r)$ $-(\beta_1\cos\beta_3 + \beta_2\sin\beta_3)(\partial\beta_3/\partial u_r)$	q_5	$S\,y_{s2}$
H_6	$\sin\beta_3(\partial\beta_3/\partial u_r)$	q_6	$S(x_{s1}x_{s2} + y_{s1}y_{s2})$
H_7	$\cos\beta_3(\partial\beta_3/\partial u_r)$	q_7	$S(x_{s1}y_{s2} - x_{s2}y_{s1})$

Table 160.b: Terms in equation 160.f

becomes

$$W_r = W_{ro} + W_{rs} \quad | W_{rs} = \partial E/\partial u_r = S(\ell-\ell_o)(\partial \ell/\partial u_r). \qquad \cdot c$$

Now in the nomenclature of Figure ·a, ℓ can be expressed in terms of relative coordinates $\beta_1, \beta_2, \beta_3$ as follows:

$$\ell = [(\beta_1 - x_{s2} + x_{s1}\cos\beta_3 - y_{s1}\sin\beta_3)^2 + (\beta_2 - y_{s2} + y_{s1}\cos\beta_3 + x_{s1}\sin\beta_3)^2]^{1/2} \qquad \cdot d$$

Then $(\partial \ell/\partial u_r)$ can be expanded as $(\partial \ell/\partial \beta_1)(\partial \beta_1/\partial u_r)+(\partial \ell/\partial \beta_2)(\partial \beta_2/\partial u_r)+(\partial \ell/\partial \beta_3)(\partial \beta_3/\partial u_r)$ leading to

$$\begin{aligned} W_{rs} = S(\ell-\ell_o)/\ell \; [&(\partial\beta_1/\partial u_r)(\beta_1 - x_{s2} + x_{s1}\cos\beta_3 - y_{s1}\sin\beta_3) \\ &+(\partial\beta_2/\partial u_r)(\beta_2 - y_{s2} + x_{s1}\sin\beta_3 + y_{s1}\cos\beta_3) \\ &+(\partial\beta_3/\partial u_r)(-\beta_1 x_{s1}\sin\beta_3 - \beta_1 y_{s1}\cos\beta_3 + \beta_2 x_{s1}\cos\beta_3 - \beta_2 y_{s1}\sin\beta_3 \\ &\quad + x_{s2}x_{s1}\sin\beta_3 + x_{s2}y_{s1}\cos\beta_3 + y_{s2}y_{s1}\sin\beta_3 - y_{s2}x_{s1}\cos\beta_3)] \end{aligned} \qquad \cdot e$$

The terms $(\partial\beta_s/\partial u_r)$ are the "influence coefficients". At any instant the influence coefficients and the relative coordinates β_s can be found by a suitable method of kinematic analysis, while the terms $S, \ell_o, x_{s1}, y_{s1}, x_{s2}, y_{s2}$ can be adjusted by the designer to control the variation of W_r. It should be noted that the equation in this general form (·e) could equally be applied to any other planar linkage mechanism and to any generalised force associated with the mechanism.

Simplification: Practical application of the above equation is considerably simplified if, following Matthew and Tesar, we specify that $\ell_o = 0$. (Springs with this characteristic are familiar from their use in statically spring-balanced table lamps). Then equations ·c, ·e reduce to

$$W_r = W_{ro} + \Sigma_{t=1}^{7} H_t q_t \qquad \cdot f$$

where H_t, q_t are defined in Table ·b.

For the particular case of a four-bar linkage, some of the terms reduce to zero. Let O_1A_1 in Figure ·a be the frame link with O_1 at the crank/frame joint, and O_2B_2 be the coupler with O_2 at the crank/coupler joint. Then:-

Coefficients		Parametric groups	
H_1'	$(\partial\beta_1/\partial u_r)(\beta_1 - x_{S2} + x_{S1}\cos\beta_3 - y_{S1}\sin\beta_3)$ $+(\partial\beta_2/\partial u_r)(\beta_2 - y_{S2} + y_{S1}\cos\beta_3 + x_{S1}\sin\beta_3)$ $+(\partial\beta_3/\partial u_r)(-\beta_1 x_{S1}\sin\beta_3 - \beta_1 y_{S1}\cos\beta_3$ $+\beta_2 x_{S1}\cos\beta_3 - \beta_2 y_{S1}\sin\beta_3 + x_{S2}x_{S1}\sin\beta_3$ $+x_{S2}y_{S1}\cos\beta_3 + y_{S2}y_{S1}\sin\beta_3 - y_{S2}x_{S1}\cos\beta_3)$	q_1'	S
H_2'	H_1'/ℓ [see equation 160.d for ℓ]	q_2'	$S\,l_o$

Table 161.a: Terms in equation 161.e

If W_r is a component of load at either of the rocker joints, $\partial\beta_1/\partial u_r = \partial\beta_2/\partial u_r = 0$ so H_1, H_2 and H_3 vanish, leaving only four variables q_t, which are independent.

If W_r is a horizontal component of load at either of the crank joints, $\partial\beta_2/\partial u_r = 0$, so H_2 vanishes leaving six variables q_t related by the auxiliary equation

$$q_3 q_4^2 + q_3 q_5^2 = q_6 q_1 q_5 - q_7 q_1 q_4 . \qquad \cdot b$$

If W_r is a vertical component of load at either of the crank joints, $\partial\beta_1/\partial u_r = 0$, $\partial\beta_1/\partial u_r = 0$, so H_3 vanishes leaving six variables q_t related by the auxiliary equation

$$q_2 q_4^2 + q_2 q_5^2 = q_6 q_1 q_4 + q_7 q_1 q_5 . \qquad \cdot c$$

Finally, if W_r is the driving torque, $(\partial\beta_1/\partial u_r)(\partial\beta_2/\partial u_r) = -\beta_2/\beta_1$ so that H_1 vanishes, leaving six variables q_t related by the auxiliary equation

$$(q_2 q_4 + q_3 q_5) q_7 = (q_2 q_5 - q_3 q_4) q_6 . \qquad \cdot d$$

Still greater simplification is possible if $x_{s1}, y_{s1}, x_{s2}, y_{s2}$ are given some prespecified values, the restriction to zero free length being removed. Then W_{rs} can be expressed as

$$W_{rs} = H_1' q_1' + H_2' q_2' \qquad \cdot e$$

where the H_t' and q_t' are defined in Table $\cdot a$. However, since this method provides only two adjustable parameters it provides less control than the previous method. Hence the previous method is preferred provided that it is practicable - as proves to be the case.

8E: SPRING SYNTHESIS

In this section a method is developed for synthesising values of the parametric groups defined as q_t in the previous section, in order to achieve (by way of example) a minimal variation in the driving torque of the four-bar mechanism referred to in the previous sections. (The principles of the method are applicable to a much wider class of problem). The driving torque is chosen as the variable to be controlled since this provides a clear cut objective, with an unambiguous index of success, namely the percentage reduction in the peak-to-peak amplitude.

Solution method (driving torque): Unlike the counterweight problem considered in Section C, the unconstrained solution in this case is not necessarily unrealistic, so there is value in seeking such a solution, at least as a first step. This removes a major difficulty of the precision-point technique. Since the derived relationship (161·d, 160·f) leads to a solution in closed form - as shown below - if exact matching at precision points is specified but not if minimum mean square error is specified, the former method will be used.

Thus it will be specified that W_r should take the same (unknown) value q_8 at each of 6 points in the cycle, Θ_p ($p=1$ to 6):

$$q_8 = W_{rop} + \Sigma_{t=2}^{7} H_{tp}\, q_t \qquad | p = 1 \text{ to } 6 \qquad \cdot a$$

that is, in matrix form

$$-\underline{w} + \dot{q}_8\, \underline{i} = \underline{H}\, \underline{q} \qquad \cdot b$$

where $\underline{w}$ is the vector of values W_{rop}, $\underline{i}$ is a vector with six elements of value unity, $\underline{H}$ is a matrix containing the H_{tp} ($t = 2$ to 7, $p = 1$ to 6) and $\underline{q}$ is a vector containing the elements q_t ($t = 2$ to 7). Examination of the expressions for H_{tp} shows that in general they are linearly independent, so that $\underline{H}$ is non-singular, and so we can write

$$\underline{q} = q_8\, \underline{\zeta} + \underline{v} \qquad | \underline{\zeta} = \underline{H}^{-1}\underline{i}, \quad v = -\underline{H}^{-1}\underline{w} \qquad \cdot c$$

This constitutes six scalar equations which linearly relate q_t ($t = 2$ to 7) to q_8. These can be substituted into the auxiliary equation (161·d) to yield a cubic in q_8:

$$U_3\, q_8^{\,3} + U_2\, q_8^{\,2} + U_1\, q_8 + U_0 = 0, \qquad \cdot d$$

U_3	$\zeta_2\zeta_4\zeta_7 + \zeta_3\zeta_5\zeta_7 - \zeta_2\zeta_5\zeta_6 + \zeta_3\zeta_4\zeta_6$
U_2	$\zeta_2\zeta_4\upsilon_7 + \zeta_2\upsilon_4\zeta_7 + \upsilon_2\zeta_4\zeta_7 + \zeta_3\zeta_5\upsilon_7 + \zeta_3\upsilon_5\zeta_7 + \upsilon_3\zeta_5\zeta_7$ $-\zeta_2\zeta_5\upsilon_6 - \zeta_2\upsilon_5\zeta_6 - \upsilon_2\zeta_5\zeta_6 + \zeta_3\zeta_4\upsilon_6 + \zeta_3\upsilon_4\zeta_6 + \upsilon_3\zeta_4\zeta_6$
U_1	$\upsilon_2\upsilon_4\zeta_7 + \upsilon_2\zeta_4\upsilon_7 + \zeta_2\upsilon_4\upsilon_7 + \upsilon_3\upsilon_5\zeta_7 + \upsilon_3\zeta_5\upsilon_7 + \zeta_3\upsilon_5\upsilon_7$ $-\upsilon_2\upsilon_5\zeta_6 - \upsilon_2\zeta_5\upsilon_6 - \zeta_2\upsilon_5\upsilon_6 + \upsilon_3\upsilon_4\zeta_6 + \upsilon_3\zeta_4\upsilon_6 + \zeta_3\upsilon_4\upsilon_6$
U_0	$\upsilon_2\upsilon_4\upsilon_7 + \upsilon_3\upsilon_5\upsilon_7 - \upsilon_2\upsilon_5\upsilon_6 + \upsilon_3\upsilon_4\upsilon_6$

Table 163·a: Coefficients of equation 162·d

S	$(q_2q_4 + q_3q_5)/q_6$
x_{s1}	q_2/S [S as above]
y_{s1}	q_3/S [" " "]
x_{s2}	q_4/S [" " "]
y_{s2}	q_5/S [" " "]

163·b: Design parameters from parametric groups

where the coefficients U are defined in Table ·a. This cubic can be solved in closed form by a standard algorithm, yielding at least one real root. Equation 162·c then provides the other q values. Reference to Table ·b, derived from Table 160·b, finally provides the necessary values of the design parameters.

The development thus far approximately parallels that of MATTHEW & TESAR(a,b), although the introduction of the additional unknown q_8 is an innovation in this context: its significance will be discussed later (page 168).

Precision-point spacing: previous work: A problem still to be resolved is how to decide which points in the cycle are to be used as the precision points, θ_p. FREUDENSTEIN proposed methods of precision point spacing in the context of kinematic synthesis, based on Chebyshev approximation theory. McLARNAN later suggested an enhancement of Freudenstein's technique. However, these methods assume that the curve to be approximated only occupies a part of the mechanism cycle, and cannot be applied directly to the case of synthesis around a closed cycle, in which there are no fixed 'end-points' to work from.

GHERONIMUS(a,b) discussed the application to mechanisms of Chebyshev's theorems and an extension due to Bernstein. The latter is formally applicable to the closed cycle problem and may be briefly stated as follows.

·c] A 'generalised polynomial of order n' is defined as a functional of the form $f = \Sigma_{i=1}^{n}(\Lambda_i \phi_i(\theta))$ where the Λ_i are adjustable parameters, and the ϕ_i are linearly independent functions of θ with the property that there cannot be more than n zeroes in f in the range in question.

·d] Using the Chebyshev criterion, the best approximation to a given function by a 'generalised polynomial' functional of order n is uniquely characterised by the error reaching its greatest value n times, with alternating sign.

In general the functions in question in this chapter do not conform to the requirements for ϕ_i stated above, so the Chebyshev-Bernstein result cannot strictly be applied, but echoes of it may be detected in the non-rigorous method to be proposed. The starting point is an alternative synthesis method, which will be described for the sake of argument only.

Fourier transform synthesis method; The time-varying terms in equation 160·f can be expanded in Fourier series:-

$$\Sigma_{k=0}^{\infty}\left[W'_{rk}\cos k\theta + W''_{rk}\sin k\theta\right] = \Sigma_{k=0}^{\infty}\left[W'_{rok}\cos k\theta + W''_{rok}\sin k\theta\right] + \Sigma_{t=2}^{7} q_t\left[\Sigma_{k=0}^{\infty}\left[H'_{tk}\cos k\theta + H''_{tk}\sin k\theta\right]\right] \qquad \cdot a$$

where $W''_{ro} \equiv 0$, $W''_{roo} \equiv 0$, and all $H_{to} \equiv 0$. Since a non-dissipative system is assumed, W'_{roo} and all H'_{to} are zero, so that W'_{ro} is also zero.

Now suppose it is specified that the first two harmonics of W_r are eliminated, that is $W'_{r1} = W''_{r1} = W'_{r2} = W''_{r2} = 0$, and also that $W'_{r3}/W''_{r3} = \tan\lambda$, where λ, the phase angle of the third harmonic, is chosen arbitrarily. Then by equality of coefficients of each orthogonal time-varying term,

$$\left.\begin{aligned} &W'_{ro1} + \Sigma_{t=2}^{7}\left[q_t H'_{t1}\right] = 0; \qquad W'_{ro2} + \Sigma_{t=2}^{7}\left[q_t H'_{t2}\right] = 0; \\ &W''_{ro1} + \Sigma_{t=2}^{7}\left[q_t H''_{t1}\right] = 0; \qquad W''_{ro2} + \Sigma_{t=2}^{7}\left[q_t H''_{t2}\right] = 0; \\ &\left[W'_{ro3} - W''_{ro3}\tan\lambda\right] + \Sigma_{t=2}^{7}\left[q_t\left[H'_{t3} - H''_{t3}\tan\lambda\right]\right] = 0. \end{aligned}\right\} \cdot b$$

In summary, this can be written

$$\underline{w}_f + q_7\,\underline{h} + \underline{H}_f\,\underline{q}_f = 0, \qquad \cdot c$$

where $\underline{q}_f$ contains terms q_2 to q_6 only. There is no reason in general for $\underline{H}_f$ to be singular, so $\underline{q}_f$ can be found as a function of q_7: $\underline{q}_f = \underline{H}_f^{-1}(\underline{w}_f + q_7\,\underline{h})$. Substitution of this relation in the auxiliary equation (161·d) yields a cubic in q_7, from whose solution the other q terms may be found, and hence the design parameters.

It is seen that the above solution method in essence follows the same course as the precision point synthesis method, except that instead of points in the curve of W_r, points in its Fourier transform are chosen. By repeated application of this method it would be possible to determine that value of λ, say λ_o, for which $(W'^{\,2}_{r3} + W''^{\,2}_{r3})$ is a minimum.

It was argued in Chapter 2D that kinematically determined functions in linkage mechanisms typically exhibit steeply falling harmonic spectra. Thus it is reasonable in the present case to expect that the terms of order four and above in equation ·a are small, and terms of order three are fairly small, in comparison with the first and second order terms. It follows that the solu-

tion given by the Fourier transform synthesis method with $W'_{r1} = W'_{r2} = W''_{r1} = W''_{r2} = 0$, $W'_{r3}/W''_{r3} = \tan\lambda_0$ can be expected to be fairly close to the true optimum, and thus that the error term W_r for the optimal case can be expected to be dominated by the third harmonic. The latter deduction provides a plausible basis for a simple method of precision point spacing.

Equal spacing solution: Since the variation of W_r after optimal balancing is likely to consist mainly of the third harmonic, the points at which it passes through zero are likely to be separated by approximately one sixth of a cycle. Thus precision points separated exactly one sixth of a cycle seem to be a suitable choice as a first approximation to the optimum spacing. The position of the first precision point (which in effect governs λ) must still be optimised by trial and error, however.

Iterative respacing: If the initial spacing θ_p gives rise to peak errors $\pm\varepsilon_p$ between points θ_p and θ_{p+1} ($\pm\varepsilon_6$ between points θ_6 and θ_1), and if not all values $|\varepsilon_p|$ are equal, it might be asked whether, by suitable adjustment of the θ_p, the largest values(s) of $|\varepsilon_p|$ might not be 'traded off' against the smaller value(s). If this proved to be possible, the end point of such a process would be when all the revised values ε'_p were of equal magnitude.

To achieve such a respacing of θ_p in the context of kinematic synthesis over part of a cycle, FREUDENSTEIN's approach was to assume that ε_p is proportional to δ_p^{η} where $\delta_p \equiv \theta_{p+1} - \theta_p$ and η is a guessed exponent greater than unity (say, 3). This leads to revised intervals δ'_p given by

$$(\delta'_p/\delta_p) = |\varepsilon_p|^{-1/\eta} \sum_p(\delta_p) / \sum_p(\delta_p |\varepsilon_p|^{-1/\eta}) \qquad \text{.a}$$

This formula is applied iteratively by Freudenstein, η being reduced if necessary to accelerate convergence or increased if necessary to damp out 'hunting'.

For application to the present case, where a complete cycle is involved, it is obviously necessary to define δ_6 as $(\theta_1 + 360^\circ - \theta_6)$. An additional problem is that the calculation of revised values of δ_p is inadequate in this case for the determination of new values of θ_p (there being, as pointed out previously, no end-point to work from). An obvious solution is to make

the arbitrary assumption that $\Theta_1' = \Theta_1$, but this is not very satisfactory, as the following simple example illustrates:-

·a] The function $\psi(\theta) \equiv \cos\Theta$ is to be approximated by the functional $(a + b \sin\Theta)$ where a and b are adjustable. Initial precision points are chosen at $\Theta_1 = 0^\circ$, $\Theta_2 = 270^\circ$, leading to $a = b = 1$. Now let Freudenstein's respacing formula be applied repeatedly with the extra condition that $\Theta_1' = \Theta_1$ at each step. The effect, whatever the value of η, is that although the ratio of the two peak errors approaches unity, their actual magnitude approaches infinity.

Thus it is here proposed that the additional condition specified is $\sum_p \Theta_p' = \sum_p \Theta_p$. ·b This can be expected to keep λ, the phase of the third harmonic of the error term, roughly constant throughout the respacing process so that the kind of instability illustrated by this example is avoided.

Synthesis procedure: The complete procedure suggested by the above investigation is as follows:-

·c] Apply the 'equal spacing' procedure using a number of different values of Θ_1 in the range 0° to 30°. Exclude any values for which the solution involves impractical values of the design parameters. Of the remaining values, choose that giving the best error curve, $\Theta_1^{\square}$. Then repeatedly apply Freudenstein's respacing formula (165·a) maintaining $\sum_p \Theta_p$ constant, until the process converges. (A further small improvement might be obtained by applying the respacing formula to equal spacing solutions with Θ_1 a little above, and a little below $\Theta_1^{\square}$.)

This procedure may need intelligent adaption in the light of the results obtained, as in the example that follows.

Application and results: The techniques described have been incorporated in a demonstration computer program written in collaboration with Dr. Esat, and applied to the four-bar mechanism with counterweights as specified in Section C. The values of H_t and W_{ro} in equation 160·1 were calculated at 64 points in the cycle using CHACE's program 'DRAM', and stored in a look-up table, an interpolation method being used for intermediate points. Eleven solutions were synthesized using approximately equally spaced precision points, with Θ_1 incremented by 1/64 of a cycle between successive solutions. The

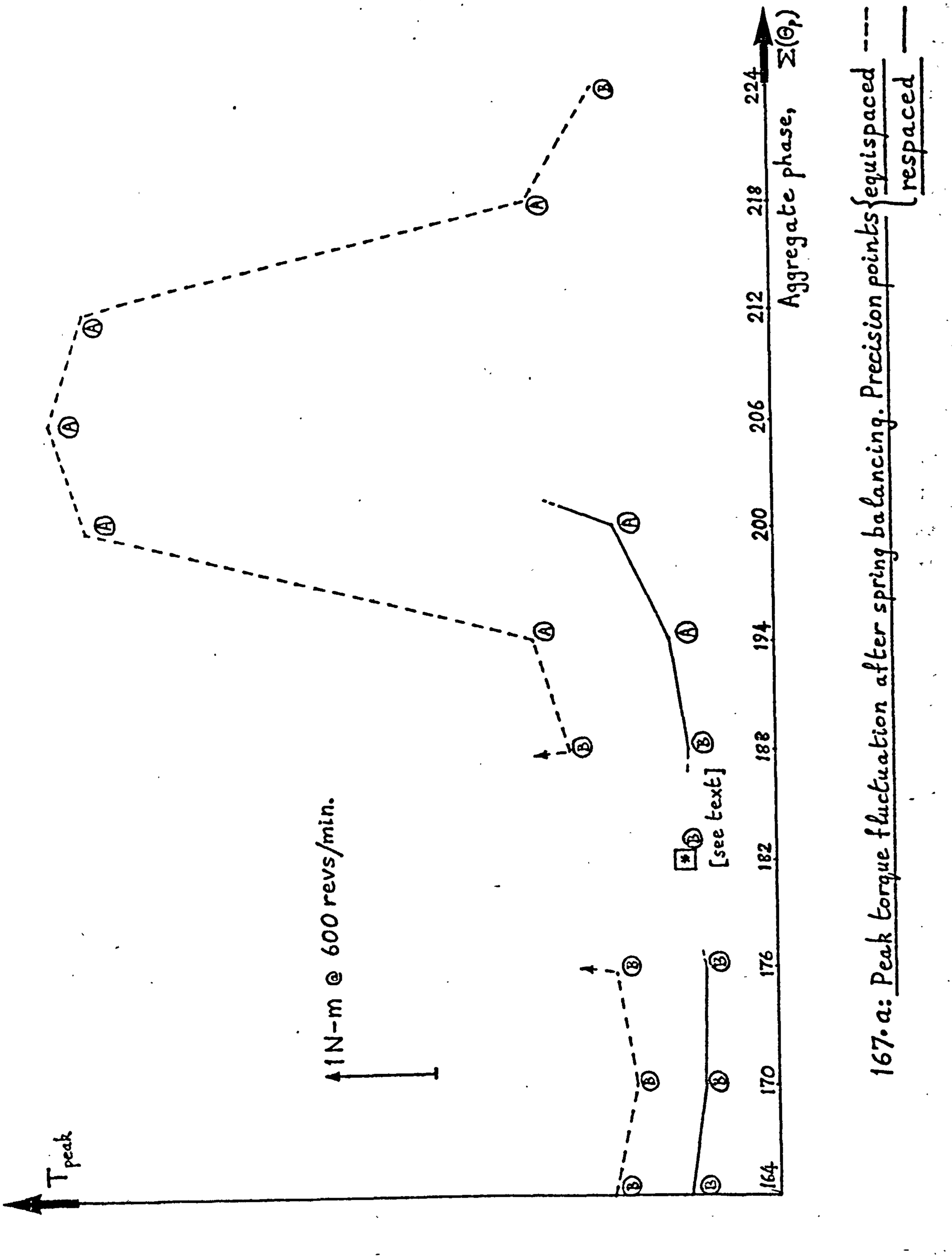

167.a: Peak torque fluctuation after spring balancing. Precision points equispaced ---, respaced ——

Tentative spring design (to suit 600 rpm)
2 springs each of 4 turns of 2 mm dia. spring steel wire to 30 mm coil diameter pretensioned to give zero free length; located at (182,147)mm on frame link and (190,-137) on coupler link (axes as shown on Fig.157.a). Working length = 13 to 53 mm.
Predicted stiffness = 1460 N/m each; max. stress = 820×10^6 N; max. helix angle $\doteq 8°$.

TABLE 167.b

peak errors obtained are shown by the broken lines in Figure •a, where the horizontal axis shows $\sum_r \Theta_r$ (in units of 1/64 cycle). For the fourth point ($\sum_r \Theta_r = 182$) the cubic was found to have only one real root, and the corresponding solution was of no practical value. At all the other points the cubic had three real roots. At the points marked Ⓐ, only one root led to a realistic stiffness value whereas at the points marked Ⓑ there were two realistic solutions leading to almost identical error curves. The solutions dismissed as unrealistic involved either negative stiffness springs, or springs with enormously high stiffnesses with fixing points almost coincident with the joint centres.

From these 'equal spacing' results the most promising value of $\sum_r \Theta_r$ is seen to be 170 units. It is therefore of interest to seek optimally respaced solutions with $\sum_r \Theta_r$ near to this value. Because of the 'gap' in the equal-spacing curve due to the appearance of imaginary roots, it was decided to explore the region of interest 'from left to right'; that is in the following manner. At first, the equally spaced solution with $\sum_r \Theta_r = 164$ is used as a starting point, and six iterations of the respacing procedure are applied, with $\eta = 5$. Then each value of Θ_r is increased by 1/64 cycle from the value obtained after respacing, and six further iterations of the respacing procedure are performed. This sequence of advancing Θ_r and respacing is repeated as often as necessary. The results are shown by the full line in Figure •a. In each case six iterations with $\eta = 5$ were sufficient for convergence, with all peak errors approximately equal, except the case where $\sum_r \Theta_r = 182$. In this case three iterations led to rough convergence (greatest peak/smallest peak $\doteqdot$ 1.5) with three real roots, but in the next iteration imaginary roots appeared, the solution derived from the remaining real root being unrealistic. The value marked ⊡ refers to the solution after three iterations.

The best balance is seen to be given by $\sum_r \Theta_r = 176$ units. However, analysis of this solution showed that the ratio of maximum to minimum spring length over the cycle is 9.9, which is difficult to realise. With $\sum_r \Theta_r = 170$ units, on the other hand, this ratio is only 4.1 while the balancing effect is almost as good. Using the latter solution, the peak-to-peak torque fluctuation is in fact only 54% of the best value obtained using equal spacing, or 18% of the value without a spring (with or without counterweights). Table •b gives the design parameters for the solution referred to, which are seen to be feasible, although the position of the fixing point on the coupler requires a supporting structure which has been neglected in the inertial analysis.

Conclusions of section: It may be concluded that spring balancing can be of practical value for this kind of problem, that equally spaced precision points with a range of values of $\sum_r \theta_r$ in general lead to a useful first-approximation solution, and that Freudenstein's respacing procedure with the modifications described can lead efficiently to considerable further improvements.

Footnote: least peak versus least range: It may be recalled that the ordinate at the precision points was set not to zero but to a further unknown, q_8. The effect of the respacing process is to minimise the variation about q_8, which is clearly equivalent to minimising the peak-to-peak range of the torque curve (since the equalised peak error magnitude ε' provides the semi-range). In practice the final curve is unlikely to differ greatly from that with a minimised peak magnitude, and it is arguable that the former is if anything a better criterion of smoothness in this context. The advantage of making q_8 variable is that the positions (on the θ axis) of six precision points can be controlled instead of five. MATTHEW & TESAR(a) achieved a rather similar result by choosing precision points in the integral of the torque curve - in other words, the stored energy curve - the constant of integration providing the extra variable in this case. The precision point spacing techniques introduced here could of course be used in conjunction with Matthew and Tesar's formulation, if a minimal range of stored energy variation is thought to meet the needs of the application in question more precisely than a minimal range of torque.

CHAPTER 9

A REVIEW OF THE INVESTIGATION

None of the material in this chapter has been published before.

Principal nomenclature for this chapter is given below.

Symbol	Meaning
E	Young's modulus for link material
g	Gravitational acceleration
H_1 H_2 H_3	Dimensionless parameters governing a 'standard' flypast.
R_u^*	Minimum contact force at joint if there was no clearance.
$\dot{R}_v^*$	Rate of change of zero-clearance contact force component perpendicular to R_u^*
μ	Mass density of link
Ω	Ratio of fundamental natural frequency to driving speed
Ω_i	Instantaneous value of Ω for drive shaft vibrations
$\bar{\Omega}$	Cyclic mean value of Ω_i for drive shaft vibrations

9. A REVIEW OF THE INVESTIGATION

9A: OVERVIEW

It is the intention in this chapter to provide both a resumé and a critique of the work presented above.

The approach: The investigation described in this thesis had the aim of advancing the body of knowledge relating to the dynamic performance of linkage mechanisms. Because of the different problems that arise with different categories of linkage, it was decided at the outset to restrict attention to one broad category of wide practical application, namely pure linkages of the planar, kinematically determinate, continously operating type. The problem was conceived as one of establishing techniques of scientific design for reducing the noise and vibration, with respect to speed, of mechanisms whose geometry was already provisionally chosen in the light of kinematic requirements.

The problem was approached in the first place by characterising four types of element thought to be representative of vibration-prone elements in practical mechanisms. The effects on these elements of a variety of factors that can in principle contribute to vibrations was estimated to an order of magnitude by means of very approximate models, and hence - with reference also to practical evidence - the dynamic effects of clearance in simple revolute joints was selected as the major topic to be given more detailed attention.

Clearance effects: After a thorough survey of the relevant published literature, the latter problem was investigated both theoretically and experimentally, with definite predictive success in some respects, though not unmixed with some surprises. The survey, the theory, the experimentation and its results will be reviewed together, in more detail, in Section B.

Drive vibrations: A second topic selected for particular study was vibrations in the drive shaft of a mechanism, with specific reference to the frequency content of the steady-state motion at the input link. This was studied by numerical analysis of the linearised system. A simple but effective method for predicting critical speeds was demonstrated; however, it was also found that off-resonance conditions could give rise to a significant high-frequency content in a case studied.

This phase of the work will be reviewed more fully in Section C; the broader question of predicting vibrations in linkage mechanisms will then be re-examined, with the two specific investigations put in context.

Synthesis: A last problem that has been studied in this thesis, as a logical counterpart to the study of vibration prediction, is the rational synthesis of designs that reduce or avoid the phenomena in question. It was argued that this could most readily be achieved in practice by the use of auxiliary devices, specifically counterweights and springs. Systematic formulations of the effects of added masses and of one type of spring device were presented, and in the light of these, methods were proposed for numerical optimisation of the design parameters of the devices; the latter appeared to be very successful in a theoretical case study. Section E will offer a brief re-examination of this whole question.

Conclusions: A formal summary of the conclusions of the thesis will constitute Section F of this chapter.

9B: THE LUDODYNAMIC INVESTIGATION

Four chapters (3 to 6) were devoted to the behaviour of revolute joints with clearance but in the absence of a hydrodynamic oil film. This was considered to be a likely source of the unexplained vibrations recorded in a number of experimental studies of linkage dynamics.

The review of previous work distinguished the study of the conditions leading to loss of pin-journal contact from the study of the ensuing impact, the latter having been treated in most cases as a one-dimensional problem. A further distinction was made between detailed simulations of the behaviour under a specific set of conditions and very simple models or rules providing a rough guide to the variation of the behaviour over a wide range of conditions. Suggested by the latter work, the term "flypast" was coined to describe the critical points in the cycle when the nominal (zero-clearance) contact force vector passed close to the origin.

The approximate theory: The new theory advanced in Chapter 4 attempted to bridge the gap between the full simulations and the heuristic models: by the use of the fullest reasonable set of formal simplifying assumptions, the multitude of variable parameters associated with a general mechanism were reduced to three dimensionless groups, H_1, H_2 and H_3. A series of numerical simulations was then used to determine the influence of these groups over a region of the parametric space.

Perhaps the most significant novelty in the model was the introduction of the "standard flypast" as an approximation to the actual external conditions imposed on the joint at flypast points in the cycle. This approximation, and the omission of small terms from the dynamic equations, were found to have very minor effects on the simulated behaviour. The other approximations made will be reviewed below in conjunction with the experimental work.

The simulations suggested that the disturbance provoked by a flypast gives rise to a series of minima in the actual contact force, and that loss of contact may occur at the later minima - termed 'terminal' - rather than at the first or 'passage' minimum in the manner usually described hitherto.

The apparatus: A limitation noted in most of the otherwise excellent experimental work reported previously was that it appeared not to be designed to discriminate between competing theories, so much as to provide a general seal of

approval for the investigators' simulations. Rather than duplicate such work, it was decided to adopt a different approach, and so a novel experimental apparatus was designed which eliminated some of the complications of a typical joint so as to permit the remaining phenomena to be studied critically. Thus, for example, the demonstrated similarity of the effects of standard and non-standard flypasts was exploited by a configuration that 'builds in' most of the simplifications associated with the former; likewise, specific measures were taken to eliminate significant misalignment and the effects of clearance at other joints.

After considerable development, two limitations in the performance of the rig were thought to be potentially significant, namely the excessive rigidity of the spider springs in the frictionless exciter units and the deterioration of the bearing surfaces. In practice, it appeared that the former effect could be neglected provided that low values of R_{μ}^{*} were avoided with the high-clearance pin, and the latter had less effect on the consistency of the results than was feared.

The experiments: The obvious remaining differences between the theoretical model and the test linkage are the presence in the latter of material elasticity, surface friction and adhesion, an air film, and profile errors. Thus the effect of testing the theoretical predictions is to test the validity of disregarding these factors. Notwithstanding a fairly wide band of variation for repeated measurements, the results showed that if the clearance is sufficiently large - 250 μm on diameter for the test bearing - the theory has considerable predictive power as regards the threshold of passage contact loss: it is considered that this result demonstrates a clear advance in the theoretical understanding of this complex subject. For smaller clearances (65 and 20 μm), on the other hand, the predicted reduction in the tendency to lose contact was not observed (for reasons that remain obscure), and the incidence of terminal contact loss was not correctly predicted at any clearance.* It was also discovered that the empirical criterion of Earles and Wu has no validity in the context of this apparatus.

* A consequence of this result is that the intriguing feature of a 'sector of sanctuary' in the proposed design chart, Figure 79.a, must (regrettably) be forgotten.

In addition to delineation of the limits of applicability of the existing theory, as considered above, considerable evidence was obtained on the nature of the factors which a more widely applicable theory must taken into account. Of particular benefit in this respect was the provision of an instrumentation and data capture system that enabled force and displacement vector loci to be plotted with corresponding instants identified, so that the rapid sequence of events could be followed in most cases with little ambiguity. By this means it became apparent that the material elasticity, although justifiably neglected in the passage phase - that is, up to the first minimum in the contact force - is a major governing factor during the terminal phase. The results of the tests on surface compliance also provided important information in this connection, showing deflections markedly greater than those anticipated theoretically.

Although the predictions of the new theory regarding impact magnitudes after contact loss were not specifically tested, the subsidiary "drop tests" and the details of the vector loci revealed a fact of considerable importance regarding this aspect of the behaviour: namely, the major role played by the air film in cushioning the impact, at least in a bearing with relatively small clearances.

Excluded factors: The factors deliberately excluded from the experiments must not be forgotten.

The difference between an inertially loaded mechanism and an externally loaded jointed structure such as that tested may appear large, but there is nothing in the physical description of the rig behaviour that suggests that the source of the joint load per se should make any difference. However, there are two consequential differences that could be significant.

The first is that in a true mechanism the drive system could introduce an additional degree of freedom unless a sufficiently heavy flywheel is used. Thus one appropriate topic for a future study would be the modification of the equations of motion of the simplified theory in order to account for the case of finite drive inertia.

The second difference between rig and reality is the presence of gross angular relative motion between the pin and journal in a true mechanism. This would alter the direction and possibly the magnitude of surface friction: for this reason it seems inadvisable to attempt to quantify the second-order "correction" for friction suggested by the rig results. Relative motion could also modify the behaviour of the air film, and the speculative "limpet" effect suggested to explain the results with small clearances; and by facilitating "running in", it could reduce the effect of profile errors.

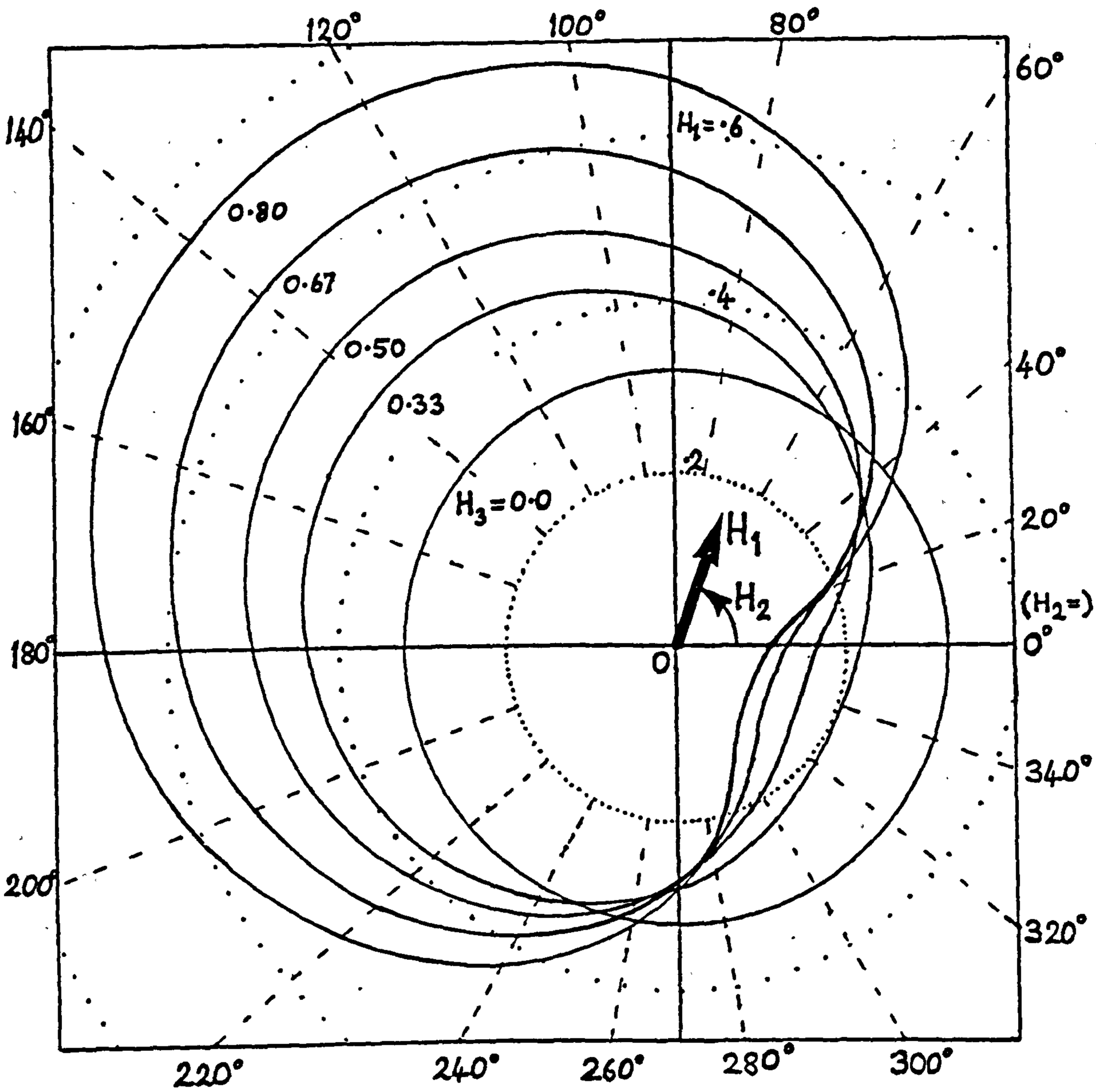

174·a: 'Design chart' – contact lost in 'passage' phase if design point is inside relevant contour.

The effect of the co-existence of two or more ludodynamic bearings in the same mechanism may be speculatively predicted on intuitive grounds: since each bearing behaves very like a zero-clearance bearing except at flypasts, the effects might be expected to be independent except when flypasts occur in two bearings at almost the same time, in which case the simple theory may well break down.

The last excluded effect is misalignment. Little can be said about this at present, except to record a suspicion that it may prove to be by no means the least significant.

Design implications: Perhaps the most suitable application for the new theory is to assume a substantially oversized clearance and identify the circumstances in which contact is predicted to be maintained in the passage phase then. In these circumstances tolerances on bearing clearances can be relaxed to a considerable extent before passage contact loss becomes likely. Where loss of contact is predicted, on the other hand, tradionally tight clearances should be used, not so much to discourage the contact loss as to minimise the ensuing impact - not least, by increasing the cushioning effect of the air film. As an aid to making this prediction, Figure .a is presented. This should be interpreted in the same manner as Figure 79.a, but the curves relate only to passage contact loss. No guidance can be offered on the terminal phase at present.

Extensions to the theory (impulse prediction): It is pertinent at this point to reconsider in what sense contact loss really matters. Certainly, in the case of large clearances the impact load following on a clearcut loss of contact is the main thing to worry about in the passage phase, so the ability to predict this is a useful advance. In the terminal phase, on the other hand, and in the passage phase when clearances are reduced, it seems to make relatively little difference to the generated impulses whether contact is lost or no. It would therefore be useful to be able to predict the magnitude and character of the impulses on the assumption that contact is always maintained.

This could be attempted by repeating the large series of runs of program BLA, with the difference that the sign of the contact force is not tested, and the information recorded for each run is such as to characterise the predicted load pulse between the first and second minima in the actual contact force: for example, the width, height and maximum rate of growth and decay of the pulse,

all reduced to dimensionless form. It could be hypothesized that if the width is greater than the (similarly reduced) longest period of elastic vibration of the system, then the force variation thus calculated would provide a good approximation to the actual variation. Furthermore, an approximate relationship could be sought between the tabulated characteristics of a pulse and its shock spectrum, as a basis for predicting the response of less rigid systems.

Air film effect: There is an obvious need for further work, both theoretical and experimental, with the aim of predicting the magnitude of the air film effect, at least to the extent of indicating in which cases it can be neglected. The existing rig would provide a suitable basis for the experimental work: a simple approach would be to repeat the "drop tests" described in Section 6B, using a tight pin, but with the effective length of the bearing progressively reduced. This could be achieved for example by machining a series of circumferential grooves in the pin. A sharp reduction in the film effect would be expected due to the shorter escape paths of the air.

Misalignment: The existing apparatus could also be used to study the effects of misalignment on contact loss during flypasts. The main difficulty lies in defining and calibrating the degree of misalignment so that externally applicable quantitative results can be obtained. Before carrying out such tests - or any other tests involving flypasts - it would be advisable to replace the bearing elements. In view of the tribological problems encountered, a recognized self-lubricating material should be used for one of the surfaces. The other surface should be ground if possible, and it would be advantageous to 'run in' the elements (for example, with the aid of a vertical milling machine) to minimise the local high spots.

Compliance: It would be desirable to check the unexpected results for surface compliance, in the first place by simply repeating the experiments reported here, but with the aluminium spacer pieces (96.e) replaced by steel or possibly eliminated entirely. Either measure would increase the pin support stiffness and so reduce one source of possible error. With the use of a more effective bearing material as suggested above, these measurements should be made both before and after the running-in procedure, to test the effect of reducing the high spots. It would also be appropriate to vary the bearing dimensions. Fig.176.a suggests a possible arrangement with diameter as well as length reduced.

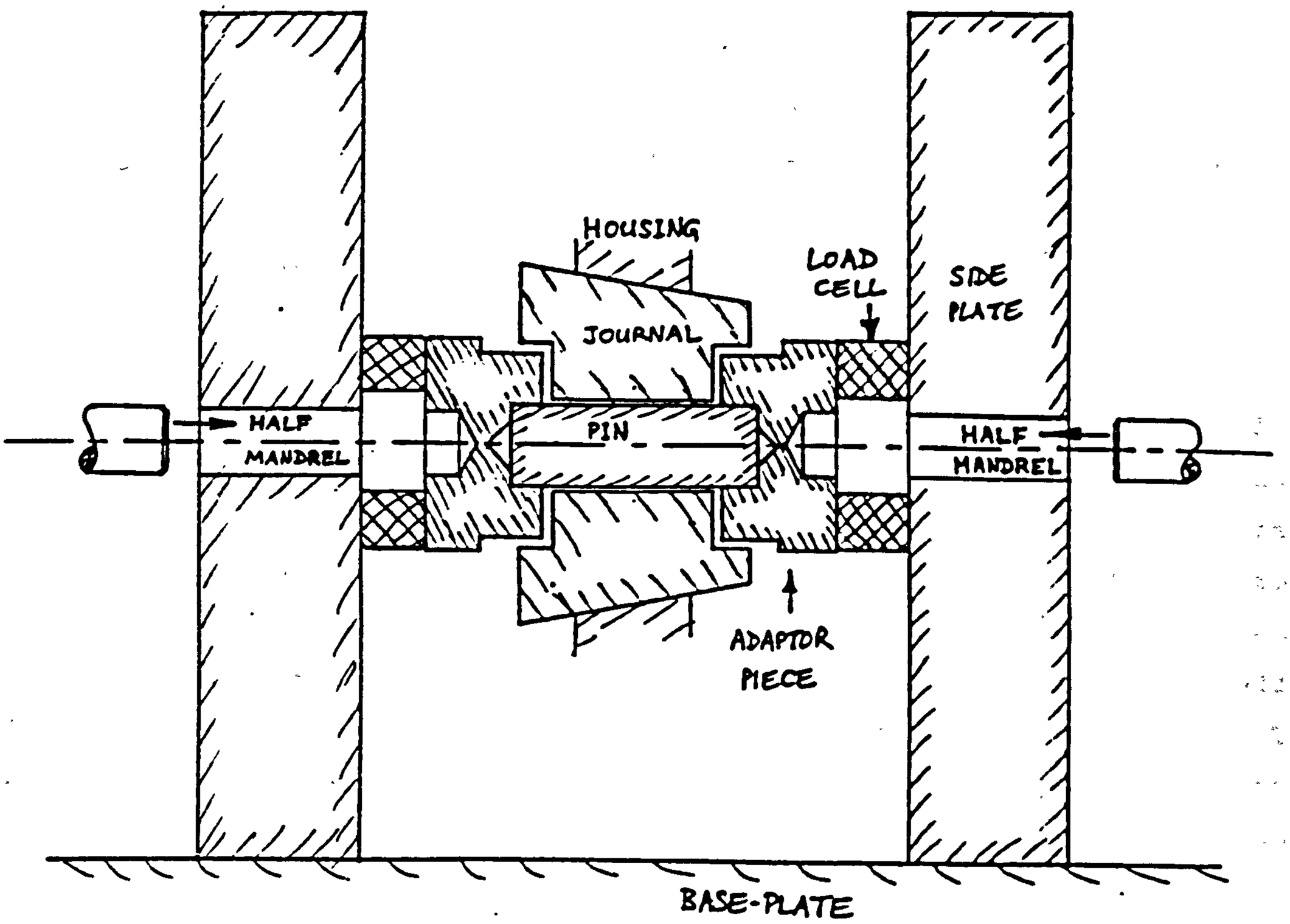

176·a: Arrangement of test bearing with reduced diameter.

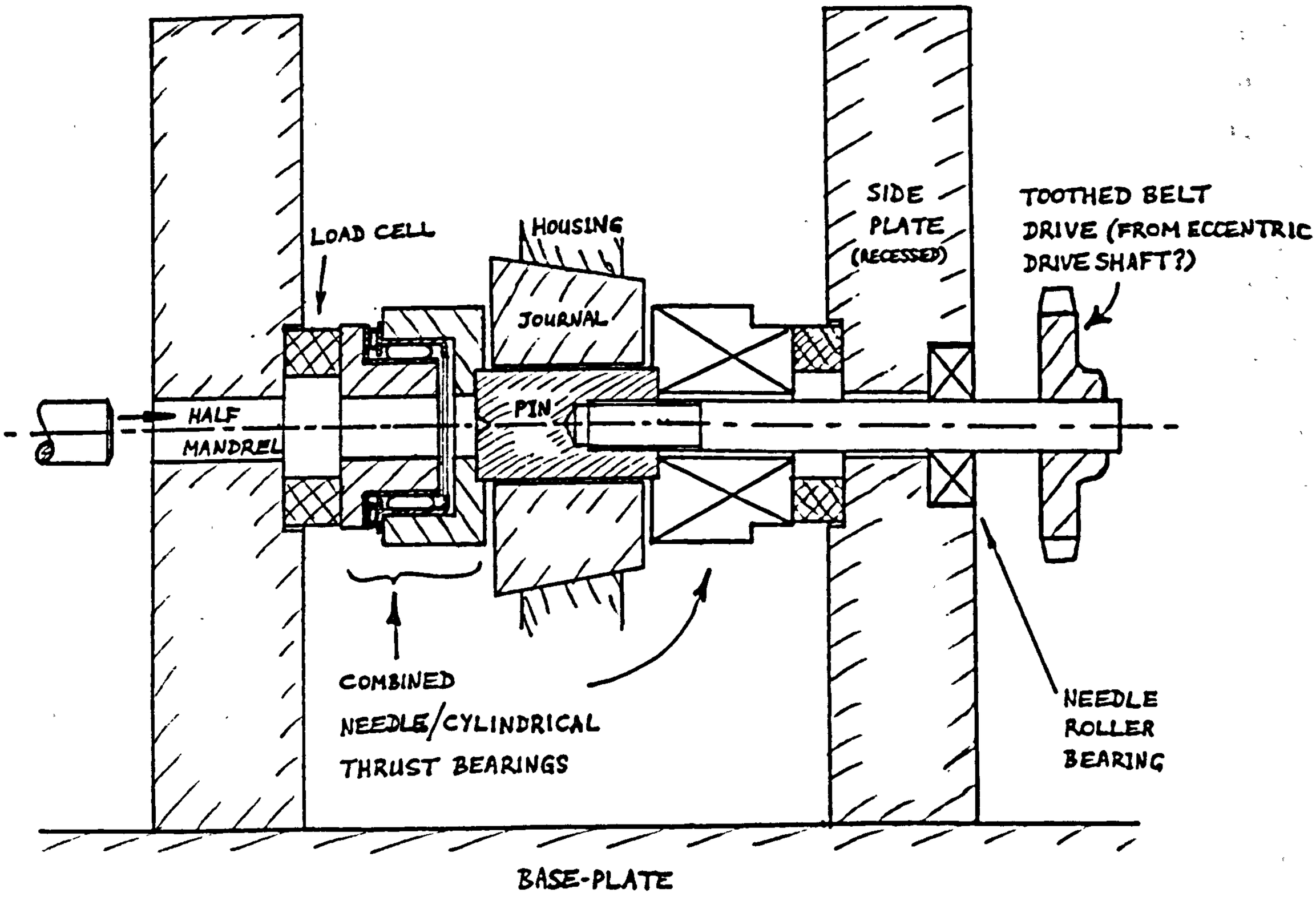

176·b: Arrangement of test bearing with rotating pin.

Pin rotation: The gross motion between the bearing elements in mechanisms could be simulated in the existing rig by mounting the pin between tapered roller bearings and applying a continuous drive via a removable shaft. Figure .b suggests a possible modification along these lines, envisaged when the rig was designed. It would be of particular interest to discover how the presence (and direction) of gross motion affects the magnitude of the angular displacement oscillations in the terminal phase, and also whether it reduced the discrepancy in the passage contact loss threshold values for small clearances.

9C: THE INVESTIGATION OF HILL'S EQUATION

In the course of the evaluation of the various factors affecting linkage vibrations, two cases emerged where the approximate governing equation took the form of an inhomogeneous Hill's equation (second order differential equation with period coefficients and forcing term). The solutions of this equation under conditions appropriate to the two applications were therefore studied. In both cases the solutions were obtained by numerical integration, transients being eliminated by the selection of initial conditions that yielded a periodic solution.

End-loaded coupler: For one application, coupler vibration under the influence of fluctuating axial loading, the solutions were used only to check the results of a more approximate analysis, which was broadly confirmed.

Drive shafts: resonance: The other application was the motion of a drive link, attached to a mechanism treated as rigid, when driven by a constant-speed prime mover by way of a flexible shaft. Owing to the variation of the effective inertia at the input as the mechanism configuration changes, the system's "instantaneous frequency ratio" Ω_i (that is, the square root of the ratio of the coefficients of the zero-order and second order terms of the equation in dimensionless form) is a function of the crank angle. Thus, one question to be answered is at what speeds maximal resonant amplication of the vibrations will occur.

It was thought to be intuitively plausible that the critical speeds would correspond to integral values of $\bar{\Omega}$, the mean value of Ω_i over a revolution of the shaft. This hypothesis was tested both for a scotch yoke mechanism and a crank-rocker mechanism. It was found in both cases that the true resonant speeds were predicted with quite a surprising accuracy, and certainly as much as is needed in practice, even when Ω_i varied by as much as a factor of 7 over the shaft revolution.

This simple but effective technique was not mentioned in any of the literature studied, and it might be wondered why it is not better known (if indeed it was previously known at all). No doubt one reason is that its merits depend on the application. The method breaks down if (Ω_i^2) is negative at any shaft angle; it cannot indicate the width of unstable speed bands but only the most unstable (or least stable) speeds; and repeated numerical evaluations of the coefficients

are necessary to determine a single critical speed. In the present application, however, these are not serious drawbacks. In the extreme cases where Ω_i^2 becomes negative or where an unstable speed band of appreciable width occurs, the linearised equation is of doubtful relevance anyway; and the complexity of the coefficients of the Hill's equation even for a simple crank-rocker mechanism is such that an analytical method requires more effort than the direct numerical evaluation of Ω_i.

Drive shafts: frequency content: The principal aim of the Hill's equation study was to explore to what extent the links of a mechanism are subjected to accelerations at their joints with a richer high-frequency content than suggested by rigid-body analysis, by virtue of vibrations at the input link. It was noted that the magnitude of this effect depended in principle on the frequency content both of the input link acceleration and of the square of its speed, but the numerical results showed the former term to be the more critical.

It was concluded that the effect under consideration could indeed be a significant one, even at off-resonance speeds; at resonant speeds it was significantly magnified, though less so than in systems with constant coefficients. Evidence was also obtained that the linear approximation used was valid for frequency ratios regarded as realistic.

Further work: The study of a single Hill's equation in this connection can only be regarded as preliminary. The suggestion that shaft flexibility can lead to serious vibrations in links that would otherwise prove adequately rigid should now be investigated more fully, by setting up the equations for a mechanism including flexibility in one link as well as the drive system. For this purpose it is probably adequate to model the link by means of equation 24.d, considering only the first mode. The steady state solution of the resulting coupled pair of Hill's equations should then be found by using subroutine SSICS in conjunction with an appropriate integration algorithm. The results of the study reported above could be used to select appropriate values for the parameters concerned. The results should be compared with results for the cases in which the link and drive in turn are treated as rigid.

It was found in the preliminary study that a large number of steps per cycle (up to 1024) were necessary to obtain satisfactory results. To some extent this is the price for seeking accuracy up to high harmonics of the response, but for further work it would be worth trying other integration algorithms: preference

should be given to algorithms that are symmetrical with respect to the sign of the independent variable, so as to minimise the effect of the numerical approximation on the system stability.

9D: THE PREDICTION OF LINKAGE MECHANISM VIBRATIONS

A careful study was made in Chapter 2 of the likely orders of magnitude of a comprehensive set of factors likely to affect vibrations in linkages. The outcome of this study was twofold: firstly, the identification of suitable approximate methods for predicting levels of vibration in those linkages to which a fairly plausible set of assumptions is applicable; and secondly, the identification of circumstances in which higher levels of vibration might be expected, owing to the breakdown of some of the assumptions. An application-oriented summary of the recommendations that emerged was provided in Section 2M (p48). The assumptions, the methods, and the exceptions will now be reviewed in turn.

The assumptions: Many of the specific assumptions made were based on an initial assumption that the linkage in question was soundly designed in rigid-body terms. This distinguishes the present from many previous investigations: however, that is not to denigrate the latter, which served a complementary purpose. A second group of assumptions had the effect of excluding from consideration linkages whose unusual functional requirements necessitate 'abnormal' kinematic characteristics. Further assumptions were made on a provisional basis, so that the effect of their relaxation could be considered at a later stage.

Five assumptions of particular importance will be restated here. It was assumed that the linkages of interest are constructed of traditional materials, with design stress levels not greatly in excess of those commonly applicable in the past; that the dominant modes of deflection are flexural rather than axial; that the drive shaft and input link are rigid; that the dominant source of excitation is the inertial loading associated with the nominal kinematic accelerations; and that the links are straight and symmetrical about a common plane.

The approximate methods: Subject to the five assumptions listed above, two important propositions were argued: that the natural frequencies of vibration of linkages would continue to be typically greater than 10 times the driving speed, and that the periodic variation of the nominal accelerations at the joints typically had a sharply declining harmonic spectrum.

For cases where these propositions were valid, it was shown that the deflections can be estimated to a good first approximation by treating the rigid-body inertial loads at any instant as though they are applied statically. If significant,

the axial loads in a binary link can be approximated by the mean of the rigid-body values at the joints.

For a more accurate prediction of the deflections, it was proposed that the total deflection be split up into the quasi-static deflection (as described above) and a dynamic error term. The advantage of this proposal, it was argued, is that the dynamic error in a given link is almost entirely associated with its fundamental (uncoupled) mode of deflection, so that only one mode per link need be considered. (In fact, this was demonstrated for a uniform link with no overhang, and it should be pointed out that in a link of very different form, the second uncoupled natural frequency could be much nearer the first; in this case its neglect would not be justified).

Under the conditions assumed, it was argued that the dynamic error for each link can normally be calculated to an appropriate level of accuracy by supposing that the joints are stationary and the link is subject only to transverse excitation. Exceptionally, coupling between adjacent links could be significant if the difference between their frequency ratios approximates to a small integer. A test of the latter intuitively-based prediction would be one appropriate task in any future investigation using a more exact analysis or an experimental linkage.

Although the high frequency part of the dynamic error term could be calculated by summing the effect of all harmonics near the natural frequency, an approximate short cut was devised whereby an "impulsive magnifier" is applied to the harmonic nearest resonance and the others are neglected. Implicit in this was the assumption that the resonant harmonic was of a similar magnitude to its neighbours.

Now the exceptions to the cases amenable to the above approximate methods will be considered in turn.

New materials: Linkages made of high strength alloys could be constructed in significantly lighter sections than has been the practice, and in some applications this could justify the greater cost. Frequency ratios of less than 10 may apply in such cases. Another possibility of increasing relevance is the replacement of metals by fibre-reinforced resins. For some materials in this group the term $[\varepsilon_i^{-1}(\mu/E_g)^{1/2}]$ in equation 17.a may be significantly smaller than for traditional materials, so that again lower values of Ω may apply. In either of these cases a full-scale kinetoelastodynamic analysis would be necessary for reliable prediction of the dynamic behaviour, and in the

second case the non-isotropicity of the material provides an additional difficulty. THOMPSON & GHANDI have tackled the latter problem with the aid of Hamilton's principle. It would be desirable to test such analyses by experimental studies on well-proportioned links run at the high speeds possible with these materials.

Axial deflections: The relationship between axial and flexural vibrations has led to some confusion in the past. Because, except for very stiff links, the first pinned-pinned axial mode has a natural frequency considerably higher than the first pinned-pinned bending mode, it has sometimes been erroneously concluded that axial vibrations can be neglected for that reason alone. Other investigators have gone to the other extreme and modelled flexural and axial effects in equal detail. In this investigation it was concluded that an intermediate approach is appropriate. The relevant axial modes, if any, will be those in which a link, undergoing small displacements in relation to its length, acts as a longitudinal spring carrying a mass at its end (representing other links) considerably heavier than itself. If the natural frequency of any such mode is of the same order as the bending natural frequencies, coupling may occur, and the approximate method described above is not applicable. However, in such cases the axial terms involving the distributed mass of the link undergoing the axial deflections may be neglected, avoiding many of the complications of a 'complete' analysis. (This conclusion rests on a consideration of the relative magnitudes of the terms, and further work is necessary to test the proposed technique: see p18-9, 38-9 and p43).

Drive deflections: The assumption that the driving link is rigid is essential to the simplified method of analysis discussed above, because it is the combination of fixed input motion and fixed link lengths that makes the trajectories of the mechanism joints independent of the vibrations, so that each link deflects with respect to its joints without interfering with its neighbours.

As the driving link can usually be designed in the form of an eccentric, or a disc-and-pin, the neglect of bending deflections can well be justified. Unfortunately, it was concluded that significant flexibility in the drive shaft and/or other drive system elements may often prove unavoidable, and this provides another important exception to the cases covered by the simplified method. The preliminary examination of such a case, with the links treated as rigid, was reviewed in the previous section.

It may be repeated that the combination of flexible links and flexible shafts deserves future study. In the same study, it would be appropriate to include external loads associated with the purpose of the mechanism, since in the cases referred to these would affect the drive link motion, and thereby the motion of all other links.

Discontinuous loads: The combination of the relatively large frequency ratios considered to be of interest and the often trivial magnitude found to characterise the corresponding harmonics of the ideal kinematic accelerations, suggested a basic change in research priorities. Rather than attempt to improve existing analyses of idealised links by retaining additional terms, it is contended that the main need is to include more realistic features in the basic model. In particular, any feature likely to cause discontinuous loading should be of interest, because at higher frequencies such loads dominate the spectra.

Such discontinuities could include the effects of motor speed controllers, friction, backlash, and external (functional) loads. The last may well be the most important source of vibration in linkages in use in industry, but their study in the context of basic research presents difficulties owing to the great variation in the nature of the loading from one application to the next. At least, a comparative study of the methods available for analysing the transient response of linkages to sudden changes of load would be valuable.

The magnitude of the effects of backlash ~~were~~ was estimated originally (p36-7) by a one-dimensional model that in the light of the subsequent discoveries must be regarded as questionable, even for order of magnitude calculations. Now that an understanding has been achieved of the behaviour of ludodynamic bearings under at least some conditions, the question of the level of vibration to be expected in links containing such bearings should be studied more fully. The method described in Section 4E for predicting the momentum exchange at impact may be of assistance here for the case of passage impact in bearings with relatively large clearances. Unfortunately the results presented as Annexe 4 cannot be used, because no distinction between passage and terminal impact was made in this tabulation.*

Perhaps the best argument for focusing attention on backlash was provided by the several experimental results which showed unexplained levels of vibration with a spectrum suggestive of discontinuous loading, although it is still not possible to say whether the speculative diagnosis of backlash as the cause was correct. In any case, the types of bearing concerned in these examples varied

*: Afterthought [Nov.'82]: The results can be used in conjunction with Fig 174·a, since if passage contact loss is there predicted, the impact magnitude prediction will relate to that contact loss.

considerably, including hydrodynamic and roller bearings as well as the ludodynamic type. Clearly, it would be desirable to understand the excitation generated at flypast points in each of these types of bearing.

Curved links etc: In one important respect the linkages usually studied, whether theoretically or experimentally, are not representative of a substantial fraction of the linkages in industrial use: the former are effectively one-dimensional, whereas the latter are frequently curved or stepped or bear some form of protuberance, in the plane of motion or otherwise. It was concluded that this provided an important field for future study, and provided a particularly suitable application for finite element methods.

9E: THE CONTROL OF LINKAGE MECHANISM VIBRATIONS

Since the preceding work had shown that link vibrations of the types studied were a function of the relevant nominal loads, the question of controlling these loads was posed. The use of auxiliary masses and springs was selected as a practical approach.

Auxiliary masses: It was shown that all the statically determinate nominal loads in a linkage at any instant are linearly related to certain fundamental parameters defining the distribution of the additional masses. (This generalised similar results obtained by previous investigators). The appropriate expression for frame shaking moment was shown to depend on whether the nominal constancy of speed was ensured by a flywheel or by a prime mover with 'stiff' torque/speed characteristics.

It was argued that, in typical problems, some of the physical constraints on the counterweight dimensions were necessarily active, and must therefore be treated explicitly. Accordingly, the use of disc counterweights with limits on the radius and thickness was assumed.

Matching of the target dynamic load values by the numerical minimisation of a weighted mean square error was shown to be a particularly efficient technique for synthesizing the counterweight dimensions and position coordinates, because a high proportion of the numerical operations required for evaluating the objective function need be performed once only at the start of the iterative process. The implementation of this technique, believed to be novel in this context, was reported to give highly satisfactory results in a case study.

For comparability with previous work, the case study was concerned with minimising shaking forces and moments. It is pertinent to add that the computer program concerned has recently been used for educational purposes. Four MSc students attempted to synthesize counterweights to minimize the driving torque fluctuation of a Watt's sixbar mechanism subject to 100% balancing of the shaking forces; upper bounds were also specified for the joint loads, one being active in practice. In this example complete convergence was not achieved in a practical number of iterations. However, the requirement of the engineer is not a formal minimum, but for a major improvement in the specified criterion of performance, and that was achieved in a practical manner in every case.

It should be noted that the effect of mass balancing on drive shaft vibrations is somewhat unpredictable. On the one hand, the parametric excitation is reduced along with the forcing term; on the other, the mean frequency ratio is reduced. A future examination of the actual effect in a realistic case would be illuminating.

Auxiliary springs: Attention was drawn to the diversity of possible applications and arrangements for auxiliary springs. A four-bar mechanism with a zero free-length tension spring between the coupler and frame links was taken as an example, and formulae were derived for the changes to the driving force fluctuation and joint loads due to the attachment of the spring. The synthesis of spring parameters to achieve a constant driving torque at six specified precision points was demonstrated.

In the main, this method for spring synthesis followed the lines of a method published by MATTHEW & TESAR (a,b), although the application to joint reactions was novel and an alternative criterion of torque smoothing was introduced. The major advance, however, was an answer to an important question left unanswered by the previous work, namely the optimal spacing of the precision points. Firstly, good reasons were given for choosing a set of equi-spaced points as a first approximation, a systematic search being required to choose the set with the best phase. Secondly, it was shown how to adapt a technique of kinematic synthesis introduced by FREUDENSTEIN, to respace the points iteratively towards a local optimum by the Chebyshev criterion.

In a case study this technique proved very effective, six iterations leading to a solution with a much improved predicted performance, as far as the nominal driving torque is concerned. It would be expected that the input link accelerations associated with shaft flexibility would also be reduced. Insufficient time was available to incorporate the effect of the optimal balancing spring in the Hill's equation program, so that this could be tested.

Future developments: It is considered that the work reviewed above overcame the main outstanding difficulties in the way of device synthesis for the 'traditional' applications of frame load and driving torque balancing. In the context of this thesis, the further application of most interest would be the synthesis of devices to reduce the severity of flypasts at ludodynamic joints, as an alternative to the 'force-form closed' bearings proposed by FAWCETT (cf p82).

Such an extension is not a simple matter, however, since the relevant expressions (such as $R_u^*/\dot{R}_v^{*2/3}$) are neither linear nor polynomial functions of the design parameters. One favourable factor is that the variation of the joints loads between flypasts can be disregarded. Thus one possible approach is to start with a design optimized by other criteria, and then to try to shift the load curve away from the origin at the most critical flypast(s) by small changes to the design. This might be achieved by setting an approximate non-zero target value for one or both components of the load at this point in the cycle with a large weighting factor, or by specifying a series of closely-spaced precision points on the load vector locus.

Another practical approach might be to establish a set of almost equally good solutions by the other criteria, and to use the flypast parameters as a final 'filter' to eliminate unsatisfactory designs. This would be consistent with the 'sequential filtering' technique advocated by SPITZNAGEL & TESAR.

As a postscript (September 1982), it is of interest that O. Perera & W. Seering have just published an alternative technique for tackling this problem, in ASME paper 82-DET-134. A spring is synthesized, for attachment to a four-bar linkage, that maintains one component of the contact force above a specified value throughout the cycle. In this writer's view, the effectiveness of this technique depends on the chosen component being in the general direction of R_u^* at the most critical flypast.

9F: SUMMARY OF CONCLUSIONS

Analysis: Under plausible specified conditions, elastic deflections in planar linkage mechanisms can be found to an adequate first approximation by quasi-static methods, with axial loads approximated by the mean of their end-point values where relevant.

The dynamic error associated with the quasi-static approximation can normally be estimated, under the conditions assumed, by considering only the first uncoupled bending mode per link, excited only by transverse inertial loading. Exceptionally, coupling may be significant if the natural frequencies associated with adjacent links differ by a small integral multiple of the driving speed (+). It is advisable to apply an 'impulsive magnifier' as well as the conventional 'dynamic magnifier' to the resonant component of the dynamic error.

The above methods are not reliable if non-traditional materials with high design stress or strain levels are used (+); if axial vibrations or drive link vibrations occur at natural frequencies of the same order as the natural frequencies referred to above; if significant sources of discontinuous loading are present, including drive system irregularities, joint backlash, and impulsive external loading (+); or if the links are not straight or act in different parallel planes.

Significant axial vibrations are possible if components of widely diverse inertia and lengths are used. In these cases such vibrations can reasonably be estimated by treating the lighter links as massless springs (+).

Critical speeds in shafts driving systems of cyclically varying effective inertia correspond closely to integral values of the cyclic mean of the instantaneous frequency ratio. Even between critical speeds, the accelerations imposed on the links when the drive is flexible can have a far greater high-frequency content than if the drive was rigid.

The correct method for calculating the total moment transmitted to the ground due to the inertia loads in a constant-speed linkage mechanism depends on whether the constant speed is maintained by virtue of high inertia or high stiffness of the drive system.

Backlash: In joints with clearance and little if any liquid lubricant, significant impulsive loads may be generated during the rapid displacement of the contact point when the nominal contact force vector passes near the origin, even if contact is maintained throughout. If contact loss does occur in these

circumstances, it may occur either before or after the first load pulse ('passage' and 'terminal' loss respectively.)

For larger clearances, the conditions of passage contact loss can be adequately expressed as a function of three dimensionless parameters in accordance with the simple theory presented in Chapter 4.

The air film in bearings with small clearances has a highly significant effect on the observed behaviour (+). Possibly for this reason, the conditions of passage contact loss in such bearings hardly differ from those for larger clearances, contrary to the theory (+).

Terminal contact loss is in part a consequence of the elastic properties of the components (+), and is not correctly predicted by the theory.

The empirical criterion for contact loss proposed by Earles and Wu is not valid under the conditions of the experiments reported here.

The measured elastic compliance of the contacting surfaces in a bearing was found to be considerably lower and less linear than predicted by Hertzian theory (+).

Synthesis: All the loads in a rigid mechanism with ideal joints and drive can be expressed as linear functions of certain parameters defining the mass distribution. In consequence, counterweights can be efficiently synthesised to modify the dynamic performance of a linkage by the numerical minimisation of the weighted mean square error with respect to the desired performance, subject to constraints on the counterweight radii, thicknesses and location coordinates.

If a zero free-length tension spring is attached between the coupler and frame link of a four-bar mechanism, the effects on the joint loads as well as the driving torque can be expressed in a form suitable for precision point synthesis. A method has been developed for choosing precision points to match a desired performance curve over a complete cycle of operation, the solution being locally optimal in the Chebyshev sense.

Future research: Each phase of the investigation has raised questions deserving further study, including those indicated thus (+) above. Other important topics for further study are the effects of misalignment on joint behaviour and synthesis to avoid contact loss at joints.

CHAPTER 10

APPENDICES

Section 10B is reproduced from Trans. ASME, Journal of Applied Mechanics, 46, p 716-7.

Sections 10A and 10C-D are in part based on material published in HAINES(a).

Sections 10H-K have been published as part of HAINES(c), except that page A18 is suitably modified.

The remaining sections of this chapter of collected appendices have not been published before in any form.

Nomenclature: The principal nomenclature for each appendix is consistent with that for the chapter to which the appendix refers, namely:-

10A - G : Chapter 2
10H - L : Chapter 4
10M - N : Chapter 5
10P - R : Chapter 6
10S - T : Chapter 7
10U : Chapter 8

10A: THE INFLUENCE OF DESIGN SPEED AND STRESS LEVEL ON THE FREQUENCY RATIO. (APPENDIX TO SECTION 2C, page 17)

(i) Given beam mass m, length L, transverse acceleration $\bar{A}_m$, height $2h$, rigid body bending moment M_m at midpoint:

$$M_m = m\bar{A}_m L/8 \qquad \cdot a$$

$$\therefore \text{ stress } \sigma = hm\bar{A}_m L/8I$$

$$= (\mu \bar{A}_m L/8g)(h/K^2) \leqslant \sigma_l \quad \Big| \; m = \mu a L/g \,,\; I = aK^2 \qquad \cdot b$$

Natural frequency of bending, by THOMPSON(1):

$$\omega_1 = \frac{\pi^2}{L^2}\sqrt{\frac{EIL}{m}} = K\left(\frac{\pi^2}{L^2}\sqrt{\frac{Eg}{\mu}}\right) \qquad \cdot c$$

From $\cdot b, \cdot c$ $$\omega_1 \geqslant \left(\frac{\pi^2}{8}\right)\left(\frac{h}{K}\right)\sqrt{\frac{E\mu}{g}}\,\frac{\bar{A}}{\sigma_l} \qquad \cdot d$$

$$\therefore \quad \Omega \geqslant \left(\frac{\pi^2}{8}\right)\left(\frac{h}{K}\right)\left(\frac{1}{\varepsilon_l}\right)\left(\sqrt{\frac{\mu}{Eg}}\right)\left(\frac{\bar{A}}{\omega^2}\right)\omega \quad \Big| \; \Omega = \omega_1/\omega,\; \varepsilon_l = \sigma_l/E \qquad \cdot e$$

(ii) Transverse acceleration $C_1\omega^2$ and angular acceleration $B\omega^2$ experienced by mass m_w overhung by l_w causes bending moment:

$$M = m_w C_1 \omega^2 l_w + m_w K_w^2 B\omega^2 \qquad \cdot f$$

$$\therefore \text{ stress } \sigma_b = h m_w l_w \omega^2 C/I \leqslant \sigma_l \quad \Big| \; C = [C_1 + BK_w^2/l_w]_{\text{maximum}} \qquad \cdot g$$

Frequency $$\omega_1 = \sqrt{3EI/(mK_f^2 + m_w l_w^2)L} = h^2\sqrt{3E(I/h^4)/(mK_w^2 + m_w l_w^2)L} \qquad \cdot h$$

$$\cdot g, \cdot h \rightarrow \quad \Omega \geqslant (m_w l_w)^{2/3}\,(Lm_w(K_w^2 + l_w^2))^{-1/2}\,(I/h^4)^{-1/6} E^{-1/6} \varepsilon_l^{-2/3} C^{2/3} \qquad \cdot i$$

(iii) Peak rigid body stress in drive-shaft, radius r_s:

$$\tau \propto \omega^2/r_s^3 \quad \Big| \text{ linkage unchanged} \qquad \cdot j$$

$$\omega_{1T}^2 \propto r_s^4 \propto \omega^{8/3} \quad \Big| \; \tau = \tau_l \qquad \cdot k$$

$$\therefore \quad \Omega \propto \omega^{1/3} \quad \Big| \; \tau \cdot \tau_l,\; \Omega = \omega_{1T}/\omega. \qquad \cdot l$$

(iv) Mass m, given acceleration $\bar{A}_a$ by rod, area a, gives rise to stress:

$$\sigma = \bar{A}_a m/a \leq \sigma_l \qquad \cdot a$$

Longitudinal natural frequency:

$$\omega_{1L} = \sqrt{(Ea/Lm)} \geq \sqrt{(E\bar{A}_a/L\sigma_l)} \qquad \cdot b$$

$$\therefore \qquad \Omega \geq \sqrt{C/L\varepsilon_l} \qquad \left| \Omega = \omega_{1L}/\omega_1 \;\; C = \bar{A}_a/\omega^2 \right. \qquad \cdot c$$

10B: UPPER BOUNDS FOR AMPLITUDES OF HARMONIC COMPONENTS OF EXCITATION (APPENDIX TO SECTION 2D, page 20).

This Appendix is reproduced from the Brief Note published in the Transactions of ASME, Journal of Applied Mechanics, Vol. 46, p 716-7 (September 1979).

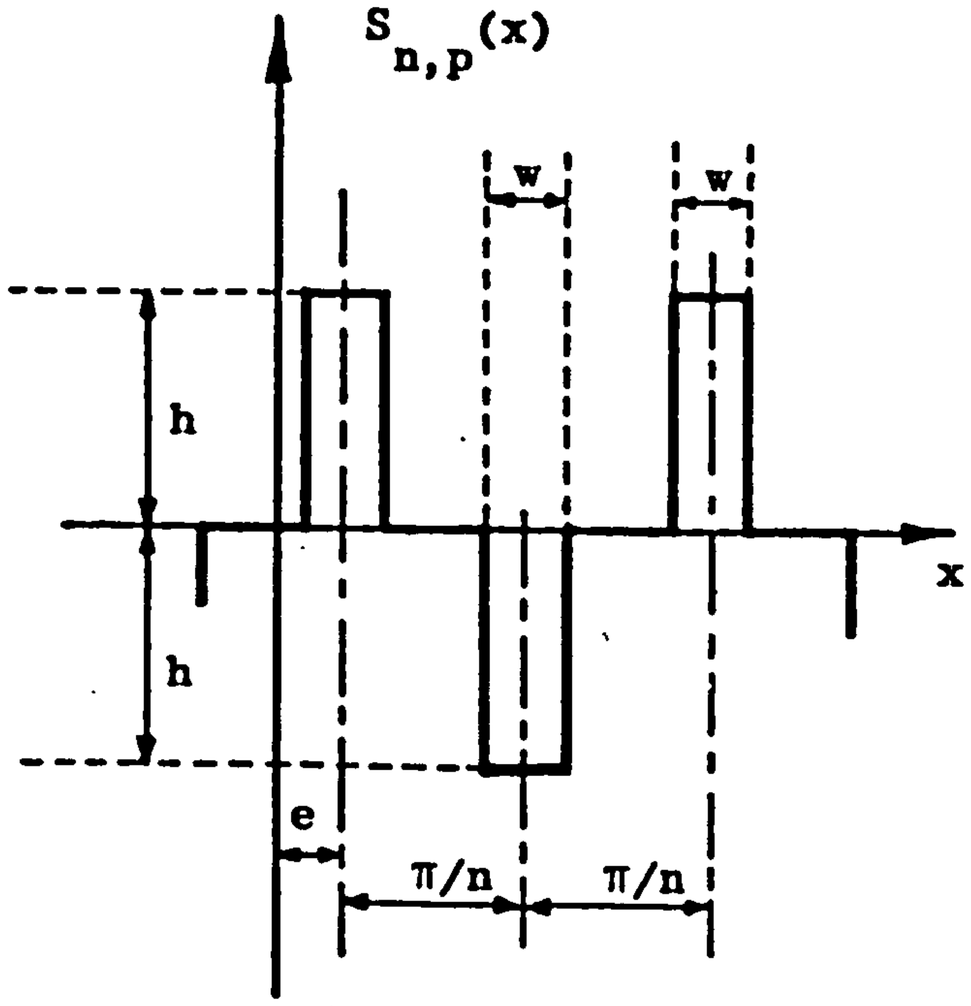

Fig. 1 Periodic waveform $S_{n,p}(x)$

The amplitude of the nth harmonic component of a known waveform has upper bounds which can be derived from inspection of the waveform. By indicating when the Fourier analysis of (for example) vibratory excitations can be circumvented, this technique may usefully shorten iterative or desk-top design calculations.

Introduction

The analysis of a known periodic waveform into harmonic components is a classic technique presenting no difficulties in principle for the "well-behaved" waveforms obtained, for example, in most problems of mechanical vibration analysis. It is, however, somewhat tedious for hand calculations, and for use in design synthesis techniques of an iterative nature. In these circumstances it may be useful to establish some upper bound for the amplitude (a_n) of the nth harmonic of a defined excitation by inspection of its waveform. If this bound is less than some threshold value, further calculation could then be omitted.

It has long been known [see, for example, Courant and Hilbert [1]] that for a waveform with period 2π and at least q bounded derivatives, (assumed to be piecewise continuous) there exist upper bounds on (a_n) of the form

$$[0 \leqslant p \leqslant q+1:] \quad a_n \leqslant A_p n^{-p} \tag{1}$$

where A_0, A_1, etc., are constant coefficients.

What is required is a convenient algorithm giving appropriate values for A_p. Such an algorithm is given here, which despite its elementary nature has not previously been published to the author's knowledge. Use is made of the concept of the "cumulative range" of a periodic waveform. This is defined as the sum of the ordinates at all local maxima less the sum of the ordinates at all local minima, within a single period. R_{p-1} denotes the cumulative range of $f^{(p-1)}(x)$, and R'_p denotes the range of $f^{(p)}(x)$, where $f^{(p)}(x)$ signifies the p'th derivative of the periodic function $f(x)$.

Derivation of Upper Bounds

First, write the Fourier expansion of $f(x)$ in the form

$$f(x) = a_0 + \sum_{n=1}^{\infty} a_n \cos(nx - l_n) \tag{2}$$

Differentiating p times, we obtain

$$[p \geqslant 0:] \quad f^{(p)}(x) = \sum_{n=1}^{\infty} (n^p a_n) \cos(nx - l_n + p\pi/2) \tag{3}$$

Comparing coefficients with those obtained [2] from the Fourier expansion of $f^{(p)}x$,

$$[n > 0, p \geqslant 0:] \quad (n^{(p)} a_n) = \pi^{-1} \times \int_0^{2\pi} f^p(x) \cos(nx - l_n + p\pi/2)dx \tag{4}$$

Second, the cumulative range of $g(x)[\equiv \int f(x)dx]$ may be seen, by piecewise integration between turning points, to be given by

$$R_{-1} = \frac{1}{2} \int_{x=0}^{2\pi} |dg(x)|;$$

that is,

$$2R_{-1} = \int_0^{2\pi} |f(x)|\, dx.$$

In words the latter integral is the area enclosed by $f(x)$ and the x-axis: call this the "enclosed area of $f(x)$."

Then a periodic waveform $S_{n,p}(x)$ of the form shown in Fig. , with $h = R'_p/2$, $w = 2R_{p-1}/nR'_p$, and $e = (l_n - p\pi/2)/n$, has an enclosed area equal to $2R_{p-1}$ and thus to the enclosed area of $f^{(p)}(x)$; moreover the range of $S_{n,p}(x)$ is equal to R'_p, the range of $f^{(p)}(x)$. By considering possible waveforms $f^{(p)}(x)$ as variations from $S_{n,p}(x)$ without any change of enclosed area or of range, it may be seen that the integral in equation (4) has a maximum value, namely, $2R'_p \sin(R_{p-1}/R'_p)$, when $f^{(p)}(x) \equiv S_{n,p}(x)$. Thus

$$a_n \leqslant 2\pi^{-1} R'_p \sin(R_{p-1}/R'_p) n^{-p} \tag{5}$$

Choice of Coefficients

From equation (5) it may be seen that equation (1) is true if

$$A_p = 2\pi^{-1} R'_p \sin(R_{p-1}/R'_p) \tag{6}$$

(Note that by the definitions of R and R' the angle in brackets

cannot exceed $\pi/2$ rad, the value when $f^{(p)}(x)$ is a square wave of period 2π). Since $\sin(x) < x$ and $\sin(x) < 1$, we can obtain two simpler formulas that give values that are also permissible, albeit less constraining

$$A_p = 2\pi^{-1}R'_p \tag{7}$$

$$A_p = 2\pi^{-1}R_{p-1} \tag{8}$$

In practice the lower of the two latter values is often very nearly as low as that given by equation (6), being never more than 19 percent higher (the case when $R'_1 = R_{p-1}$).

The values R_0, R'_0, R_1, and R'_1 can easily be found by inspection of the waveform $f(x)$, yielding values for A_0, A_1, and A_2 to give by equation (1) upper bounds on (a_n) proportional to n^0, n^{-1}, and n^{-2}, respectively.

If derivatives of $f(x)$ have already been calculated for other purposes, equations (6)–(8) with (1), define curves that bound (a_n) more tightly for higher orders.

Application

Fig. 2 shows the angular acceleration of the rocker of a four bar chain, with crank: coupler: rocker: frame link lengths in the ratio 1: 2:2:2 and crank running at constant speed. The maximum and minimum gradients of this curve are estimated graphically as shown, and give a cumulative range $R_1 + 55000$ acceleration units per radian. Thus $A_2 + 35000$ so that the amplitude of the fifth harmonic (for example) is immediately known to be no more than 1400. In fact, Fourier analysis shows it to be 990 in this case. (The bound using A_2 is increasingly conservative for orders greater than 5).

Since the calculation of the rocker acceleration is a relatively simple matter using a programmable calculator, this entire analysis is suitable for desk-top application. The author has also used the technique as an aid to a more general assessment of the limits of quasi-static analysis [3].

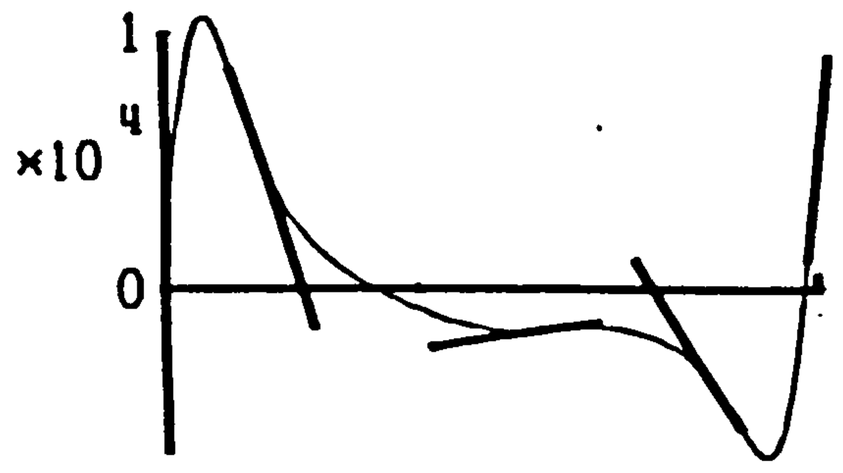

Fig. 2 Periodic excitation, showing cumulative range of gradient

Conclusion

A useful algorithm for determining upper bounds for the harmonic amplitudes (a_n) of a periodic waveform is as follows:

Scale the abscissa of the waveform so that the period is 2π. Note the range (R'_0) and cumulative range (R_0) of the waveform, and the cumulative range (R_1) of its gradient. Then (a_n) is less than the least of $(2R'_0/\pi)$, $(2R_0/\pi n)$, $(2R_1/\pi n^2)$. If this limit is between 100 and 120 percent of the threshold for the purpose in hand, then note the range (R'_1) of the gradient, and calculate a closer limit of $(2R'_1 \sin(R_0/R'_1)/\pi n)$. Closer bounds can be found for the higher orders if higher derivatives of the waveform are available.

References:

[1] COURANT & HILBERT, p 74.

[2] COURANT & HILBERT, pp 69-70.

[3] HAINES(a).

10C: . DEVELOPMENT OF APPROXIMATE EQUATIONS FOR COUPLER-LINK VIBRATIONS. (APPENDIX TO SECTION 2F)

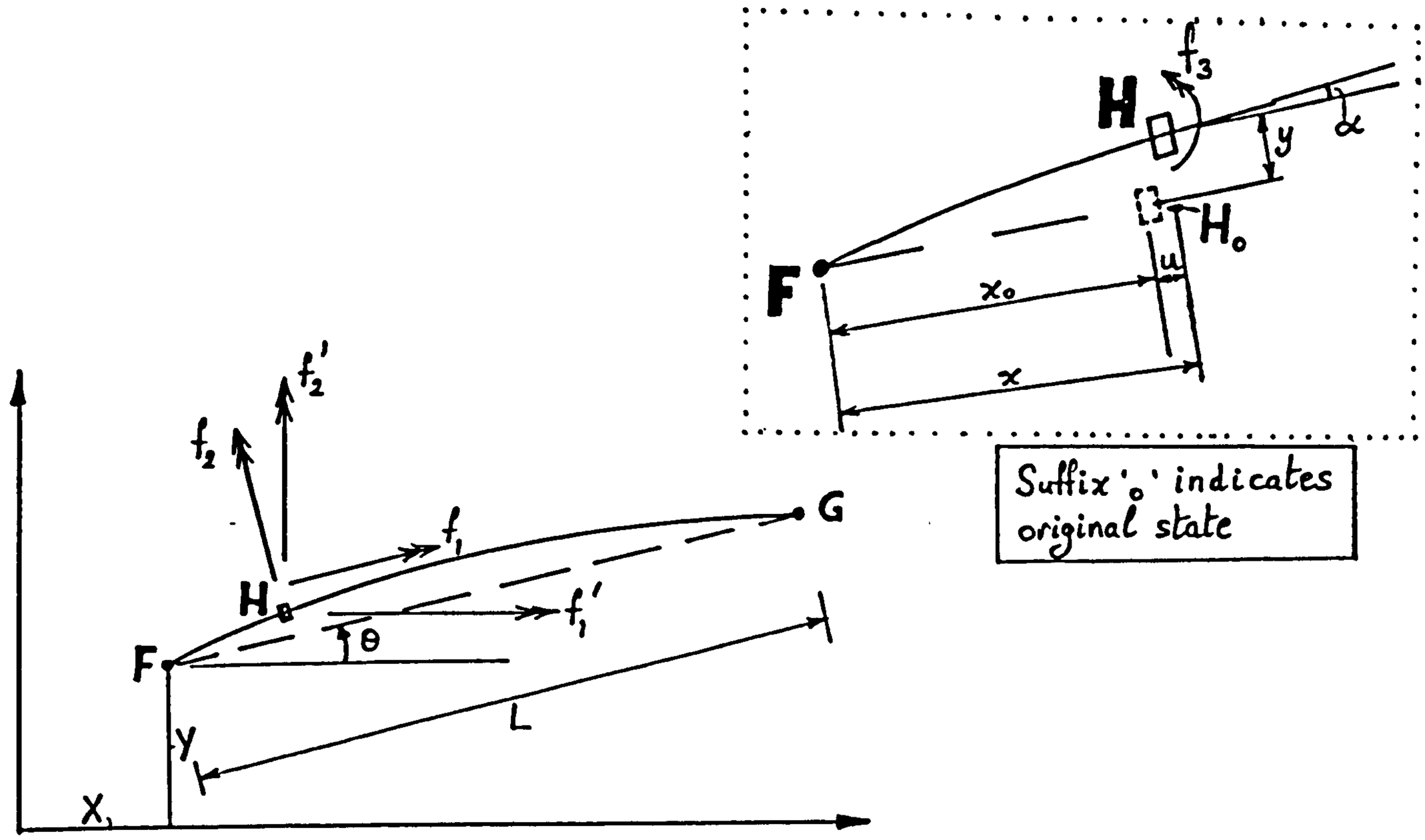

A5·a: FLEXIBLE LINK - NOMENCLATURE

Position: $X_F + iY_F + (x+iy)\exp(i\theta)$ [Note $\dot{x} \equiv \dot{u}$] ·b

Acceleration:

$$f_1' + if_2' = \ddot{X}_F + i\ddot{Y}_F + (\ddot{u} + i\ddot{y})\exp(i\theta) + i(x+iy)\exp(i\theta) - (x+iy)\dot{\theta}^2\exp(i\theta) + 2i(\dot{u}+i\dot{y})\dot{\theta}\exp(i\theta) \quad \cdot c$$

where ' indicates $\partial/\partial t$ for constant x_o.

$$f_1 + if_2 = (f_1' + if_2')\exp(i\theta) \quad \cdot d$$

$$\therefore \quad \left.\begin{aligned} f_1 &= \ddot{X}_F\cos\theta + \ddot{Y}_F\sin\theta - x\dot{\theta}^2 + \ddot{u} - y\ddot{\theta} - 2\dot{y}\dot{\theta} \\ f_2 &= -\ddot{X}_F\sin\theta + \ddot{Y}_F\cos\theta + x\ddot{\theta} - \ddot{y} - y\dot{\theta}^2 + \underline{2\dot{u}\dot{\theta}} \end{aligned}\right\} \cdot e$$

neglect pro tem.

Let $$\left.\begin{aligned} A_m &\equiv (-\ddot{X}_F\sin\theta + \ddot{Y}_F\cos\theta + L\ddot{\theta}/2) \\ A_e &\equiv -L\ddot{\theta}/2 \end{aligned}\right\} \cdot f$$

Then $$f_2 = A_m + A_e(1 - 2x/L) - \ddot{y} - y\dot{\theta}^2 . \quad \cdot g$$

Also $$f_3 = \ddot{\theta} + \ddot{\alpha} \quad \cdot h$$
$$= \ddot{\alpha} - 2A_e/L$$

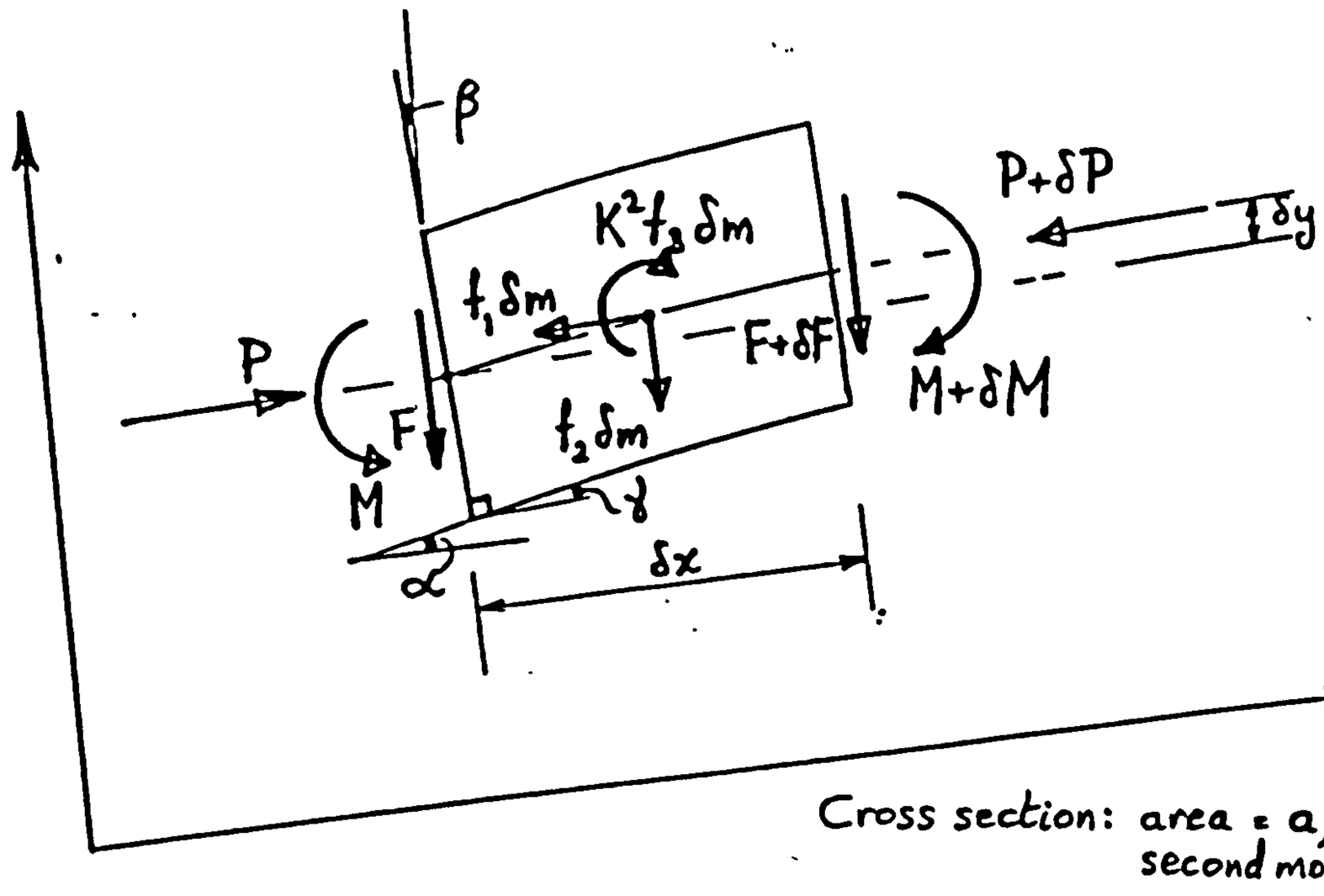

ELEMENT 'H'

A6·a: ELEMENT 'H' - NOMENCLATURE

$$\delta m = m\,\delta x_o/L_o \triangleq m\,\delta x/L \quad \text{where } m = \text{mass of FG} \qquad \cdot b$$

$$\therefore (\uparrow) \quad \partial S/\partial x = f_2\, m/L$$
$$(\rightarrow) \quad \partial P/\partial x = -f_1 m/L$$
$$(\circlearrowleft) \quad \partial M/\partial x = F + P(\partial y/\partial x) - K^2 m\, f_3/L \qquad \cdot c$$

$$\therefore \quad \partial^2 M/\partial x^2 = f_2 m/L + P\,\partial^2 y/\partial x^2 \underbrace{- K^2 m/L\;\partial f_3/\partial x - m f_1/L\;\partial y/\partial x}_{\text{neglect pro tem.}} \qquad \cdot d$$

Taking $\sin\alpha \triangleq \alpha$, $\cos\alpha \triangleq 1$ (etc.) $\qquad \cdot e$

$$\gamma = (F + P\beta)/Ga$$
$$\partial u/\partial x = -[P/aE + \alpha^2/2]$$
$$\partial\beta/\partial x = -M/EI \qquad \cdot f$$

Assume axial and shear deformations are negligible;

thus $x \triangleq x_o$, $L \triangleq L_o$, $\alpha \triangleq \beta$ $\qquad \cdot g$

$$\therefore \quad \partial^2 y/\partial x^2 \triangleq \partial\alpha/\partial x \triangleq -M/EI \qquad \cdot h$$

$$\therefore \quad \partial^2 M/\partial x^2 \triangleq -EI\,\partial^4 y/\partial x^4 \qquad \cdot i$$

From . A5·g, A6·d, A6·i:

$$E I \partial^4 y/\partial x^4 + A_m m/L + A_e m/L\,[1-2x/L] + m/L\,[\ddot{y}+y\dot{\theta}^2] + P\partial^2 y/\partial x^2 = 0 \qquad \cdot a$$

Let $y = \sum_{k=1}^{\infty}[y_k \sin(k\pi x/L)]$ (check: $x=0 \rightarrow y=0,\ \ddot{y}=0$). ·b

Neglect variation of P with x, taking the mean of the values at $x=0$ & $x=L$.

Now $A_m m/L \cdot \sum_{k=1}^{\infty}[2/k\pi(1-\cos k\pi)(\sin k\pi x/L)] = \begin{cases} A_m m/L & \big|_{0<x<L} \\ 0 & \big|_{\substack{x=0 \\ x=L}} \end{cases}$ 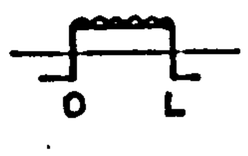

and $A_e m/L \cdot \sum_{k=1}^{\infty}[2/k\pi(1+\cos k\pi)(\sin k\pi x/L)] = \begin{cases} A_e m/L\,[1-2x/L] & \big|_{0<x<L} \\ 0 & \big|_{\substack{x=0 \\ x=L}} \end{cases}$ 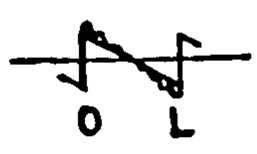 ·c

(Fourier series expansions of square wave, saw tooth wave respectively).

$$\therefore \quad A_m m/L + A_e m/L\,(1-2x/L) = \sum_{k=1}^{\infty}[(4A_k m/k\pi L)\sin k\pi x/L] \Big|_{0<x<L} \qquad \cdot d$$

where $A_k \equiv \begin{cases} A_m & \big|_{k\ \text{odd}} \\ A_e & \big|_{k\ \text{even}} \end{cases}$. ·e

From ·a, ·b, ·d, ·e (equating coefficients)

$$m\ddot{y}_k/L + m y_k \dot{\theta}^2/L + [(EIk^4\pi^4/L^4) - (Pk^2\pi^2/L^2)]y_k = 4A_k m/k\pi L \qquad \cdot f$$

that is $\ddot{y}_k + \omega^2\Omega^2 k^4 (1-P/k^2P_c) y_k + \underbrace{\dot{\theta}^2 y_k}_{\text{neglect pro tem.}} = 4A_k/\pi k$ ·g

where $\omega\Omega = (\pi^2/L^2)\sqrt{EIL/m}$ ·h

and $P_c = \pi^2 EI/L^2$. ·i

Let $y_{ks} = y_k \big|_{\ddot{y}_k \rightarrow 0}$ (quasi-static solution).

Then $\omega^2\Omega^2 k^4 (1-\underbrace{P/k^2P_c}_{\text{neglect pro tem.}}) y_{ks} = 4A_k/\pi k$ ·j

Let $z_k \equiv y_k - y_{ks}$ ·k

and include a small damping term;

then $\ddot{z}_k + 2\omega\Omega k^2 c_k \dot{z}_k + \omega^2\Omega^2 k^4 z_k = -4\ddot{A}_k/(\pi k^5 \omega^2\Omega^2)$. ·l

Expand $$z_k = \sum_{j=0}^{\infty}[z_{kj}\exp(i(j\omega t - \kappa_j))] \qquad |i^2=-1 \qquad \cdot a$$

and $$A_k = \sum_{j=0}^{\infty}[A_{kj}\exp(i(j\omega t - \lambda_j))] \qquad \cdot b$$

Substituting in A 7.ℓ and equating coefficients of $\exp(ij\omega t)$

$$[-\omega^2 j^2 + 2ij\omega^2\Omega k^2 c_k + \omega^2\Omega^2 k^4]z_{kj}\exp(-i\kappa_j) = [4j^2/k^5\pi\Omega^2]A_{kj}\exp(-i\lambda_j) \qquad \cdot c$$

$$\therefore \quad z_{kj} = [4j^2/\pi\omega^2\Omega^4 k^9]D_{kj}A_{kj} \qquad |D_{kj} = |[1-(i/\Omega k^2)^2 + (2c_k j/\Omega k^2)i]|^{-1} \qquad \cdot d$$

Now $\bar{y}_s \doteqdot y_{1s}$

so A7.j$\rightarrow$ $\bar{y}_s \doteqdot 4\bar{A}/\pi\omega^2\Omega^2$ $\cdot e$

$$\therefore \quad \frac{z_{kj}}{\bar{y}_s} \doteqdot \frac{j^2}{\Omega^2 k^9}\,\frac{A_{kj}D_{kj}}{\bar{A}} \qquad \left|\begin{array}{l} A_{kj} = A_{mj}\ (k\ \text{odd}) \\ A_{kj} = A_{ej}\ (k\ \text{even}) \end{array}\right. \qquad \cdot f$$

10 D: <u>THE EFFECT ON RESONANT VIBRATIONS OF AN IMPULSE-LIKE COMPONENT IN THE PERIODIC EXCITATION</u> (APPENDIX TO SECTION 2F, page 25-6)

This appendix concerns a representative system comprising a mass m on a spring of stiffness S with damping factor c, subject to a periodic impulse Π at circular frequency $\Omega\omega_1$ where $\omega_1^2 = S/M$ .a

It is desired to find the peak deflection $(\bar{z})$ in relation to the amplitude (z_r) of the resonant harmonic (see Figure .h).

The response between impulses takes the textbook form:

$$z(t) = \exp(-c\omega_1 t)(v_1 \cos \omega_1 t\sqrt{1-c^2} + v_2 \sin \omega_1 t\sqrt{1-c^2}) \quad .b$$

Let $\Omega = \sqrt{1-c^2}/N$ (resonant case: N integral, $c^2 \ll 1$) .c

Now $z(0) = z(2\pi/\Omega\omega_1)$ (steady state solution)

and $\dot{z}(0) = \dot{z}(2\pi/\Omega\omega) + \Pi/m$ (conservation of momentum). } .d

Therefore $v_1 = 0$

and $v_2 = \Pi/[\omega_1 m\sqrt{1-c^2}(1-\exp(-2\pi c/\Omega))]$ } .e

so that $\bar{z} \doteq \Pi/[\omega_1 m(1-\exp(-2\pi c/\Omega))]$

By Fourier analysis, resonant component of excitation is given by $\Pi\Omega\omega_1/\pi$ giving rise to a quasi-static deflection $\Pi\Omega\omega_1/\pi S$

Thus $z_r = \Pi\Omega\omega_1/2\pi Sc$ (dynamic magnifier = $1/2c$). .f

Therefore $$\frac{\bar{z}}{z_r} \doteq \frac{2\pi c/\Omega}{1-\exp(-2\pi c/\Omega)} \Bigg|_{c^2 \ll 1} \quad .g$$

This expression may be regarded as defining an "impulsive magnifier" $D_I = \bar{z}/z_r$ by which the resonant amplitude must be multiplied to obtain the peak dynamic error in the limiting case that the high-frequency excitation approaches the form of a periodic impulse.

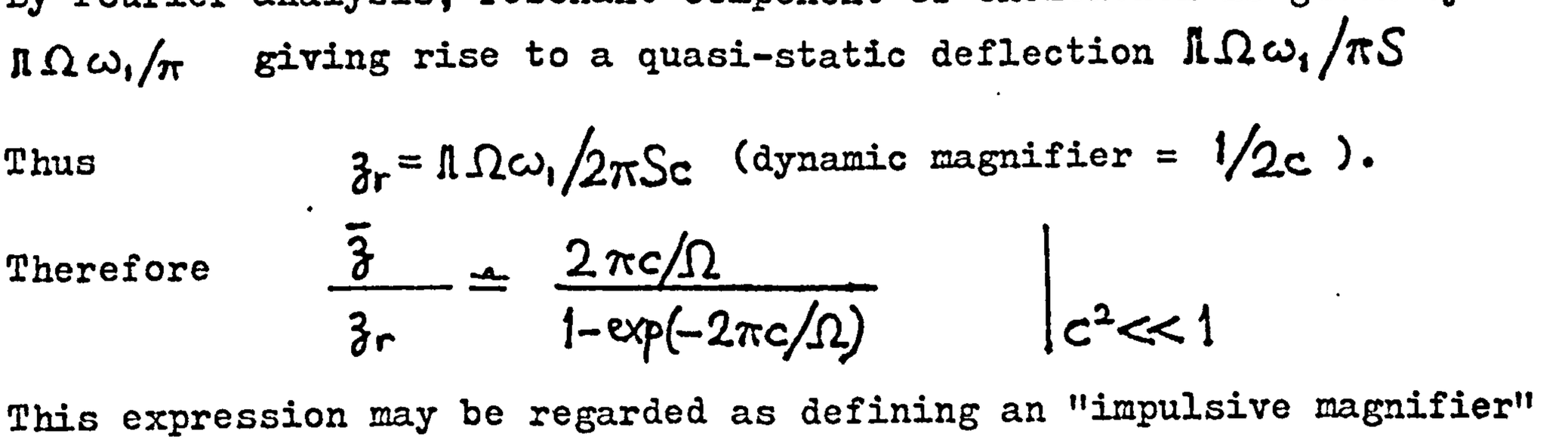

Response to a repeated impulse .h

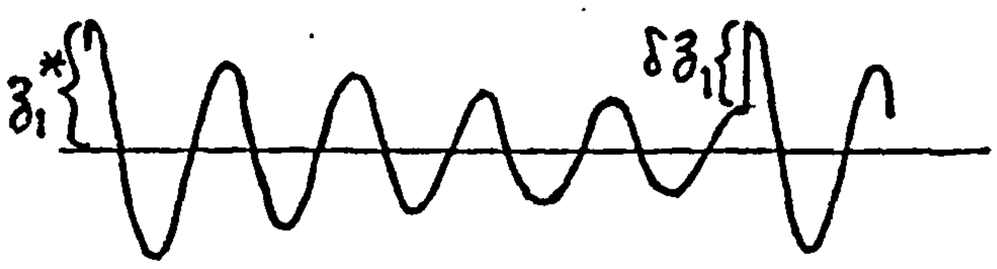

A10·a: Effect of periodic step in end-load (resonant case).

10E: THE EFFECT OF A STEP CHANGE IN THE END LOAD ON COUPLER VIBRATIONS. (APPENDIX TO SECTION 2G, page 29)

Consider a pinned-pinned beam with quasi-static first-mode transverse deflection (y_{1s}/R_1) at the instant when a once-per-cycle step change in the end load from P to $P+\delta P$ occurs; y_{1s} is the corresponding deflection in the absence of end-load. Since H_1 equals $1-(P/P_c)$ (see Section 2G), H_1 changes by $-\delta P/P_c$, and thus (y_{1s}/H_1) changes by $(y_{1s}/H_1^2)(\delta P/P_c)$ approximately, for small $(\delta P/P_c)$.

By virtue of the step change in the end load, the steady state dynamic deflection will differ from (y_{1s}/H_1) by a fluctuating amount, z_1, say. Since the total deflection cannot change instantaneously, there must be a step change δz_1 in z_1 at the instant in question, equal in magnitude to the change in (y_{1s}/H_1), that is $|\delta z_1| = |(y_{1s}/H_1^2)(\delta P/P_c)|$. In the resonant case, this change is in phase with the residual vibration from previous cycles, so z_1 increases from $(z_1^* - \delta z_1)$ (say) to (z_1^*) (see Figure .a).

Between the step changes, the amplitude of oscillation of z_1 dies away. The actual waveform through the cycle will be affected by slow changes in end-load between the steps, but these changes will not greatly affect the total energy dissipation over the cycle, so it may be assumed, as in the constant end-load case, that z_1 falls to $(z_1^* - \delta z_1 =)\ z_1^* \exp(-2\pi\Omega c)$, where c is the damping ratio and Ω the mean frequency ratio over the cycle, as in Chapter 2. Therefore,

$$z_1^* = \delta z_1 / (1 - \exp(-2\pi\Omega c)) \qquad .b$$

The step change in P gives rise to harmonics $P_j = \delta P/\pi j$, so that δ_1 can be written $(\pi j P_j)(y_{1s}/H_1^2 P_c)$ or equivalently $(\pi j H_{1j})(y_{1s}/H_1^2)$. Then the peak dynamic error z_1^* can be written as

$$z_1^* = (\pi j H_{1j})(y_{1s}/H_1^2)/(1 - \exp(-2\pi\Omega c)) \qquad .c$$

In the worst case y_{1s} is equal to its peak value $\bar{y}_{1s}$ and H_1 equals its minimum value 0·75. The error normalised with respect to the peak quasi-static deflection $(\bar{y}_{1s}/H_1)$ is then

$$[z_1^* H_1/\bar{y}_{1s}] = (\pi j H_{1j}/0{\cdot}75)/(1-\exp(-2\pi\Omega c), \approx 9 j H_{1j} \Big|_{c=.01}^{\Omega=10} \qquad .d$$

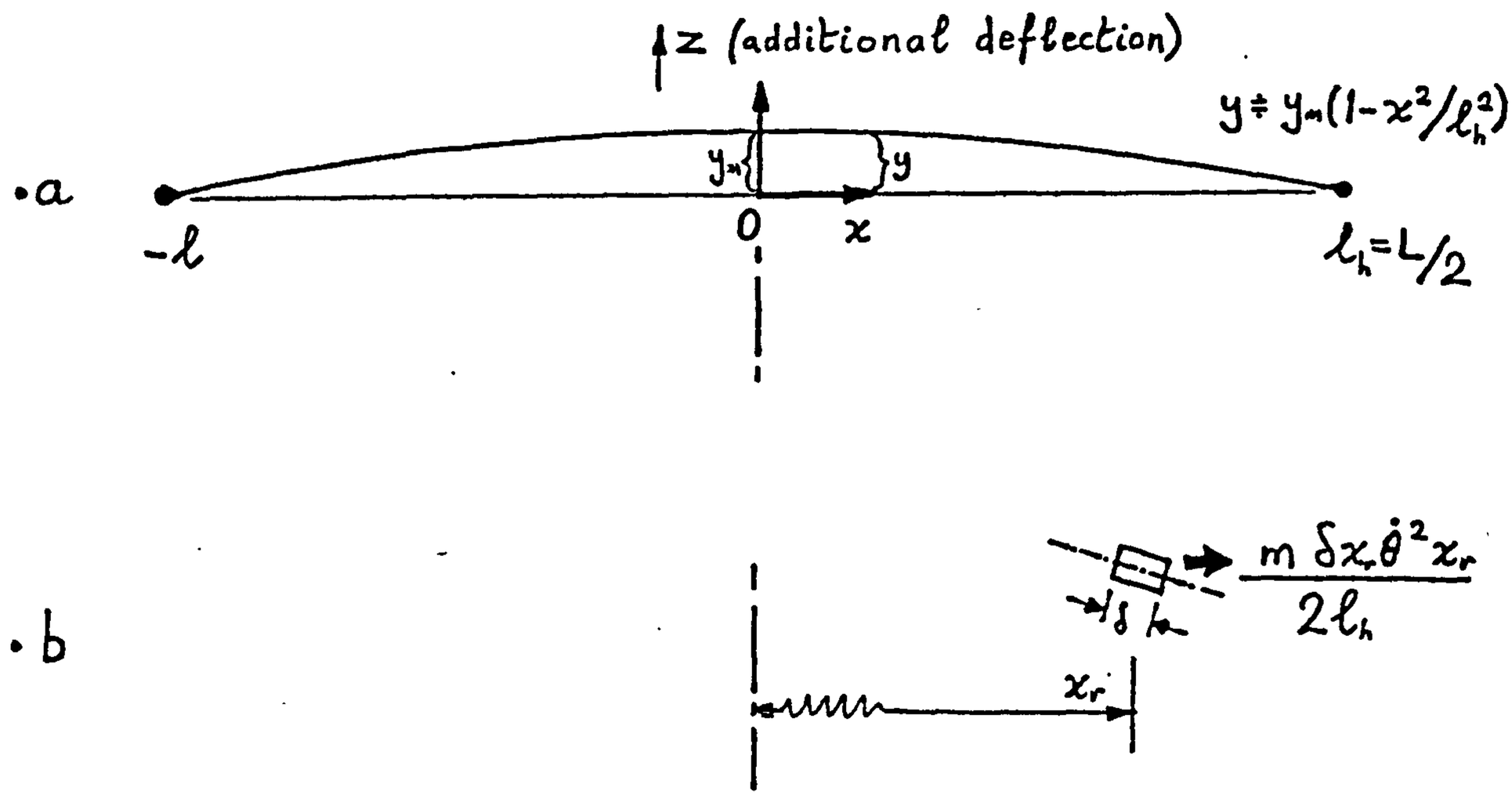

All • a/b: <u>Inertial load on deflected beam due to rotation.</u>

10 F: THE EFFECT OF ROTATION ON A SLIGHTLY CURVED BEAM.

(APPENDIX TO SECTION 2G, page 30)

Problem: A uniform beam of length $L = 2\ell_h$ is slightly curved in the plane of motion so that the deflection y is given approximately by $y = y_m(1 - x^2/\ell_h^2)$ where x is measured in this case from the mid-point of the beam (see Figure ·a). Rotation of the beam at angular velocity $\dot{\theta}$ gives rise to a distributed d'Alembert force whose component in the x direction has the effect of putting the beam into tension. It is desired to find how much this straightens the beam, assuming the change of deflection z to be small compared with y.

Solution: Figure ·b shows the d'Alembert load on an element at $x = x_r$. The bending moment at $x = x_s$ due to this load is

$$(m x_r \dot{\theta}^2 \, \delta x_r / 2\ell_h)(y_r - y_s)$$

that is:
$$M(x_s) = \int_s^{\ell} (m x_r \omega_t^2 / 2\ell_h)(y_m x_s^2/\ell_h^2 - y_m x_r^2/\ell_h^2)\, dx_r \qquad \cdot c$$

But (from ·h) $-M(x_s) = EI\, d^2z/dx_s^2$ ·d

$$\therefore \qquad EI\, d^2z/dx_s^2 = (m y_m \dot{\theta}^2/8\ell_h^3)(\ell_h^4 - 2\ell_h^2 x_s^2 + x_s^4) \qquad \cdot e$$

Integrating twice with boundary conditions $dz/dx_s = 0,\ z = 0 \,|\, x_s = 0;\quad z = 0 \,|\, x_s = \ell_h$

$$z_m = 11 m y_m \dot{\theta}^2 \ell_h^3 / 240 EI \qquad \cdot f$$

Simplification: Compare with the expression for the first transverse natural frequency (c.f. A1·c):

$$\omega_1^2 = \Omega^2 \omega^2 = \pi^4 EI / 8\ell_h^3 m \qquad \cdot g$$

Thus we can write

$$\frac{z_m}{y_m} = -\left(\frac{11\pi^4}{1920\Omega^2}\right)\left(\frac{\dot{\theta}}{\omega}\right)^2 \doteqdot -\frac{0{\cdot}56}{\Omega^2}\left(\frac{\dot{\theta}}{\omega}\right)^2 \qquad \cdot h$$

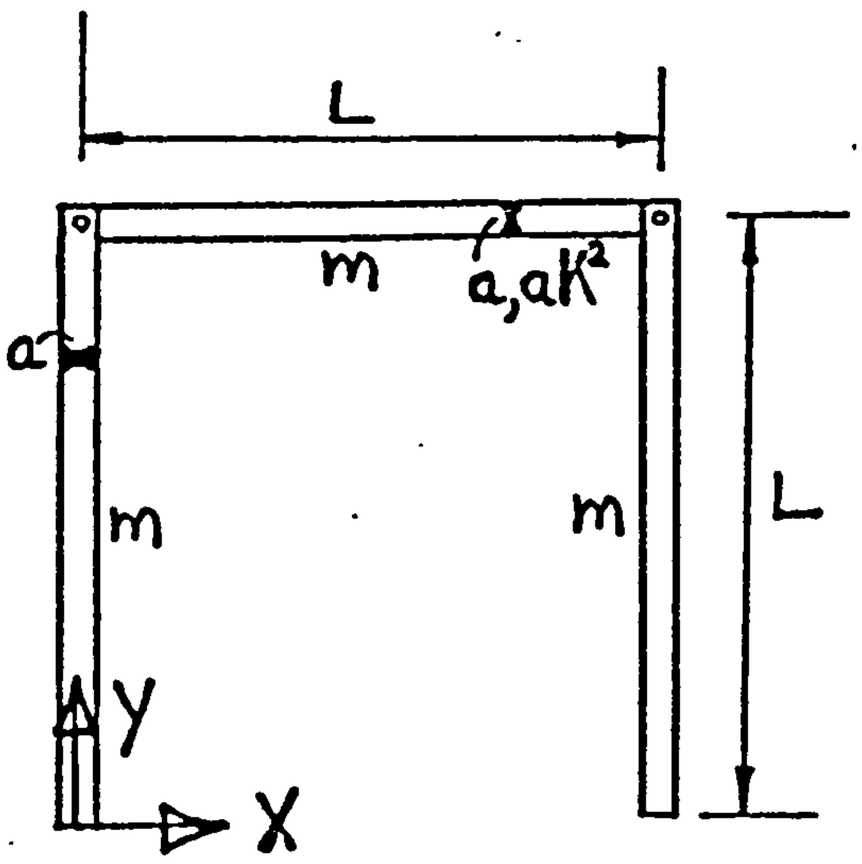

A12·a: Structure with axial/bending mode

```
*     1.          PI=ATAN(1.0)*4.0
*     2.          PIN=1.0/PI
*     3.          WRITE(6,101)
*     4.          B=0.0
*     5.          DO 1 I=1,10
*     6.          B=B+0.02
*     7.          C=3+24*PIN*B+10*B*B
*     8.          A=2*B*C/(6*PIN+5*B)-4*B*B
*     9.          AI=1.0/A
*    10.          S=PI*PI*SQRT(AI)
*    11.          WRAT=SQRT(3*(1+4*B*B*AI)/C)
*    12.          WRITE(6,100)S,B,WRAT
*    13.     1    CONTINUE
*    14.          STOP
*    15.     100  FORMAT(3F8.3)          { [Δ]     [Γ]
*    16.     101  FORMAT(///' L/K        { BETA    FREQRAT'/)
*    17.          END
*
```

A12-b: Program for analysis of .a by Rayleigh-Ritz method

10 G: EFFECT OF AXIAL COMPLIANCE OF ADJACENT LINKS ON BENDING VIBRATIONS. (APPENDIX TO SECTION 2J, page 38)

Let deflection of structure in the Y direction (see Figure ·a) be y, and assume y is approximately of the form:

$$y = [v \sin(\pi X/L) + \Delta v\, Y/L] \sin \omega_1^* t. \qquad \cdot c$$

$$\therefore \quad \partial y/\partial t = \omega_1^* [v \sin(\pi X/L) + (\Delta v\, Y/L)] \cos \omega_1^* t, \qquad \cdot d$$

$$\partial^2 y/\partial x^2 = -(v\pi^2/L^2) \sin(\pi X/L) \sin \omega_1^* t \qquad \cdot e$$

$$\partial y/\partial Y = (\Delta v/L) \sin \omega_1^* t \qquad \cdot f$$

The maximum kinetic energy of the system is given by:

$$KE_{max} = (2 \times \tfrac{1}{2}) \int_0^L m/L \left(\partial y/\partial t\right)^2_{\substack{max \\ X=0}} dY + \tfrac{1}{2} \int_0^L m/L \left(\partial y/\partial t\right)^2_{\substack{max \\ Y=L}} dX$$

$$= m \omega_1^{*2} v^2/12 \,[10\Delta^2 + (24/\pi)\Delta + 3] \qquad \cdot g$$

The maximum potential energy of the system is given by:

$$PE_{max} = (2 \times \tfrac{1}{2}) \int_0^L E a \left(\partial y/\partial Y\right)^2_{\substack{max \\ X=0}} + \tfrac{1}{2} \int_0^L E a K^2 \left(\partial^2 y/\partial X^2\right)^2_{\substack{max \\ Y=L}} dX$$

$$= E a v^2/4L \,[4\Delta^2 + \pi^4/s^2] \;\Big|_{s=L/K} \qquad \cdot h$$

Equating maximum kinetic and potential energy, we have:

$$\frac{\omega_1^{*2}}{\omega_1^2} = \frac{\pi^4 + 4\Delta^2 s^2}{3 + (24/\pi)\Delta + 10\Delta^2} \times \frac{3}{\pi^4} \qquad \cdot i$$

where

$$[\omega_1^{*2}]_{min} \rightarrow \quad 8\Delta s^2 [3 + (24/\pi)\Delta + 10\Delta^2] = [(24/\pi) + 20\Delta][\pi^4 + 4\Delta^2 s^2] \qquad \cdot j$$

$$\therefore \quad s = \pi^2 \left\{ \frac{2\Delta [3 + (24/\pi)\Delta + 10\Delta^2]}{(6/\pi) + 5\Delta} - 4\Delta^2 \right\}^{-1/2} \qquad \cdot k$$

These relations are programmed in FORTRAN as shown opposite (·b).

(APPENDIX TO SECTION 4B, p75)

10 H: APPROXIMATIONS FOLLOWING FROM THE SMALL-CLEARANCE ASSUMPTION

A partial derivative such as $(\partial X_r/\partial\theta)$ can be expanded as a double Taylor series in u and v, in terms of the nominal (u=v=0) values at the same crank angle; thus

$$(\partial X_r/\partial\theta) = (\partial X_r/\partial\theta)^* + u(\partial^2 X_r/\partial\theta\ \partial u)^* + v(\partial^2 X_r/\partial\theta\ \partial v)^* + \ldots\ldots \qquad \cdot a$$

Now, according to Assumption f of Section 4A the clearance radius e is much smaller than any property of the nominal mechanism having the dimension of length. Thus $(\partial X_r/\partial\theta)^*/(\partial^2 X_r/\partial\theta\ \partial u)^* >> e$, whereas $u \approx e$, so that by comparison with the first term in the Taylor series we can neglect the second, and likewise all subsequent terms. The components of force between the pin and the journal necessary for equilibrium of the system at some (u,v) when the crank is stationary, namely S_u and S_v, can similarly be expressed as Taylor series in which S_u^* and S_v^* are the only significant terms. In summary, the instantaneous partial derivatives and static force components may both be replaced by their nominal values.

Applying this to equation 75·a, dividing through by $\dot\theta^2$ so that every term has the dimension of length, and re-arranging, we obtain

$$(\ddot X_r/\dot\theta^2)=[(\partial X_r/\partial\theta)^*(\ddot\theta/\dot\theta^2)+(\partial^2 X_r/\partial\theta^2)^*]+[(\partial X_r/\partial u)^*(\ddot u/\dot\theta^2)+(\partial X_r/\partial v)^*(\ddot v/\dot\theta^2)]$$
$$+[(\partial^2 X_r/\partial u^2)^*(\dot u^2/\dot\theta^2)+(\partial^2 X_r/\partial v^2)^*(\dot v^2/\dot\theta^2)+2(\partial^2 X_r/\partial u\partial\theta)^*(\dot u/\dot\theta)$$
$$+2(\partial^2 X_r/\partial v\partial\theta)^*(\dot v/\dot\theta)+2(\partial^2 X_r/\partial u\partial v)(\dot u/\dot\theta)(\dot v/\dot\theta)] \qquad \cdot b$$

The first bracket on the right hand side is a property of the nominal mechanism, and is therefore much larger than e. Turning to the third bracket, we note that $|u|$ is of the order of e, and in the following mode $\dot u=0$ at $u=+e$ so the maximum value of $\dot u^2$ is of the order of $|\ddot u e|$. Thus

$$(\dot u^2/\dot\theta^2) \approx |\ddot u/\dot\theta^2|\ e << |\ddot u/\dot\theta^2| \times |(\partial X_r/\partial u)^*/(\partial^2 X_r/\partial u^2)^*| \qquad \cdot c$$

and so the first term in the third bracket can be neglected by comparison with the first in the second. The elimination of the second term in the third bracket can be justified in a similar manner. The last term in the

third bracket is of the same order as the first and second terms taken together, and can therefore be neglected as well. The third term in the third bracket is much smaller than the first bracket when $|\dot{u}/\dot{\theta}| \approx e$ or $<<e$, and much smaller than the first term in the second bracket when $|\dot{u}/\dot{\theta}| >> e$, since then $|\ddot{u}/\dot{\theta}^2|/|\dot{u}/\dot{\theta}| \approx |\dot{u}/\dot{\theta}e| >> 1$. The third term in the third bracket, and likewise the fourth term, can therefore be omitted in every case. In summary, every term in the third bracket of A13.b can always be neglected during the following mode. (In fact, this can be extended to the period immediately after loss of contact, since there is nothing to make the relative orders of magnitude change suddenly). $\ddot{Y}_r$ and $\ddot{\lambda}_r$ can be treated similarly.

(APPENDIX TO SECTION 4B, p76)

10 I: DERIVATION OF FOLLOWING MODE EQUATION

With (u,v) on the clearance circle and aligned with the contact force vector, the equations of motion (76·a,·b) can be written in polar coordinates as

$$-R\cos\gamma = M_{uu}(-e\dot{\gamma}^2\cos\gamma - e\ddot{\gamma}\sin\gamma) + M_{uv}(e\ddot{\gamma}\cos\gamma - e\dot{\gamma}^2\sin\gamma) - R^*\cos\gamma^*$$

$$-R\sin\gamma = M_{uv}(-e\dot{\gamma}^2\cos\gamma - e\ddot{\gamma}\sin\gamma) + M_{vv}(e\ddot{\gamma}\cos\gamma - e\dot{\gamma}^2\sin\gamma) - R^*\sin\gamma^* \qquad \}\cdot a$$

The elimination of R from these equations gives

$$e\dot{\gamma}^2((M_{vv}-M_{uu})\sin\gamma\cos\gamma + M_{uv}(\cos^2\gamma - \sin^2\gamma)) + e\ddot{\gamma}(-M_{uu}\sin^2\gamma - M_{vv}\cos^2\gamma$$

$$+ 2M_{uv}\sin\gamma\cos\gamma) + R^*(\sin\gamma^*\cos\gamma - \cos\gamma^*\sin\gamma) = 0 \qquad \cdot b$$

Writing M_{uu} as $M_o(1-\varepsilon\cos2\eta)$, M_{vv} as $M_o(1+\varepsilon\cos2\eta)$, M_{uv} as $\varepsilon M_o \sin2\eta$, and simplifying the resulting trigonometrical expressions, we obtain

$$M_o e\dot{\gamma}^2\varepsilon\sin(2\eta+2\gamma) - M_o e\ddot{\gamma}(1+\varepsilon\cos(2\eta+2\gamma)) + R^*\sin(\gamma^*-\gamma) = 0 \qquad \cdot c$$

With $(\gamma^*-\gamma)$ written as α, $\ddot{\alpha}$ may then be extracted as shown in Equation 76·c. R is found similarly, after eliminating γ from the left hand sides of ·a.

Equations 77·a to 77·c evidently follow from the substitutions above. Note that the line joining $(M_{uu},-M_{uv})$ and (M_{vv},M_{uv}) is a diameter (with inclination 2η) of a Mohr's circle of radius (εM_o) centred at $(M_o,0)$. In addition to the simplification that is made possible, the advantages of replacing (M_{uu},M_{uv},M_{vv}) by (M_o,ε,η) are that ε and η are dimensionless and that M_o and ε are invariant under rotations of the axes (u,v).

(APPENDIX TO SECTION 4B, p78)

10 J: DERIVATION OF STANDARD FLYPAST EQUATION

It is assumed (see 78.a & .b) that $\dot{R}^*_u$ and $\dot{R}^*_v$ are constant, and axes are chosen so that R^*_u is constant. Then differentiating the relation $\tau=\tan\gamma^* =(R^*_v/R^*_u)$ we obtain $\dot{\tau}=\dot{\gamma}^*\sec^2\gamma^* =\dot{\gamma}^*\cdot(1+\tau^2)=(\dot{R}^*_v/R^*_u)$, and then $\ddot{\tau}=\ddot{\gamma}^*(1+\tau^2) + 2\dot{\gamma}^*\,\tau\dot{\tau}=0$. Thus $\dot{\gamma}^* = (1+\tau^2)^{-1}(\dot{R}^*_v/R^*_u)$ and $\ddot{\gamma}^*=-2\tau(1+\tau^2)^{-2}(\dot{R}^*_v/R^*_u)^2$. } .a

Furthermore, $R^* = R^*_u \sec\gamma^* = R_u(1+\tau^2)^{\frac{1}{2}}$, $\dot{\alpha}=(\dot{R}^*_v/R^*_u)d\alpha/d\tau$, and $\ddot{\alpha} = (\dot{R}^*_v/R^*_u)^2 d^2\alpha/d\tau^2$. Substituting these relations in Equation 76.c and dividing through by $(\dot{R}^*_v/R^*_u)^2$, we obtain } .b

$$d^2\alpha/d\tau^2= -2\tau(1+\tau^2)^{-2} -[(R^{*3}_u/R^{*2}_v M_o e)(1+\tau^2)^{\frac{1}{2}}\sin\alpha - \varepsilon(d\alpha/d\tau$$

$$- (1+\tau^2)^{-1})^2 \sin(2\alpha-2\eta-2\gamma^*)[1+ \varepsilon\cos(2\alpha-2\eta-2\gamma^*)]^{-1} \quad .c$$

Expressed in terms of the parameters H defined in Equations 78.d to 78.f, this is equivalent to Equation 78.c.

(APPENDIX TO SECTION 4B, p79)

10 K: PROCEDURE USED FOR CONSTRUCTING FIGURE 79.a

Integration of equation of motion:

For a set of values H_1, H_2, H_3, equation 78c was integrated using the Runge-Kutta algorithm, with a step length given by the formula $0.04/H_3$ (This was found for sample cases to give results close to those obtained using shorter steps). The terms $\sin(2\alpha - H_3 - 2\gamma^*)$ and $\cos(2\alpha - H_3 - 2\gamma^*)$ were evaluated by expanding in terms of the separate sines and cosines, and using the relations $\sin 2\gamma^* = 2/(1+\tau^2)$, $\cos 2\gamma^* = (1-\tau^2)/(1+\tau^2)$. The initial conditions in every case were $\tau = -10$, $\dot{\alpha}=0$, and a value of α, found iteratively, such that $\ddot{\alpha}=0$. The integration was continued until α had changed sign 8 times. Each successive local minimum R was noted, say R_1, R_2....R_N....R_8.

Construction of single contour.

For a given value of H_3, an integration as described above was performed for every point on a grid in the (H_1, H_2) plane, covering ten values of H_1 by eighteen values of H_2. For a given N, values of H_1 for which $R_N = 0$ were found by linear interpolation at each successive value of H_2 and joined by straight lines to give approximate contours. "Patches" of additional grid points were incorporated where the original grid was found to give a poor definition of these contours. A final set of integrations was carried out for points just inside and just outside the approximate contour, so that a revised contour could be drawn (freehand), accurate to $\pm$ 0.01 in the H_1 direction at each grid value of H_2.

Construction of chart.

Contours were found as described above for each value of N from 1 to 6, and the evelope of all the contours was plotted. This was repeated for each value of H_3 as shown to produce Fig. 79.a.

The entire procedure was written in Fortran and implemented on the IBM 370 computer at Newcastle University. The program for performing the integrations is called BLA, which writes the parameters and results sequentially to file. A second program BRIDGE reads from this file and carries out the interpolation and graph plotting functions, storing or adjusting the contour point coordinates in an indexed file. These programs constitute Annexes 2 and 3 respectively.

10L: DERIVATION OF FREE-FLIGHT TRAJECTORY & IMPACT EQUATIONS

(APPENDIX TO SECTION 4E, page 84 & 85)

In this Appendix it is assumed that the conditions of a 'standard flypast' are in force (78·a) and that the motion up to $t = t_\ell$ is known.

Free-flight phase: From 84·a, ·b

$$\left.\begin{aligned} \ddot{u} &= [R_u^* M_{vv} - R_v^* t\, M_{uv}]/[M_{uu}M_{vv} - M_{uv}^2] \\ \ddot{v} &= [-R_u^* M_{uv} + R_v^* t\, M_{uu}]/[M_{uu}M_{vv} - M_{uv}^2] \end{aligned}\right\} \cdot a$$

Converting M_{uu}, M_{vv}, M_{uv} to M_0, ε, η (c.f. 77·a-·c) and t to $\tau R_u^*/\dot{R}_v^*$:

$$\left.\begin{aligned} (\dot{R}_v^*/R_u^*)^2\, d^2u/d\tau^2 &= R_u^*\,[1 + \varepsilon\cos 2\eta - \tau\varepsilon\sin 2\eta]/[M_0(1-\varepsilon^2)] \\ (\dot{R}_v^*/R_u^*)^2\, d^2v/d\tau^2 &= R_u^*\,[-\varepsilon\sin 2\eta + \tau(1-\varepsilon\cos 2\eta)]/[M_0(1-\varepsilon^2)] \end{aligned}\right\} \cdot b$$

At $\tau = \tau_\ell$, trajectory is tangential to the contact circle, so:

$$\left.\begin{aligned} u &= e\cos\gamma_\ell \qquad (du/d\tau) = -e\sin\gamma_\ell\,(d\gamma/d\tau)_\ell \\ v &= e\sin\gamma_\ell \qquad (dv/d\tau) = \;\; e\cos\gamma_\ell\,(d\gamma/d\tau)_\ell \end{aligned}\right| _{\tau=\tau_\ell} \Bigg\} \cdot c$$

Integrating ·b twice (writing $\tau - \tau_\ell$ as $\delta\tau$):

$$\left.\begin{aligned} u &= e\cos\gamma_\ell - e\sin\gamma_\ell(d\gamma/d\tau)_\ell\,\delta\tau + [R_u^{*3}/M_0\dot{R}_v^{*2}(1-\varepsilon^2)]\,[(1-\varepsilon\cos 2\eta\cdot\tau_\ell\varepsilon\sin 2\eta)\delta\tau^2/2 \\ &\qquad -(\varepsilon\sin 2\eta)\delta\tau^3/6] \\ v &= e\sin\gamma_\ell + e\cos\gamma_\ell(d\gamma/d\tau)_\ell\,\delta\tau + [R_u^{*3}/M_0\dot{R}_v^{*2}(1-\varepsilon^2)]\,[(\tau_\ell - \tau_\ell\varepsilon\cos 2\eta - \varepsilon\sin 2\eta)\delta\tau^2/2 \\ &\qquad +(1-\varepsilon\cos 2\eta)\delta\tau^3/6] \end{aligned}\right| \cdot d$$

Expressed in terms of $[H_1, H_2, H_3]$ this corresponds to 84·c-·f.

Impact phase: Since $R_u^* \doteqdot 0, R_v^* \doteqdot 0, R_u = R\cos\gamma_i, R_v = R\sin\gamma_i$, 76·a-·b become

$$\left.\begin{aligned} -R\cos\gamma_i &= M_{uu}\ddot{u} + M_{uv}\ddot{v} = M_0(1-\varepsilon\cos 2\eta)\ddot{u} + M_0(\varepsilon\sin 2\eta)\ddot{v} \\ -R\sin\gamma_i &= M_{uv}\ddot{u} + M_{vv}\ddot{v} = M_0(\varepsilon\sin 2\eta)\ddot{u} + M_0(1+\varepsilon\cos 2\eta)\ddot{v} \end{aligned}\right\} \cdot e$$

Let r = component of relative displacement in γ_i direction,

i.e. $r = u\cos\gamma_i + v\sin\gamma_i$

$\therefore\quad \ddot{r} = \ddot{u}\cos\gamma_i + \ddot{v}\sin\gamma_i$ ·f

Eliminating $\ddot{u},\ddot{v}$ from A19·e, A19·f and simplifying,

$$R = -M_o(1-\varepsilon^2)\ddot{r}/(1+\varepsilon\cos(2\eta+2\gamma_i)) \qquad \cdot a$$

Integrating over the small impact time $(\dot{r} = \dot{r}_i \rightarrow -E\dot{r}_i)$, the impulse is

$$|I| = [M_o(1-\varepsilon^2)/(1+\varepsilon\cos(2\eta+2\gamma_i))]\,\dot{r}_i(1+E). \qquad \cdot b$$

The dimensionless form (85·f) is then obtained using

$$V_N = d(r/e)/d\tau = \dot{r}_i R_u^*/e\dot{R}_v^*. \qquad \cdot c$$

10M: · PROCEDURE FOR CONSTRUCTING FIGURE 104•a/•b

(APPENDIX TO SECTION 5J, pages 103 - 4)

Pin 'A' was installed, and the journal was aligned parallel to the pin as well as could be judged (cf. Section 5F). The displacement transducers were adjusted (cf. Section 5H), and the output channels, I to IV, were tape-recorded* on tape channels 1 to 4 respectively.

The journal was /top-sprung/ (see 96•*l*) and the vertical link was pressed against a rigid stop incorporating slip gauges. The horizontal link was gently pushed up and down several times, so that light contact between pin and journal occurred. Thus the journal axis traced out an arc of 125 mm radius, which closely approximates to a vertical chord of the clearance circle. This was repeated, using different combinations of slip gauges. (Inch' slip gauges were used, so a convenient increment was 0.001" = 25.4μm).

The journal was then /suspended/ by an effectively rigid hook, the point of suspension incorporating a screw adjustment. The vertical link was gently rocked to and fro several times, so that light contact between pin and journal occurred, Thus the journal traced out an arc (radius about 115 mm) which closely approximates to a horizontal chord of the clearance circle. This was repeated, with the suspension point adjusted vertically each time. The increment was again 25.4 μm, but since the suspension point shown at 96•*k* was used, the journal axis moved in vertical increments of 20.3 μm. (This was recognized subsequently).

The journal was again /top-sprung/, and moved by hand so that its axis slowly traced out the clearance circle twice, with pin/journal contact firmly maintained.

The recording was played back* at first with channels 1 and 2 connected to the 'X' and 'Y' terminals of the pen plotter. The gain was adjusted until a chosen (nearly diametral) chord was drawn with a gradient of 1 : 1 on the graph paper, and Figure 104•a was then drawn in full.

The recording was played back* a second time with channels 3 and 4 connected to the plotter. The gains on both axes were adjusted, using the same portion of the recording as before, until the chord was drawn with a gradient of 1 : 1 and a length equal to the previous length; Figure 104•b was then drawn.

*: A tape speed of 1.5 inches/sec was used for both recording and playback for this test.

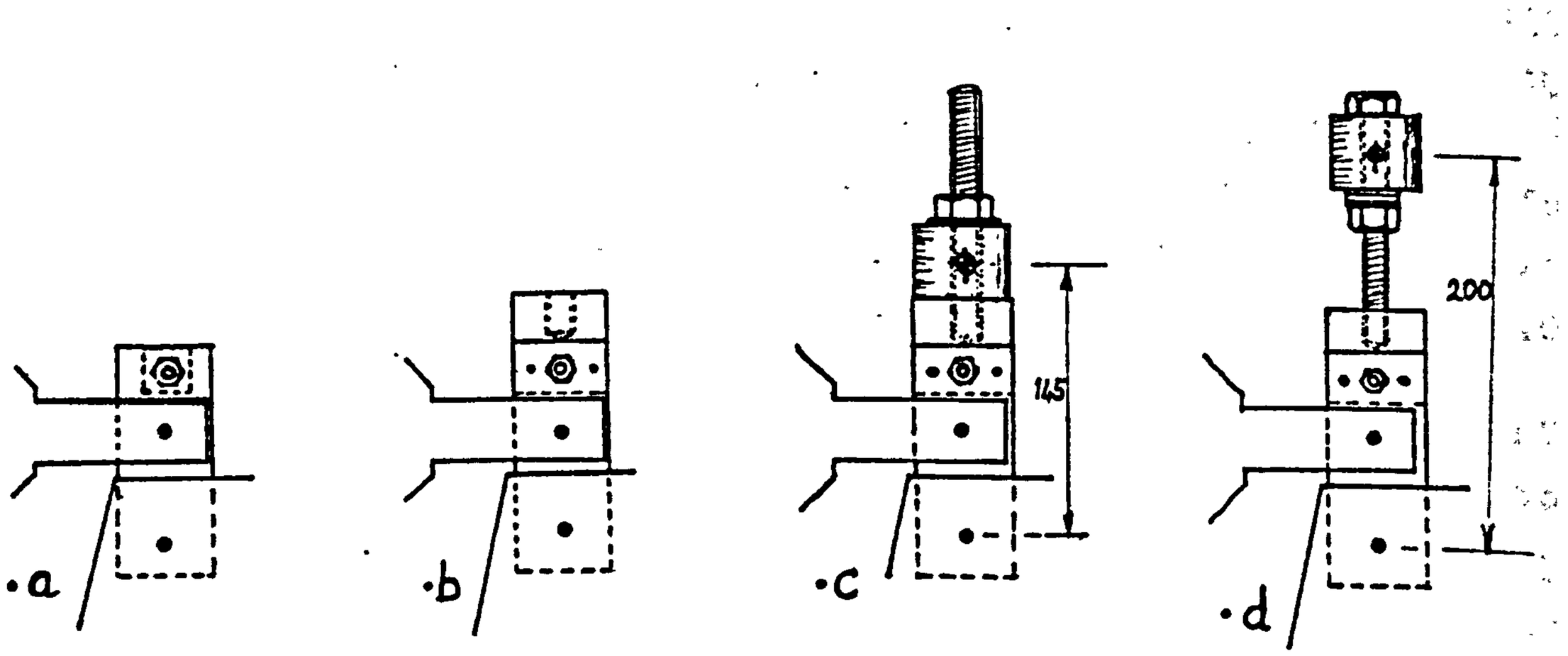

A22·a-d: Variants of vertical link

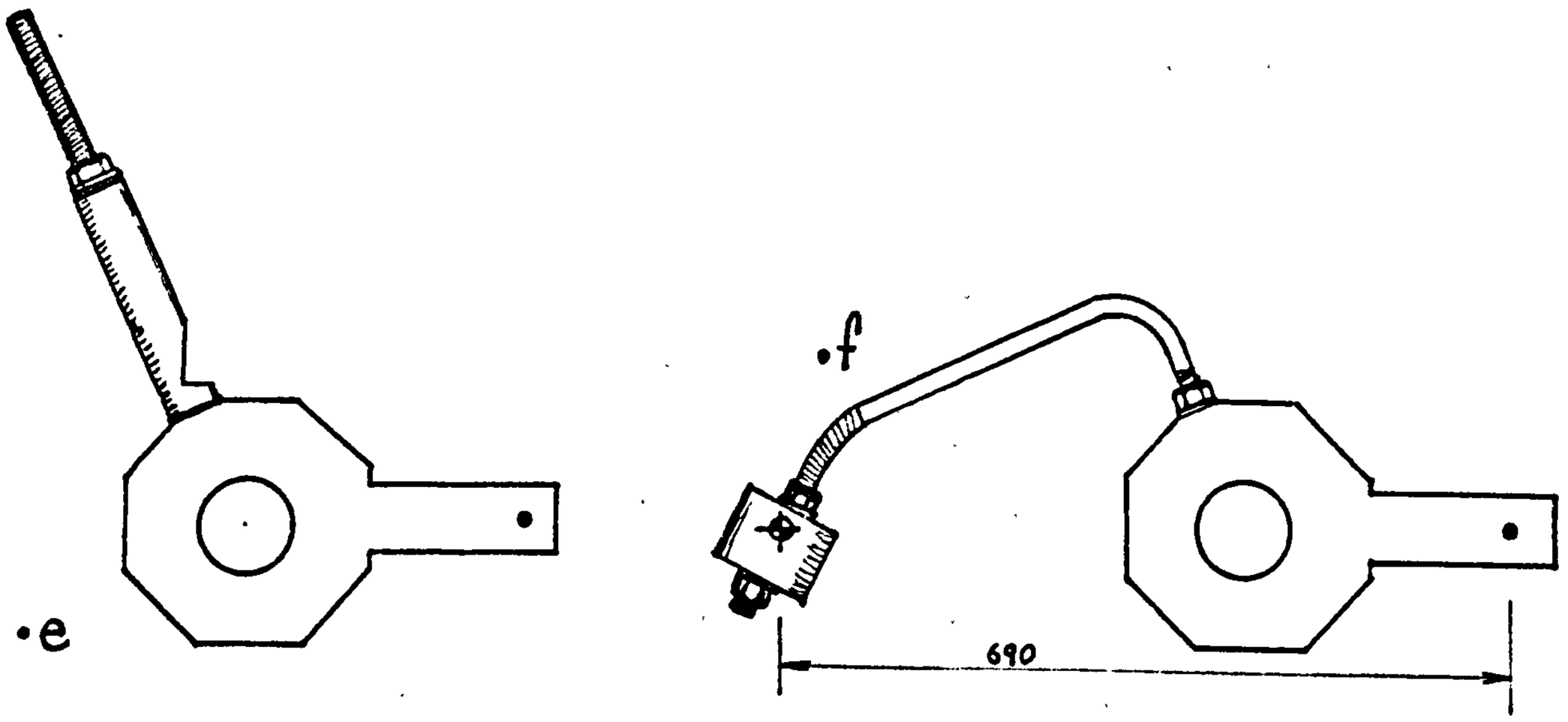

A22·e - ·f: Variants of horizontal link

10N: VARIATION OF INERTIAL PARAMETERS (APPENDIX TO CHAPTER 5, p105)

The inertial parameters of the linkage may be expressed as M_{HH}, M_{VV}, and M_{HV} where H and V refer to the horizontal axes respectively. The vertical link only contributes to M_{HH}; the horizontal link contributes to all three values.

The sign of M_{HV} is determined as follows: consider the case $R_H^*>0$, $R_V^*=0$ (that is, force is right to left in .a to .f), with an offset mass on the horizontal link as in .e, and no pin/journal contact. Then $\delta_H>0$, $\ddot{\delta}_V<0$ (journal accelerates to left and upwards). Now from 76.a/.b, $R_V^* = 0 = M_{VV}\ddot{\delta}_V + M_{HV}\ddot{\delta}_H$. Therefore, since $M_{VV}>0$, $M_{HV}>0$ also.

Vertical link: Five variants were used, as follows, with the contribution to M_{HH}, in kg, shown in the right margin:-

		M_{HH}	M_{VV}	M_{HV}
/A	The two forks of the vertical link bolted together at the top through a 25x25x24 mm spacer 'cube' (sketch .a)	1.7		
/B	The two forks bolted together through a 50x50x24 mm spacer piece (sketch .b).	3		
/C	The spacer piece as in /B carrying an M16 screwed rod together with a nut and washers.	6		
/D	The screwed rod as in C carrying a cylindrical mass weighing 0.5 kg at its lower end (sketch .c).	10		
/E	The screwed rod as in /C carrying a 0.5 kg cylindrical mass between nuts at its upper end (sketch .d).	15		

Horizontal link: Four variants were used, as follows, with the contributions to the inertial parameters shown in kg at the right:-

a/	The basic link with no attachments.	4	3.25	0
b/	The link with a 25mm diameter stem attached to the journal housing as in sketch .e .	4.5	4.75	0.5
c/	The link with the stem as in b/ carrying 2.5kg (laboratory weights) on the screwed end.	7	16	4
d/	The link with a long bent 10mm bar attached to the journal housing, carrying 0.5 kg (sketch .f).	4.75	8	0

Conversion: M_{HH}, M_{VV}, M_{HV} can be converted to M_{uu}, M_{vv}, M_{uv} according to the directions of the applied loads, as follows:

Build	M_{uu}	M_{vv}	M_{uv}
/Top-sprung/; gravity > spring load, R_H^* increasing	M_{VV}	M_{HH}	$+M_{HV}$
/Top-sprung/, gravity < spring load, R_H^* increasing	M_{VV}	M_{HH}	$-M_{HV}$
/Side-sprung/, R_V^* increasing.	M_{HH}	M_{VV}	$-M_{HV}$

Change sign of M_{uv} for decreasing load; use 77.a-.c to convert to M_o, ε, γ.

10P: ADJUSTMENT & ALIGNMENT OF EXPERIMENTAL RIG (APPENDIX TO CHAPTER 6)

Outlined below are the most efficient procedures found for each adjustment. These are not necessarily the procedures used for the tests described in Chapter 6, since the procedures were progressively improved during the investigation. The complete procedure can take a number of hours.

Re-assembly: (This assumes the pin has been removed for polishing etc.)

.a Assemble bearing between side-plates (96.g) with mandrel inserted.

.b Note that height of datum lines on either side of the load transducers should be equal (check with scriber/block). If not, slacken horizontal clamps (96.i), rotate transducers on mandrel and reclamp.

.c Push out mandrel: if too tight, slacken clamps slightly, push out, reclamp.

.d Check that right-hand end of pivot stand (as seen in 90.a-.t) is held just clear of floor by levelling screws.

.e Check that 'vertical' link is vertical by set square. If not, loosen holding down screws on pivot stand (90.i) and/or vertical clamp on far 'side plate' (90.d) to adjust, then retighten. Install and tighten down vertical clamp on near side-plate (far one not normally moved).

.f Journal housing to be /isolated/, located axially midway along pin, and /clamped/ with top face horizontal (check by placing ball on top).

.g Horizontal link should fit symmetrically to housing; if not, adjust pivot stand position. Reassemble horizontal link with bearing housing, and tighten screws before unclamping journal from pin.

.h Inductances should be parallel to flats on journal housing and all gaps should be similar, say 10 times diametral clearance.

Displacement transducers: tests: (for use in conjunction with adjustments).

.i Display A/C bridge output signal for one channel (see 90.j) on oscilloscope externally triggered by the $\frac{28.5}{2\pi}$ kHz supply. Set time base to show $\approx$ $1\frac{1}{2}$ cycles of waveform (cf 103.a). Move journal: waveform should not change sign, and

.j points where waveform crosses axis should not move (phase constant).

.k As .i/.j for other three channels.

.l Display demodulated output signal on oscilloscope. Oscillate journal by hand and note extreme range of signals. 'Pinch' terminals of one inductance then the other, so as to saturate the system. Extreme values should lie well outside working extremes. Ditto for other channels.

.m With journal /top-sprung/ to take most of weight, and /held/ against

horizontal jack (or /propped/ on vertical jack), move journal across most of vertical (horizontal) diameter, but without contact with pin. The four demodulated signals should all change by the same amount (compare a pair at a time on oscilloscope).

Displacement transducers: adjustment: As the adjustments interact, iterative use of .a-.c may be necessary.

.a Loosen clamping screws on pair of inductances. Moving both in opposite directions alters gain of channel (A23.m), moving in same direction shifts working range cf. saturation (A23.i/.l); phase stability (A23.j) may also be affected in either case. (Tool 90.p may be useful).

.b Trimming potentiometers and capacitors on bridge circuit (plugged into control box 90.j) affect phase stability and working range.

.c Gain control potentiometers (knobs on 90.j) provide fine (non-linear) control of gain; working range also affected.

Bearing alignment: With journal /top-sprung/ to take most of load...

.d Push journal to and fro along bearing axis: should be equally free in both directions. If not, tap right-hand of pivot stand (90.i) to align it with direction in which journal is free-est.

.e Then with (provisionally adjusted) displacement signals displayed on two oscilloscopes in X-Y mode (I vs II, IV vs III respectively), slowly press journal against pin in various directions, in the plane of the linkage; to avoid inadvertant out-of-plane loading, use loop of string round vertical link to apply horizontal component, and adjust top spring tension for vertical component. Contact should be seen to be made at the back (IV/III) and front (I/II) of the bearing at the same time. If not:

.f very gingerly adjust levelling screws on pivot stand 90.i (affects 'yawing' as well as 'rocking' alignment) and/or

.g firmly tap right-hand end of pivot stand one way or the other (mainly affects yawing alignment).

Owing to errors of form of the pin and journal, the optimum alignment usually varies slightly with the direction of the contact force, so a compromise alignment must be sought. If the errors of form are excessive, it may be beneficial to rotate or reverse the pin. Procedure for rotation:

.h insert mandrel, put grub screw in mandrel through hole in spacer collar (96.e) using screwdriver rod (90.n), locate grubscrew in notch in pin,

release horizontal clamps (96.i), rotate pin using mandrel, reclamp, remove grubscrew, remove mandrel; NB repeat check A23.b.

When the bearing alignment has been completed, the displacement transducers should be checked, and if necessary re-adjusted.

Exciters: With the journal top-sprung to take its weight.....

.a insert the 16 mm load balls between the journal housing/horizontal link and the exciters to be used.

.b Release the clamping screws in the extension cylinders (98.b), and slacken the limit stop nuts (98.f) using the mini-spanner (90.o). Open the gas charging valves by the appropriate master cylinders (93.f) and introduce gas at a low pressure, say 4 bar (50 psi on gauge). While pulling one extension cylinder out as far as it will go, finger-tighten its limit stop nuts; then tighten each nut about half a turn more, and tighten the clamping screw. Repeat for the opposite cylinder.

.c Position the load balls by eye in the centre of the load pads, with the aid of the inspection mirror (90.r) and the bent hooks available.

.d Increase gas pressure to around 25 bar (400 psi); with the horizontal and vertical load transducer signals displayed on an oscilloscope at an appropriate scale, close one master cylinder gas valve and check for significantly increased drift of the measured load (indicating gas leak). Open the valve, close the other, and repeat to check other exciter.

.e Cure leaks if necessary: if master cylinder piston seal found to be grooved, rub on fine emery (renew silicon grease) - or replace piston.

.f Close both valves, run motor, and compare waveform with journal /clamped/ and unclamped, as described on p101. If the difference is much greater than shown in Fig. 101.f, try to cure as follows:-

.g Stop the eccentric in the position where the discrepancy is greatest (extreme throw one way or the other), release the extension cylinder clamp screws and adjust the limit stop nuts very slightly, noting the change in the load signal. The stop on one cylinder will probably have a much greater effect than the other: the former should be adjusted one way or the other until the effect is reduced. Reclamp and repeat the test until success.

With the active master cylinder gas charging valves open, and the displacement transducer signals displayed as for bearing alignment, adjust the tension spring above the journal until the latter is either /floated/

out of contact or only lightly contacting the pin. Then

.a vary the gas pressure between about 3 and 20 bar (say) and check that the two displacement vectors move, if at all, in the same direction and by the same amount. If not, the exciters are exerting a moment on the journal, and one or both load balls must be moved slightly parallel to the bearing axis until the effect is eliminated.

If the pair of horizontal exciters are being used, the vertical alignment of the balls is also critical. To test this, the total vertical load transducer signal should be displayed on an oscilloscope, with the zero set (see 10Q) and a suitable scale chosen. Then

.b set the gas pressure to about 20 bar, push the journal in the $+R_H$ direction, gently release it and record the vertical load; repeat for the $-R_H$ direction; take the mean of the recorded loads (which will differ owing to friction). Repeat with the gas pressure at about 3 bar. If the high pressure load is higher (in the downwards direction), the ball nearer the vertical link is too high relative to the other ball, and one or other must be marginally adjusted: then repeat preceding check (.a).

It is advisable at this stage to repeat check 25.f . Further delicate adjustments to the pivot stand may be necessary while performing fly-past tests in order to minimise differences between the **(I/II)** and **(IV/III)** displacement trajectories

10Q: CALIBRATION OF TRANSDUCERS (APPENDIX TO CHAPTER 6)

Amplifiers: The gains of the stepwise amplifiers of the oscilloscopes, pen plotter and charge amplifier units were found to be consistent, and were therefore accepted as correct, except that the gain of the (elderly) Telequipment DMS3A was about 15% below par. Thus the latter instrument was not used for quantitative measurement but only for comparison.

Load transducers: It was known from previous experiments that the sensitivity of the four shear force transducer channels was the same, to adequate accuracy. After alignment of the transducers (A23.b), the two vertical load channels were connected to a single charge amplifier, as in 94.a . The journal was /isolated/ and /clamped/, and a 2 kg weight repeatedly placed on top and removed, while the charge amplifier gain was adjusted until the output voltage changed by 1 volt as the weight was removed. This was repeated using the other charge amplifier. The vernier gain was left unchanged thereafter, although the stepwise gain was altered and allowed for where appropriate.

To establish the zero load, the journal was positioned out of contact with the pin, guided by the displayed displacement transducer signals. This was normally achieved by momentarily raising the jack (97.b), with equal pressure in the horizontal exciters if in use. If the vertical exciters were in use, the drive shaft (93.d) was turned by hand with the motor switched off until the journal was halfway up the clearance, and the horizontal jack (97.d, upper position) used to eliminate contact on the horizontal diameter.

Displacement transducers: The procedure for equalising the gains of the four transducers was described at A23.m.

The diametral clearances for the three pins, having been estimated as described on page 105, were subsequently used as standard displacements. That is, a displacement/volt ratio, assumed constant, was determined by dividing the estimated clearance ~~clearance~~ diameter for the pin in use by the voltage range of the transducer circuit output as the clearance circle periphery was traced out.

Tape recordings: At the start of each tape-recorded experiment, after the recorder input amplifier gains had been set to give a suitable recording level, three calibration records were made. For the first, a load was applied in a convenient direction and the load signal for that direction was recorded on both 'load' channels of the tape. At the same time the magnitude of the load was noted from an oscilloscope display of the input signal. Note that during the experiment proper both charge amplifiers were set to the same gain, namely that used for the calibration record.

The second and third records were of the displacement signals, as the journal was pushed, respectively, around the periphery of the clearance circle and across a horizontal or vertical chord (cf p A21).

On playback, the ranges of the first two calibration records provided reference levels for load and displacement signals respectively, which were traced in the margins of the pen plotter output; the third signal enabled the gain of the two displacement signals to be equalised on the plotter.

10R: RECORDING OF EXPERIMENTAL SIGNALS (APPENDIX TO CHAPTER 6)

Use of equipment: The equipment used is indicated on page 95. All the traces shown in Sections 6B and 6C (compliance tests and drop tests) were recorded on the digital storage oscilloscope and played back to the pen plotter. All the traces shown in Sections 6D to 6G were first tape-recorded (at high speed). The flypast sequences [117.a - .d] were played back direct to the plotter (at low speed), the time-base of an oscilloscope being used to drive the horizontal ordinate. For all other traces the signals were first played back in pairs (at low speed) to the digital storage oscilloscope; this in turn was played back to the pen plotter, with the time-base of the former adjusted to give the clearest possible trace in each case.

Synchronisation: The flypast sequences were first played back to oscilloscopes and points of interest noted, and marked by 'clicks' recorded over one of the displacement channels. When constructing Figure [117.a-.d], one such click was repeatedly used to trigger the time-base, while each recorded channel in turn was played back to the plotter.

For the detailed study of flypasts, the digital storage oscilloscope was typically triggered externally from one of the recorded clicks to record two channels simultaneously; each recorded waveform was played back in turn to the plotter, against the 'ramp' generated by the oscilloscope time-base for this purpose, and then one was played against the other to produce a vector locus plot. This was repeated for the other two channels, triggered by the same click. Thus four synchronised traces of signal against time were plotted. Points of interest were marked by vertical lines; the ordinates at each point were then read off and used to identify the corresponding points on the vector loci, as shown in Figure 115.g - .p.

10S: STEADY STATE SOLUTIONS OF A HILLS EQUATION WITH FORCING TERM (APPENDIX TO CHAPTER 7)

Form of equation: The inhomogeneous Hill's equation will be considered in the form

$$d^2y/dx^2 + H(x)\, dy/dx + \Omega^2 Q(x)\, y = \Omega^2 P(x) \qquad .a$$

where H, Q and P are periodic functions of x with period 2π, $\int_0^{2\pi} Q(x)\,dx = 1$ and $\int_0^{2\pi} H(x)\,dx = 4c\pi$. If the periodic coefficients are in fact constant, this reduces to the simple damped 'spring-mass' equation with natural frequency Ω times the fundamental forcing frequency and damping factor c. If Ω is sufficiently large, the steady-state solution then approaches the quasi-static solution $y = P(x)$.

The problem is to generate a steady-state numerical solution of this equation and to check on its stability. None of the textbooks or papers consulted considered such a problem in a form convenient for the present purposes, but all the techniques necessary were found therein, and are embodied in the treatment from first principles that follows. In this Appendix a method of finding a periodic particular solution is developed. The following Appendix derives a stability criterion which, if satisfied, ensures that the periodic solution is in fact the steady-state solution.

General solution: Since the system is second order, the state at any instant can be represented by a state vector $\underline{y}(x)$ with two elements, namely $(y(x), dy(x)/dx)^T$, and the general solution will contain two arbitrary constants, a_1 and a_2. Let $\underline{y}_o(x)$ be the particular solution with initial conditions $\underline{y}_o(0) = (0, 0)^T$, and let $\underline{y}_1(x)$, $\underline{y}_2(x)$ be two solutions of the corresponding homogeneous (unforced) equation, following from the initial conditions $\underline{y}_1(0) = (1, 0)^T$ and $\underline{y}_2(0) = (0, 1)^T$ respectively. Then it can be seen that $\underline{y}(x)$ is also a solution provided that

$$\underline{y}(x) = \underline{y}_o(x) + a_1 \underline{y}_1(x) + a_2 \underline{y}_2(x), \qquad .b$$

```
      SUBROUTINE SSICS(X,NX,FINT,B,Y,A,AA,W,*)

GIVEN PERIODIC LINEAR SYSTEM WITH STATE VECTOR OF ORDER NX,
RETURNS INITIAL CONDITION VECTOR X WHICH GIVES STEADY STATE
(PERIODIC) SOLUTION. CALLING ROUTINE MUST DECLARE THE
SUBROUTINE PASSED AS 'FINT' AS EXTERNAL; THIS SUBROUTINE
FINT(X) MUST INTEGRATE OVER A WHOLE PERIOD, GIVEN X AS
INITIAL CONDITION VECTOR & RETURNING X AS FINAL CONDITIONS.
IF PERIODIC SOLUTION IS NOT STABLE, EXITS VIA RETURN 1

THEORY: IN MATRIX NOTATION, XF=(I-A)XI+B WHERE I IS THE UNIT MATRIX.
THUS IF XI=XF=X, A.X=B.    (AA,W ARE WORKING SPACES)
* NOTE: LAST CALCULATED VALUE OF MATRIX A IS USED IF ON ENTRY Y(1)>=1

      IMPLICIT REAL*8(A-H,O-Z)
      DIMENSION X(NX),B(NX),Y(NX),A(NX,NX),AA(NX,NX),W(NX,2)

      IFL=1
      C0=0.D0
      C1=1.0D0
      DO 1 J=1,NX
    1 B(J)=C0
      CALL FINT(B)
      IF (Y(1) .GE. 0.99999999)GO TO 6

      DO 2 JJ=1,NX
      DO 3 J=1,NX
    3 Y(J)=C0
      Y(JJ)=C1
      CALL FINT(Y)
      DO 4 J=1,NX
    4 A(J,JJ)=-Y(J)+B(J)
    2 CONTINUE

      DO 5 J=1,NX
    5 A(J,J)=A(J,J)+C1

      IF(NX.EQ.2) GO TO 7
    6 CALL F04ATF(A,NX,B,NX,X,AA,NX,W(1,1),W(1,2),IFL)   [NAG LIBRARY SUBROUTINE]
SOLVES EQUATION A.X=B; AA & W ARE WORKING SPACES
      IF(IFL.GT.0)GO TO 9

      RETURN

CHECK STABILITY (FOR NX=2 CASE)
    7 T11=C1-A(1,1)
      T22=C1-A(2,2)
      WRONSK=T11*T22-A(1,2)*A(2,1)
      IF ((C1 + WRONSK) .GT. DABS(T11+T22)) GO TO 6

UNSTABLE...
      RETURN 1

    9 WRITE(6,100)IFL
  100 FORMAT(' F04: IFAIL=',I1)
      RETURN 1
      END
```

A31.a Listing of FORTRAN subroutine SSICS for finding steady state initial conditions

and that this represents the general solution. It is noted that the initial state vector $y(0)$ equals $(a_1, a_2)^T$, so we can write the general solution in the form:

$$y(x) = y_0(x) + \underline{T}(x)\, y(0) \qquad \text{.b}$$

where the columns of matrix $\underline{T}(x)$ are $y_1(x)$ and $y_2(x)$. The linearity of the system is reflected in the form of this general solution.

Periodic particular solution: If the conditions after a complete period ($x = 2\pi$) are identical to the initial conditions, the solution from $x = 2\pi$ must match that from $x = 0$, so the complete solution is periodic. That is, the periodic solution $y_p(x)$ is characterised by $y_p(2\pi) = y_p(0)$, so that

$$y_0(2\pi) + \underline{T}(2\pi)\, y_p(0) = y_p(0). \qquad \text{.c}$$

Therefore $y_p(0)$ can be obtained as

$$y_p(0) = -(\underline{T}(2\pi) - \underline{I})^{-1} y_0(2\pi) \qquad \text{.d}$$

| $\underline{I}$ is the unit matrix

provided that $(\underline{T}(2\pi) - \underline{I})$ is non-singular. Thus in this case the periodic solution is unique. If $(\underline{T}(2\pi) - \underline{I})$ is singular there is evidently no periodic solution.

$\underline{T}(2\pi)$ and $y_0(2\pi)$ can easily be evaluated by numerical integration over a period from the initial conditions $y_0(0)$, $y_1(0)$ and $y_2(0)$; then $y_p(0)$ can be found from .d above, and the complete periodic solution found by a further numerical integration. This method has been implemented in the FORTRAN subroutine SSICS shown opposite.

If $y_{p1}(x)$ is the periodic solution associated with a forcing function $P_1(x)$ and $y_{p2}(x)$ is likewise associated with $P_2(x)$, then it can be seen that $y_{p1}(x) + y_{p2}(x)$ is also periodic and is a solution to equation A30.a with the forcing function $P_1(x) + P_2(x)$. Thus the periodic response to a general $P(x)$ may be found as the sum of the periodic responses associated with each harmonic of $P(x)$ acting separately.

? Same period

10T: STABILITY OF SOLUTIONS OF HILL'S EQUATION
(APPENDIX TO CHAPTER 7)

This Appendix uses the same nomenclature as the previous one. Let the general solution $y(x)$ be expressed as the sum of an aperiodic part $y_a(x)$ and the periodic solution considered above; that is, $y_a(x) \equiv y(x) - y_p(x)$. By subtraction it is seen that

$$y_a(x) = \underline{T}(x)\, y_a(0). \qquad \text{.a}$$

Since the Hill's equation is unchanged when the origin of x is shifted by an integral number of periods, $y_a(2\pi n + \delta x)$ bears the same relation to $y_a(2\pi n)$ as $y_a(\delta x)$ bears to $y_a(0)$; that is

$$y_a(2\pi n + \delta x) = \underline{T}(\delta x)\, y_a(2\pi n) \qquad \text{.b}$$

where δx is defined as in the range $0 \leq \delta x < 2\pi$ and n is integral.

Now writing $y_a(x)$ as $(\alpha \underline{u}_1 + \beta \underline{u}_2)$ where $\underline{u}_1$, $\underline{u}_2$ are the eigenvectors of $\underline{T}(2\pi)$, assumed to be distinct, we have

$$y_a(2\pi) = \alpha\, \underline{T}(2\pi)\, \underline{u}_1 + \beta\, \underline{T}(2\pi)\, \underline{u}_2 = \alpha\lambda_1 \underline{u}_1 + \beta\lambda_2 \underline{u}_2 \qquad \text{.c}$$

where λ_1, λ_2 are the corresponding eigenvalues; and so similarly

$$y_a(2\pi n) = \alpha\lambda_1^n \underline{u}_1 + \beta\lambda_2^n \underline{u}_2. \qquad \text{.d}$$

On physical grounds we can be sure that for the applications in question $\underline{T}(\delta x)$ remains finite for $0 \leq \delta x < 2\pi$, so that the stability of $y_a(x)$ depends on the magnitude of the eigenvalues. If $|\lambda_1| < 1, |\lambda_2| < 1$ then $y_a(x)$ approaches zero for large x, so that $y(x)$ approaches $y_p(x)$ and therefore the periodic solution is also the "steady state" solution.

10U: EDITED OUTPUT OF PROGRAM 'MUSCLE' (APPENDIX TO CHAPTER 8, p156-7)

The listing below is based on the output produced by program 'MUSCLE' when applied to the case study described on page 156. It has been edited only to improve clarity and save space.

```
NON-INTERACTIVE DATA FILE:-  DEFINES ORIGINAL LINKAGE
&LDATA NDYAD=2, NSTEP=72, RPM=300, ITOP=0,-1,1,
GEOM=.2, .05, .0, .275, .25, .0,
DYNE=0, 0, 0, 0,  0, 0, 0, 0,
.1, .0, .33235, .001278,   .1375, .0, .47445, .00405   &END
-------------------------------------------------------------------------
&LOAD MCC5:TIMEDMUSCLE
T=0.239 DR=0
&START 1=MCC5:CS.KEYTABLE 2=MCA7:CARSON.DATA 3=-KILFIN
 4=-KILOUT 7=*SINK* 8=-AMTRX 9=-DMTRX  0=MCA7:TITLE.NEW(LAST)
-------------------------------------------------------------------------

              **********
              * MUSCLE *:  MULTICRITERION SYNTHESIS OF COUNTERWEIGHTS
              **********   FOR LINKAGE ENHANCEMENT

-------------------------------------------------------------------------
INTERACTIVE DATA INPUT PHASE BEGINS...        0.249 CPU SEC.
" UPPER/X=3*.8 U/Y=3*.8 U/RADIUS=3*.8 U/THICKNESS(2)=.02,.05
" LOWER/X=3*-.8 LO/Y=3*-.8
" FIX/RAD(1)=.1 F/THIC(1)=.05  #(CRANK C/WT MASS DOESN'T AFFECT SOL.)
;
" OPCONTROL(5)=0 MAXITR=150  #(CONTROL PRINTOUT & TERMINATION)
" TFFORCE=1 TFMOMENT=1  #(TARGET RMS FRAME FORCE & MOMENT)
"
" # IF COUNTERWEIGHTS START AT POOR LOCATIONS, PROGRAM WILL TRY
" # TO ELIMINATE THEM. LOWER BOUND ON R AND FIXING OF T
" # AVOIDS THIS. THICKNESS CAN BE UNFIXED IN SECOND STAGE.
" LOWER/RADIUS(2)=.03,.03   FIX/THICKNESS(2)=.02,.05
"
" SEED=10001 RANDOMISE/PARAMETERS      OPTIMISE
-------------------------------------------------------------------------

*** ENTERING EXECUTE PHASE ***         0.622 CPU SEC.
TIME TO PRODUCE MATRIX A =    0.354 CPU SECONDS
TIME TO PRODUCE MATRIX D =    0.327 CPU SECONDS

     ROOT MEAN SQUARES OF INITIAL LOADS (WITHOUT COUNTERWEIGHTS)
     ---- ---- ------- -- ------- -----
FRAME FORCE        FRAME MOMENT      DRIVING TORQUE
 1.6494E+01          1.2499E+00          4.9955E-01
JOINT   1 FX:   8.7821E+00  FY:   2.1069E+01
JOINT   2 FX:   8.7821E+00  FY:   2.1069E+01
JOINT   3 FX:   2.2400E+00  FY:   1.1197E+01
JOINT   4 FX:   7.8765E+00  FY:   4.9995E+00

RANDOMISED INITIAL COUNTERWEIGHT PARAMETERS (#: FIXED):-
CWT          X              Y              RAD              TH
 1    -3.8956E-02     6.6256E-02     1.0000E-01#     5.0000E-02#
 2    -5.1861E-02     9.2532E-02     7.2678E-02      2.0000E-02#
 3     9.8836E-02    -4.4144E-03     5.4397E-02      5.0000E-02#
```

continued →

```
*** OPTIMISATION COMPLETED - FUNCTION VALUES HAVE CONVERGED ***
TIME IN OPTIMISING ROUTINE    =   0.381 CPU SECONDS
TIME FOR OBJ. FN. EVALUATION =   0.212 CPU SECONDS
 ITNS      FN EVALS          INITIAL OBFUN     FINAL OBFUN
 129          219              4.1431E+07       1.6744E+02

INTERIM SOLUTION FOR COUNTERWEIGHT PARAMETERS:-
CWT          X                Y                RAD              TH
 1    -6.4679E-03    -1.4698E-03     1.0000E-01#    5.0000E-02#
 2    -6.2665E-03    -5.2558E-02     5.2930E-02     2.0000E-02#
 3    -3.3773E-02     3.4710E-02     4.8430E-02     5.0000E-02#

    ROOT MEAN SQUARES OF FINAL LOADS
    ---- ---- ------- -- ----- -----
FRAME FORCE        FRAME MOMENT     DRIVING TORQUE
 1.4484E-01          1.5111E+00       4.9657E-01
JOINT   1 FX:   2.4456E+01   FY:   6.0749E+00
JOINT   2 FX:   6.7344E+01   FY:   5.8829E+01
JOINT   3 FX:   1.1416E+01   FY:   1.2009E+01
JOINT   4 FX:   2.4417E+01   FY:   6.0446E+00

-------------------------------------------------------------------------
RETURN TO INTERACTIVE DATA INPUT PHASE...        2.016 CPU SEC.
" # NOW UNFIX THICKNESS AND SEE IF IMPROVEMENT IS POSSIBLE. ALSO
" # REMOVE WEIGHTING FROM FRAME MOMENT SO RESIDUAL FORCE ELIMINATED
" -FIX/TH(2) -F/TH(3)    TFFORCE=.0001 TFMOMENT=0    OPTIMISE
-------------------------------------------------------------------------

*** ENTERING EXECUTE PHASE ***        2.063 CPU SEC.
TIME TO PRODUCE MATRIX D =    0.032 CPU SECONDS

*** AN UNDERCONSTRAINED MINIMUM HAS BEEN FOUND , EXIT CODE    3 ***
TIME IN OPTIMISING ROUTINE    =   0.064 CPU SECONDS
TIME FOR OBJ. FN. EVALUATION =   0.073 CPU SECONDS
 ITNS      FN EVALS          INITIAL OBFUN     FINAL OBFUN
  17           84              3.0211E+08       2.1973E-03

FINAL SOLUTION FOR COUNTERWEIGHT PARAMETERS:-
CWT          X                Y                RAD              TH
 1    -6.4660E-03    -1.4741E-03     1.0000E-01#    5.0000E-02#
 2    -6.7098E-03    -5.2621E-02     5.2928E-02     2.0000E-02U
 3    -3.4016E-02     3.4351E-02     4.8442E-02     5.0000E-02U

    ROOT MEAN SQUARES OF FINAL LOADS
    ---- ---- ------- -- ----- -----
FRAME FORCE        FRAME MOMENT     DRIVING TORQUE
 1.1338E-08          1.5393E+00       4.9247E-01
JOINT   1 FX:   2.4483E+01   FY:   6.1572E+00
JOINT   2 FX:   6.7509E+01   FY:   5.8854E+01
JOINT   3 FX:   1.1471E+01   FY:   1.2051E+01
JOINT   4 FX:   2.4483E+01   FY:   6.1572E+00
-------------------------------------------------------------------------
RETURN TO INTERACTIVE DATA INPUT PHASE        2.310 CPU SEC.
" STOP
```

BIBLIOGRAPHY

AFIMIWALA, K.A & MAYNE, R.W:
"A Contour Plotting Scheme for Design Optimization", ASME, J Mech Des, 101, pp 349-354 (1979).

BADLANI, M & MIDHA, A:
"Member Initial Curvature Effects on the Elastic Slider-Crank Mechanism Response", ASME, J Mech Des, 104(1), pp 159-167 (1982).

BAHGAT ET ALIA:
(Bahgat, B.M, Osman, M.O.M & Sankar, T.S), "On the Effect of Bearing Clearances in the Dynamic Analysis of Planar Mechanisms", J Mech Eng Sci, 21(6), pp 429-437 (1979).

BARKAN, P & TUOHY, E.J:
"Impact Behaviour of the Four-Bar Linkage", Trans. 7th Mechanisms Conf., Purdue University, USA, pp 139-145 (1962).

BECKETT ET AL:
(Beckett, R.C, Pan, K.C & Chu, S.C), "A Numerical Method for the Dynamic Analysis of Mechanical Systems in Impact", Trans. ASME, J.Engng Ind., 99B, pp 665-672 (1977).

BERKOF ET AL:
(Berkof, R.S, Lowen, G.G & Tepper, F.R), "Balancing of Linkages", Shock & Vibn Digest, 9(6), pp 3-10 (1977).

BERKOF, R.S & LOWEN, G.G(a):
"A New Method for Completely Force Balancing Simple Linkages", ASME, J. Engng for Industry, 91B, pp 21-26 (1969).

BERKOF, R.S & LOWEN, G.G(b):
"Theory of Shaking Moment Optimization of Force-Balanced 4-bar Linkages", ASME, J.Engng for Industry, 93B, pp 53-60 (1971).

BRACH, R.M:
"Moment Between Impacting Rigid Bodies", ASME, J Mech Des, 103, pp 813-817 (1981).

BROOKE, R.E:
"Where the Mechanical Way Makes Sense", Mach. Des, 51(1) pp 80-83 (1979).

CARSON, W.L & STEPHENS, J.M:
"Feasible Parameter Design Spaces for Force and Root Mean Square Shaking Moment Balancing an In-line 4R 4-bar Synthesized for Kinematic Criteria", Mech & Mach Theory 13, pp 649-658 (1978).

CHACE, M.A:
"Users Guide to DRAM (Dynamic Response of Articulated Machinery)", Report Tel4, Dept Mech Engng, University of Newcastle upon Tyne (1974).

CROSSLEY ET AL:
(Crossley, F.R.E, Olędzki, A & Szydlowski, W), "On Modelling of Impacts of Two Bodies having Flat and Cylindrical Surfaces with Application to Cam Mechanisms", Proc. V World Congress, IFToMM, Montreal, Canada, pp 1090-1092 (1979).

COURANT, R & HILBERT, D:
"Series Expansions of Arbitrary Functions", in "Methods of Mathematical Physics", Interscience, New York, 1 pp 69-70,74 (1953).

DATSERIS, P & FREUDENSTEIN, F:
"Optimum Synthesis of Mechanisms Using Heuristics for Decomposition and Search", ASME, J Mech Des, 101, pp 380-385 (1979).

DIX, R.C:
Discussion on HERBERT & McWHANNEL, Trans. ASME, J Engng Ind. 99b, p 917 (1977).

DIX, R.C & AGRAWALLA, D:
"Balancing Using a General Mechanism Program", Proc. 4th Appl. Mechanisms Conf, OSU, Paper 24 (Nov. 1975).

DRESIG, H & SCHONFELD, D:
"Computer-Aided Optimisation of the Input Torque and Frame Forces in Planar Linkages", Mech & Mach Theory 11, (Part I) pp 363-370, (Part II) pp 371-379 (1976).

DUBOWSKY, S:
"On Predicting the Dynamic Effects of Clearances in Planar Mechanisms", Trans. ASME, J Engng Ind. 96B, pp 317-323 (1974).

DUBOWSKY, S & GARDNER, T.N(a):
"Dynamic Interactions of Link Elasticity and Clearance Connections in Planar Mechanical Systems", Trans. ASME, J Engng Ind. 97B, pp 652-661 (1975).

DUBOWSKY, S & GARDNER, T.N(b):
"Design and Analysis of Multilink Flexible Mechanisms with Multiple Clearance Connections", Trans. ASME, J Engng Ind. 99B, pp 88-96 (1977).

DUBOWSKY, S & FREUDENSTEIN, F:
"Dynamic Analysis of Mechanical Systems with Clearances", (Parts I & II), Trans. ASME, J Engng Ind. 93B, pp 305-316 (1971).

DUBOWSKY, S & MOENING, M.F:
"An Experimental and Analytical Study of Impact Forces in Elastic Mechanisms with Clearances", Mech & Mach Theory, 13, pp 451-465 (1978).

DUBOWSKY, S & YOUNG, S.C:
"An Experimental and Analytical Study of Connection Forces in High-Speed Mechanisms", Trans. ASME, J Engng Ind. 97B, pp 1166-1174 (1975).

DUBOWSKY, ET AL:
(Dubowsky, S, Prentis, J.M & Valero, R.A), "On the Development of Criteria for the Prediction of Impact in the Design of High Speed Systems with Clearances", Proc. V. World Congress, IFToMM, Montreal, Canada, pp 968-971 (1979).

EARLES, S.W.E.& KILICAY, O(a):
"Predicting Impact Conditions due to Bearing Clearances in Linkage Mechanisms", Proc. V World Congress, IFToMM, Montreal, Canada, pp 1078-1081 (1979).

EARLES, S.W.E & KILICAY, O(b):
"A Design Criterion for Maintaining Contact at Plain Bearings", Proc. Inst. Mech Engrs, 194 (25), pp 249-258 (1980).

EARLES, S.W.E & WU, C.L.S(a):
"Motion Analysis of a Rigid-Link Mechanism with Clearance at a Bearing, using Lagrangean Mechanics and Digital Computation", Mechanisms, pp 83-89: Institution of Mechanical Engineers, London, (1973).

EARLES, S.W.E & WU, C.L.S(b):
"Predicting the Occurrence of Contact Loss and Impact at a Bearing from a Zero-Clearance Analysis", Proc.IV World Congress, IFToMM, Newcastle upon Tyne, pp 1013-1018 (1975).

EARLES, S.W.E & WU, C.L.S(c):
"Designing to Minimise Impacts in Bearings", Engineering, Lond. 217, pp 866-867 (1977).

ELLIOTT, J.L:
"Mass Synthesis for Multiple Balancing Criteria of Complex, Planar Mechanisms", PhD Thesis, Univ. of Florida; Univ. Microfilms Intl 80-29056 (1980).

ERDMAN, A.G & SANDOR, G.N:
"Kineto-Elastodynamics - a Review of the State of the Art and Trends", Mechanism & Machine Theory, 7, pp 19-33 (1972).

ESAT, I.I & HAINES, R.S:
"The Use of Springs to Control the Dynamic Performance of Planar Linkage Mechanisms", Report Ta57, Dept Mech Engg, University of Newcastle upon Tyne (1982).

ESHWAR, V.A:
"Analysis of Clearance Fit Pin Joints", Int. J. Mech. Sci. 20, pp 477-484 (1978).

FAWCETT, J.N:
"Maintaining Contact Brings Rewards", Engineering,Lond. 215, pp 741-743 (1975).

FAWCETT, J.N & BURDESS, J.S:
"Effects of Bearing Clearance in a Four-Bar Linkage", Proc. III World Congress, IFToMM, Kupari, Yugoslavia, C, pp 111-126 (1971).

FREUDENSTEIN, F:
"Structural Error Analysis in Plane Kinematic Synthesis", ASME, J of Engng for Ind, 81, pp 15-21 (1959).

FUJITA, T & HATTORI, S:
"Periodic Vibration & Impact Characteristics of a Nonlinear System with Collision", Bull JSME, 23 (177) pp 409-418 (1980).

FUNABASHI, H & OGAWA, K:
"A Dynamic Synthesis of Non-Uniform Motion Mechanisms" Bull JSME, 19 (130) pp 446-453 (1976).

FUNABASHI ET ALIA(a):
(Funabashi, H, Ogawa, K & Horie, M), "A Dynamic Analysis of Mechanisms with Clearances", Bull. JSME, 21 (161) pp 1652-1659 (1978).

FUNABASHI ET ALIA(b):
(Funabashi, H, Ogawa, K, Horie, M & Iida, H), "A Dynamic Analysis of the Plane Crank-and-Rocker Mechanisms with Clearances", Bull. JSME, 23 (177) pp 446-452 (1980).

FURUHASHI ET AL(a):
(Furuhashi, T, Morita, M & Matsuura, M), "Research on Dynamics of Four-Bar Linkages with Clearances, 1st report". Bull. JSME, 21, pp 518-523 (1978).

FURUHASHI ET AL(b):
(Furuhashi, T, Morita, M & Matsuura, M), "Research on Dynamics of Four-Bar Linkages with Clearances, 4th report". Bull. JSME, 21, pp 1299-1305 (1978)

GHERONIMUS, Ya.L:
"On the Application of Chebyshev's Methods to the Problem of Balancing Mechanisms" (translation), J. Mechanisms, 3, pp 235-281 (1948, tr.1968).

GOLDSMITH, W:
"Impact", Arnold, London (1960).

GOLEBIEWSKI, E.P & SADLER, J.P:
"Analytical and Experimental Investigation of Elastic Slider-Crank Mechanisms", ASME, J Engg Ind., 98,B, (4), pp 1266-1271 (1976).

GRANT, S.J:
"Dynamic Effects of Bearing Clearances in Mechanisms", Ph.D Thesis, University of Newcastle upon Tyne, England (1976).

GRANT, S.J & FAWCETT, J.N(a):
"Control of Clearance Effects in Mechanisms", ASME paper 77-WA/DE-2 (1977).

GRANT, S.J & FAWCETT, J.N(b):
"Comparison of Relative Motion at Form-Closed and Force-Form-Closed Connections", Proc. II IFToMM International Symposium on Linkages and Computer Aided Design Methods, Bucharest, Romania, 1-2, pp 269-280 (1977).

HAIN, K:
"Einfluß von Gelenkspiel und Reibung auf die im Getriebe wirkenden Kräfte", Fortschritt Bericht, VDI-Zeitschrift, Series 1 (17)(1969).

HAINES, R.S(a):
"On Predicting Vibrations in Realistically Proportioned Linkage Mechanisms", ASME, J Mech Des, 103, pp 706-711 (1981).

HAINES, R.S(b):
"Survey, 2-Dimensional Motion and Impact at Revolute Joints", Mech & Mach Theory, 15, pp 361-370 (1980).

HAINES, R.S(c):
"A Theory of Contact Loss at Revolute Joints with Clearance", J.Mech.Engg Sci., 22(3), pp 129-136 (1980).

HAINES, R.S(d):
"Minimum RMS Shaking Moment or Driving Torque of a Force-Balanced 4-Bar Linkage Using Feasible Counterweights", Mech & Mach Theory, 16, pp 185-190 (1981).

HAINES, R.S(e):
"The Spacing of Precision Points in Full-Cycle Mechanism Synthesis", accepted for publication in ASME, J.Mech Des.

HALTER, J.M:
"Force System Synthesis to Produce a Desired Time Response of Mechanisms", PhD Thesis, University of Missouri in Columbia; University Microfilms Intl 76-1017 (1975).

HALTER, J.M & CARSON, W.L:
"Mechanism-Force System Synthesis to Obtain a Desired Motion-Time Response", Proc IV World Congress, IFToMM, Newcastle upon Tyne, 2, pp 399-404 (1975).

HALTER ET AL:
(Halter, J.M, Smith, R.E & Carson, W.L), "Dynamic Time Response Synthesis of Mechanisms", ASME Paper 72-MECH-69 (1972).

HAMMERSCHMIDT, C:
"Dynamische Wirkung des Spiels in Gelenken von Getrieben", Proc. IV World Congress, IFToMM, Newcastle upon Tyne, England, pp 1001-1006 (1975).

HAMMERSCHMIDT, C & STRUMPFEL, H:
"The Effect of Clearance and Tolerances in Linkages Motion" (in German), Proc. V World Congress, IFToMM, Montreal, Canada, pp 1093-1096 (1979).

HAYASHI ET AL:
(Hayashi, T, Crossley, F.R.E & Larionescu, D), "Analog Simulation of Repetitive Impacts", Proc. IV World Congress, IFToMM, Newcastle upon Tyne, England, pp 1073-1077 (1975).

HERBERT, R.G & McWHANNELL, D.C:
"Shape and Frequency Composition of Pulses from an Impact Pair", Trans. ASME, J.Engng Ing. 98B, 513-518 (1977).

HUNT, K.H & CROSSLEY, F.R.E:
"Coefficient of Restitution Interpreted as Damping in Vibroimpact", Trans. ASME, J.Appl.Mech. 42E, pp 440-445 (1975).

IMAM ET AL:
(Imam, I, Skreiner, M and Sadler, J.P), "A New Solution to Coulomb Friction in Mechanism Bearings: Theory and Application", ASME, J. Mech Des., 103 pp 764-775 (1981).

INGLIS, C:
"Applied Mechanics for Engineers", Dover, NY, pp 201, 332-333 (1963).

JANDRASITS, W.G & LOWEN, G.G(a):
"The Elastic-Dynamic Behaviour of a Counterweighted Rocker Link with an Overhanging Endmass in a Four-Bar Linkage, Part I: Theory", ASME, J Mech Des, 101, pp 77-88 (1979).

JANDRASITS, W.G & LOWEN, G.G(b):
Ibid: "Part II: Application and Experiment", ASME, J. Mech Des, 101, 89-98 (Jan. 1979).

JOHNSTON, R.C:
"Impact Forces in Mechanisms", Mach.Des. 30, pp 138-146 (1958).

KAUFMAN, R.E:
"Mechanism Design by Computer", Mach Des 50 (24) pp 94-100 (1978).

KRANIAUSKAS, P.V:
"A Dynamic Analysis of Serially Connected Planar Linkages", PhD Thesis, University of Newcastle upon Tyne, (1974).

LAWRENCE, K.L & ALEXANDER, R.M:
"Elastic Mechanism Dynamic Strains", Proc. IV World Congress, IFToMM, 1, p 133 (1975).

LOWEN, G.G & BERKOF, R(a):
"Survey of Investigations into the Balancing of Linkages", J.Mechanisms, 3(4) pp 221-231 (1968).

LOWEN, G.G & BERKOF, R(b):
"Determination of Force-Balanced 4-Bar Linkages with Optimum Shaking Moment Characteristics", ASME, J Engg for Industry, 93B, pp 39-46 (1971).

LOWEN, G.G & JANDRASITS, W.G:
"Survey of Investigations into the Dynamic Behaviour of Mechanisms Containing Links with Distributed Mass and Elasticity", Mech & Mach Theory, 7, pp 3-17 (1972).

MANSOUR, W.M & TOWNSEND, M.A:
"Impact Spectra and Intensities for High-Speed Mechanisms", Trans. ASME, J. Engg Ind. 97B, pp 347-353 (1975).

MATTHEW, G.K & TESAR, D(a):
"Synthesis of Spring Parameters to Satisfy Specified Energy Levels in Planar Mechanisms", ASME, J Engg for Ind. 99B, pp 341-346 (1977).

MATTHEW, G.D & TESAR, D(b):
"Synthesis of Spring Parameters to Balance General Forcing Functions in Planar Mechanisms", ASME, J Engg for Ind, 99B pp 347-352 (1977).

MAW ET AL:
(Maw, N, Barber, J.R.& Fawcett, J.N), "The Oblique Impact of Elastic Spheres", Wear 38.1 pp 101-114 (1976).

McCALLION, H:
"Vibration of Linear Mechanical Systems", Longman, London, p 120 (1973).

McLARNAN, C.W:
"On Linkage Synthesis with Minimum Error", J Mechanisms, 3, pp 101-105 (1968).

MEYER-zur-CAPELLEN, W:
"Torsional Vibrations in the Shafts of Linkage Mechanisms", ASME, J.Engg Ind., 89B, pp 126-136 (1967).

MIDHA, A & BADLANI, M.L:
"On a Numerical Method for Solution of the Mathieu-Hill Type Equations", ASME, J Mech Des, 102, pp 619-625 (1980).

MIDHA ET AL:
(Midha, A, Erdman, A.G & Frohrib, D.A), "A Closed-Form Numerical Algorithm for the Periodic Response of High-Speed Elastic Linkages", ASME, J Mech Des, 101 (1) pp 154-162 (1979).

MIEDEMA, B & MANSOUR, W.M:
"Mechanical Joints with Clearance: a Three-Mode Model", Trans. ASME, J. Engg Ind. 98B, pp 1319-1323 (1976).

MILNER, J.R & SMITH, D:
"Kinematic Analysis of Planar Mechanisms Using Programmable Calculators", Paper No. 10, Vth OSU Applied Mechanisms Conf, Oklahoma City, Nov 1977.

MORITA ET AL:
(Morita, N, Furuhashi, T & Matsuura, M), "Research on Dynamics of Four-Bar Linkages with Clearances at Turning Pairs (2nd & 3rd repots)", Bull. JSME, 21, pp 1284-1298 (1978).

NAG:
"NAG Fortran Library Manual" (Mk8), Chapter E04, Numerical Algorithms Group, Oxford (1981).

NATH, P.K & GHOSH, A:
"Kineto-Elastodynamic Analysis of Mechanisms by Finite Element Method", Mech & Mach Theory, 15, pp 179-197 (1980).

OLDHAM, K(a):
"Advantages of Dyadic Planar Linkages for Kinematic Synthesis", Second IFToMM Intl Symp on Linkages and CAD Methods, Bucharest, Romania, I-2 (38) pp 455-462 (1977).

OLDHAM, K(b):
"The Kinematics and Vibration of Planar Linkage Mechanisms", PhD Thesis, University of Newcastle upon Tyne (1977).

OLDHAM, K & WALKER, M.J:
"A Procedure for Force-Balancing Planar Linkages Using Counterweights", J Mech Engg Sci, 20(4), pp 177-182 (1978).

OLEDZKI, A & SZYDLOWSKI, W:
"On the Modelling of the Energy Dissipation in Kinematic Pairs with Backlash", Proc. IV World Congress, IFToMM, Newcastle upon Tyne, England, pp 1007-1011 (1975).

OLEZDKI ET AL:
(Olęzdki, A, Szydlowski, W & Orkan-Lęcki, K), "Modelling of Impact in a Kinematic Pair" (in Polish). Research work review, Group for modelling and computer simulation in machine design, Warsaw Technical University (1978).

OSMAN, M.O.M, BAHGAT, B.M & SANKAR, T.S:
"On the Prediction of Journal-Bearing Separation in High Speed Mechanisms with Clearances", ASME Paper 80-WA/DSC-36,(1980).

PAUL, B:
"Analytical Dynamics of Mechanisms - A Computer Oriented Overview", Mech & Mach Theory, 10, pp 481-507 (1975).

PERREIRA, N.D & DUBOWSKY, S:
"Predicting Acoustic Noise Generation in Complex Mechanical Systems", ASME, J Mech Des., 101, pp 199-209 (1979).

RAO, A.C:
"An Accurate Analysis of Slider-Crank Mechanism", J Inst Engg (India), Mech Engg Div., 59ME, pp 177-180 (1978).

ROARK, R.J & YOUNG, W.C:
"Formulas for Stress and Strain", 5th edition. McGraw-Hill Kogakusha Ltd., Tokyo (1975).

ROGERS, R.J & ANDREWS, G.C:
"Dynamic Simulation of Planar Mechanical Systems with Lubricated Bearing Clearances using Vector-Network Methods", Trans. ASME, J Engg Ind. 99B, pp 131-138 (1977).

ROGERS, R.J & PICK, R.J:
"On the Dynamic Spatial Response of a Heat Exchanger Tube with Intermittent Baffle Contacts", Nuclear Engineering & Design, 36, pp 81-90 (1976).

ROONEY, G.T & DERAVI, P:
"Coulomb Friction in Mechanism Sliding Joints", Mech & Mach Theory 17(3) pp 207-212 (1982).

SANDERS, J.R.& TESAR, D:
"The Analytical and Experimental Evaluation of Vibratory Oscillations in Realistically Proportioned Mechanisms", ASME, Journal of Mech Des, 100(4) pp 762-768 (1978).

SCHOLES, A & STROVER, E.M:
"The Piecewise-Linear Analysis of Two Connecting Structures Including the Effect of Clearance at the Connections", Int.J. Numerical Methods in Engg, 3 pp 45-51 (1971).

SERGEEV, W.I & YUDIN, K.M:
"On a Problem of the Dynamics of Mechanisms with Clearance" (in Russian), Proc. III World Congress, IFToMM, Kupari, Yugoslavia, A, pp 197-208 (1971).

SHERWOOD, A.A & HOCKEY, B.A:
"The Optimisation of Mass Distribution in Mechanisms using Dynamically Similar Sytems", J Mechanisms 4, pp 243-280 (1969).

SHIMOJIMA ET AL:
(Shimojima, H, Ogawa, K & Matsumoto, K), "Dynamic Characteristics of Planar Mechanisms with Clearance", Bull. JSME, 21, pp 303-308 (1978).

SKREINER, M:
"Dynamic Analysis used to Complete the Design of a Mechanism", Jnl Mechanisms, 5 pp 105-119 (1970).

SMITH, M.R:
"The Dynamics of Rigid & Flexible Four-Bar Linkages", PhD Thesis, University of Newcastle upon Tyne, (1972).

SPITZNAGEL, K.L & TESAR, D:
"Multiparametric Optimization of Four-Bar Linkages", ASME, J.Mech Des,101, pp 386-391 (1979).

STARR, P.J:
"Dynamic Synthesis of Linkages - An Emerging Field", ASME Paper 74-DET-64 (1974).

SUNADA, W & DUBOWSKY, S:
"The Application of Finite Element Methods to the Dynamic Analysis of Flexible Spatial and Co-Planar Linkage Systems", ASME Paper 80-DET-87 (1980).

TAMURA, H
"A Dynamic Analysis of a Linkage having Flexible Drive Shafts", Internal Report, Department of Mechanical Engineering, University of Newcastle upon Tyne, (1979).

TATARA, Y:
"Effects of External Force on Contacting Times and Coefficients of Restitution in a Periodic Collision", Trans. ASME, J.Appl.Mech. 44E, pp 773-775 (1977).

THOMPSON, B.S(a):
"A Survey of Analytical Path-Synthesis Techniques for Plane Mechanisms", Mech & Mach Theory, 10, pp 197-205 (1975).

THOMPSON, W.T(b):
"Vibration Theory and Applications", George Allen & Unwin, London, Ch 8, p 275 (1966).

THOMPSON, B.S & GHANDI, M.V:
"The Finite Element Analysis of Mechanism Components Made from Fiber-Reinforced Composite Materials", ASME Paper 80-DET-63 (1980).

THRELFALL, D.C:
"The Inclusion of Coulomb Friction in Mechanisms with Particular Reference to DRAM", Mech & Mach Theory, 13(4), pp 475-482 (1978).

TOWNSEND, M.A & MANSOUR, W.M(a):
"A Pendulating Model for Mechanisms with Clearances in the Revolutes", Trans. ASME, J.Engg Ind. 97B, pp 354-358 (1975).

TOWNSEND, M.A & MANSOUR, W.M(b):
"Approximating the Times between Closely-Spaced Impacts in Mechanisms with Clearances", Mech & Mach Theory, 11, pp 259-265 (1976).

VELUSWAMI ET AL:
(Veluswami, M.A, Crossley, F.R.E & Horvay, G), "Multiple Impacts of a Ball between Two Plates" (Part II), Trans. ASME, J.Engg Ind. 97B, pp 828-835 (1975).

VISCOMI, B.V & AYRE, R.S:
"Nonlinear Dynamic Response of Elastic Slider-Crank Mechanism", ASME Trans, J.Engg for Ind., 93B, pp 251-262 (1971).

WALDRON, K & KUMAR, Alok:
"Numerical Burmester Synthesis on a Pocket Calculator", Paper 9, Fifth OSU Appl. Mech. Conf., Oklahoma, (1977).

WALKER, M.J:
"Balancing Planar Linkage Mechanisms", PhD Thesis, University of Newcastle upon Tyne, (1979).

WALKER, M.J & HAINES, R.S:
"An Experimental Study of the Effects of Counterweights on a Six-Bar Chain", accepted for publication in Mech & Mach Theory.

WIEDERRICH, J.L:
"Analysis of Drive Shaft Speed Variations in a Scotch Yoke Mechanism", ASME, J Mech Des., 103,pp 239-246 (1982).

WIEDERRICH, J.L & ROTH, B:
"Momentum Balancing of Four-Bar Linkages", ASME, J Engg Ind, 98B, pp 1289-1295 (1976).

WILLMERT ET AL:
(Willmert, K.D, Thornton, W.A & Khan, M.R), "A Hierarchy of Methods for Analysis of Elastic Mechanisms with Design Applications", ASME Paper 78-DET-56.

WILSON, R:
"The Dynamics of the Slider-Crank Mechanism with Clearance in the Sliding Bearing", PhD Thesis, University of Newcastle upon Tyne, (1971).

WILSON, R & FAWCETT, J.N:
"Dynamics of the Slider-Crank Mechanism with Clearance in the Sliding Bearing", Mech and Mach Theory, 9, pp 61-80 (1974).

WU, C.L.S:
"A Determination of Contact-Loss at a Bearing of a Linkage Mechanism", PhD Thesis, Queen Mary College, University of London, England (1974).

WU, C.L.S & EARLES, S.W.E:
"A Determination of Contact-Loss at a Bearing of a Linkage Mechanism", Trans. ASME. J.Engg Ind. 99B, pp 375-380 (1977).